

Air Force Institute of Technology

**AFIT Scholar**

---

Theses and Dissertations

Student Graduate Works

---

3-2000

## Improving UAV Handling Qualities Using Time Delay Compensation

Andrew J. Thurling

Follow this and additional works at: <https://scholar.afit.edu/etd>



Part of the [Aerospace Engineering Commons](#)

---

### Recommended Citation

Thurling, Andrew J., "Improving UAV Handling Qualities Using Time Delay Compensation" (2000). *Theses and Dissertations*. 4871.

<https://scholar.afit.edu/etd/4871>

This Thesis is brought to you for free and open access by the Student Graduate Works at AFIT Scholar. It has been accepted for inclusion in Theses and Dissertations by an authorized administrator of AFIT Scholar. For more information, please contact [richard.mansfield@afit.edu](mailto:richard.mansfield@afit.edu).



**IMPROVING UAV HANDLING QUALITIES  
USING TIME DELAY COMPENSATION**

**THESIS**

**Andrew J. Thurling, Major, USAF**

**AFIT/GAE/ENY/00M-01**

**DEPARTMENT OF THE AIR FORCE  
AIR UNIVERSITY**

**AIR FORCE INSTITUTE OF TECHNOLOGY**

---

---

**Wright-Patterson Air Force Base, Ohio**

**APPROVED FOR PUBLIC RELEASE; DISTRIBUTION UNLIMITED.**

**20000613 089**

**DIC QUALITY INSPECTED 3**

**DIC QUALITY INSPECTED 4**

# REPORT DOCUMENTATION PAGE

*Form Approved*  
**OMB No. 0704-0188**

Public reporting burden for this collection of information is estimated to average 1 hour per response, including the time for reviewing instructions, searching existing data sources, gathering and maintaining the data needed, and completing and reviewing this collection of information. Send comments regarding this burden estimate or any other aspect of this collection of information, including suggestions for reducing this burden to Department of Defense, Washington Headquarters Services, Directorate for Information Operations and Reports (0704-0188), 1215 Jefferson Davis Highway, Suite 1204, Arlington, VA 22202-4302. Respondents should be aware that notwithstanding any other provision of law, no person shall be subject to any penalty for failing to comply with a collection of information if it does not display a currently valid OMB control number. **PLEASE DO NOT RETURN YOUR FORM TO THE ABOVE ADDRESS.**

<b>1. REPORT DATE (DD-MM-YYYY)</b> 24-02-2000	<b>2. REPORT TYPE</b> Master's Thesis	<b>3. DATES COVERED (From - To)</b> 17-09-1997 to 24-02-2000
<b>4. TITLE AND SUBTITLE</b> IMPROVING UAV HANDLING QUALITIES USING TIME DELAY COMPENSATION		<b>5a. CONTRACT NUMBER</b>
		<b>5b. GRANT NUMBER</b>
		<b>5c. PROGRAM ELEMENT NUMBER</b>
<b>6. AUTHOR(S)</b>  Andrew J. Thurling, Major, USAF		<b>5d. PROJECT NUMBER</b>
		<b>5e. TASK NUMBER</b>
		<b>5f. WORK UNIT NUMBER</b>
<b>7. PERFORMING ORGANIZATION NAME(S) AND ADDRESS(ES)</b>  Air Force Institute of Technology Graduate School of Engineering and Management (AFIT/EN) 2950 P Street, Building 640 WPAFB OH 45433-7765		<b>8. PERFORMING ORGANIZATION REPORT NUMBER</b>  AFIT/GAE/ENY/00M-01
<b>9. SPONSORING / MONITORING AGENCY NAME(S) AND ADDRESS(ES)</b> USAF Test Pilot School Attn: Lt. Col. Tom Buter 395 North Flightline Road Edwards AFB CA 93524      DSN: 527-3000		<b>10. SPONSOR/MONITOR'S ACRONYM(S)</b> USAF/TPS
		<b>11. SPONSOR/MONITOR'S REPORT NUMBER(S)</b>

**12. DISTRIBUTION / AVAILABILITY STATEMENT**  
  
APPROVED FOR PUBLIC RELEASE; DISTRIBUTION UNLIMITED

**13. SUPPLEMENTARY NOTES**  
Prof. Bradley Liebst, ENY, DSN: 785-3069, Bradley.Liebst@afit.af.mil

**14. ABSTRACT**

This research investigated control loop time delay and its effect on UAV handling qualities. Compensation techniques to improve handling qualities in the presence of varying amounts of time delay were developed and analyzed. One technique was selected and successfully flight-tested on a UAV.

Flight-testing occurred at a constant flight condition with varying levels of additional time delay introduced into the control loop. Research pilots performed a pitch tracking task and gave Cooper-Harper ratings and comments. Tracking errors were used as a quantitative measure of Pilot/Display/UAV system performance.

Predictive pitch compensation was found to significantly reduce pilot workload and improve Cooper-Harper ratings. Using the predictive display doubled the amount of system time delay that research pilots could tolerate while tracking the task bars. Overall system tracking performance, however, was not improved. Parameter variations of  $\pm 20\%$  in the aerodynamic model used to generate the predictive display produced statistically significant, although not operationally significant, changes in both pilot opinion and performance.

Analysis of flight test data and follow-on simulations resulted in predictor improvements that increased predictor accuracy to the point of restoring system tracking performance to equal that of the system with no additional time delay.

**15. SUBJECT TERMS**  
Time Delay, Delay Compensation, Pilot-in-the-loop Oscillations, UAV Handling Qualities, Handling Qualities, UAV Flight Test, Predictive Display, Quickened Display

<b>16. SECURITY CLASSIFICATION OF:</b>			<b>17. LIMITATION OF ABSTRACT</b>  UL	<b>18. NUMBER OF PAGES</b>  296	<b>19a. NAME OF RESPONSIBLE PERSON</b> Maj. Andrew J. Thurling
<b>a. REPORT</b> UNCLASSIFIED	<b>b. ABSTRACT</b> UNCLASSIFIED	<b>c. THIS PAGE</b> UNCLASSIFIED			<b>19b. TELEPHONE NUMBER</b> (include area code) (661) 277-6554

The views expressed in this thesis are those of the author and do not reflect the official policy or position of the Department of Defense or the United States Government.

AFIT/GAE/ENY/00M-01

IMPROVING UAV HANDLING QUALITIES  
USING TIME DELAY COMPENSATION

THESIS

Presented to the Faculty of the Graduate School of Engineering and Management  
of the Air Force Institute of Technology

Air University

In Partial Fulfillment of the  
Requirements for the Degree of  
Master of Science in Aeronautical Engineering

Andrew Joseph Thurling, B.S.

Major, USAF

March 2000

Approved for public release; distribution unlimited

IMPROVING UAV HANDLING QUALITIES  
USING TIME DELAY COMPENSATION

Andrew Joseph Thurling, B.S.

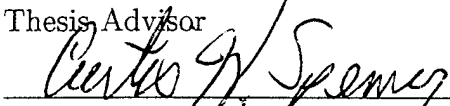
Major, USAF

Approved:

 24 Feb 00


Dr. Bradley Liebst  
Thesis Advisor

Date

 27 Feb 2000

Dr. Curtis Spenny  
Committee Member

Date

 24 Feb 00

Lt. Col. Tom Buter  
Committee Member

Date

## *Preface*

The effects of control system time delays on manned aircraft handling qualities are well understood. Unmanned aircraft have similar control system delay, but have an additional latency caused by the datalink of the human operator's commands from control station to aircraft. The purpose of this thesis is to investigate the effects of time delay on the handling qualities of Unmanned Aerial Vehicles (UAV) and develop compensation strategies to mitigate the adverse effects of the delay. It is my hope that with techniques developed and investigated in this thesis future UAV operators will be able to employ UAVs from anywhere in the world thus increasing the flexibility of this already versatile platform.

I would like to thank the professors at the Air Force Institute of Technology, particularly my committee members Dr. Brad Liebst and Dr. Curtis Spenny, for their instruction and advice. My heartfelt appreciation is expressed to Tony Frackowiak, Alex Sim, Howard Ng, Jim Murray and the other outstanding individuals at NASA Dryden Flight Research Center for their excellent support and aid in preparing for and conducting the flight test. I also wish to thank Steve Bowline of Computer Sciences Corporation for his ceaseless efforts on my behalf. A big "thank you" goes to the Have Reckon test team of Dana Purifoy, Kevin Ford, Andy Adams, Kelly Greene, and Shahnaz Punjani without whom all the effort would have been for naught. My sincere thanks to Dr. Tom Buter for supporting this research from beginning to end and wading through endless drafts of this document.

Finally, I'd like to thank my long suffering wife, Lesley, who has put up with this research being a part of my life for the last two years. Her support and encouragement when obstacles obscured my path kept me focused and sane enough to carry on until the way was once again clear.

Andrew Joseph Thurling

## *Table of Contents*

	Page
Preface . . . . .	iii
List of Figures . . . . .	ix
List of Tables . . . . .	xviii
List of Symbols . . . . .	xxi
List of Abbreviations . . . . .	xxiv
Abstract . . . . .	xxvi
I. Introduction . . . . .	1-1
1.1 Handling Qualities for UAVs? You Must Be Joking! . . . . .	1-1
1.1.1 A Brief History of the UAV . . . . .	1-1
1.1.2 What's a UCAV? . . . . .	1-2
1.1.3 No, I'm Not Joking . . . . .	1-4
1.2 Objectives . . . . .	1-6
1.3 Thesis Overview . . . . .	1-7
II. Theoretical Development . . . . .	2-1
2.1 Signals . . . . .	2-1
2.1.1 Time Domain Characteristics . . . . .	2-1
2.1.2 Temporal Sensitivity . . . . .	2-1
2.2 Systems . . . . .	2-2
2.2.1 Open Loop . . . . .	2-2
2.2.2 Closed Loop . . . . .	2-3



	Page
2.2.3 Pade Approximations . . . . .	2-5
2.3 Time Delay Effect on Human Control Behavior . . . . .	2-6
2.3.1 Handling Qualities Rating Scale . . . . .	2-7
2.3.2 Measuring Time Delay . . . . .	2-9
2.3.3 Pilot Compensation Effects . . . . .	2-9
2.3.4 Time Delay Effects on Handling Qualities . . . . .	2-12
2.4 Mathematical Methods for Estimating Pilot Rating . . . . .	2-14
2.4.1 Bandwidth Criteria . . . . .	2-15
2.4.2 Neal-Smith Criteria . . . . .	2-17
2.4.3 Optimal Control Model . . . . .	2-23
2.4.4 Modified Optimal Control Model . . . . .	2-26
2.4.5 Time-Domain/Frequency-Domain Combination Techniques . . . . .	2-27
2.5 Transport Delay Compensation Techniques . . . . .	2-28
2.5.1 Lead-Lag Networks . . . . .	2-29
2.5.2 Velocity Predictor Algorithm . . . . .	2-32
2.5.3 State Predictors . . . . .	2-33
III. Analysis . . . . .	3-1
3.1 Mathematical Analysis, Effect of Delay . . . . .	3-1
3.1.1 Overall Results . . . . .	3-1
3.1.2 F-8 DFBW Data Analysis . . . . .	3-4
3.1.3 Princeton VRA Data Analysis . . . . .	3-7
3.1.4 NASA Utility UAV Data Analysis . . . . .	3-8
3.2 Lead-Lag Compensation Results . . . . .	3-15
3.2.1 Lead/Lag Compensator Analysis . . . . .	3-22
3.2.2 Simulink Simulations . . . . .	3-29
3.3 State Predictor Compensation . . . . .	3-38

	Page
3.3.1 Compensator Design . . . . .	3-38
3.3.2 Full State Feedback Predictor Results . . . . .	3-40
3.3.3 State Predictor Compensator Analysis . . . . .	3-47
3.3.4 Output Feedback Based Compensation . . . . .	3-52
3.3.5 Simulink Model Simulations . . . . .	3-57
IV. Flight Test . . . . .	4-1
4.1 Introduction . . . . .	4-1
4.1.1 General . . . . .	4-1
4.1.2 Program Chronology . . . . .	4-1
4.2 Model-Based Predictive Algorithm Design . . . . .	4-2
4.2.1 Deadband Modeling . . . . .	4-11
4.2.2 Washout Filter Design . . . . .	4-11
4.3 Test Item Description . . . . .	4-14
4.4 Test Objectives . . . . .	4-19
4.5 Test and Execution . . . . .	4-20
4.5.1 General . . . . .	4-20
4.5.2 Test Procedures . . . . .	4-20
V. Flight Test Results and Analysis . . . . .	5-1
5.1 Baseline UAV Handling Qualities . . . . .	5-1
5.1.1 Modeling and Simulation . . . . .	5-1
5.1.2 Flight Test . . . . .	5-1
5.2 Improvement of UAV Handling Qualities using Model- Based Predictive Compensation . . . . .	5-3
5.2.1 Modeling and Simulation . . . . .	5-4
5.2.2 Flight Test . . . . .	5-5
5.3 Sensitivity of Model-Based Predictive Compensation Al- gorithm . . . . .	5-16

	Page
5.3.1	Modeling and Simulation . . . . . 5-16
5.3.2	Flight Test . . . . . 5-16
5.4	Flight Test Time Histories . . . . . 5-21
5.5	Post Flight Test Analysis . . . . . 5-28
5.5.1	UAV Mathematical Models . . . . . 5-28
5.5.2	Atmospheric Disturbances . . . . . 5-36
5.5.3	Kalman Filter Design . . . . . 5-37
5.5.4	Simulation Error . . . . . 5-38
VI.	Conclusions and Recommendations for Further Research . . . . . 6-1
Appendix A.	Experimental Data . . . . . A-1
A.1	F-8 DFBW . . . . . A-1
A.2	Princeton Variable-Response Research Aircraft (VRA) . . . . . A-3
Appendix B.	Additional Simulation Results . . . . . B-1
B.1	F-8 DFBW, Lead/Lag Compensation . . . . . B-1
B.2	F-8, Full State Predictor Compensation . . . . . B-5
B.3	F-8, Output Feedback State Predictor Compensation . . . . . B-8
Appendix C.	Instrumentation . . . . . C-1
C.1	Parameter List . . . . . C-1
C.2	Utility UAV Flight Data . . . . . C-2
C.3	Pilot Station . . . . . C-3
C.4	SGI Workstation . . . . . C-3
C.4.1	Delay . . . . . C-3
C.4.2	Display . . . . . C-4
Appendix D.	Test Point Matrices . . . . . D-1

	Page
Appendix E. Pilot Comments and Ratings . . . . .	E-1
Appendix F. Data Analysis Methods . . . . .	F-1
F.1 Required Data . . . . .	F-1
F.2 Data Analysis . . . . .	F-2
F.2.1 Baseline UAV Handling Qualities . . . . .	F-2
F.2.2 Statistical Methodologies . . . . .	F-2
F.2.3 Learning Curve Validation . . . . .	F-9
F.3 Improvements of UAV Handling Qualities Using Model- Based Predictive Compensation . . . . .	F-11
F.3.1 Data Reduction . . . . .	F-11
F.3.2 Statistical Methodologies . . . . .	F-12
F.4 Sensitivity of the Model-Based Predictive Compensation Algorithm . . . . .	F-19
F.4.1 Statistical Methodologies . . . . .	F-19
Appendix G. UAV Aerodynamic Model and Time Delay Budget . .	G-1
G.1 UAV Aerodynamic Model . . . . .	G-1
G.2 Time Delay Budget . . . . .	G-3
Bibliography . . . . .	BIB-1
Vita . . . . .	VITA-1

## *List of Figures*

Figure		Page
2.1.	Simple Time Delayed System . . . . .	2-3
2.2.	Delay System Response, $K = .8$ . . . . .	2-4
2.3.	Delay System Response, $K = 1.0$ . . . . .	2-4
2.4.	Pilot/Vehicle Closed Loop System . . . . .	2-6
2.5.	Pilot/Vehicle System with Feedback Delay . . . . .	2-7
2.6.	The Cooper-Harper Rating Scale . . . . .	2-7
2.7.	Computing Effective Time Delay (51) . . . . .	2-10
2.8.	F-8 Study Data (51) . . . . .	2-13
2.9.	Task Influence on Time delay effects (51) . . . . .	2-14
2.10.	NT-33 Data from Hodgkinson (29) . . . . .	2-14
2.11.	Definition of Bandwidth for Pitch Angle Response . . . . .	2-19
2.12.	Bandwidth Requirements, Category A and C . . . . .	2-20
2.13.	Neal-Smith Tracking Performance . . . . .	2-20
2.14.	Neal-Smith Handling Qualities Level Boundaries . . . . .	2-21
2.15.	Neal-Smith Criteria Nichols Chart . . . . .	2-22
2.16.	Control Model of Optimal Human Behavior, from (31) . . . . .	2-24
2.17.	Conceptual block diagram of modified optimal control model, from (13) . . . . .	2-27
2.18.	Block Diagram used by Crane (12) . . . . .	2-30
2.19.	First Compensator Flight Tested in Hodgkinson (29) . . . . .	2-32
2.20.	Second Compensator Flight Tested in Hodgkinson (29) . . . . .	2-33
2.21.	State Predictor System Diagram from Sobiski and Cardullo (52)	2-34
3.1.	VRA, Cat A Task, $Y_p Y_c$ Closed Loop Bandwidth versus Delay	3-2
3.2.	VRA, Cat A Task, Bacon-Schmidt Criteria . . . . .	3-3

Figure		Page
3.3.	F-8 DFBW, Landing Task, Pitch SAS, Bandwidth Criteria . . .	3-4
3.4.	F-8 DFBW, Landing Task, Pitch SAS, Neal-Smith Criteria . . .	3-5
3.5.	F-8 DFBW, Cat A Task, Pitch SAS, Bandwidth Criteria . . . . .	3-7
3.6.	F-8 DFBW, Cat A Task, Pitch SAS, Neal-Smith Criteria . . . . .	3-8
3.7.	VRA, Tracking Task, Bandwidth Criteria . . . . .	3-10
3.8.	VRA, Tracking Task, Neal-Smith Criteria . . . . .	3-11
3.9.	VRA, Lower $\omega_c$ Requirement . . . . .	3-11
3.10.	VRA, Landing, 75 KIAS, Bandwidth Criteria . . . . .	3-12
3.11.	VRA, Landing, 75 KIAS, Neal-Smith Criteria . . . . .	3-13
3.12.	Utility UAV, Cat A Task, Bandwidth Criteria . . . . .	3-13
3.13.	Utility UAV, Cat A Task, Neal-Smith Criteria . . . . .	3-14
3.14.	NASA UAV Flight Test Results . . . . .	3-14
3.15.	Lead/Lag Compensated System . . . . .	3-15
3.16.	F-8 DFBW, Pitch SAS, Lead/Lag Compensation . . . . .	3-16
3.17.	F-8 DFBW, Landing Task, Pitch SAS, Lead/Lag Compensation . . . . .	3-16
3.18.	F-8 DFBW, Pitch SAS, Lead/Lag Compensation . . . . .	3-17
3.19.	F-8 DFBW, Landing Task, Pitch SAS, Lead/Lag Compensation . . . . .	3-18
3.20.	VRA, 75 KIAS Landing Task, Lead/Lag Compensation . . . . .	3-19
3.21.	VRA, Formation Task, Lead/Lag Compensation . . . . .	3-20
3.22.	VRA, 75 KIAS Landing Task, Lead/Lag Compensation . . . . .	3-20
3.23.	VRA, Formation Task, Lead/Lag Compensation . . . . .	3-21
3.24.	Utility UAV, Cat A Task, Lead/Lag Compensation, Bandwidth Criteria . . . . .	3-22
3.25.	Utility UAV, Cat A Task, Lead/Lag Compensation, Neal-Smith Criteria . . . . .	3-23
3.26.	Lead/Lag Compensator Comparison . . . . .	3-24
3.27.	Lead/Lag Compensator Phase Error Comparison . . . . .	3-25

Figure		Page
3.28.	VRA, 105 KIAS Landing, Lead/Lag Compensation, Franklin-Powell . . . . .	3-25
3.29.	Lead/Lag Compensation at Varying $\omega_c$ . . . . .	3-27
3.30.	Phase error for Lead/Lag Compensation at Varying $\omega_c$ . . . . .	3-28
3.31.	VRA, 105 KIAS Landing Task, Compensated for Cat A . . . . .	3-29
3.32.	Comparison of Varying Amounts of Lead/Lag Compensation . . . . .	3-30
3.33.	Phase Error of Varying Amounts of Lead/Lag Compensation . . . . .	3-31
3.34.	VRA, 105 KIAS Landing, Varying Amounts of Lead/Lag Compensation . . . . .	3-31
3.35.	Pilot Model Used In Simulation . . . . .	3-32
3.36.	Aircraft Short Period Model . . . . .	3-32
3.37.	VRA Command Tracking Model . . . . .	3-33
3.38.	VRA Gust Rejection Model . . . . .	3-34
3.39.	VRA Command Tracking, 100 msec Delay, Lead/Lag Compensation . . . . .	3-35
3.40.	VRA Command Tracking, 200 msec Delay, Lead/Lag Compensation . . . . .	3-36
3.41.	VRA Command Tracking, 300 msec Delay, Lead/Lag Compensation . . . . .	3-36
3.42.	VRA Command Tracking, 400 msec Delay, Lead/Lag Compensation . . . . .	3-37
3.43.	VRA Gust Rejection, 400 msec Delay, Lead/Lag Compensation . . . . .	3-38
3.44.	Full State Predictor Compensated System . . . . .	3-39
3.45.	Full State Feedback Predictor Compensator . . . . .	3-39
3.46.	F-8 DFBW, Pitch SAS, State Predictor Compensation . . . . .	3-41
3.47.	F-8 DFBW, Landing Task, Pitch SAS, State Predictor Compensation . . . . .	3-41
3.48.	F-8 DFBW, Pitch SAS, State Predictor Compensation . . . . .	3-42

Figure		Page
3.49.	F-8 DFBW, Landing Task, Pitch SAS, State Predictor Compensation . . . . .	3-42
3.50.	VRA, 75 KIAS Landing Task, State Predictor Compensation . . . . .	3-43
3.51.	VRA, Formation Task, State Predictor Compensation . . . . .	3-44
3.52.	VRA, 75 KIAS Landing Task, State Predictor Compensation . . . . .	3-44
3.53.	VRA, Formation Task, State Predictor Compensation . . . . .	3-45
3.54.	Utility UAV, Cat A Task, Full State Compensation, Bandwidth Criteria . . . . .	3-45
3.55.	Utility UAV, Cat A Task, Full State Compensation, Neal-Smith Criteria . . . . .	3-46
3.56.	VRA, 105 KIAS Landing Task, Perturbed $\omega_{n_{sp}}$ . . . . .	3-48
3.57.	VRA, 105 KIAS Landing Task, Perturbed $\zeta_{sp}$ . . . . .	3-48
3.58.	VRA, 105 KIAS Landing Task, Perturbed $T_{\theta_2}$ . . . . .	3-49
3.59.	VRA, 105 KIAS Landing Task, Perturbed $K_{\theta}$ . . . . .	3-49
3.60.	F-8 DFBW, Pitch SAS, Landing Task, Perturbed $\omega_{n_{sp}}$ . . . . .	3-50
3.61.	F-8 DFBW, Pitch SAS, Landing Task, Perturbed $\zeta_{sp}$ . . . . .	3-50
3.62.	F-8 DFBW, Pitch SAS, Landing Task, Perturbed $T_{\theta_2}$ . . . . .	3-51
3.63.	F-8 DFBW, Pitch SAS, Landing Task, Perturbed $K_{\theta}$ . . . . .	3-51
3.64.	VRA, 105 KIAS, State Predictor Compensation, Varying Amounts . . . . .	3-52
3.65.	F-8, SAS, State Predictor Compensation, 50 msec Incremental Amounts . . . . .	3-53
3.66.	Output Feedback Based State Predictor System Diagram . . . . .	3-53
3.67.	System Model with Luenberger Observer . . . . .	3-54
3.68.	VRA, 105 KIAS Landing Task, Output Feedback State Predictor Compensation . . . . .	3-55
3.69.	F-8, Pitch SAS, Landing Task, Output Feedback State Predictor Compensation . . . . .	3-55
3.70.	UAV, Cat A Task, Output Feedback State Predictor Compensation . . . . .	3-56



Figure		Page
3.71.	VRA Command Tracking Model, Full State Predictor Compensation . . . . .	3-58
3.72.	VRA Gust Rejection Model, Full State Predictor Compensation	3-59
3.73.	VRA Command Tracking, 100 msec Delay, Full State Predictive Compensation . . . . .	3-60
3.74.	VRA Command Tracking, 200 msec Delay, Full State Predictive Compensation . . . . .	3-61
3.75.	VRA Command Tracking, 300 msec Delay, Full State Predictive Compensation . . . . .	3-61
3.76.	VRA Command Tracking, 400 msec Delay, Full State Predictive Compensation . . . . .	3-62
3.77.	VRA Command Tracking, Displayed Pitch, 400 msec Delay, Full State Predictive Compensation . . . . .	3-63
3.78.	VRA Gust Rejection, 400 msec Delay, Full State Predictive Compensation . . . . .	3-64
3.79.	VRA Command Tracking Model, Output Feedback State Predictor Compensation . . . . .	3-66
3.80.	VRA Gust Rejection Model, Full Output Feedback State Predictor Compensation . . . . .	3-67
3.81.	VRA Command Tracking, 400 msec Delay . . . . .	3-68
3.82.	VRA Command Tracking, Displayed Pitch, 400 msec Delay . . . . .	3-69
3.83.	VRA Gust Rejection, 400 msec Delay . . . . .	3-70
4.1.	System Block Diagram . . . . .	4-3
4.2.	New System Block Diagram . . . . .	4-5
4.3.	Typical UAV Video Frame . . . . .	4-6
4.4.	Straight and Level Flight . . . . .	4-7
4.5.	Pitch Capture Commanded . . . . .	4-8
4.6.	Predicted Pitch Response to Pilot Input . . . . .	4-8
4.7.	Predicted Pitch Capture . . . . .	4-9

Figure		Page
4.8.	Delayed UAV Response . . . . .	4-9
4.9.	New Pitch Attitude Set . . . . .	4-10
4.10.	System Block Diagram with Washout Filter . . . . .	4-13
4.11.	Block Diagram of Test Configuration . . . . .	4-15
4.12.	NASA Utility UAV . . . . .	4-16
4.13.	Have Reckon Support Vehicles . . . . .	4-17
4.14.	Pilot Station . . . . .	4-18
4.15.	Pilot Station With CSC Computer in Model Shop Van . . . . .	4-18
4.16.	Reference Angles for CSC Display . . . . .	4-19
4.17.	Pilot-In-The-Loop Oscillation Rating Scale . . . . .	4-23
5.1.	Average Cooper-Harper Rating with 90% Confidence Interval	5-7
5.2.	Average Cooper-Harper Rating with Minimum and Maximum	5-8
5.3.	Average PIO Rating with 90% Confidence Interval . . . . .	5-9
5.4.	Average PIO Rating with Minimum and Maximum . . . . .	5-10
5.5.	Average Root Mean Square Tracking Error with 90% Confidence Interval . . . . .	5-12
5.6.	Average Root Mean Square Tracking Error with Minimum and Maximum . . . . .	5-13
5.7.	Average Predictor Performance with 90% Confidence Interval	5-14
5.8.	Average Predictor Performance with Minimum and Maximum	5-15
5.9.	Bode Magnitude Response of Washout Filter . . . . .	5-20
5.10.	Flight Test Data, Test Point 1214, 120 msec Additional Delay, Baseline . . . . .	5-22
5.11.	Flight Test Data, Test Point 2213, 120 msec Additional Delay, Predictive Compensation . . . . .	5-23
5.12.	Flight Test Data, Test Point 1221, 55 msec Additional Delay, Baseline . . . . .	5-23

Figure		Page
5.13.	Flight Test Data, Test Point 2223, 55 msec Additional Delay, Predictive Compensation . . . . .	5-24
5.14.	Flight Test Data, Test Point 1235, 154 msec Additional Delay, Baseline . . . . .	5-24
5.15.	Flight Test Data, Test Point 2234, 154 msec Additional Delay, Predictive Compensation . . . . .	5-25
5.16.	Flight Test Data, Test Point 1222, 156 msec Additional Delay, Baseline . . . . .	5-25
5.17.	Flight Test Data, Test Point 2226, 156 msec Additional Delay, Predictive Compensation . . . . .	5-26
5.18.	Flight Test Data, Test Point 2221, 389 msec Additional Delay, Predictive Compensation . . . . .	5-26
5.19.	Flight Test Data, Test Point 1245, 55 msec Additional Delay, Baseline . . . . .	5-27
5.20.	Flight Test Data, Test Point 2246, 55 msec Additional Delay, Predictive Compensation . . . . .	5-27
5.21.	Utility UAV Simulink Model . . . . .	5-29
5.22.	$\alpha$ and $q$ Feedback Compensation Simulink Model . . . . .	5-30
5.23.	$\alpha$ and $q$ Feedback Compensation Simulink Algorithm Model . . . . .	5-31
5.24.	$\alpha$ , $q$ , and $\theta$ Feedback Compensation Simulink Model . . . . .	5-32
5.25.	$\theta$ Feedback with Kalman Filter Compensation Simulink Model . . . . .	5-33
5.26.	Kalman Filter Compensation Algorithm . . . . .	5-34
5.27.	Kalman Filtered $\alpha$ , $q$ , and $\theta$ Feedback Compensation Simulink Model . . . . .	5-35
5.28.	Nominal Turbulence and Gust Disturbance . . . . .	5-36
5.29.	Simulation Time History, 133 msec Additional Delay, $\alpha$ and $q$ Feedback Compensation . . . . .	5-39
5.30.	Simulation Time History, 133 msec Additional Delay, $\alpha$ , $q$ , and $\theta$ Feedback Compensation . . . . .	5-40

Figure		Page
5.31.	Simulation Time History, 133 msec Additional Delay, Kalman Filtered $\alpha$ , $q$ , and $\theta$ Feedback Compensation . . . . .	5-41
5.32.	Simulation Results, $\alpha$ and $q$ Feedback Compensation . . . . .	5-43
5.33.	Simulation Results, Kalman Filtered $\alpha$ , $q$ , and $\theta$ Feedback Compensation . . . . .	5-44
A.1.	F-8 SAS Simulink Model . . . . .	A-11
A.2.	F-8 Pitch Direct Simulink Model . . . . .	A-12
B.1.	F-8 DFBW Command Tracking Model . . . . .	B-1
B.2.	F-8 DFBW Command Tracking, 20 msec Delay, Lead/Lag Compensation . . . . .	B-2
B.3.	F-8 DFBW Command Tracking, 60 msec Delay, Lead/Lag Compensation . . . . .	B-2
B.4.	F-8 DFBW Command Tracking, 100 msec Delay, Lead/Lag Compensation . . . . .	B-3
B.5.	F-8 DFBW Command Tracking, 140 msec Delay, Lead/Lag Compensation . . . . .	B-3
B.6.	F-8 DFBW Command Tracking, 200 msec Delay, Lead/Lag Compensation . . . . .	B-4
B.7.	F-8 DFBW Command Tracking, 20 msec Delay, Full State Predictive Compensation . . . . .	B-5
B.8.	F-8 DFBW Command Tracking, 60 msec Delay, Full State Predictive Compensation . . . . .	B-6
B.9.	F-8 DFBW Command Tracking, 100 msec Delay, Full State Predictive Compensation . . . . .	B-6
B.10.	F-8 DFBW Command Tracking, 140 msec Delay, Full State Predictive Compensation . . . . .	B-7
B.11.	F-8 DFBW Command Tracking, 200 msec Delay, Full State Predictive Compensation . . . . .	B-7
B.12.	F-8 DFBW Command Tracking, Output Feedback, 20 msec Delay . . . . .	B-8

Figure		Page
B.13.	F-8 DFBW Command Tracking, Output Feedback, 60 msec Delay . . . . .	B-9
B.14.	F-8 DFBW Command Tracking, Output Feedback, 100 msec Delay . . . . .	B-9
B.15.	F-8 DFBW Command Tracking, Output Feedback, 140 msec Delay . . . . .	B-10
B.16.	F-8 DFBW Command Tracking, Output Feedback, 200 msec Delay . . . . .	B-10
C.1.	UAV Onboard Data Acquisition System . . . . .	C-2
C.2.	Frame of Video With Displayed Data . . . . .	C-4
C.3.	Computer Workstation Data Flow Diagram . . . . .	C-5
C.4.	Computer Workstation Top-Level Threads of Execution . . . . .	C-6
C.5.	Computer Workstation Update Current Variable Table (CVT) . . . . .	C-7
C.6.	Computer Workstation Video Processing . . . . .	C-8
F.1.	Display Symbology Definitions . . . . .	F-3
G.1.	Parameter Identification Flight Test Data and pEst Model Response . . . . .	G-2

## *List of Tables*

Table		Page
2.1.	Neal-Smith Bandwidth Requirements . . . . .	2-17
3.1.	F-8 DFBW Landing Task Flight Test Results . . . . .	3-6
3.2.	F-8 DFBW Tracking Task Flight Test Results . . . . .	3-9
3.3.	VRA Tracking Task Flight Test Results . . . . .	3-10
3.4.	VRA Landing Task Flight Test Results . . . . .	3-12
5.1.	Flying Qualities Simulator PIO Ratings . . . . .	5-2
5.2.	Simulation Results, $\alpha$ and $q$ Feedback Compensation . . . . .	5-42
5.3.	Simulation Results, $\alpha$ , $q$ , and $\theta$ Feedback Compensation . . . . .	5-42
5.4.	Simulation Results, $\theta$ Feedback with Kalman Filter Compensation . . . . .	5-43
5.5.	Simulation Results, Kalman Filtered $\alpha$ , $q$ , and $\theta$ Feedback Compensation . . . . .	5-44
A.1.	F-8 Short Period Parameters . . . . .	A-3
D.1.	Research Pilots . . . . .	D-1
D.2.	Objective 1 Test Matrix- Baseline UAV HAndling Qualities . . . . .	D-1
D.3.	Objective 2 Test Matrix- Predictor Handling Qualities . . . . .	D-2
D.4.	Objective 3 Test Matrix - Aerodynamic Sensitivity ( $\tau_d = 100$ msec) . . . . .	D-2
D.5.	Objective 3 Test Matrix - Time Delay Uncertainty . . . . .	D-3
E.1.	Objective 1 - Baseline Handling Qualities, MOP 2 - Research Pilot 1, Comments and Ratings . . . . .	E-1
E.2.	Objective 1 - Baseline Handling Qualities, MOP 2 - Research Pilot 2, Comments and Ratings . . . . .	E-2

Table		Page
E.3.	Objective 1 - Baseline Handling Qualities, MOP 2 - Research Pilot 3, Comments and Ratings . . . . .	E-3
E.4.	Objective 1 - Baseline Handling Qualities, MOP 2 - Research Pilot 4, Comments and Ratings . . . . .	E-3
E.5.	Objective 1 - Baseline Handling Qualities, MOP 2 - Research Pilot 5, Comments and Ratings . . . . .	E-4
E.6.	Objective 1 - Baseline Handling Qualities, MOP 2 - Research Pilot 6, Comments and Ratings . . . . .	E-4
E.7.	Objective 2 - Predictor Handling Qualities, MOP 2 - Research Pilot 1, Comments and Ratings . . . . .	E-5
E.8.	Objective 2 - Predictor Handling Qualities, MOP 2 - Research Pilot 2, Comments and Ratings . . . . .	E-6
E.9.	Objective 2 - Predictor Handling Qualities, MOP 2 - Research Pilot 3, Comments and Ratings . . . . .	E-7
E.10.	Objective 2 - Predictor Handling Qualities, MOP 2 - Research Pilot 4, Comments and Ratings . . . . .	E-8
E.11.	Objective 2 - Predictor Handling Qualities, MOP 2 - Research Pilot 5, Comments and Ratings . . . . .	E-9
E.12.	Objective 2 - Predictor Handling Qualities, MOP 2 - Research Pilot 6, Comments and Ratings . . . . .	E-10
E.13.	Objective 3 - Sensitivity Analysis, MOP 1 - Aerodynamic Sensitivity . . . . .	E-11
E.14.	Objective 3 - Sensitivity Analysis, MOP 1 - Aerodynamic Sensitivity cont. . . . .	E-12
E.15.	Objective 3 - Sensitivity Analysis, MOP 1 - Aerodynamic Sensitivity cont. . . . .	E-13
E.16.	Objective 3 - Sensitivity Analysis, MOP 2 - Time Delay Sensitivity . . . . .	E-14
E.17.	Objective 3 - Sensitivity Analysis, MOP 2 - Time Delay Sensitivity cont. . . . .	E-15

Table		Page
F.1.	Baseline Maximum Additional Time Delay Data . . . . .	F-3
F.2.	Baseline Maximum Additional Time Delay Descriptive Statistics	F-4
F.3.	Objective One, Processed Baseline Data . . . . .	F-5
F.4.	Baseline PIO Rating Descriptive Statistics . . . . .	F-6
F.5.	Baseline Cooper-Harper Rating Descriptive Statistics . . . . .	F-7
F.6.	Baseline Root Mean Square Tracking Error Descriptive Statistics . . . . .	F-8
F.7.	Flying Qualities Simulator PIO Ratings . . . . .	F-9
F.8.	Flying Qualities Simulator PIO Ratings Descriptive Statistics	F-10
F.9.	Predictor Data . . . . .	F-13
F.10.	Predictor Data, cont. . . . .	F-14
F.11.	Predictor PIO Rating Descriptive Statistics . . . . .	F-15
F.12.	Predictor Cooper-Harper Rating Descriptive Statistics . . . . .	F-16
F.13.	Predictor Root Mean Square Tracking Error Descriptive Statistics . . . . .	F-17
F.14.	Predictor Root Mean Square Display Error Descriptive Statistics	F-18
F.15.	Time Delay Uncertainty Data . . . . .	F-20
F.16.	Time Delay Uncertainty PIO Rating Descriptive Statistics . . . . .	F-20
F.17.	Time Delay Uncertainty Cooper-Harper Rating Descriptive Statistics . . . . .	F-21
F.18.	Time Delay Uncertainty Root Mean Square Tracking Error Descriptive Statistics . . . . .	F-21
F.19.	Time Delay Uncertainty Root Mean Square Display Error Descriptive Statistics . . . . .	F-21
F.20.	Aerodynamic Sensitivity Analysis Data . . . . .	F-22



## *List of Symbols*

Symbol	Page
$n_z$ Normal acceleration . . . . .	1-5
$\tau$ Time delay . . . . .	2-1
$Y_p$ Pilot transfer function . . . . .	2-6
$Y_c$ Controlled element transfer function . . . . .	2-6
$K_p$ Pilot steady-state gain . . . . .	2-9
$T_L$ Pilot lead compensation time constant . . . . .	2-9
$T_I$ Pilot lag compensation time constant . . . . .	2-9
$T_N$ Neuromuscular time constant . . . . .	2-9
K Gain . . . . .	2-10
s Laplace operator . . . . .	2-10
$\omega_c$ Crossover frequency . . . . .	2-11
$\tau_e$ Effective time delay . . . . .	2-11
$T_{\theta_2}$ High-frequency pitch attitude zero . . . . .	2-14
$\zeta_{sp}$ Damping ratio of the short period pitch mode . . . . .	2-14
$\omega_{BW}$ Bandwidth criteria frequency . . . . .	2-16
$\tau_p$ Bandwidth criteria time delay parameter . . . . .	2-16
$\tau_{p1}$ Pilot lead compensation time constant . . . . .	2-17
$\tau_{p2}$ Pilot lag compensation time constant . . . . .	2-17
$ \theta/\theta_c $ Ratio of actual to commanded pitch angle . . . . .	2-17
e Error signal . . . . .	2-25
$\tau_d$ Time delay . . . . .	2-29
$\omega_{n_{sp}}$ Undamped natural frequency of the short period pitch oscillation	2-31
<b>A</b> State transition coefficient matrix . . . . .	2-33
<b>Bu</b> Input coefficient matrix . . . . .	2-33
<b>C</b> Output coefficient matrix . . . . .	2-33

Symbol	Page
$\mathbf{x}$ State space system state vector . . . . .	2-33
$\mathbf{Du}$ Feedforward coefficient matrix . . . . .	2-33
$\phi$ State transition matrix . . . . .	2-34
$u$ Pilot input . . . . .	3-15
$\phi_{max}$ Maximum lead compensation required . . . . .	3-23
$\omega_{max}$ Frequency at maximum lead compensation . . . . .	3-23
$\omega_{c_{des}}$ Desired crossover frequency . . . . .	3-23
$\tilde{z}$ Predicted system output . . . . .	3-39
$\Phi$ State transition matrix integrated over period of time delay . . . . .	3-40
$\omega_{n_{sp}}$ Undamped natural frequency of short period pitch oscillation . . . . .	3-47
$K_{\theta}$ Pitch angle transfer function steady state gain . . . . .	3-47
$\alpha_0$ Initial angle of attack . . . . .	4-2
$\theta_0$ Initial pitch angle . . . . .	4-2
$V_0$ Initial airspeed . . . . .	4-2
$y$ System Output . . . . .	4-2
$x_s$ Stick position . . . . .	4-2
$q$ Pitch rate . . . . .	4-2
$\alpha$ Angle of attack . . . . .	4-3
$U_0$ Nominal test airspeed . . . . .	4-4
$K_G$ Stick gain . . . . .	4-4
$q_{pred}$ Predicted pitch rate . . . . .	4-5
$\theta_D$ Delayed pitch angle . . . . .	4-12
$\theta_B$ Boresight reference angle . . . . .	4-12
$\delta_e$ Elevator deflection . . . . .	4-15
$\tau_{d_{max}}$ Maximum allowable time delay . . . . .	4-21
$C_{L_{\delta_e}}$ Nondimensional stability derivative, change in lift coefficient due to elevator deflection . . . . .	5-16

Symbol	Page
$C_{L\alpha}$ Nondimensional stability derivative, lift curve slope . . . . .	5-16
$C_{M\alpha}$ Nondimensional stability derivative, change in pitching moment due to angle of attack . . . . .	5-16
$C_{Mq}$ Nondimensional stability derivative, change in pitching moment due to pitch rate . . . . .	5-16
$C_{M\delta_e}$ Nondimensional stability derivative, change in pitching moment due to elevator deflection . . . . .	5-16
$\theta$ Pitch angle . . . . .	5-28
$w$ Process white noise . . . . .	5-37
$v$ Measurement white noise . . . . .	5-37
$z$ Turbulence model state vector . . . . .	5-37
$\mathbf{A}_z$ Turbulence model coefficient matrix . . . . .	5-37
$\mathbf{B}_z$ Turbulence model input matrix . . . . .	5-37
$\mathbf{C}_z$ Turbulence model output matrix . . . . .	5-37
$\mathbf{D}_z$ Turbulence model feedforward matrix . . . . .	5-37
$L$ Observer Gain . . . . .	5-38

*List of Abbreviations*

Abbreviation	Page
UAV Unmanned Aerial Vehicle . . . . .	iii
RPV Remotely Piloted Vehicles . . . . .	1-1
UCAV Unmanned Combat Aerial Vehicle . . . . .	1-2
SEAD Suppression of Enemy Air Defenses . . . . .	1-2
DARPA Defense Advanced Research Projects Agency . . . . .	1-2
OTH Over-The-Horizon . . . . .	1-6
HQR Handling Quality Rating . . . . .	1-6
CH Cooper-Harper . . . . .	2-7
LOES Lower Order Equivalent System . . . . .	2-9
PIO Pilot Induced Oscillation . . . . .	2-11
CAP Control Anticipation Parameter . . . . .	2-14
OCM Optimal Control Model . . . . .	2-14
POR Pilot Opinion Rating . . . . .	2-16
HQ Handling Qualities . . . . .	2-22
OCM Optimal Control Model . . . . .	2-23
MOCM Modified Optimal Control Model . . . . .	2-26
CGI Computer Generated Imagery . . . . .	2-28
VRA Variable-Response Research aircraft . . . . .	3-1
SAS Stability Augmentation System . . . . .	3-4
CHR Cooper-Harper ratings . . . . .	4-1
PIO Pilot-In-The-loop Oscillation . . . . .	4-1
PIOR Pilot-In-The-Loop Oscillation Ratings . . . . .	4-1
TPS Test Pilot School . . . . .	4-1
PID Parameter Identification . . . . .	4-1
RP Research Pilot . . . . .	4-14

Abbreviation	Page
R/C Radio-Controlled . . . . .	4-14
SP Safety Pilot . . . . .	4-14
DAS Data Acquisition System . . . . .	4-14
CSC Computer Sciences Corporation . . . . .	4-14
PCM Pulse Code Modulated . . . . .	4-15
NTSC National Television System Committee . . . . .	4-16
AFFTC Air Force Flight Test Center . . . . .	4-20
msec millisecond . . . . .	4-20
TPS FQ USAF Test Pilot School's Flying Qualities . . . . .	4-20
TC Test Conductor . . . . .	4-21
HQ Handling Qualities . . . . .	4-22
TPS FQ USAF Test Pilot School's Flying Qualities . . . . .	5-1
RSM Response Surface Methodology . . . . .	5-17
MOP Measure of Performance . . . . .	5-21
MOPs Measures of Performance . . . . .	F-2
GPS Global Positioning System . . . . .	G-1
Pest Parameter Estimation . . . . .	G-1
KIAS Knots Indicated Airspeed . . . . .	G-2

*Abstract*

This study investigated control loop time delay and its effect on UAV handling qualities. Compensation techniques to improve handling qualities in the presence of varying amounts of time delay were developed and analyzed. One technique was selected and successfully flight-tested on a UAV.

Flight-testing occurred at a constant flight condition with varying levels of additional time delay introduced into the control loop. Research pilots performed a modified MIL-STD-1797A discrete pitch tracking task and gave Cooper-Harper ratings and comments. Tracking errors were used as a quantitative measure of Pilot/Display/UAV system performance.

Predictive pitch compensation was found to significantly reduce pilot workload and improve Cooper-Harper ratings. Using the predictive display doubled the amount of system time delay that research pilots could tolerate while tracking the task bars. Overall system tracking performance, however, was not improved.

Parameter variations in amount of time delay compensated did not result in degraded handling qualities. There was little significant difference in pilot opinion or performance for time delay uncertainties of  $\pm 33\%$ . Parameter variations of  $\pm 20\%$  in the aerodynamic model used to generate the predictive display produced statistically significant, although not operationally significant, changes in both pilot opinion and performance.

Analysis of UAV flight test data and follow-on simulations revealed that including UAV pitch attitude in the feedback signal greatly increased the gust rejection capability of the model-based predictive algorithm. For these simulations, algorithm accuracy was improved to the point of restoring system tracking performance to equal that of the system with no additional time delay.

# IMPROVING UAV HANDLING QUALITIES USING TIME DELAY COMPENSATION

## *I. Introduction*

### *1.1 Handling Qualities for UAVs? You Must Be Joking!*

We don't want to constrain our thinking on Unmanned Aerial Vehicles as strictly surveillance platforms. They may eventually be employed for communications relay, electronic warfare and even strike missions.

*-Gen. Ronald R. Fogleman, U.S. Air Force chief of staff*

This is not our fathers' Air Force.

*-Gen. Michael E. Ryan, U.S. Air Force chief of staff*

*1.1.1 A Brief History of the UAV.* Barely four years have passed since Gen. Fogleman spoke those words and yet already the first two of his expanded roles for Unmanned Aerial Vehicles, communications relay and electronic warfare, have been flight tested in Air Force wargames. The Air Force is committed to flight testing a proof-of-concept vehicle for the third role, strike, by 2002.

The successful performance of Remotely Piloted Vehicles (RPV), as UAVs were called at the time, with the Israeli Air Force (59) and during the Vietnam and Gulf War has prompted Air Force long range planners to advocate development of UAVs to fill future Air Force combat roles.

Pioneer RPVs flew 1,011 hours during 307 sorties in Operation Desert Storm (21). Missions flown were primarily reconnaissance with specific tasks ranging from route surveillance to target acquisition and artillery spotting. Currently, UAVs are primarily employed in similar types of reconnaissance missions. Predator UAVs have

flown numerous missions in support of Operation Deny Flight and other low intensity conflicts with exceptional performance (8). The operators and aircraft have proven themselves as an important asset for monitoring ground troop movement and, if required, target selection. Global Hawk, a predominantly autonomous high altitude reconnaissance UAV, is now in full scale flight test and is intended to be used as a theater or even national asset.

The success of UAVs in filling current mission requirements has prompted the Air Force Scientific Advisory Board (58) to recommend developing UAVs capable of delivering weapons. The mission of choice for the first combat capable UAV, named Uninhabited Combat Aerial Vehicle (UCAV) is the Suppression of Enemy Air Defenses (SEAD). Correctly or not, this mission is seen by Air Force planners as the mission most amenable to being accomplished by an unmanned platform with available technology or technology soon to be available. Consequently the Defense Advanced Research Projects Agency (DARPA) and the USAF jointly have contracted with major U.S. defense contractors to enter a competition to develop and demonstrate a "low life-cycle cost, highly survivable design for a SEAD/Strike unmanned air vehicle" (32).

*1.1.2 What's a UCAV?* Perhaps the most perplexing and important question facing the designers of the UCAV is not "What is a UCAV?" but "What should a UCAV do?". Andrew Probert addresses some of these issues in his article *Uninhabited Combat Aerial Vehicles: Remove The Pilot?* (43). The DARPA/USAF briefing to industry teams (32) provides very specific guidance as to "what" the UCAV must do leaving the "how" entirely up to the design team. While these questions (and their answers) indeed should be at the core of any UCAV design, whatever form or function the UCAV takes, it will *still need to be flight tested*.

Recent experience with flight testing the highly autonomous Darkstar UAV has demonstrated the difficulty of conducting flight test in a predominantly autonomous



mode. This is largely due to the fact that autonomous control systems are designed using data from a mathematical model of the aircraft derived from aerodynamic equations and augmented by wind tunnel studies and Computational Fluid Dynamic data. However, present capability to accurately model many of the non-linear aerodynamics is limited. Flight test is still necessary to verify and correct predicted aerodynamics. Autonomous control systems designed from inaccurate aerodynamic models will be less than optimal, perhaps to the point of becoming unstable in certain flight regimes. Traditional aircraft stability and control augmentation systems are designed in similar fashion. However, the presence of a test pilot on board the aircraft during initial envelope expansion and data collection provides a "back-up" system that will not be available in an exclusively autonomous UAV.

Another daunting task autonomous systems present both the flight tester and operational user is flight planning. Autonomous vehicles need extensive flight planning when defining both mission tasks and contingency plans. Errors in flight plans are often hard to find and can lead to disaster. Human pilots, however, use airmanship gained over thousands of flight hours to cope with contingencies perhaps not even addressed in flight planning. Flight test is certainly one of the environments where unusual occurrences are likely to occur. Having a human pilot in the loop during initial flight test of a UCAV may actually be more efficient, when costs and time for flight planning and potential mishaps resulting from flight plan "bugs" are considered.

Human pilots adapt their control inputs, within their limitations, as necessary to maintain aircraft control, provide acceptable stability margins, and perform the given task. They use experience and piloting skill rather than a detailed understanding of the aircraft's aerodynamic and control system characteristics. The great success McDonnell-Douglas and NASA enjoyed with the X-36 project (48) demonstrates that a UAV may be flight tested fully pilot-in-the-loop. The X-36 was designed to be a subscale, remotely piloted, technology demonstrator for a highly ag-

ile, tailless fighter. It was unmanned and flown by a test pilot from a ground control station. The test program was an unqualified success. Experience with Darkstar and the X-36 has prompted DARPA and the USAF to provide guidance that the UCAV Advanced Technology Demonstrator be flight tested using a low risk approach, "full pilot-in-the-loop for initial envelope expansion", prior to a "systematic build-up to semi-autonomous operation" (32).

*1.1.3 No, I'm Not Joking.* It would appear that a test pilot will be flying and evaluating the UCAV, at least until the aircraft's flight envelope has been adequately explored and accurate aerodynamic models are obtained. For this reason it is important that any potential UCAV be sufficiently controllable by a test pilot operating from a remote piloting station that the tasks necessary for proper collection of data at different test points throughout the aircraft flight envelope may be accomplished safely, expeditiously, and accurately. This is less a requirement as it is a simple statement of fact. Compare the above statement to how Cooper and Harper (10) define handling qualities,

Handling Qualities - those qualities or characteristics of an aircraft that govern the ease and precision with which a pilot is able to perform the tasks required in support of an aircraft role.

The aircraft role, in this case, is the successful expansion of the operating envelope. Thus it is apparent that some discussion of handling qualities for UAVs needs to be undertaken.

The first specification for the required flying qualities of an aircraft was written in 1907 and stated,

... it must be steered in all directions without difficulty and at all times under perfect control and equilibrium. (57)

Flying qualities requirements for manned aircraft have become quite a bit more complex, realistic, and lengthy since the days of the Wright Flyer. However, as we enter an age in which the pilot may be removed from the cockpit and associated

in-flight environment, a new definition of flying qualities for UAVs may be in order. *RPV Flying Qualities Design Criteria* (44) provided initial guidelines for UAV handling qualities. The authors expected the stability and response characteristics of an RPV to be different from a piloted aircraft. With the pilot removed from the proprioceptive ("seat-of-the-pants") feedback cues in the cockpit, traditional values for response parameters may not apply. In other words, with the pilot out of the cockpit, parameters constrained in the past to accommodate pilot likes and dislikes may now be assigned more freely. For example, normal accelerations that had been limited to the range of +9 to -3 g due to the pilot's physiological limitations may now realistically approach, with sufficient structural strength,  $\pm 20$  g, the current turbine engine  $n_z$  limitation. Additionally, a human pilot may require slower aircraft control responses than would be considered desirable for an automatic control system. Limited experience with UAVs at the time prevented a redefinition of flying qualities parameters or values.

The development of theUCAV will place a bit more urgency on such a discussion. By removing the cockpit and associated life support systems, designers may reduce the weight and volume of any potential design by up to 40 percent (20). This, coupled with no human physiological load factor limitations will potentially make for a highly maneuverable aircraft. While the upper bandwidth limitation of the human pilot is slightly less than 10 rads/sec, similar limitations on modern digital flight computers are at much higher frequencies. It should be assumed that designers will configure the UAV stability and control characteristics to take advantage of the increased capability of onboard autonomous control rather than accommodate the test pilot who is to fly theUCAV through its envelope expansion test profiles.

Since the desired "end-product" ofUCAV development is an autonomous platform, any element of the design to accommodate the human test pilot will only be used in flight test. Thus it would seem appropriate to accomplish the pilot-in-the-loop flight test without devoting large amounts of funding to the human interface.

The X-36 design team avoided the time delay issue by making sure they had sufficient bandwidth to keep delays, both datalink and control system, within the MIL-STD-1797A requirements for satisfactory handling qualities.

Flight Simulators have been successfully using delay compensation algorithms to remove the effects of transport delays instead of the more expensive strategy of buying faster, more powerful computers. Delay Compensation for UAVs may allow more inexpensive testing by liberalizing bandwidth requirements for the datalink. Delay compensation may also find use on today's pilot-in-the-loop UAVs such as the Predator. The aircraft is flyable for non-precision tasks using Over-The-Horizon(OTH) communications in which delays of several hundred milliseconds due to satellite relays are not uncommon. A landing, however, has never been attempted. Perhaps with compensation techniques investigated in this thesis, or more complex techniques currently enjoying success in the field of robotic teleoperation, operators will be able to employ UAVs from anywhere in the world thus increasing the flexibility of this already versatile platform.

## *1.2 Objectives*

This thesis addresses the issue of time delay in the transmission of pilot commands to the UAV and how the delay effects handling qualities. Compensation techniques to mitigate deleterious effects are also investigated. In particular, the objectives of this research were:

1. Study existing pilot models and mathematical metrics used in predicting pilot Handling Quality ratings (HQR).
2. Apply metrics to previously accomplished in-flight studies of time delay for initial verification. Modify, if necessary, to achieve good match with flight test data.

3. Implement one or more of the above methods to predict HQR on a UAV mathematical model for various transport delays.
4. Develop compensation techniques to reduce the effects of transport delay.
5. Employ the mathematical method developed above to draw conclusions about which technique offers the most benefit.
6. Verify the efficacy of the compensation technique in actual flight test on a UAV.

### *1.3 Thesis Overview*

This thesis is divided into six sections. This chapter contains a brief discussion of UAV roles, the motivation for the research and general background information.

In the second chapter the characteristics of time delay systems are discussed with a focus on how transport delay affects human control behavior and aircraft handling qualities. Current methods for estimating test pilot rating of handling qualities from a mathematical model of the aircraft are discussed. The theory behind techniques to compensate for time delay is presented.

The third chapter contains an application of the mathematical methods discussed in the second chapter to existing data from in-flight test of time delay effects. Data is analyzed and methods are fine tuned to function as accurate predictors of pilot HQR. Different compensators are designed and evaluated for efficacy in improving the predicted HQR of delayed systems.

Flight test methodology and flight test results are discussed in the fourth and fifth chapters respectively. Conclusions drawn from the thesis work as well as recommendations for further research in this exciting area of study are presented in the sixth and final chapter.

## II. Theoretical Development

The characteristics of time delay systems with focus on how transport delays affect human control behavior and aircraft handling qualities are presented in this chapter. Current methods for estimating test pilot ratings of handling qualities from a mathematical model of the aircraft are introduced and discussed. Finally, the theory behind techniques to compensate for the time delay is developed.

### 2.1 Signals

*2.1.1 Time Domain Characteristics.* When a pure time delay,  $\tau$ , is applied to a signal,  $x(t)$ , the result is a time shifted version of the original,  $x(t - \tau)$ . Transforming to the Laplace domain,

$$\mathcal{L}\{x(t - \tau)\} = \int_0^{\infty} e^{-s\tau} x(t - \tau) dt \quad (2.1)$$

since no signal is present prior to time  $t = \tau$ , this expression may be rewritten as,

$$\mathcal{L}\{x(t - \tau)\} = \int_{\tau}^{\infty} e^{-s\tau} x(t - \tau) dt \quad (2.2)$$

and making the variable change  $\lambda = t - \tau$  Equation 2.2 becomes

$$\mathcal{L}\{x(t - \tau)\} = e^{-s\tau} \int_0^{\infty} e^{-s\lambda} x(\lambda) dt \quad (2.3)$$

Thus the Laplace domain relationship for the pure delay is  $e^{-s\tau} X(s)$ , where  $X(s)$  is the Laplace transform of the original signal,  $x(t)$  and  $\tau$  is the magnitude of the time delay in seconds.

*2.1.2 Temporal Sensitivity.* Consider the linear system  $G(s) = Y(s)/X(s)$  where  $Y(s)$  and  $X(s)$  are the Laplace transform of output and input respectively. When placed in cascade with a pure time delay  $e^{-s\tau}$ , the overall transfer function

becomes  $G(s)e^{-s\tau}$ . The new output  $Z(s)$  is the delayed output of the original system  $Y(s)$ . Thus  $z(t) = y(t - \tau)$ . Taking the Laplace transform of  $\partial z/\partial\tau$  gives,

$$\mathcal{L}\left\{\frac{\partial z}{\partial\tau}\right\} = X(s)G(s)se^{-s\tau} = sZ(s) \quad (2.4)$$

The  $s$  operator is equivalent to time differentiation and thus the temporal sensitivity of the system is defined by the derivative of the system output (33). This makes intuitive sense considering that systems whose output does not change rapidly are less likely to be affected by time delay as a system with rapidly changing output. It can be seen from this short discussion that the delay in a system's open loop dynamics is apt to have an effect on closed-loop dynamics and operators trying to control time delayed systems.

## 2.2 Systems

**2.2.1 Open Loop.** Frequency domain techniques are used extensively in the analysis and synthesis of classical control systems. The Bode diagram, a plot of system gain and phase shift versus frequency, is one of the most popular frequency domain tools. To examine the effect that time delay has on the Bode diagram, let  $s = j\omega$  and use Euler's identity to rewrite  $e^{-j\omega\tau}$  as  $re^{j\theta}$ . One can see by inspection that the gain,  $r$ , of  $e^{-j\omega\tau}$  is unity while the phase contribution is given by  $-\omega\tau$  or,

$$G(\omega) = |e^{-s\tau}|_{s=j\omega} = 1 \quad (2.5)$$

and,

$$\phi(\omega) = \arg(e^{-s\tau})_{s=j\omega} = -\omega\tau \quad (2.6)$$

Two major points may be gleaned from Equations 2.5 and 2.6. The first is that the delay does not affect system gain. All frequencies are passed with no attenuation; the output is an exact, time-delayed, copy of the input. Secondly, the phase shift

is a function of frequency and the final value of open loop phase shift is no longer finite.

2.2.2 *Closed Loop.* Consider now the system in Figure 2.1 consisting of a gain and a transport delay of .1 seconds. One can see that the closed loop transfer

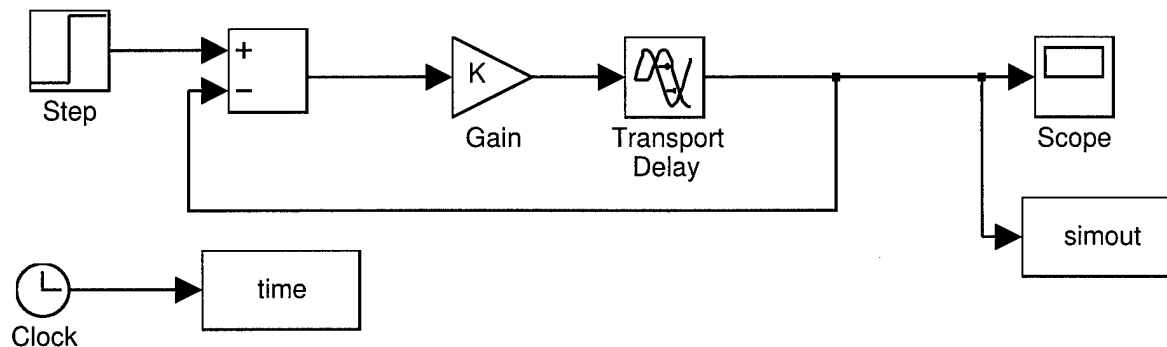


Figure 2.1 Simple Time Delayed System

function,  $Y(s)$ , is given by,

$$Y(s) = \frac{Ke^{-s\tau}}{1 + Ke^{-s\tau}} = \frac{K}{K + e^{s\tau}} \quad (2.7)$$

With system response for gains of 0.8 and 1.0 respectively illustrated in Figures 2.2 and 2.3.



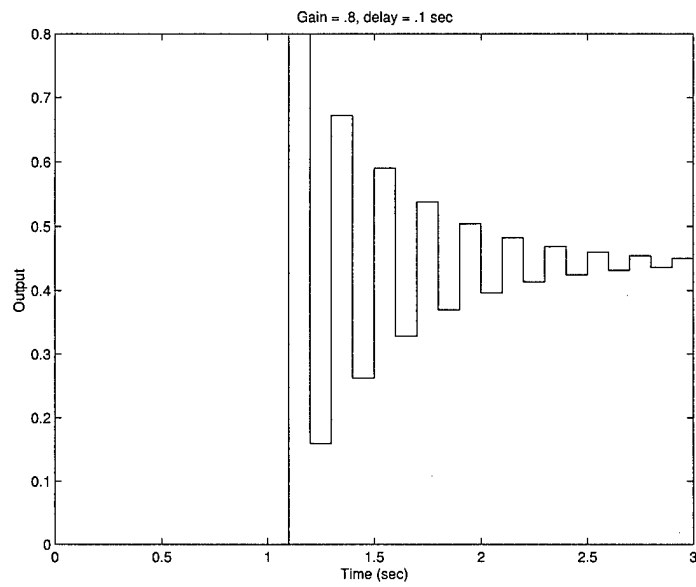


Figure 2.2 Delay System Response,  $K = .8$

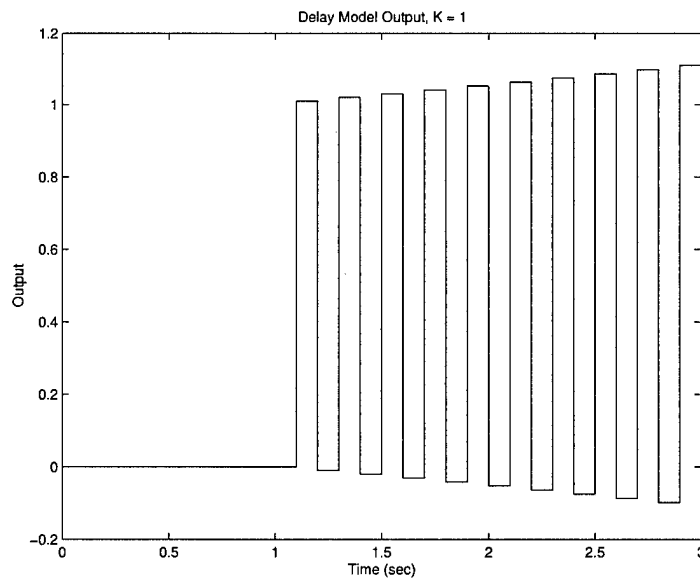


Figure 2.3 Delay System Response,  $K = 1.0$

The poles of  $Y(s)$  are defined as the values for  $s$  that make the denominator of Equation 2.7 equal to zero or,  $e^{s\tau} = -K$ . Using Euler's identity,  $-K = Ke^{j\pi \mp 2\pi q}$  where  $q = 1, 2, 3, \dots, n$ . Applying this identity to Equation 2.7 gives

$$e^{s\tau} = Ke^{j\pi \mp 2\pi q} \quad (2.8)$$

Taking the natural logarithm of both sides yields,

$$s\tau = \ln(K) + j(\pi \mp 2\pi q) \quad (2.9)$$

For  $K = 1$  this yields purely imaginary poles on the imaginary axis spaced by  $2\pi/\tau$  (33). Figures 2.2 and 2.3 demonstrate the effect of delay on the simple feedback model of Figure 2.1. The presence of delay made a system that had been stable for all values of  $K$  go unstable for gains  $K \geq 1$ . It also added an infinite number of poles to a system that had none previously. The effect of turning a finite dimensional system into an infinitely dimensional problem makes working with delay terms mathematically difficult. For this reason, approximations are often used in place of the exponential term.

*2.2.3 Pade Approximations.* A technique for approximating exponential terms was developed by the French mathematician H. Pade. It involves the ratio of two polynomials,  $P(s)/Q(s)$ , each a truncation of a Taylor series expansion. When the additional relationship  $P(s) = Q(-s)$  is imposed, the resulting approximant has the correct modulus,  $G(s) = 1$  and an approximate phase shift that increases in accuracy as the order of  $P(s)$  and  $Q(s)$  increase. The first order Pade approximant is,

$$e^{-sT} \approx \frac{1 - sT/2}{1 + sT/2} \quad (2.10)$$

and the second order is

$$e^{-sT} \approx \frac{1 - sT/2 + (sT)^2/12}{1 + sT/2 + (sT)^2/12} \quad (2.11)$$

where  $T$  is the amount of delay to be approximated. Pade approximations are commonly used to render the non-linear effects of pure time delay into a linear system. This thesis will make use of second order Pade approximations when including equivalent time delay in state space representations of aircraft dynamics.

### 2.3 Time Delay Effect on Human Control Behavior

The effects of time delay on human control behavior has been studied extensively by human factors experts and is applied extensively in the fields of telerobotics and aircraft handling qualities. This thesis will be primarily concerned with time delay in uninhabited aircraft flight control systems and the effects on pilot's control behavior.

The classical pilot/aircraft closed loop system is shown in Figure 2.4, where  $Y_p$  is the pilot transfer function and  $Y_c$  is the transfer function of the controlled element, in this case UAV. From the pilot's perspective, the flight control system and feedback time delays may be lumped together to form one delay block, thereby simplifying analysis. In other words, delay may be defined as the amount of "dead time" from when the pilot first moves the stick to his perception of the aircraft initial response. Thus for the discussion and analysis in this study the system shown in Figure 2.5 will be the basic model.

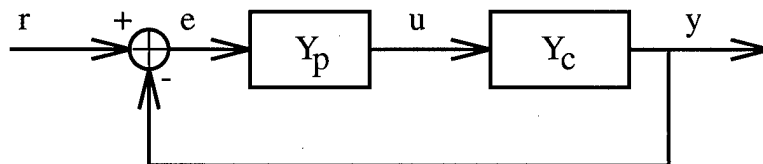


Figure 2.4 Pilot/Vehicle Closed Loop System

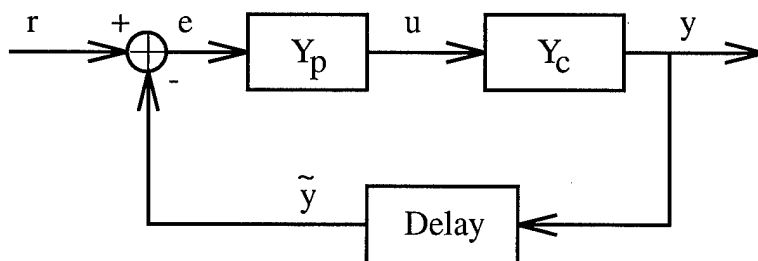


Figure 2.5 Pilot/Vehicle System with Feedback Delay

2.3.1 Handling Qualities Rating Scale. Any discussion of the effect of delay on Pilot Opinion rating must include a discussion of the Cooper-Harper(10) rating scale. The Cooper-Harper (CH) scale, see Figure 2.6, is the most common evaluation scale for aircraft handling qualities. It provides for three different levels of handling qualities.

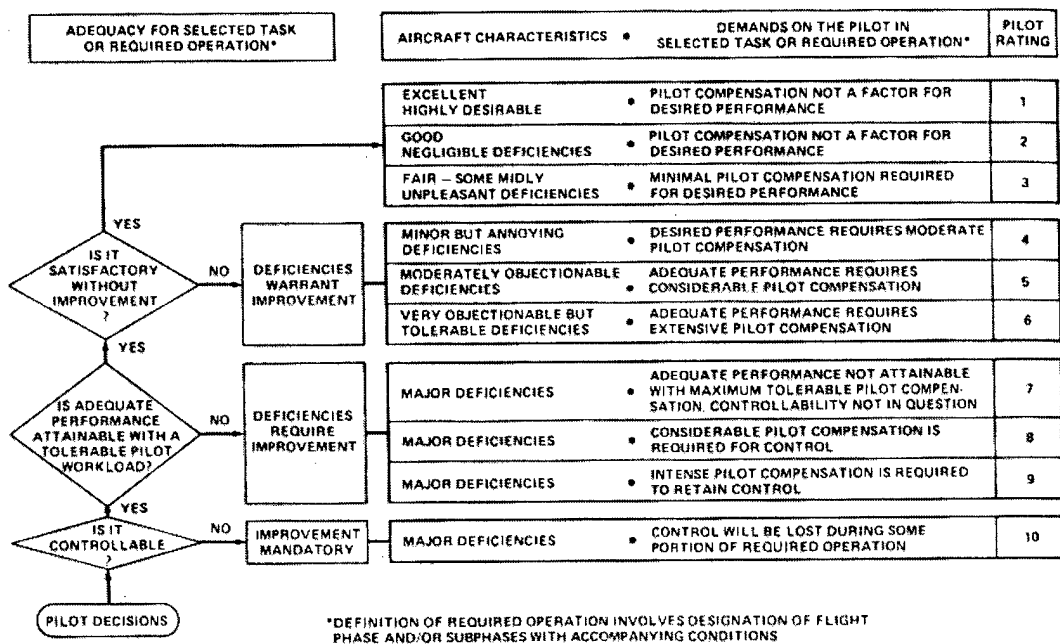


Figure 2.6 The Cooper-Harper Rating Scale

An aircraft receiving a "Level 1" rating is judged to have satisfactory handling qualities. The pilot is able to achieve the desired performance with minimal pilot compensation. A "Level 2" rating indicates adequate handling qualities and the ability to complete the mission. However, some increasing pilot workload or performance degradation is present. A "Level 3" rating indicates handling qualities that are inadequate to complete the mission; the aircraft, however, is still controllable. A CH rating of "10" or sometimes called "Level 4" indicates that aircraft control will be lost at some point in the mission profile. In calm air, the numeric values of 1-3 equate to Level 1, 4-6 to Level 2, and 6-9 to Level 3. It can be seen that the Cooper-Harper rating scale makes use of the concepts of performance and workload. The questions that need to be answered are does the aircraft have adequate performance to complete the mission satisfactorily and will the pilot have to work inordinately hard to obtain adequate performance. These questions are not independent of the task being completed; more challenging tasks tend to expose poor handling qualities. Three different task categories have been defined, categories A, B, and C. The most demanding tasks such as air-to-air combat and inflight refueling are placed in category A while Category C consists of approach and landing tasks. Category B encompasses all other, mainly non-precision tasks.

The ideas of performance and workload are at the core of the Cooper-Harper scale. While it was designed for use by human pilots in evaluating part of the man-machine interface, namely handling qualities; the concepts of performance and workload may apply to robotic aircraft as well. Performance in this scenario is easy to understand; the UAV must have sufficient performance to accomplish the mission. Workload is more nebulous in robotic systems but is often associated with control deflection. Increased performance at the expense of increased workload is still undesirable, even in robotic systems. One need only to consider the adverse effects on radar signature that result from large control deflections to see how robotic UAVs may also benefit from "handling qualities" analysis.

2.3.2 *Measuring Time Delay.* Time delay may come from many sources. Digital time delay, or transport delays, are caused by computation latency introduced when control laws are computed in discrete time. System delays may also come from analog portions of the flight control system. Higher order effects whether from high frequency poles in complex control laws or from aircraft stick dynamics and actuators also contribute to the effective time delay. There are two ways to measure the time delays: effective and equivalent. "Equivalent" time delay inherent to the controlled element is derived from frequency response analysis and is computed from a Lower Order Equivalent System (LOES) match to the actual frequency response of the system. The equivalent time delay inherent to the pilot is modelled as the  $e^{-s\tau}$  delay term in a frequently used pilot model transfer function (14), Equation 2.12

$$Y_p = \frac{K_p e^{-\tau_e s} (T_L s + 1)}{(T_I s + 1)(T_N s + 1)} \quad (2.12)$$

where  $K_p$  is the pilot's gain,  $T_L$ ,  $T_I$ , and  $T_N$  are the time constants associated with the pilot's lead compensation, lag compensation, and the first order model of his neuromuscular system. "Effective" time delay is a time domain analysis method and is calculated from the response of the system in question to a step input, see Figure 2.7. It is defined as the difference between the time of application of a step input and the time axis intersection of the maximum slope tangent to the response.

It should be noted that effective and equivalent time delay for the same system may not be the same. Systems that can not be accurately modelled in LOES form generally show poor correlation between equivalent and effective delay.

2.3.3 *Pilot Compensation Effects.* Numerous studies (37, 28, 18) have investigated the effects time delay has on the human operator's control behavior. Hess (28) used a fixed base simulator and compensatory tracking task to evaluate the effects time delay had on the pilot's transfer function,  $Y_p$ . He found that time delays cause significant reduction in pilot/vehicle system crossover frequencies, the

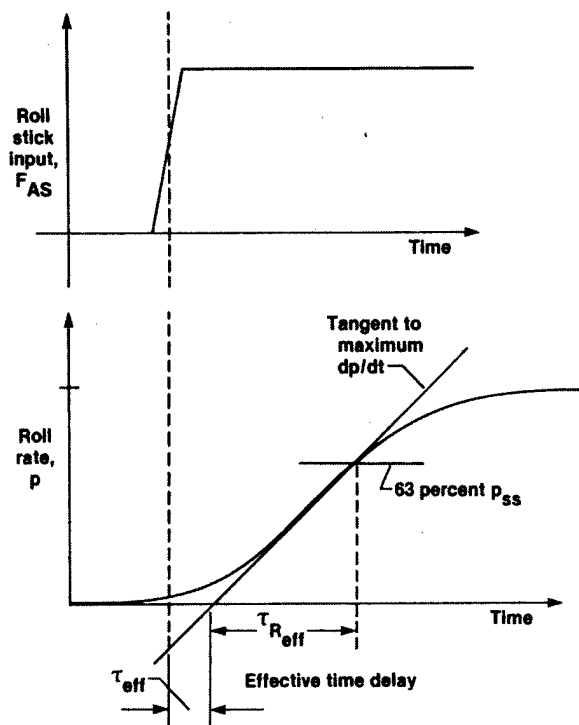


Figure 2.7 Computing Effective Time Delay (51)

effective frequency bandwidth of the pilot/vehicle system. Since the delay adds  $-\omega\tau$  to the open loop system phase shift, the operator must decrease his gain in order to preserve an acceptable phase margin. The reduced pilot gain in turn causes a regression in the pilot/vehicle system crossover frequency.

Hess also found that operators generated significant amounts of lead compensation in order to preserve adequate system performance. This effect was independent of the controlled system dynamics, i.e. operators generated lead for a variety of controlled elements with transfer functions,  $Y_c = K, K/s, K/s^2$ . Hess also found that operators tended to generate lead compensation that was not attributable to them attempting to maintain  $K/s$ , or "ideal plant", characteristics near the pilot/vehicle crossover frequency. He found that this produced broad frequency ranges in which the slope of the gain curve was less than the desired -20 dB/dec characteristic of the crossover model. This effectively increased the operators likelihood to enter into a Pi-

lot Induced Oscillation (PIO). A small increase in pilot gain results in a large increase in crossover frequency,  $\omega_c$ , and a corresponding decrease in phase margin which could result in a PIO if phase margin degenerated to zero. Pilot lead generation is often associated with the pilot's workload. This concept will become important when time delay effects on pilot HQR is discussed later in this chapter. The other important aspect of pilot opinion is the precision with which he can control the aircraft. Hence system error plays a large part in the HQR as well.

Miller (37) used a motion based simulator to investigate the effects that time delay in visual and proprioceptive feedback had on pilot performance in a pursuit tracking task. Ema (18) used a fixed base compensatory tracking task. Both researchers found that error increased almost linearly with increasing time delay,  $\tau$ . Ema used signal processing techniques to recover pilot transfer functions from his experimental data. Using a numerical algorithm he fit the numerical data to an assumed pilot transfer function of the form,

$$Y_p(s) = \frac{K_p(1 + T_2s)}{1 + T_1s} \frac{\omega_n^2}{s^2 + 2\zeta\omega_n s + \omega_n^2} e^{-\tau_e s} \quad (2.13)$$

where  $\zeta$  and  $\omega_n$  are characteristics of the neuromuscular system model.  $T_2$  and  $T_1$  are the pilot's lead and lag time constants respectively, and  $\tau_e$  is the pilot's effective time delay. He also found the pilot gain,  $K_p$ , decreased with increasing time delay. Similarly,  $T_2$ , or pilot lead compensation, increased. Ema found for  $\tau_e \geq 0.5$  the damping factor,  $\zeta$ , decreased below 0.35 and PIO tendency was observed. Ema varied his time delays from zero to three seconds. His results point to a more open loop strategy being applied by the test subjects once the time delay increased above one second. Indeed pilot comments (14) characterizing the landing flare on some heavy aircraft, B-747, DC-10, and C-5 as an open loop maneuver tend to support this finding.



2.3.4 *Time Delay Effects on Handling Qualities.* Control difficulties during the 1977 Space Shuttle Approach and Landing Tests and YF-17 development resulted in efforts to investigate whether time delays associated with digital flight computers might be a contributing factor to the handling qualities problems. As discussed above, delays in flight control systems may come from a variety of sources. The effects of phase lag due to higher order effects, or analog time delay, had been studied (15) and were relatively well understood. A detailed study of the effects of pure delay, transport delay due to digital systems, had yet to be accomplished. In 1978 a NASA study employed an F-8 fighter aircraft modified with a digital flight control system to accomplish a detailed study of the effects of pure time delays on aircraft handling qualities (7, 4, 6). In 1979, Hodgkinson and others (29) conducted a study on the USAF/Calspan NT-33 inflight simulator in which they tested how mismatches between the higher order system and the LOES affected pilot opinion. They also investigated how well the delay term,  $e^{-s\tau}$ , in the LOES approximated the higher order phase lags and if the difference caused variations in pilot opinion. Both studies showed a strong correlation between pilot rating and the magnitude of the time delay, see Figures 2.8 and 2.10. The NT-33 data also showed that the degradation in pilot rating was similar for both digital transport delay and analog delay, or delay due to phase lag from higher order effects. The insidious nature of time delay's effects on handling qualities is demonstrated in a pilot comment during the F-8 research (7)

Pilots desire some response immediately upon stick input. It doesn't have to be much, but if he doesn't get response, his gains skyrocket.

The pilots in the NT-33 study also voiced similar concerns with delay after control inputs and the rapidity of the response following the delay. The authors of the F-8 study (7) make a further observation that aircraft dynamics have an impact on system sensitivity to time delay.

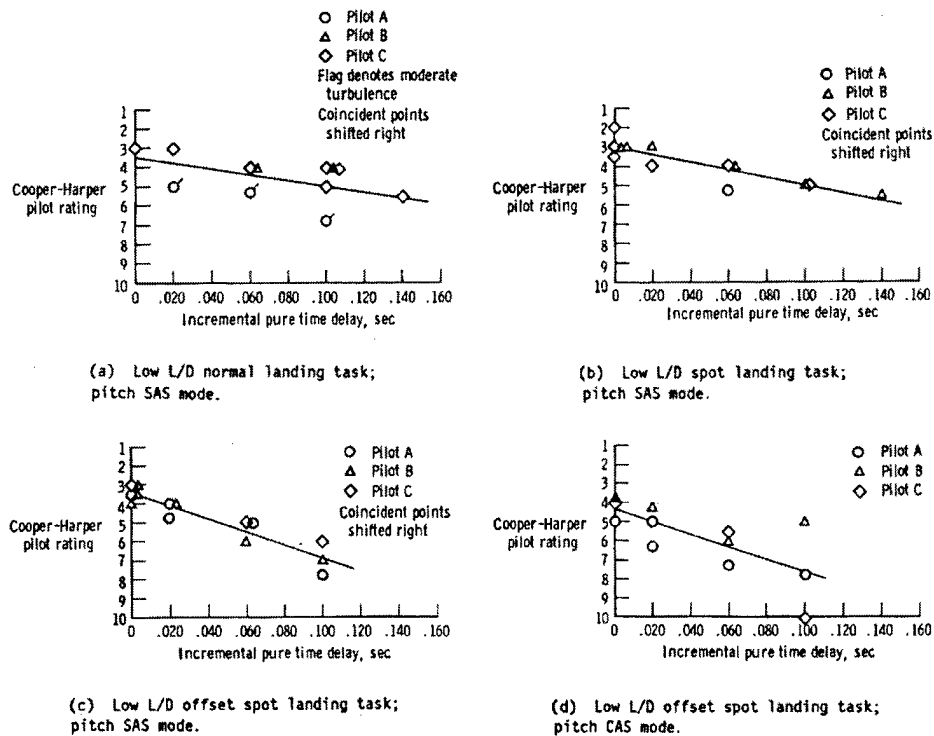


Figure 2.8 F-8 Study Data (51)

Disharmony between the initial time delay and a subsequent “snappy” response suggests that large or basically sluggish aircraft may be less sensitive than fighter aircraft to time delays.

Experimental data has verified the theoretical result derived in Equation 2.4. That is the temporal sensitivity of a system is directly proportional to the system output rate of change. It has been shown (37) that permissible time delay is a function of the “bare” airframe’s handling qualities. Aircraft handling qualities have an affect on how much delay may be tolerated; permissible time delays decrease as the delay free Cooper-Harper ratings increase. This effect is not limited to longitudinal handling qualities. Monagan and others (39) found that lateral flying qualities ratings were very sensitive to delay as well. They found that the allowable time delay is a function of the roll mode time constant.

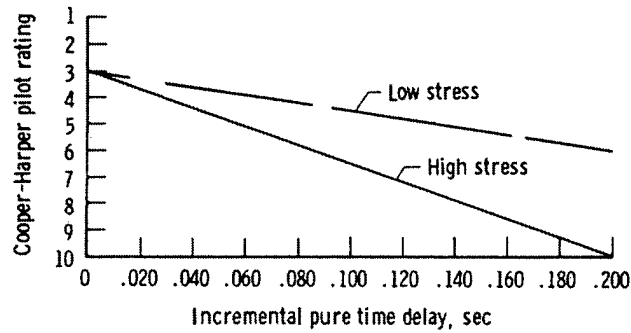


Figure 2.9 Task Influence on Time delay effects (51)

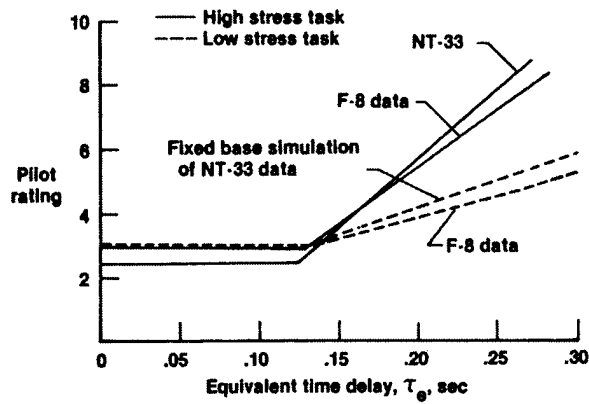


Figure 2.10 NT-33 Data from Hodgkinson (29)

#### 2.4 Mathematical Methods for Estimating Pilot Rating

There are three basic categories of mathematical methods for determining pilot HQR. Classical methods deal with computing "literal" factors such as Control Anticipation Parameter(CAP),  $T_{\theta_2}$ ,  $\zeta_{sp}$ , etc. and comparing them to existing databases of known aircraft ratings. The arrival of highly augmented control systems in the late 1960s led to the development of the second group of methods, the pilot-in-the-loop analysis techniques. These include methods such as the one developed by Neal and Smith (41). The final group of analysis techniques makes use of the advance in optimal control theory of the 1970s and is based on the well known Optimal Control Model(OCM). Caution should be used when applying any one of these cri-

teria indiscriminantly, “nor should one criteria be chosen as an extensive guide or panacea” (5). Each has types of plants on which it has proven successful in the past; likewise, they each have shortcomings. This research sought to employ one method from each of the three major subgroups. The Bandwidth Criteria from the classical division; Neal-Smith from the pilot-in-the-loop group, and an algorithmic method based on the Optimal Control Model. Each of which has been employed successfully in previous handling qualities research.

*2.4.1 Bandwidth Criteria.* Although the Bandwidth Criteria was developed as a response to the inaccuracy with which classical methods evaluated highly augmented control systems and has been referred to as a “pilot-in-the-loop” criterion (30), the analysis does not involve a dynamic pilot model and is listed in MIL-STD-1797A (14) as an “open-loop” technique. Thus, for the purpose of this research, it is considered a classical method of HQR prediction. MIL-STD-1797A suggests employing the Bandwidth Criteria when aircraft response dynamics do not have classical characteristics, i.e. short period and phugoid longitudinal modes. Thus it is perhaps the only “classical” method that is capable of making an accurate assessment in the face of a pure transport delay and non-classical aircraft dynamics as are likely to be found in UAV systems. The simplicity of the method and the fact that it was developed specifically to rate the newer flight control systems with substantial higher order dynamics made it the best method from the classical category for use in this research.

The bandwidth of a system used in this criterion is defined as the highest frequency at which the phase margin is at least 45 degrees while the gain margin is at least 6 dB, see Figure 2.11. The bandwidth is the lesser of the two frequencies,  $\omega_{BW_{Gain}}$  or  $\omega_{BW_{Phase}}$  and systems are defined as either “gain-margin-limited” or “phase-margin-limited” depending on which criteria specified the bandwidth.

The shape of the phase curve was also found to play a part in pilot HQR prediction. A rapid phase roll-off at frequencies above  $\omega_{BW}$  results in a large decrease in phase margin for a small increase in pilot gain. The gain margin limit of 6 dB discussed above lets a pilot double his gain and still not cause instability. Systems with rapid phase roll-off are most often "gain-margin-limited". Since rapid phase roll-off is well represented by pure time delay;  $e^{-j\omega\tau}$ , a parameter  $\tau_p$  representing a measure of the phase curve shape is calculated from Equation 2.14 from MIL-STD-1797A (14),

$$\tau_p = -\frac{(\Phi_{2\omega_{180}} + 180 \text{ deg})}{57.3 * 2\omega_{180}} \quad (2.14)$$

where  $\omega_{180}$  is the frequency corresponding to -180 degree phase shift, and  $\Phi_{2\omega_{180}}$  is the phase angle at twice that frequency.

When  $\tau_p$  and  $\omega_{BW}$  are plotted versus one another, see Figure 2.12, regions of the plot have been shown through numerous studies to correlate with different levels of handling qualities rather than a specific numerical HQR or Pilot Opinion Rating(POR). In fact, most techniques are limited to predicting only the overall level of handling qualities. This is most likely a result of military specifications where all requirements are given as general level and not specific CH number. For the purposes of this research, however, a specific CH number would be more desirable. Mitchell, Aponso, and Hoh (38) applied linear regression techniques to past data and derived formulae to derive the numerical CH rating from bandwidth criterion parameters,  $\tau_p$ , and  $\omega_{BW}$ ,

$$\hat{R}_\theta = 3.47 - .48 * \omega_{BW} + 7.2\tau_p \quad (2.15)$$

$$\hat{R}_\theta = 3.8 - .27 * \omega_{BW} + 5.7\tau_p \quad (2.16)$$

where Equation 2.15 correlates to data from fixed base simulations and Equation 2.16 correlates to full-motion and in-flight data.

2.4.2 *Neal-Smith Criteria.* The Neal-Smith method is an analytical procedure to evaluate the handling qualities of fighter type aircraft with augmented short period pitch dynamics. It is based on the assumption that accurate pitch attitude control is essential for good flying qualities. Flying qualities boundaries were developed through correlation with in-flight simulation data. The closed loop pitch tracking performance is related to the dynamic compensation generated by the pilot necessary to achieve the required closed loop bandwidth. Current bandwidth requirements (14) are contained in Table 2.1.

Table 2.1 Neal-Smith Bandwidth Requirements

Flight Phase	Bandwidth
Category A	3.5 rad/sec
Category B	1.5 rad/sec
Landing	2.5 rad/sec
Other Category C	1.5 rad/sec

Since Neal-Smith is a closed loop criteria it requires a pilot model which is assumed to consist of a fixed delay, variable gain, and variable first order compensation network. The model takes the form (41),

$$Y_p = K_p e^{-0.3s} \frac{\tau_{p1}s + 1}{\tau_{p2}s + 1} \quad (2.17)$$

where  $\tau_{p1}$  and  $\tau_{p2}$  are the pilot lead and lag compensation time constants respectively. MIL-STD-1797 modifies the original Neal-Smith model somewhat. The pilot delay is defined as 0.25 seconds and a low frequency integration term,  $(5s + 1)/s$ , is added to the model if there is no free "s" in the denominator of the plant model. Neal-Smith assumes that the pilot attempts to accomplish three tasks which, if successful, will result in good tracking performance (41)

1. The pilot tries to achieve a particular value of the open-loop gain-crossover frequency,  $\omega_c$  (the frequency at which  $|\theta/\theta_c| = 0$  dB)

2. The pilot tries to minimize any low-frequency, closed-loop “droop” (hold  $|\theta/\theta_c|$  as near 0 dB as possible, for  $\omega \leq \omega_c$ )
3. The pilot tries to maintain good high-frequency stability by keeping the damping ratio of any closed-loop oscillatory modes greater than 0.35, and by maintaining a phase margin of 60 to 110 degrees.

Put more simply, a pilot adjusts his gain and compensation to achieve the required bandwidth while minimizing “droop” and closed loop resonance, see Figure 2.13.

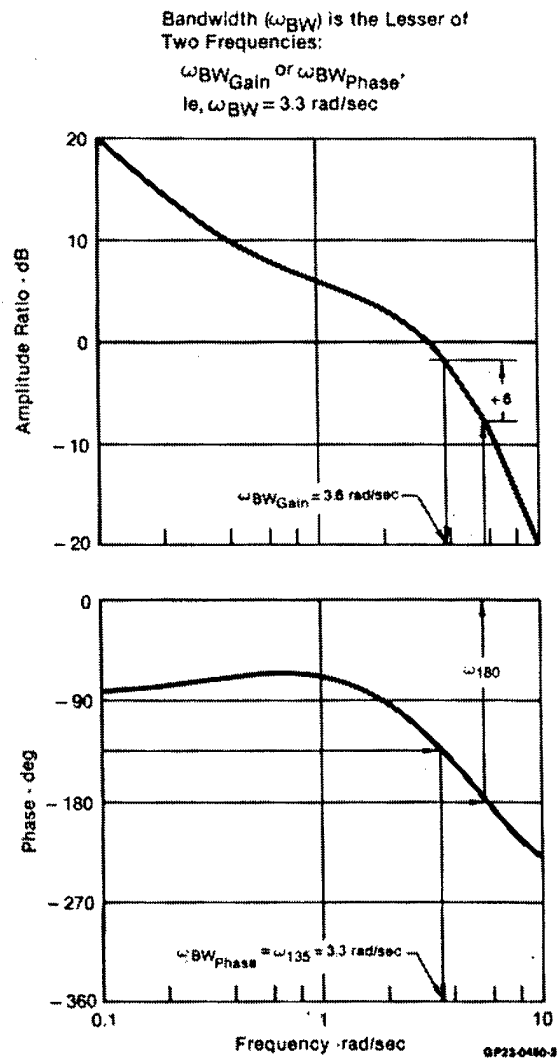


Figure 2.11 Definition of Bandwidth for Pitch Angle Response from Hodgkinson, Wood, and Hoh (30)



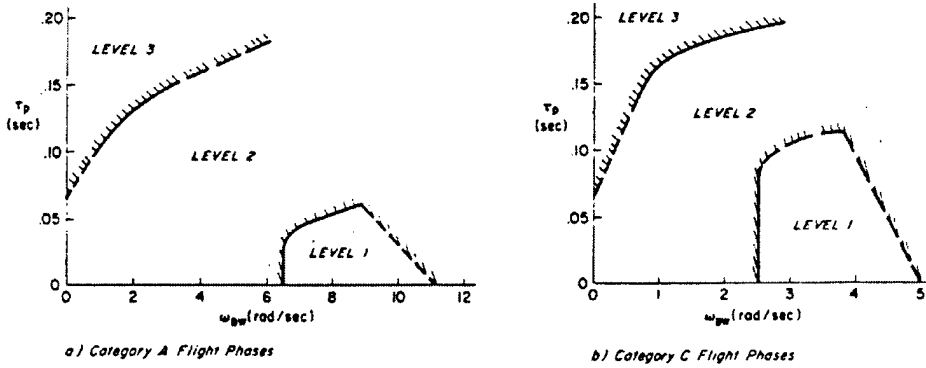


Figure 2.12 Bandwidth Requirements from MIL-STD-1797 (14)

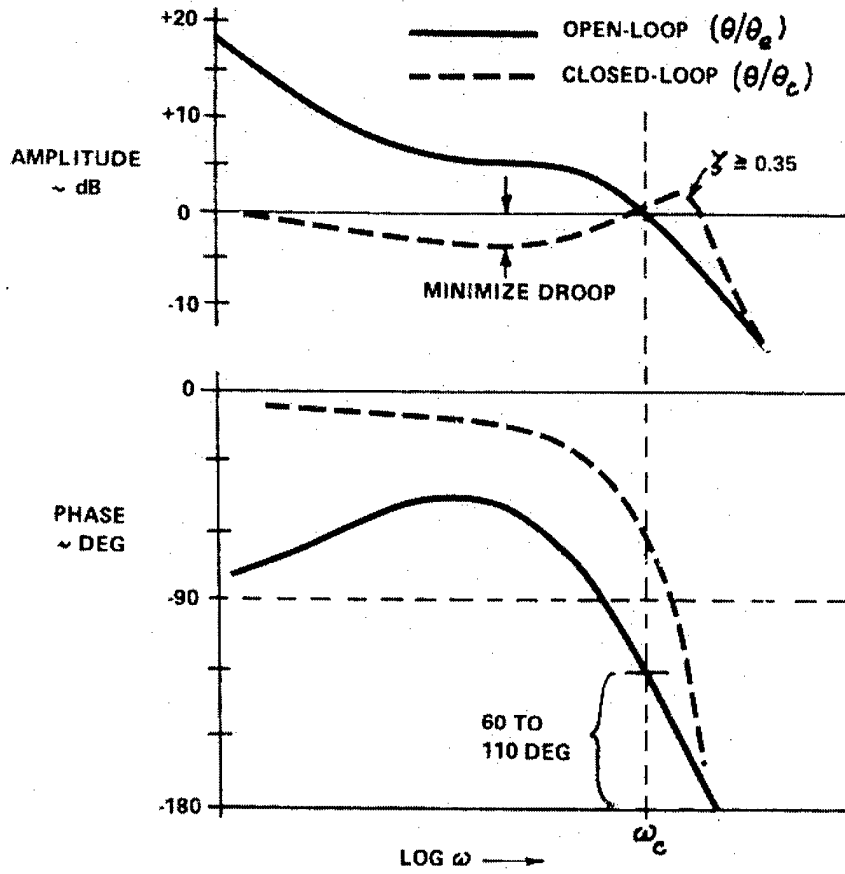


Figure 2.13 Neal-Smith Tracking Performance, from Neal and Smith (41)

In the original Neal-Smith analysis, the values of closed loop resonance and pilot compensation provided by the pilot model fulfilling the three criteria previously discussed are plotted versus one another. Experimental data was plotted and correlated to form regions corresponding to the predicted level of POR, Figure 2.14.

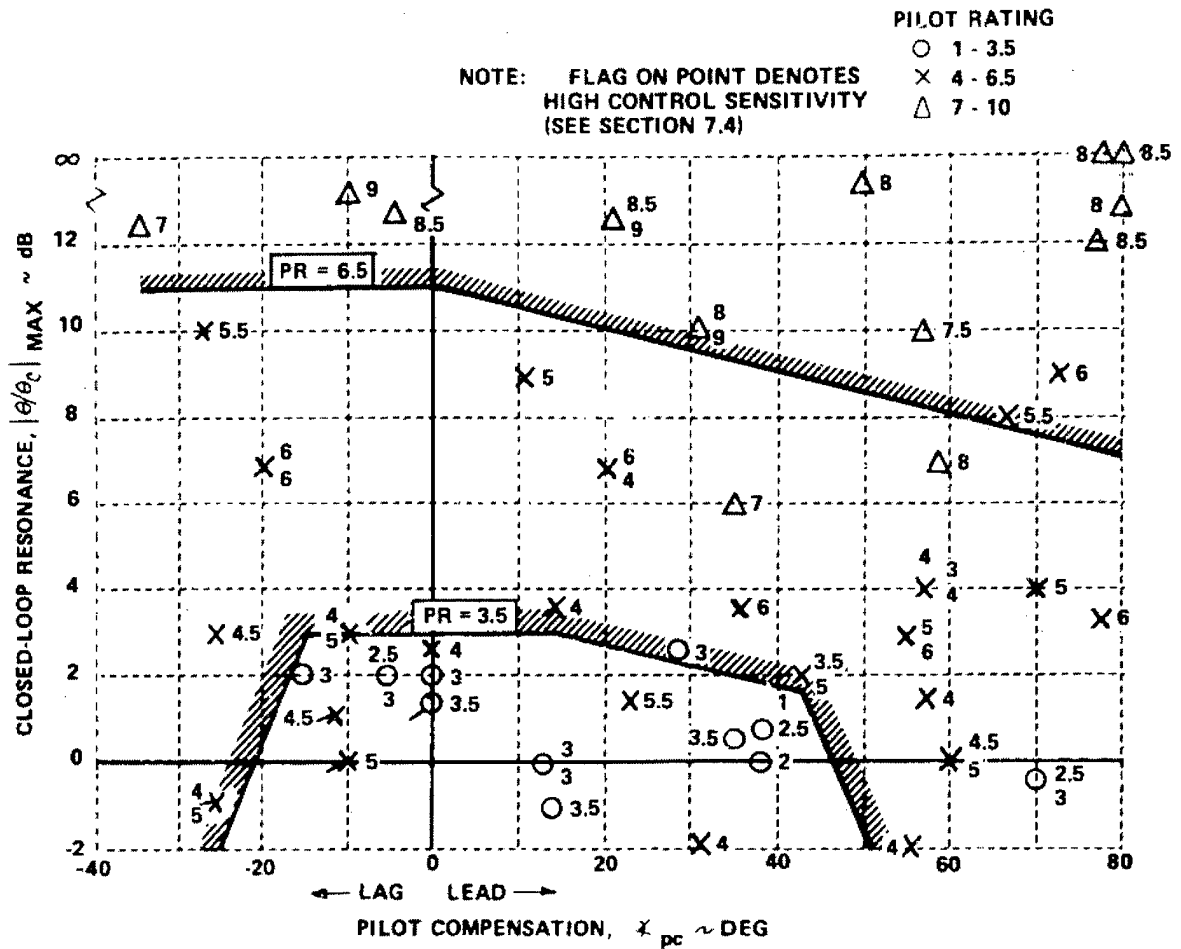


Figure 2.14 Neal-Smith Handling Qualities Level Boundaries, from Neal and Smith (41)

When plotted on a Nichols chart, the Neal-Smith Criteria provides a simple, graphical method from which the overall Handling Qualities (HQ) level may be determined, Figure 2.15.

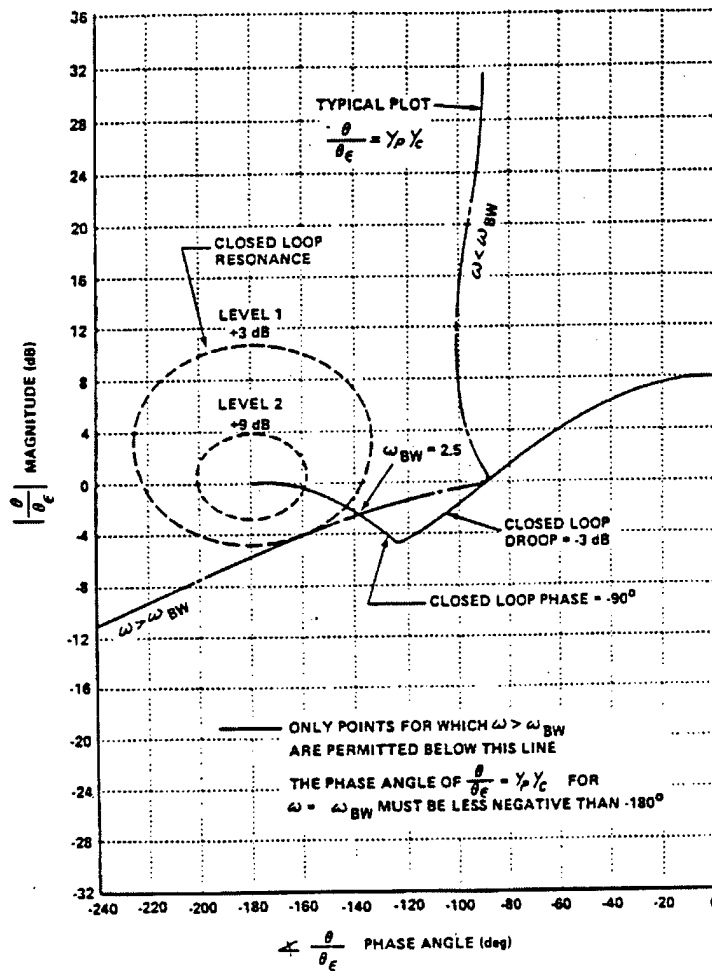


Figure 2.15 Neal-Smith Criteria Nichols Chart, from MIL-STD-1797a (14)

2.4.3 *Optimal Control Model.* The methods of predicting pilot opinion discussed so far have been frequency domain methods that employed relatively simple linear models of the human pilot. A different approach introduced in 1969 by Kleinman, Baron and Levison (31, 3) employed modern control and optimization theory in a state-space framework resulting in an Optimal Control Model (OCM) of the human operator. The approach is based on the assumption that the pilot acts "optimally" in some sense. It assumes that a well motivated and well trained human operator behaves in a nearly optimal manner subject to his inherent limitations and physical constraints, specifically neuromuscular lag, processing delays and perceptual thresholds (31).

The OCM model includes the desirable features of the human operator, the ability to adapt control compensation and strategy, as well as the undesirable, non-linear remnant and time delay. Time delay in the pilot model was discussed previously and is included in the Neal-Smith model as well. However, the operator's remnant, that portion of human output that is not linearly related to input is obviously not considered in linear models. The OCM model takes the remnant to be the component of human response that can not, except in a statistical sense, be predicted. Thus in the OCM model, the remnant is accounted for by introducing noise into the pilot's observation and control response. Figure 2.16 shows the structure of the OCM pilot model. The concept behind the model is elegant and relatively simple. The task modeled is compensatory tracking. The pilot attempts to minimize the error induced by a disturbance forcing function modelled by white Gaussian noise passed through a coloring filter. The pilot observes the state of the dynamic system being controlled,  $y(t)$ , but cannot derive perfect information from his displays, the observations are noisy,  $V_y(t)$ , and subject to perceptual thresholds. Thus the pilot must make an estimate of the actual state of the system, delayed by a finite amount as he processes the information presented,  $\hat{x}(t - \tau)$ . In the OCM all pilot delays are lumped into the one delay  $\tau$ . The pilot is aware of this inherent delay and, using

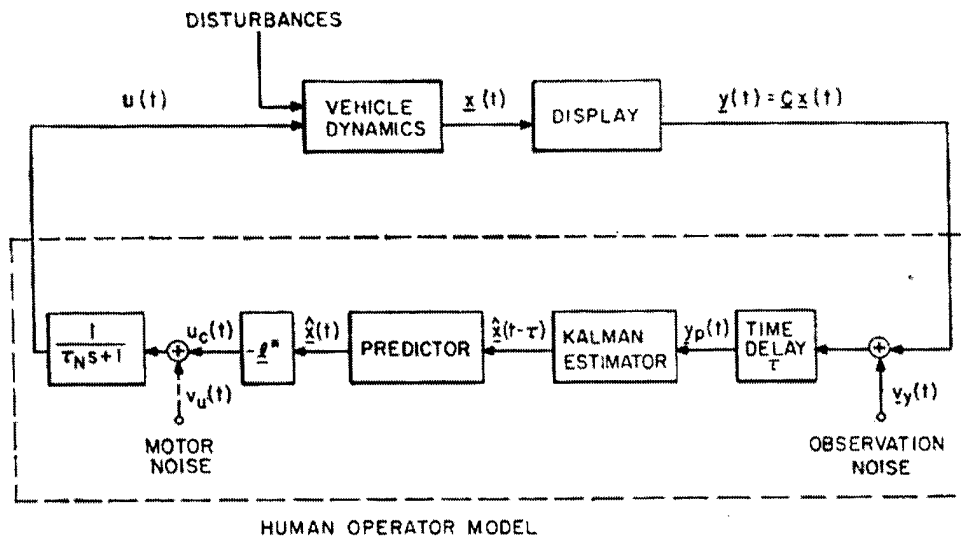


Figure 2.16 Control Model of Optimal Human Behavior, from (31)

knowledge of the controlled system dynamics, is able to generate an estimate of the undelayed display data vector,  $\hat{x}(t)$ . Display noise is uncorrelated white Gaussian noise with a spectral density proportional to the mean squared value of the displayed component. The noise represents a part of the pilot's non-linear remnant as well as random observation error. Signal-to-noise ratios of 0.01 are commonly seen in single loop situations and have been shown to be relatively invariant over a wide range of input spectra and controlled system dynamics (35). In the model, estimation of the delayed state vector is accomplished by a Kalman Filter. The delayed state information is then passed through a least mean square predictor to yield the undelayed estimated state vector.

The "optimal" pilot places appropriate gains on the system states to produce a control law that optimizes his performance,  $u_c(t)$ . Since a human cannot make control movements with infinite precision, the operator's output is corrupted by motor noise,  $V_u(t)$ . Lastly, the pilot's output is passed through his neuromuscular system modelled by a first order lag with time constant  $\tau_N$ . The optimal pilot gain matrix is computed by solving the Linear Quadratic Gaussian Regulator problem

for a cost function,

$$J(u) = E \left\{ \lim_{T \rightarrow \infty} \frac{1}{T} \int_0^T y^T Q y + u^T R u + \dot{u}^T G \dot{u} dt \right\} \quad (2.18)$$

The first part of the integrand,  $y^T Q y$ , is related to performance, while the second and third,  $u^T R u + \dot{u}^T G \dot{u}$ , place penalties on control and control rate. Simply put, this quadratic performance index says that the optimal pilot desires good performance while maintaining an acceptable workload. It was found (31) that the neuromuscular system could be implicitly modelled if the penalty is placed on control rate. Thus for a single-input/single-output compensatory task, the cost function simplifies to,

$$J(u) = E \left\{ \lim_{T \rightarrow \infty} \frac{1}{T} \int_0^T (e^2 + G \dot{u}^2) dt \right\} \quad (2.19)$$

where  $e$  is the compensatory error and  $\dot{u}$  is the control rate. The penalty,  $G$ , is selected iteratively to yield the appropriate  $\tau_N$ . A value of 0.1 sec is commonly used for  $\tau_N$ .

The motor noise,  $V_u(t)$ , is zero mean Gaussian white noise with a spectral density proportional to the mean squared operator output. Motor signal-to-noise ratios of 0.003 have been found to provide a good match to experimental data (35). A detailed discussion of the mathematics used in solving the OCM problem is beyond the scope of this work. The interested reader is directed to Kleinman (31).

OCM has been shown to be very effective in deriving a model of pilot behavior (3). Pilot compensation measured in simulator studies involving different controlled elements has been accurately predicted by OCM algorithms (17). Additional work has been done relating the optimal value of the cost function,  $J$ , to a numerical Cooper-Harper pilot rating (25, 27, 26, 23). The Minimum Flying Qualities study (38) found the OCM method very accurate in predicting HQR except in plants where lag generation near crossover was required. The authors derived a

simple formula to calculate a numerical Cooper-Harper rating,

$$HQR = 5.5 + 3.7 \left[ \log_{10} \left( \frac{J}{\sigma_c^2} \right) - \log_{10} (\omega_w^2) \right] \quad (2.20)$$

where  $\sigma_c$  is the RMS error amplitude and  $\omega_w$  is the forcing function noise bandwidth. The “task” portion of the handling qualities rating is enforced by selecting a coloring filter to yield the appropriate forcing function noise bandwidth. However, in systems that exhibited pure time delays, Hess (24) found that the value of  $J$  alone was unacceptable as a metric. Other studies (47) have also sought to relate the minimum value of the cost function to Cooper-Harper rating. Unfortunately, the equations for HQR derived vary widely and the use of OCM as a HQR predictor has not been adopted in Mil-STD-1797A. Another drawback of OCM is that the use of the linear predictor and exponential time delay makes it impossible to directly express the optimal pilot model,  $Y_p$ , as a simple transfer function.

*2.4.4 Modified Optimal Control Model.* An alternative to the OCM model was developed by Davidson and Schmidt (13). The Modified Optimal Control Model (MOCM) is a variation of the OCM developed by Kleinmann et al (31) and the simplified optimal pilot models developed by Hess (25) and Schmidt (47). The model is input compatible with the OCM and retains its key features. Unlike the OCM, the MOCM structure allows the direct calculation of pilot and overall system transfer functions. The predicted pilot compensation derived by MOCM has been shown (13) to be a very good model of actual closed-loop pilot performance and compares more favorably to actual pilot performance than does the full OCM. The structure of the MOCM is illustrated in Figure 2.17. It differs primarily in that the pilot's effective time delay is modelled by a second order Pade approximation and placed at each of the pilot's outputs and is treated as part of the plant dynamics. In the multiple-input/multiple-output structure, this yields a lower order operator model since pilots typically have fewer outputs than inputs.

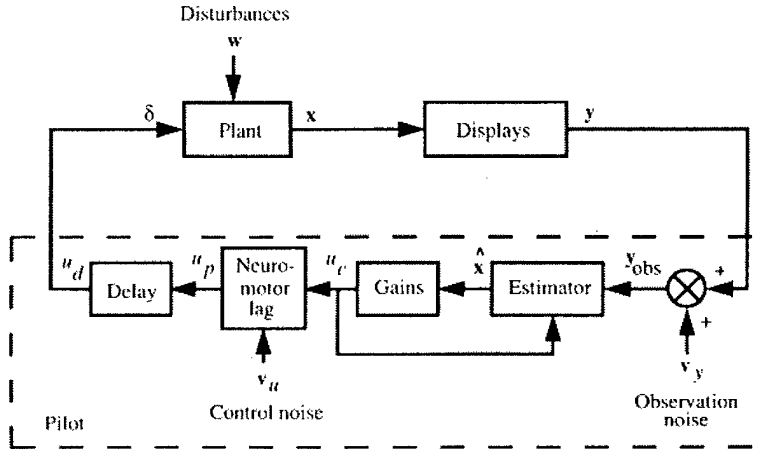


Figure 2.17 Conceptual block diagram of modified optimal control model, from (13)

The pilot model is derived in a similar fashion to the OCM solution. Pilot gain matrix is determined by solving the LQR problem such that the neuromuscular lag,  $\tau_N$ , is implicitly modelled. The Kalman filter is solved in a similar manner to the OCM. Since the pilot delay has been moved to the output, there is no need for the linear estimator and the pilot describing function can be determined in state-space form directly.

The proven accuracy of MOCM in modelling pilot compensation as well as the ease with which one may derive pilot transfer functions,  $Y_p$ , makes this approach superior to OCM for the analysis in this thesis.

*2.4.5 Time-Domain/Frequency-Domain Combination Techniques.* We have discussed both time-domain, OCM and MOCM, as well as frequency domain, Bandwidth and Neal-Smith techniques to predict HQR. Research has been done by Bacon and Schmidt (2) and more recently by Efremov (17) that seeks to combine time-domain and frequency-domain techniques. Specifically, pilot models and closed-loop system models are determined using OCM. Performance in the form of closed-loop resonance peak, and pilot effort in terms of phase compensation may be directly



derived from these models and applied to Neal-Smith derived criteria. Bacon and Schmidt use pilot compensation at crossover frequency as their measure of pilot workload. Efremov, on the other hand, calculates the difference in pilot compensation between the system being evaluated and a system with "ideal" dynamics. This allows him to make pilot compensation comparisons across the frequency spectrum and not just at crossover. Both methods provide approximately equally good correlation with actual pilot rating. However, Bacon and Schmidt's approach was chosen for investigation in this thesis due to the comparative simplicity of their method.

### *2.5 Transport Delay Compensation Techniques*

The revolution in digital technology flowed into flight simulator design in the late 1970s. The transition from "flying cameras" and model landscapes (terrain boards) to modern Computer Generated Imagery (CGI) was not initially smooth. Transport delays inherent to the digital algorithms combined with CGI delay and system synchronization problems contributed to significant overall delays that adversely effected pilot performance to the point of rendering the design unusable without improvement (22).

Research has shown (11) that, when "flying" a simulator, pilots cannot distinguish between simulator visual delay and flight control delay. This is due to the pilot deriving a large proportion of his perceived aircraft response from a computer generated display, especially during precision visual landing and formation flying. All the deleterious effects of time delay discussed previously come into play to reduce pilot/vehicle performance. Since simulators are used primarily as training devices any reduction in pilot/vehicle performance will adversely effect training and acquisition of new skills (46).

Computer delays in processing the equations of motion and control laws can be reduced or eliminated by using predicted values for aircraft states that are already calculated and stored by numerical integration algorithms. However, the delays

due to computer processing for CGI, on the order of 100 msec (12), can only be eliminated by increasing the speed at which the displayed image was updated, and this was an expensive solution in the late 1970s. Simulator designers and controls engineers sought less expensive alternatives. A survey by Cardullo and George (9), discusses three methods that have proven successful in compensating for CGI delay: lead/lag networks, velocity predictor algorithms, and state predictors.

Consider now the problem of the UAV where aircraft performance feedback to the pilot is delayed by transmission time. For a given datalink delay,  $\tau_d$ , the pilot must wait  $2\tau_d$  to see the effects of his control inputs on aircraft performance. This is essentially similar to the simulator delay problem in that a UAV pilot will not be able to distinguish between delay due to datalink latency and control system delay. To the pilot they are one and the same and the pilot/vehicle system stability and performance will be degraded. To illustrate this point one can perform a thought experiment in which a pilot is sitting at a UAV control system “flying” a simulated mission. Delays that he experiences are due to computational and CGI latency and can be reduced by faster computers and image update rates. Now the “plug” is pulled on the simulation and “plugged in” to a real UAV at the same flight parameters as its simulated twin. If the simulated UAV has high enough fidelity and the delay time was similar, the pilot would not notice that he was no longer flying a simulation on a computer and the equations of motion and control laws were instead “running” on the real thing! Now let us consider the compensation methods mentioned above and how they might be applied to the UAV datalink latency.

*2.5.1 Lead-Lag Networks.* Crane performed fixed base (12) and full-motion (11), compensatory tracking experiments to investigate the efficacy of simple lead/lag networks in compensating for the effects of time delay. Compensators were employed as shown in Figure 2.18 and were of the form,

$$G_c = K_d \frac{T_n s + 1}{T_d s + 1} \quad (2.21)$$

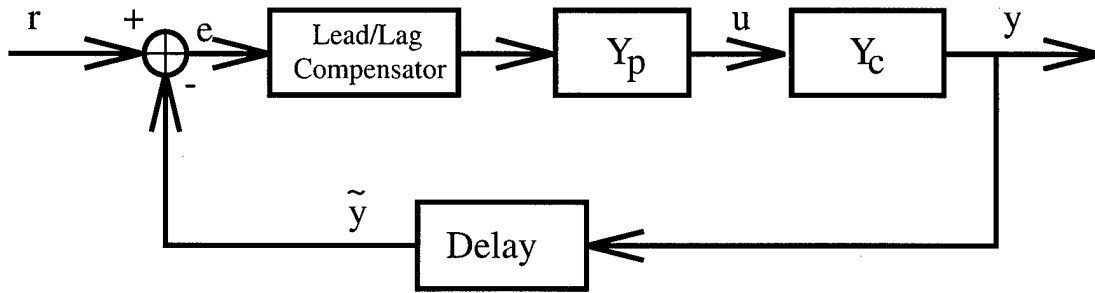


Figure 2.18 Block Diagram used by Crane (12)

The design algorithm consisted of two steps. First determine the amount of lead compensation required using Equation 2.22, locate the filter zero at  $\omega_c$ , the crossover frequency for the task to be accomplished, and use Equation 2.23 to solve for  $T_d$ .

$$\phi_f|_{\omega=\omega_c} = \omega_c T_d \quad (2.22)$$

$$\phi_f|_{\omega=\omega_c} = \arctan(\omega_c T_n) - \arctan(\omega_c T_d) \quad (2.23)$$

Secondly, distribute resulting gain distortion by adjusting  $K_d$  such that,

$$|G_c(j\omega)|_{\omega=\omega_c} = 1. \quad (2.24)$$

The simple lead/lag filter designed by this method provides lead that is a function of frequency and the maximum phase lead is a function of the filter pole-zero separation. The filter has the desirable property that it provides little lead at frequencies  $\omega \leq \omega_c$ . However it has the undesirable property that filter gain is also a function of frequency and is also proportional to filter pole-zero separation. Since the pure delay contributes nothing to the system gain, compensation to reduce delay effects should not appreciably effect gain. Consequently, the lead/lag network “purchases phase lead at the cost of gain distortion” (12). Such was the case in attempting to compensate for delays in simulators. The fact that the UAV pilot is removed from the cockpit and will never experience the actual flight characteristics of the UAV

makes gain distortion much less of a factor in UAV delay compensation. Having never physically flown in the UAV, the pilot would not know the difference between the original and delay compensated handling qualities.

The results of Crane's experiment showed that compensation increased average pilot performance by fifty percent and measures of pilot workload and system stability approached no-delay baseline values. Additionally, he found pilot-to-pilot variability in  $\omega_c$  was small. Ricard investigated lead/lag compensation effects on the acquisition of control skill in delay compensated system (46). Again compensation proved to be effective; test subjects needed approximately half as many trials to criterion when display delay was compensated by a lead/lag network.

Inflight tests of lead/lag delay compensation were performed by Hodgkinson (29). They tested two compensators on a configuration having  $\omega_{n_{sp}} = 2.3$ ,  $\zeta_{sp} = 0.57$ , and  $\tau_d = 0.17$  seconds. The basic configuration received a CH rating of 6. When compensated with a filter  $(.5s + 1)/(.17s + 1)$  CH rating decreased from 6 to 10. Compensation of the form  $(.1s + 1)/(.05s + 1)$  resulted in a CH rating of 9. Pilots had difficulty with the abrupt onset of the response following the time delay. When the gains were reduced to make high frequency gain similar to the basic system, the CH ratings returned to baseline. The authors comment,

It is tempting to extrapolate these results to show that delay effects could be reduced or eliminated by reducing the system gain.

They did not, however, test system gains below those of the basic system due to pilots complaining of high stick forces. It has been shown (50, 29) that pilots are more sensitive to mismatches between higher order systems and their LOES in the region of  $\omega_c$ . Looking at the compensators chosen by Hodgkinson one can see that the resulting gains in the vicinity of  $\omega_c$  are 1.42 and 1.02 respectively. However, Figures 2.19 and 2.20 show the Bode plots for these two filters are clearly not providing correct gain in the case of the first and lead at the appropriate frequency in the case of the second. The poor performance of the Lead/Lag compensators tested in the

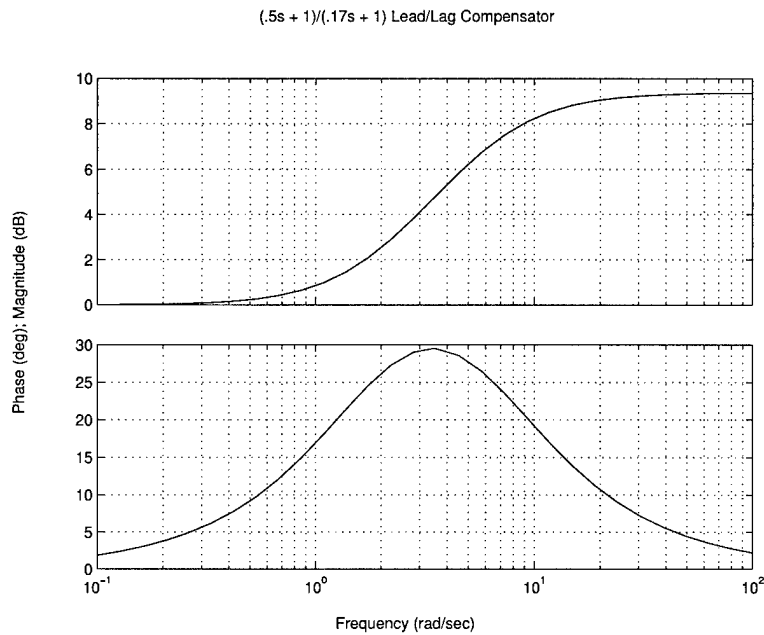


Figure 2.19 First Compensator Flight Tested in Hodgkinson (29)

limited in-flight evaluation most likely resulted from inadequate compensator design. One may conclude that the more rigorous simulator studies of Crane (12, 11) and Ricard (46) demonstrate that lead/lag compensation may be helpful in reducing the effects of datalink latency on UAV handling qualities. This compensation technique was chosen for further investigation.

*2.5.2 Velocity Predictor Algorithm.* Another technique that has been employed for mitigating simulator transport delays is the velocity predictor algorithm originated by McFarland and has proven successful on both research and training simulators. The technique uses the past two values of velocity as well as the current position to predict the future position (34),

$$U_{n+1} = U_n + b_0V + b_1V_{n-1} + b_2V_{n-2} \quad (2.25)$$

where  $U$  is position and  $V$  is rate. The algorithm assumes a bandwidth of two to three hertz for high gain tasks. Sinusoidal inputs are applied to the compensation

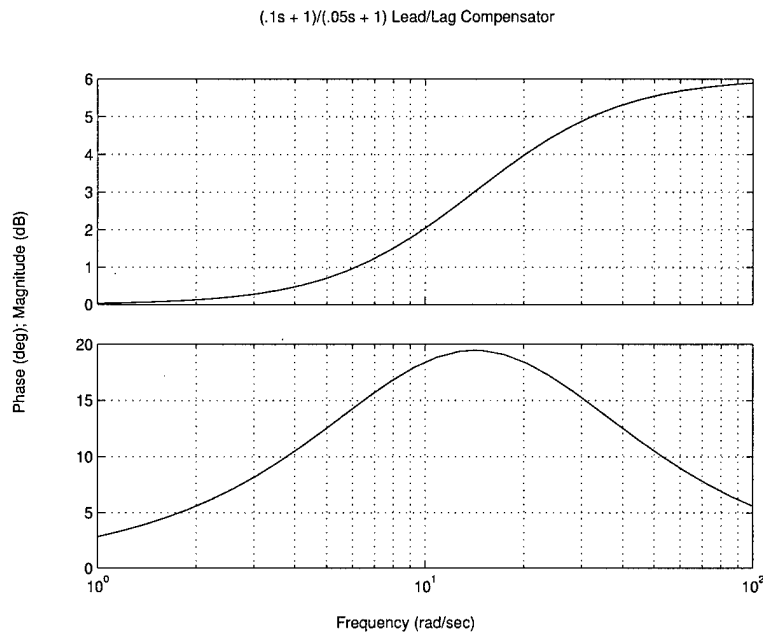


Figure 2.20 Second Compensator Flight Tested in Hodgkinson (29)

delay model in order to “tune” it at the proper frequency. The values of constants  $b_0$ ,  $b_1$ , and  $b_2$  are found as functions of delay, update rate, and bandwidth (9). Unfortunately, this technique introduces substantial gain at frequencies above  $\omega_c$ . The difficulties involved in tuning such an algorithm on a UAV in flight made this technique unsuitable for flight test and was not explored any further.

*2.5.3 State Predictors.* Perhaps the most successful compensation method, albeit the most complex, is the state predictor algorithm. This technique was originated by Sobiski and Cardullo (52) and uses state-space methods to design a state predictor using the system state transition matrix. Given the state-space system of  $n$  states, with  $m$  inputs, and  $p$  outputs,

$$\dot{\mathbf{x}}(t) = \mathbf{A}\mathbf{x}(t) + \mathbf{B}\mathbf{u}(t) \quad (2.26)$$

$$\mathbf{y}(t) = \mathbf{C}\mathbf{x}(t) + \mathbf{D}\mathbf{u}(t) \quad (2.27)$$

where,  $\mathbf{u} \in R^m$ ,  $\mathbf{x} \in R^n$ , and  $\mathbf{y} \in R^p$ . This research is concerned with primarily the single-input/single-output case. The state transition matrix,  $\phi$  is given by,

$$\phi(t, \tau) = e^{\mathbf{A}(t-\tau)} \quad (2.28)$$

One may determine both the system state,  $\mathbf{x}(t)$ , and system output,  $y(t)$ , for any time,  $t$ , given initial system state,  $\mathbf{x}(t_0)$ , and input history,  $u(\tau)$ ,  $\tau \in [t_0, t]$  by solving,

$$\mathbf{x}(t) = \phi(t, t_0)\mathbf{x}(t_0) + \int_{t_0}^t \phi(t, \tau)\mathbf{B}u(\tau)d\tau \quad (2.29)$$

If one chooses the time interval  $[t_0, t]$  to be equal to the length of time delay,  $\tau_d$ , then  $\mathbf{x}(t)$  will be the system state at the end of the delay. The resulting filter functions as a state predictor. Appropriate gains for state feedback can be determined and state feedback may be employed as if the delay did not exist, see Figure 2.21. Unfortunately, Equation 2.29 can not be solved without a priori knowledge of the fu-

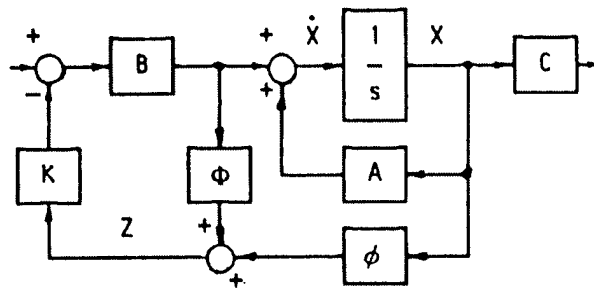


Figure 2.21 State Predictor System Diagram from Sobiski and Cardullo (52)

ture time history of the input,  $u(t)$ , which is not available. However, if the time delay is of short enough duration and the bandwidth of the input signal is low enough, one may approximate the input as constant for the period of time delay thus allowing a closed form solution to the convolution in Equation 2.29. Sobiski and Cardullo (52) showed that the state predictor filter with the piecewise constant input approximation restored gain and phase margins of a delayed system to the undelayed values.

They were able to successfully employ this technique on delays as great as 800 ms without the gain and phase distortion that accompanied the lead/lag and velocity predictor algorithms.

With this background and theory behind us, let us now investigate whether one can indeed design compensation for time delay in a pilot/UAV interface and apply the mathematical techniques for predicting POR to evaluate their effects.



### *III. Analysis*

#### *3.1 Mathematical Analysis, Effect of Delay*

The discussion of the effects of time delay on the human operator in the last chapter focused on experimental results. Mathematical tools currently used to predict HQR, specifically Bandwidth, Neal-Smith and the Bacon-Schmidt OCM method, were also discussed. This section will investigate employing these mathematical tools to predict the effect of time delay on pilot HQR. The resulting predictions will be compared to actual values obtained in flight test.

While there have been numerous flight tests investigating handling qualities in the past, the number of tests investigating the effects of time delay is much smaller. Investigations of digital, or pure time delay are few indeed. Two of the most accessible sets of data come from the NASA F-8 DFBW test (7) of the late 1970's and early 1980's and the Princeton Variable-Response Research Aircraft (VRA) (53). In both cases, researchers specifically examined the effects of pure transport delays on pilot HQR in both landing and up-and-away tasks. Appendix A contains a derivation of the models used to reproduce the results of these flight tests. Additionally, Appendix A and G contain detailed derivations of the appropriate transfer functions for analysis with the Bandwidth, Neal-Smith and OCM methods implemented in the Wright Labs Handling Qualities Toolbox (16).

*3.1.1 Overall Results.* In general both the Bandwidth and the Neal-Smith criteria provided valid predictions of time delay effect on handling qualities rating; the Neal-Smith technique proved to be the most accurate. Both techniques more accurately matched flight test data when the in-flight task requirements closely matched established task categories. Although the Bacon-Schmidt method provided somewhat accurate predictions of the baseline (no incremental delay) HQR; it proved to be unusable as incremental delay was added. This was do mainly to the fact that

the optimal pilot model enforces the task requirement by proper selection of the coloring filter which when applied to the gaussian white noise forms the disturbance signal. The coloring filter determines the disturbance signal bandwidth and is adjusted to give good agreement between the optimal pilot model produced and pilot models derived from human subject data. Hence the disturbance noise bandwidth does not vary between configurations in the Bacon-Schmidt analysis. This begins to cause trouble as incremental delay is added to the system. The optimal pilot model strives to minimize the cost function, Equation 2.19, and in doing so provides a pilot model that yields a lower crossover frequency, see Figure 3.1. This “crossover

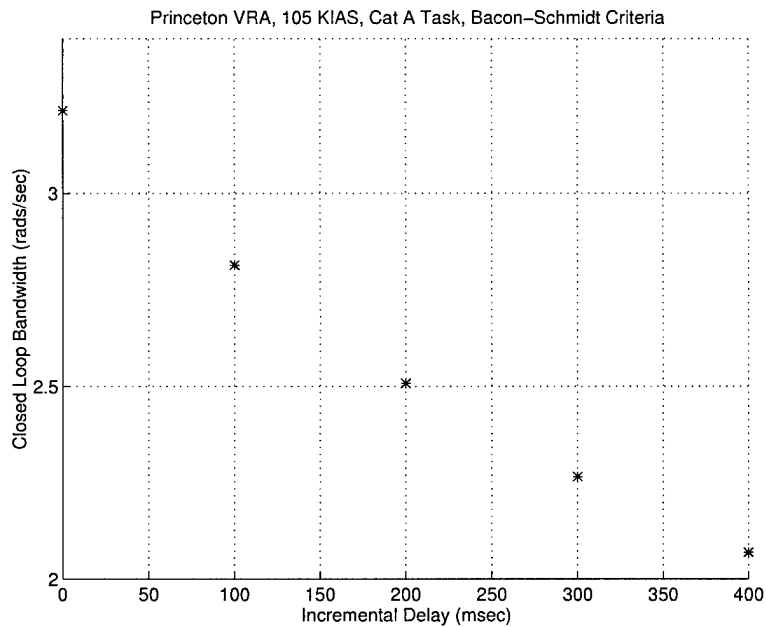


Figure 3.1 VRA, Cat A Task,  $Y_p Y_c$  Closed Loop Bandwidth versus Delay

regression” has been observed in numerous studies on human subjects (28, 45). This result is interesting in that it validates the optimal pilot model, but it also makes the Bacon-Schmidt method unusable for evaluating the effects of incremental delay without major modification. With no way to enforce the task requirement by holding  $\omega_c$  relatively constant near established values (Table 2.1, page 2-17), any analysis technique based on an optimal pilot model will provide inaccurate results,

see Figure 3.2 where the predicted POR improves as the time delay increases from 300 to 400 msec. This is a result of the pilot/vehicle bandwidth regression as seen in Figure 3.1.

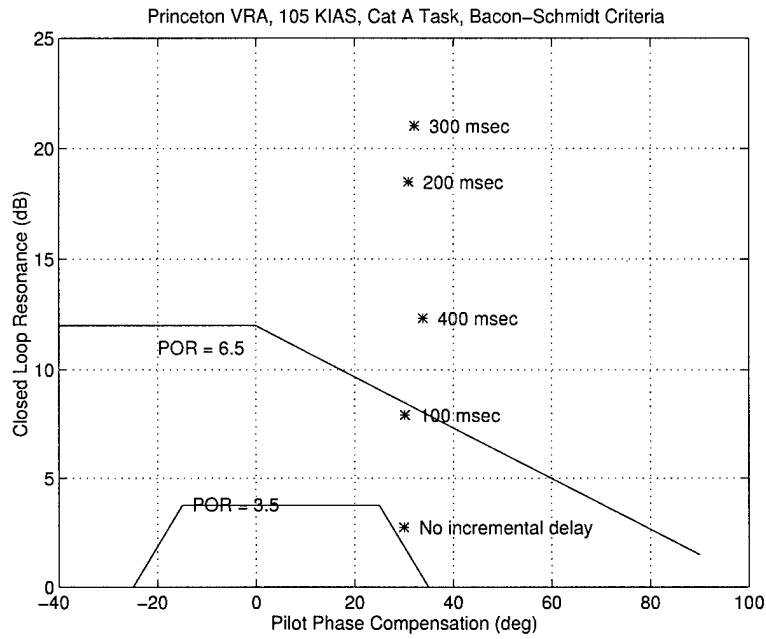


Figure 3.2 VRA, Cat A Task, Bacon-Schmidt Criteria

In fact, Bacon and Schmidt encountered this situation when the pilot models produced by their optimal methods were not producing the large resonant peaks such as were seen in the Neal-Smith analysis. They found that when faced with undesirable aircraft dynamics the “optimal pilot” accepted more low frequency error, i.e. droop, in favor of a lower resonant peak. When Bacon and Schmidt adjusted the forward pilot gain to ensure the -3 db droop criteria was met, they saw the resonant peak and PIO susceptibility increase to levels consistent with Neal and Smith (41). With added incremental delay the crossover frequency regression was too dramatic for a similar adjustment to be effective in this analysis.

*3.1.2 F-8 DFBW Data Analysis.* The Bandwidth Criteria as discussed in the previous chapter and implemented in Matlab by the Wright Laboratory Handling Quality Toolbox (16) was applied to the F-8 DFBW data set. The effect of delay on the F-8 DFBW aircraft with Stability Augmentation System (SAS) in landing (Cat C) task is shown in Figure 3.3. The increase in  $\tau_p$  and bandwidth regression is clearly evident. A more easily read assessment of the predicted HQR results is

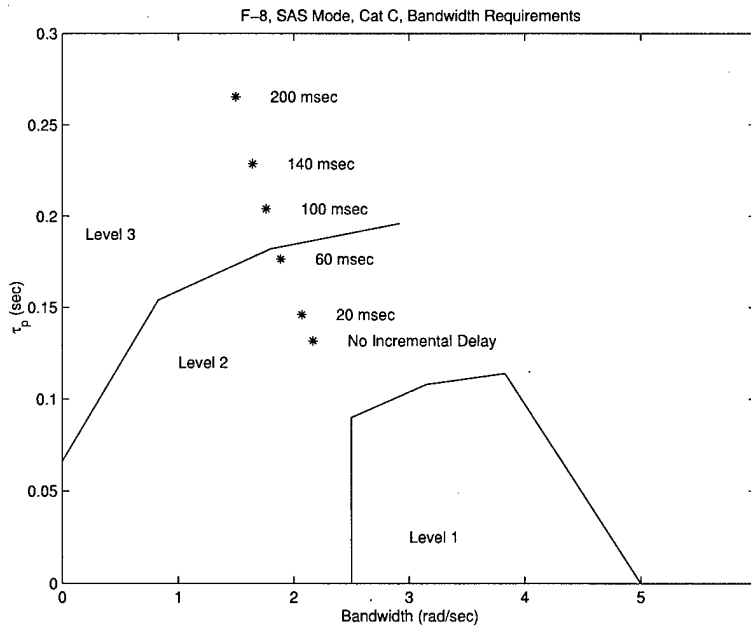


Figure 3.3 F-8 DFBW, Landing Task, Pitch SAS, Bandwidth Criteria

provided by the Neal-Smith criteria analysis presented in Figure 3.4. The decrease in performance as measured by closed-loop resonance increase is clearly displayed. Additional pilot workload caused by an increasing amount of pilot generated lead as delay increases may also be observed. It must be noted that some liberty is being

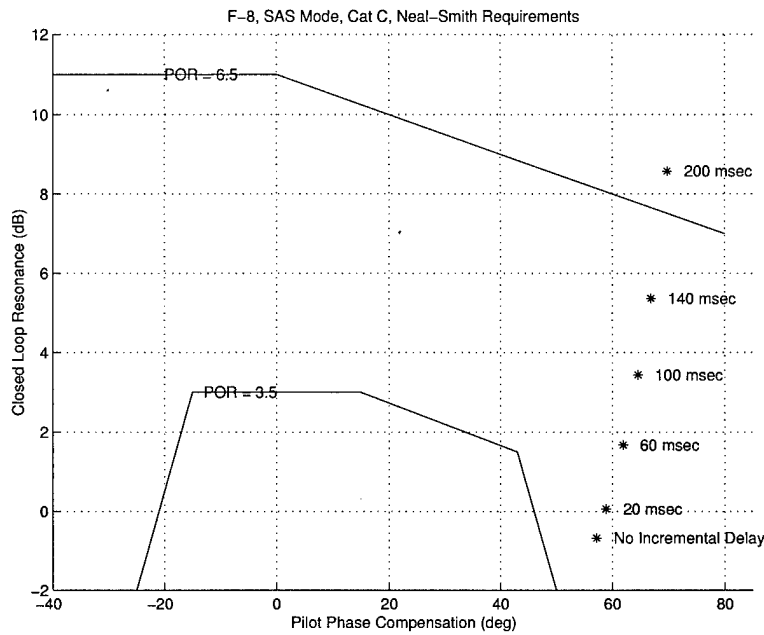


Figure 3.4 F-8 DFBW, Landing Task, Pitch SAS, Neal-Smith Criteria

taken with the traditional Neal-Smith criteria. Specifically, the original Neal-Smith criteria, employing resonant peak as a performance measure and pilot compensation at  $\omega_c$  as a measure of workload was established only for Cat A tasks. It is being used here with both Cat C and Cat A tasks with bandwidth requirements established by the Modified Neal-Smith criteria (14) listed in Table 2.1. This is done primarily so the reader can see how the pilot workload as well as resonant peak increase as delay time increases. Purists may recover the MIL-STD-1979A Modified Neal-Smith Criteria by ignoring the pilot compensation axis and concentrating solely on resonant peak.

Comparing these figures to the flight test results compiled from Figure 2.8 in Table 3.2, one can see the reasonably good correlation between the Neal-Smith

predictions and the normal and spot landing in-flight ratings. However, the Neal-Smith criteria is somewhat optimistic when compared to the offset spot landing HQR. This can be explained by the fact that the offset spot landing task is often employed to drive pilot gains up and expose poor handling qualities. This task is most likely not a 2.5 rad/sec task as is specified for Cat C tasks in the Neal-Smith criteria and most likely falls between Cat C (2.5 rads/sec) and Cat A (3.5 rads/sec). Indeed when the target frequency for closed loop  $\omega_c$  was increased to 3.0 rads/sec the Neal-Smith results more closely correlated to the in-flight ratings, Table 3.1.

Table 3.1 F-8 DFBW Landing Task Flight Test Results

Task	Mode	$\tau_d$ (msec)	HQR (average)
Low L/D Normal	Pitch SAS	None	3.5
Low L/D Normal	Pitch SAS	20	4.0
Low L/D Normal	Pitch SAS	60	4.5
Low L/D Normal	Pitch SAS	100	5.0
Low L/D Normal	Pitch SAS	140	5.5
Low L/D Spot	Pitch SAS	None	3.5
Low L/D Spot	Pitch SAS	20	4.0
Low L/D Spot	Pitch SAS	60	4.5
Low L/D Spot	Pitch SAS	100	5.0
Low L/D Spot	Pitch SAS	140	5.5
Low L/D Offset Spot	Pitch SAS	None	3.5
Low L/D Offset Spot	Pitch SAS	20	4.0
Low L/D Offset Spot	Pitch SAS	60	5.5
Low L/D Offset Spot	Pitch SAS	100	7.0
Low L/D Offset Spot	Pitch SAS	140	No Data

The F-8 DFBW study employed a formation flying task to simulate inflight aerial refueling. Category A Bandwidth criteria results for Pitch SAS mode are displayed in Figure 3.5. Results from the Neal-Smith criteria analysis for a Cat A task are displayed in Figure 3.6. Comparing Figures 3.5 and 3.6 to the flight test results compiled from (7) in Table 3.2, one can see that the Cat A Bandwidth and Neal-Smith criteria are far from being satisfied even though the in-flight rating for the baseline, no incremental delay, SAS and ISAS were Level 1.

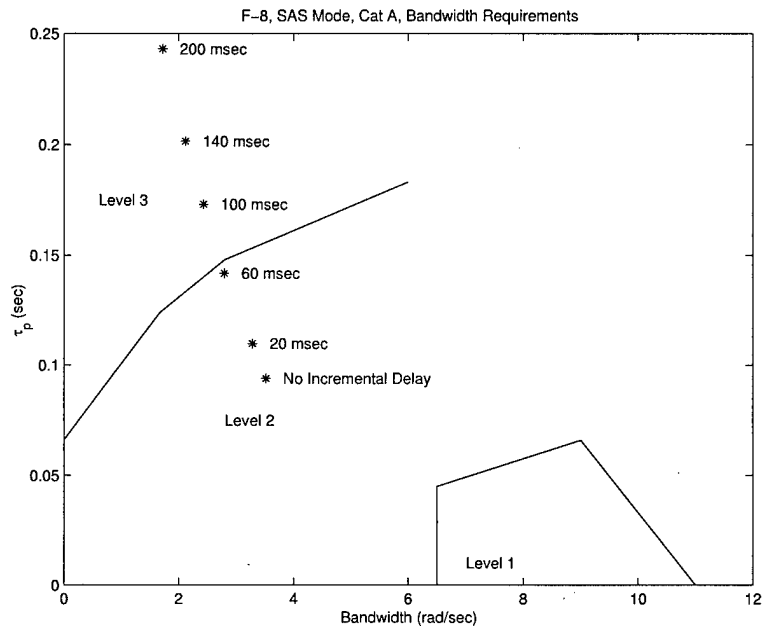


Figure 3.5 F-8 DFBW, Cat A Task, Pitch SAS, Bandwidth Criteria

*3.1.3 Princeton VRA Data Analysis.* The analysis for the Princeton VRA data proceeded in a similar manner to the above F-8 DFBW discussion. Bandwidth criteria and Neal-Smith criteria results are presented in Figures 3.7 and 3.8 respectively. As seen before with the F-8 DFBW data, both the Bandwidth and Neal-Smith predictions are overly pessimistic when compared to the actual flight test results compiled from (7) in Table 3.3.

The Cat A tracking task used in the Princeton study was the correction of flight path errors in up-and-away flight. Although the authors (53) refer to this as a "tracking" task; it seems that this particular task falls more into Category B than A. The bandwidth requirements from MIL-STD-1797A are identical for Categories A and B. However, Neal-Smith analysis specifies a target  $\omega_c$  of 1.5 rad/sec rather than 3.5 rad/sec. When Neal-Smith analysis is reaccomplished with  $\omega_c$  closer to Cat B, 2.25 rads/sec, the analysis falls more in line with the actual flight test results, Figure 3.9. This is a good example of the sensitivity of handling qualities to the task being accomplished. Bandwidth predictions for the VRA landing at 75 KIAS are

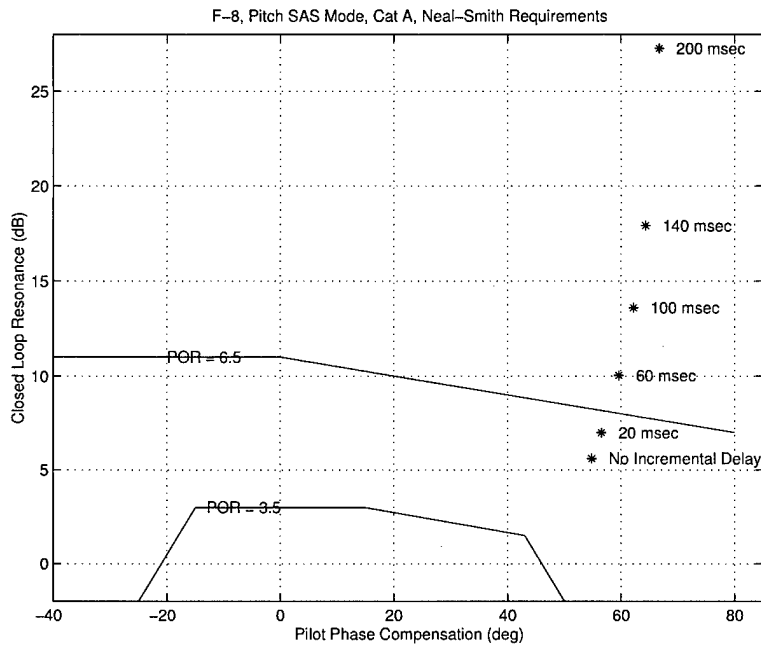


Figure 3.6 F-8 DFBW, Cat A Task, Pitch SAS, Neal-Smith Criteria

shown in in Figure 3.10. Neal-Smith criteria are displayed in Figure 3.11. Correlation between the predictions and in-flight ratings, Table 3.4, is generally quite good.

*3.1.4 NASA Utility UAV Data Analysis.* Analysis for the NASA Utility UAV data proceeded in a similar manner to the above discussions. Bandwidth criteria and Neal-Smith criteria results are presented in Figures 3.12 and 3.13 respectively. As seen before with the F-8 DFBW and VRA data, both the Bandwidth and Neal-Smith predictions are overly pessimistic when compared to the actual flight test results compiled from flight test (56) in Tables E.1 to E.6 on page E-1 and depicted in Figure 3.14.

Correlation between the predictions and in-flight ratings is generally poor. The Cat A tracking task used in the UAV flight test was the MIL-STD-1797A (14) discrete pitch tracking task. It is possible that research pilots were less aggressive during the tracking task due to the overall poor handling qualities of the UAV tested. This



Table 3.2 F-8 DFBW Tracking Task Flight Test Results

Mode	$\tau_d$ (msec)	HQR (average)
Pitch SAS	None	2.7
Pitch SAS	20	3.0
Pitch SAS	60	4.0
Pitch SAS	100	5.0
Pitch SAS	140	5.5
Pitch SAS	200	6.5
Pitch ISAS	None	2.7
Pitch ISAS	20	3.0
Pitch ISAS	60	4.0
Pitch ISAS	100	5.0
Pitch ISAS	140	5.5
Pitch ISAS	200	6.5
Pitch Direct	None	5.0
Pitch Direct	20	5.5
Pitch Direct	60	6.5
Pitch Direct	100	7.5
Pitch Direct	140	8.5
Pitch Direct	200	10.0

would have the effect of producing pilot ratings more optimistic than Bandwidth and Neal-Smith predictions.

Table 3.3 VRA Tracking Task Flight Test Results

A/S	$\tau_d$ (msec)	HQR (average)
105 KIAS	None	2.5
105 KIAS	100	3.0
105 KIAS	200	4.0
105 KIAS	300	5.0
105 KIAS	400	6.5

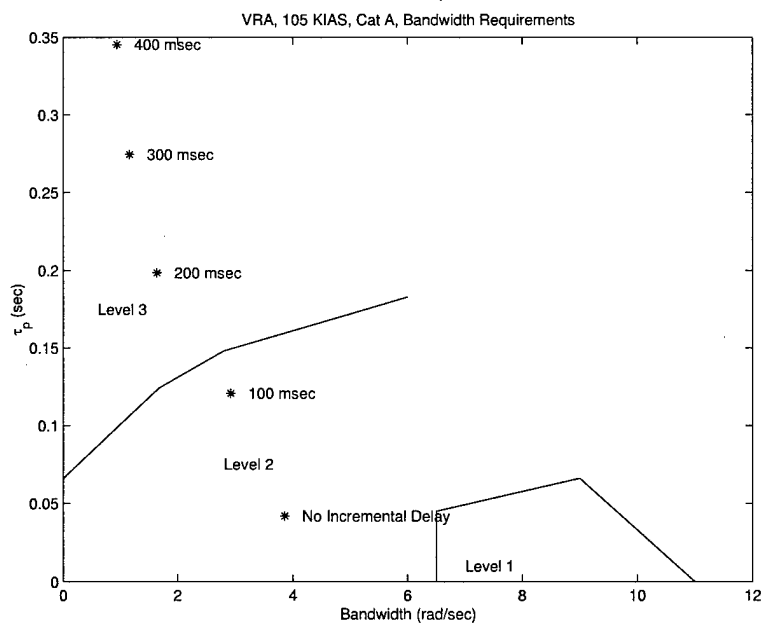


Figure 3.7 VRA, Tracking Task, Bandwidth Criteria

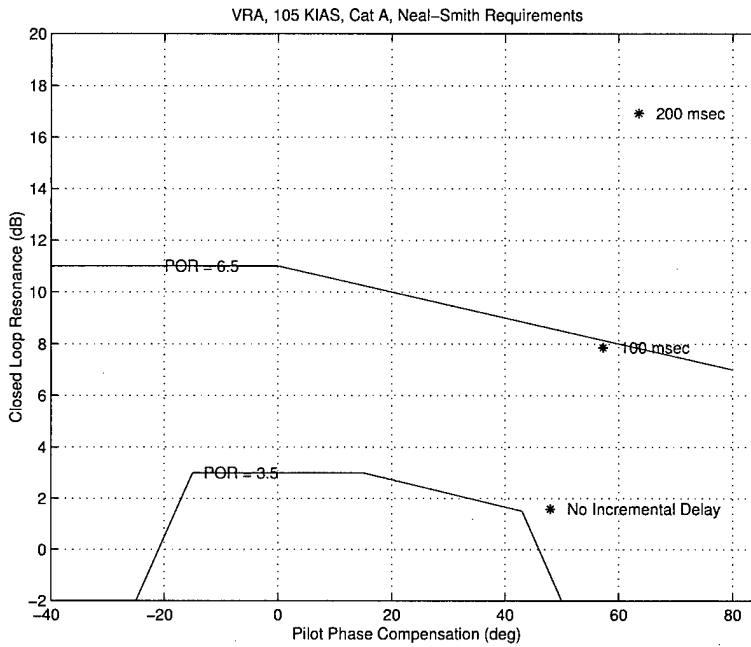


Figure 3.8 VRA, Tracking Task, Neal-Smith Criteria

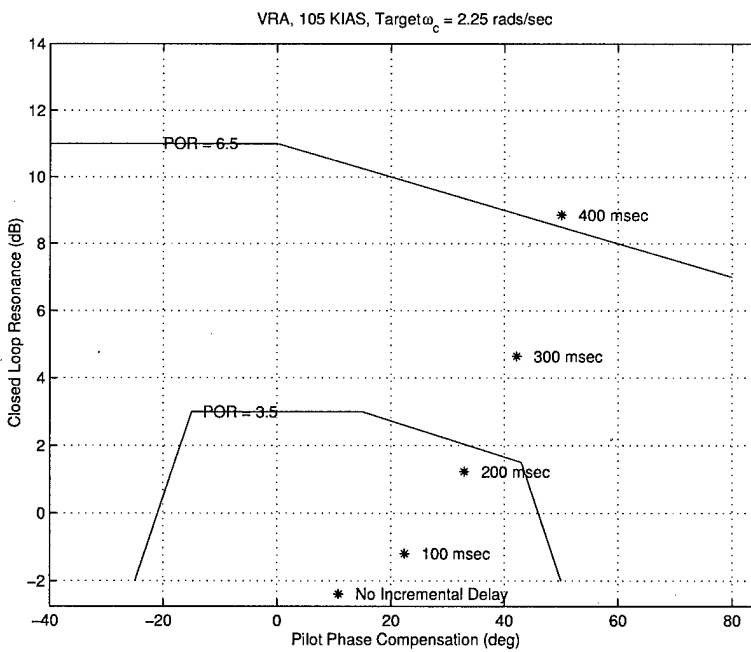


Figure 3.9 VRA, Lower  $\omega_c$  Requirement

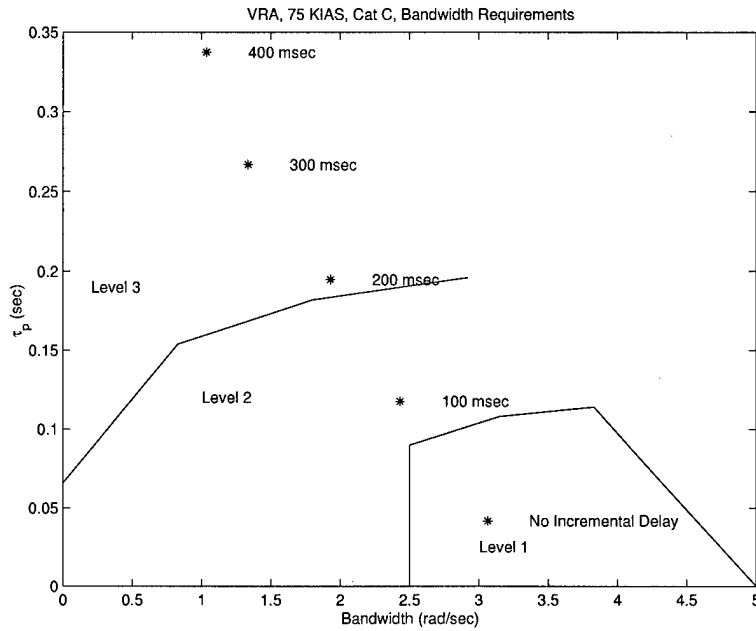


Figure 3.10 VRA, Landing, 75 KIAS, Bandwidth Criteria

Table 3.4 VRA Landing Task Flight Test Results

A/S	Landing	$\tau_d$ (msec)	HQR (average)
75 KIAS	Normal	None	2.0
75 KIAS	Normal	100	3.0
75 KIAS	Normal	200	4.0
75 KIAS	Normal	300	5.5
75 KIAS	Normal	400	7.0
86 KIAS	Field Carrier	None	2.5
86 KIAS	Field Carrier	100	3.5
86 KIAS	Field Carrier	200	6.0
86 KIAS	Field Carrier	300	No Data
86 KIAS	Field Carrier	400	No Data
105 KIAS	Field Carrier	None	3.0
105 KIAS	Field Carrier	100	4.0
105 KIAS	Field Carrier	200	3.0
105 KIAS	Field Carrier	300	6.0
105 KIAS	Field Carrier	400	No Data

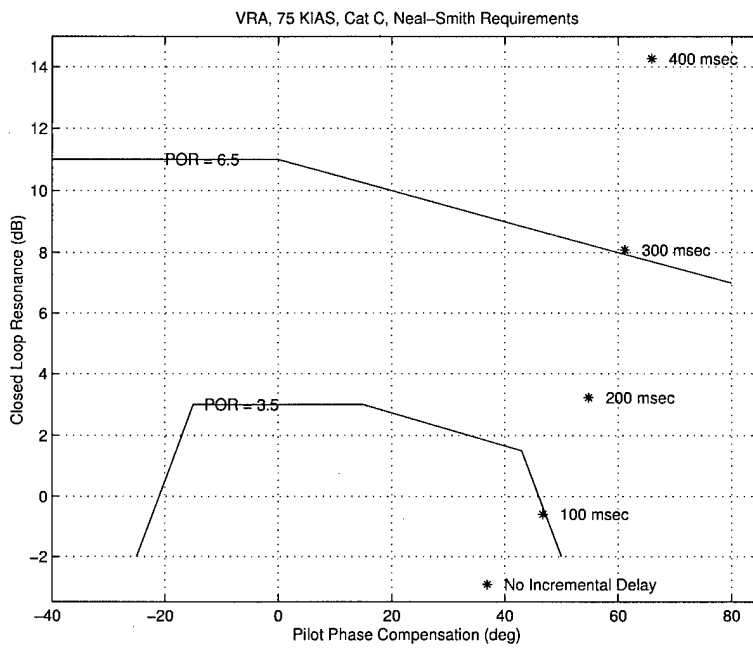


Figure 3.11 VRA, Landing, 75 KIAS, Neal-Smith Criteria

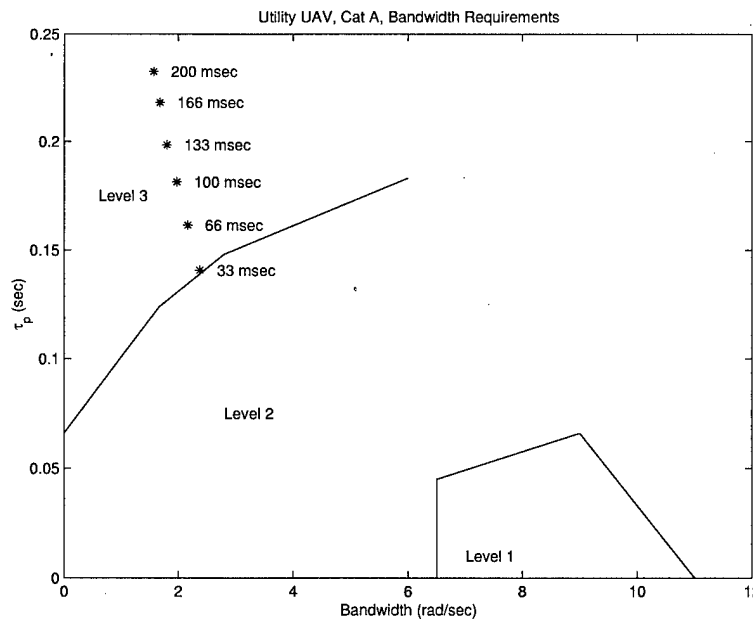


Figure 3.12 Utility UAV, Cat A Task, Bandwidth Criteria

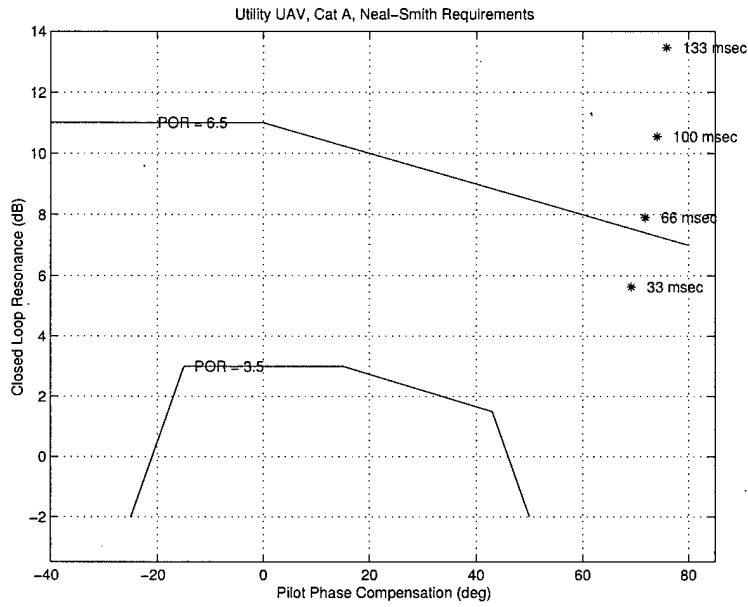


Figure 3.13 Utility UAV, Cat A Task, Neal-Smith Criteria

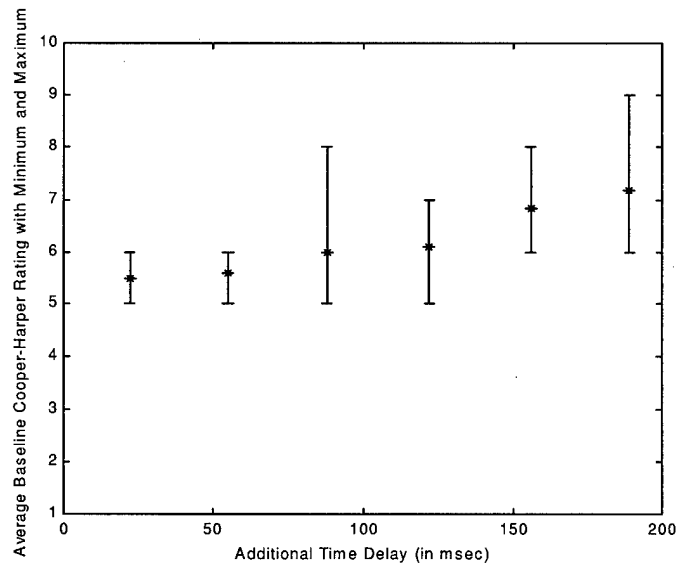


Figure 3.14 NASA UAV Flight Test Results

### 3.2 Lead-Lag Compensation Results

Lead-Lag compensation as discussed in chapter two and Equations 2.22 and 2.23 was applied to the F-8 DFBW data. Compensation bandwidth was appropriate for the task accomplished. Refer to Figure 3.15 for a block diagram of the compensated system. The transfer function used in Bandwidth and Neal-Smith analysis

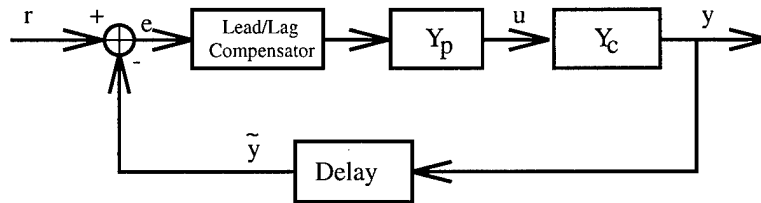


Figure 3.15 Lead/Lag Compensated System

was the open loop transfer function from the pilot's output,  $u$ , to the output of the compensator. Sampling delays and incremental feedback delay were lumped together into a single system delay.

Bandwidth Criteria results, see Figures 3.16 and 3.17 show some success at restoring delay free handling qualities.

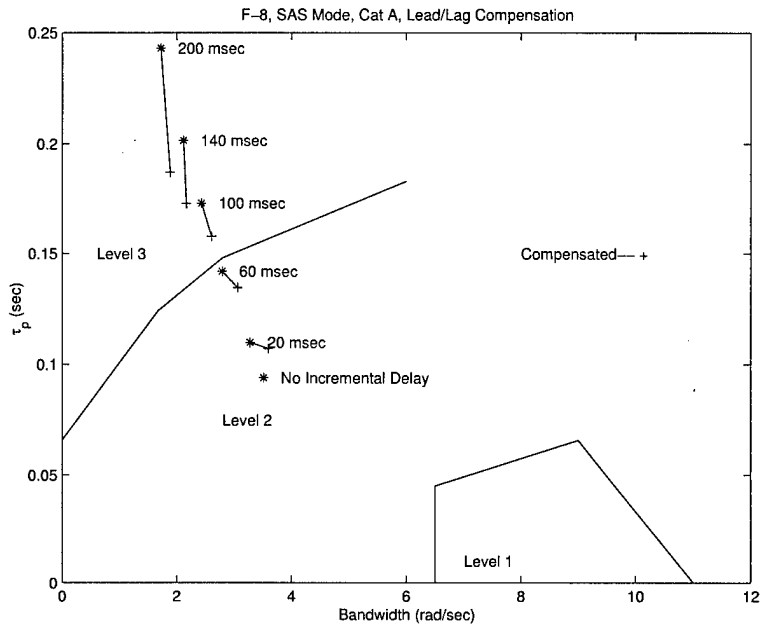


Figure 3.16 F-8 DFBW, Pitch SAS, Lead/Lag Compensation

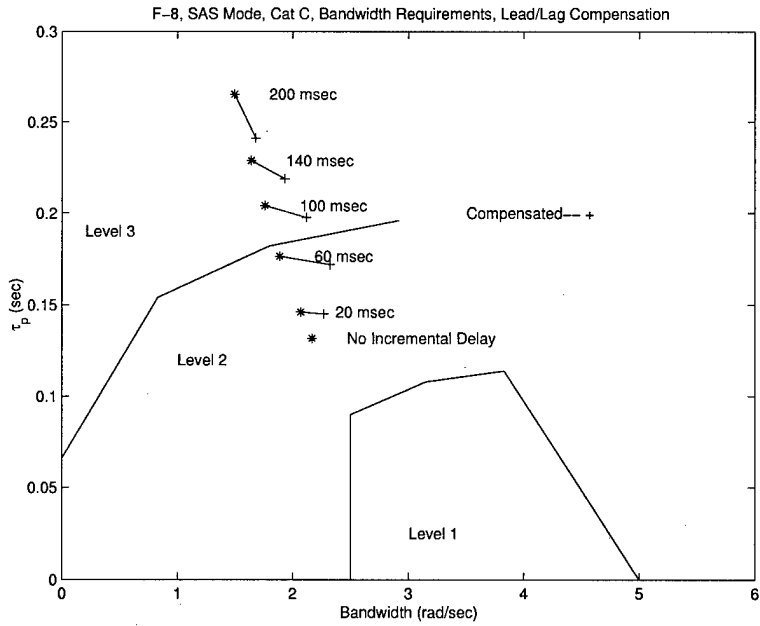


Figure 3.17 F-8 DFBW, Landing Task, Pitch SAS, Lead/Lag Compensation



Neal-Smith Criteria results, see Figures 3.18 and 3.19 show that Lead/Lag compensation provides some improvement, but does not return handling qualities to the no delay baseline.

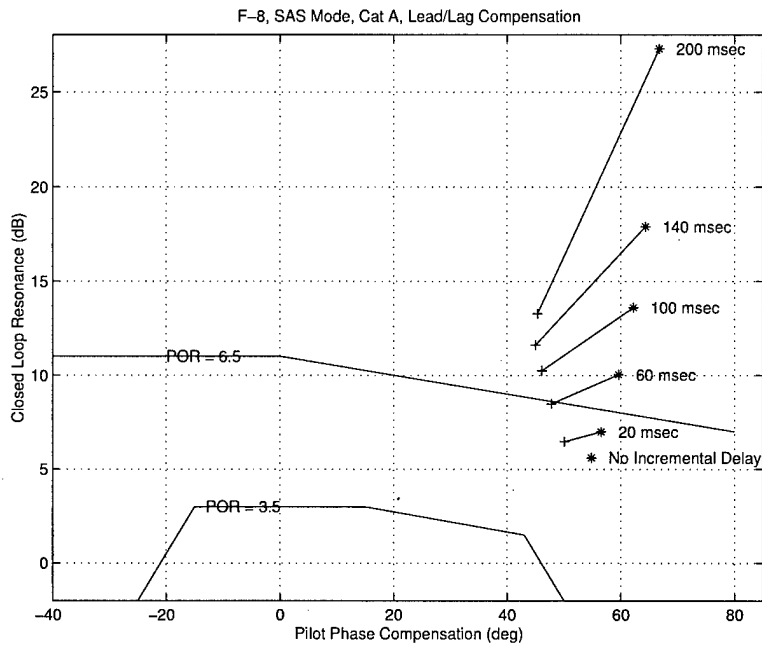


Figure 3.18 F-8 DFBW, Pitch SAS, Lead/Lag Compensation

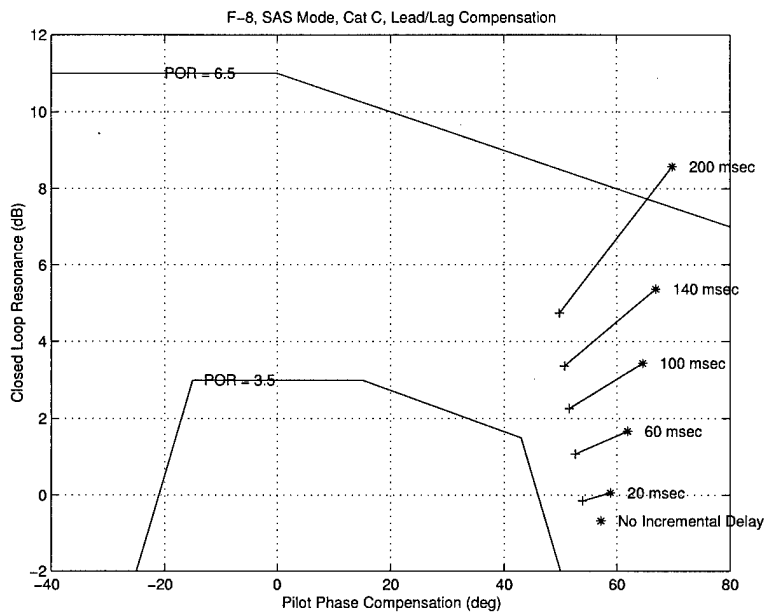


Figure 3.19 F-8 DFBW, Landing Task, Pitch SAS, Lead/Lag Compensation

Lead/Lag compensation appeared to provide better results in the case off the Princeton VRA. Figure 3.20 and 3.21 show that compensation provided significantly better handling qualities, although still not reaching the no delay case.

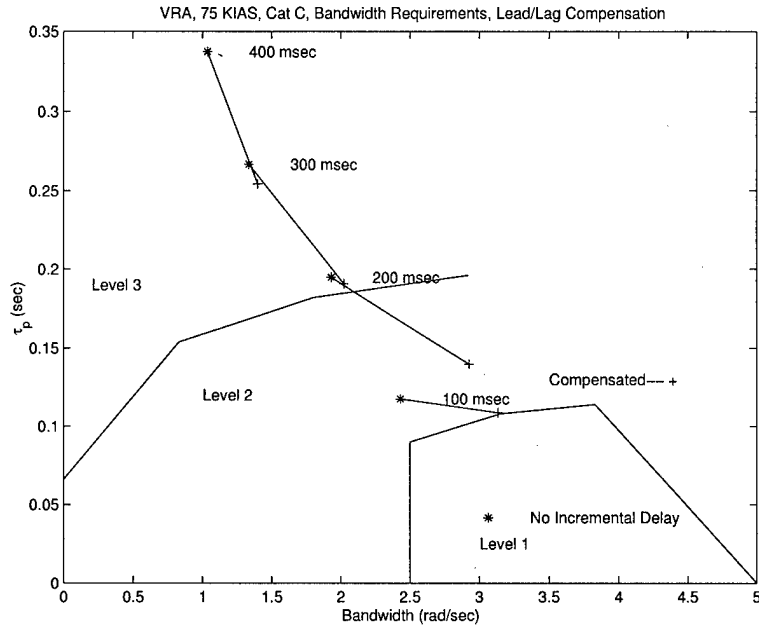


Figure 3.20 VRA, 75 KIAS Landing Task, Lead/Lag Compensation

Figures 3.22 and 3.23 again show significant improvement in handling qualities. Lead/Lag compensation did not return HQR to baseline, however, it did succeed in moving HQR back to Level 1 for delays of 100 and 200 msec.

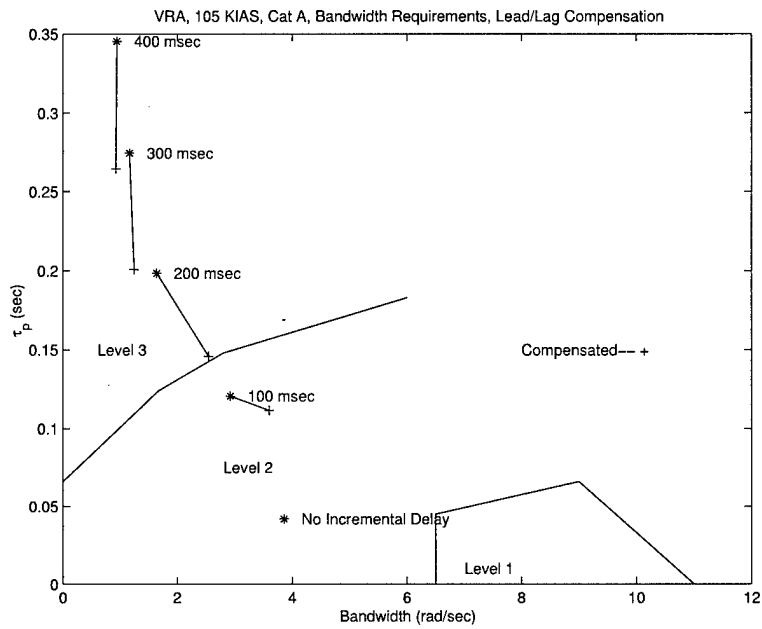


Figure 3.21 VRA, Formation Task, Lead/Lag Compensation

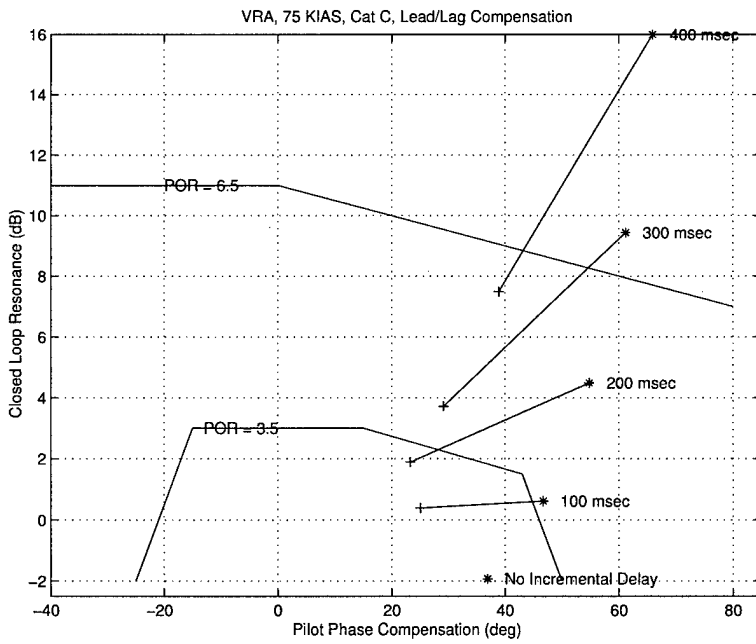


Figure 3.22 VRA, 75 KIAS Landing Task, Lead/Lag Compensation

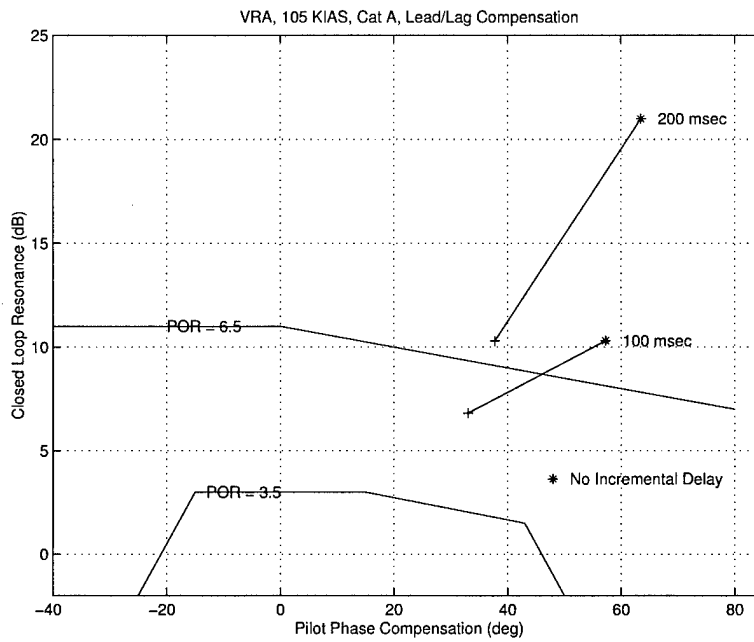


Figure 3.23 VRA, Formation Task, Lead/Lag Compensation

Previous studies (37, 39) have shown that the effects of time delay are more pronounced on “poorer” handling aircraft. A comparison of the Lead/Lag compensators efficacy on the F-8 and VRA shows that Lead/Lag compensation is also less effective in restoring acceptable handling qualities on “poorer” handling aircraft. This is evident in the poor performance of Lead/Lag compensation on the Utility UAV. Figures 3.24 and 3.25 show that compensation provided only slightly improved handling qualities.

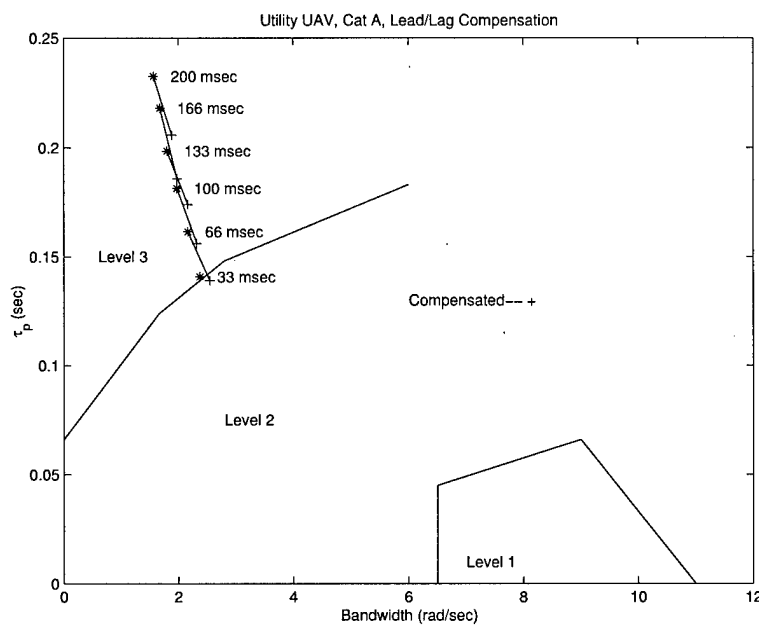


Figure 3.24 Utility UAV, Cat A Task, Lead/Lag Compensation, Bandwidth Criteria

**3.2.1 Lead/Lag Compensator Analysis.** An analysis of the Lead/Lag compensator tested in the above section was undertaken to determine if compensator performance could be improved.

**3.2.1.1 Compensator Design.** Lead compensation is a popular classical design technique used to improve system stability and increase damping. The techniques used to design such classical compensators are well established. An example of which is the procedure discussed in Franklin and Powell (19). A lead/lag

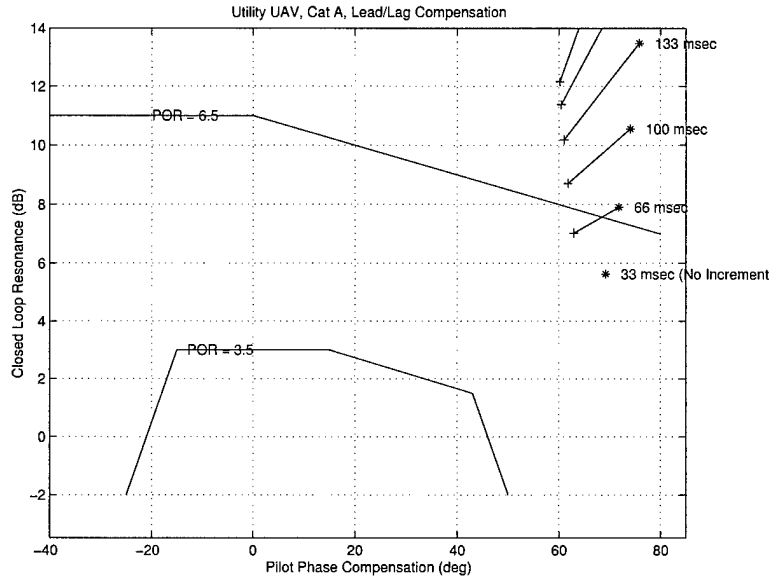


Figure 3.25 Utility UAV, Cat A Task, Lead/Lag Compensation, Neal-Smith Criteria

network of the form

$$G_c = K_d \frac{Ts + 1}{\alpha Ts + 1} \quad (3.1)$$

is designed by first calculating the amount of lead required,  $\phi_{max}$ , at frequency  $\omega_{max}$  and then determining the factor  $\alpha$  from

$$\alpha = \frac{1 - \sin\phi_{max}}{1 + \sin\phi_{max}} \quad (3.2)$$

The value of  $T$  is defined by

$$\omega_{max} = \frac{1}{T\sqrt{\alpha}} \quad (3.3)$$

The amount of lead required was determined by the amount of delay being compensated,  $\tau_d$ , at the desired frequency,  $\omega_{c_{des}}$ . For a Cat A task,  $\omega_{max}$  was set at 3.5 rads/sec and  $\phi_{max}$  determined from

$$\phi_{max} = \omega_{max}\tau_d \quad (3.4)$$

Bode diagrams for a compensator designed by the method discussed above and one designed by Crane's method outlined in Equation 2.21 on page 2-29 are presented in Figure 3.26. Phase difference from the 200 msec delay being compensated is displayed in Figure 3.27. One can see from Figure 3.26 that the Franklin-Powell

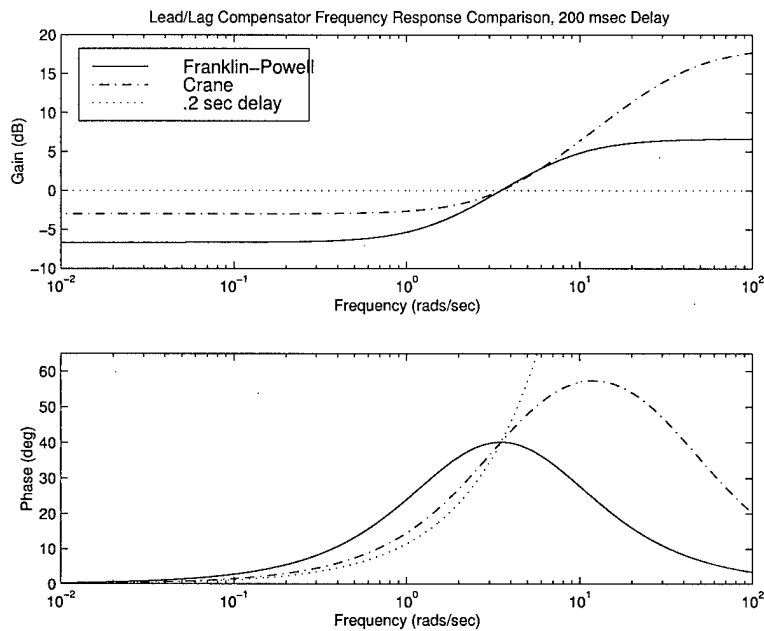


Figure 3.26 Lead/Lag Compensator Comparison

compensator distributes lead evenly on either side of  $\omega_{max}$  while the phase of the Crane compensator much more closely matches that of the 200 msec pure delay. Phase error below  $\omega_{c_{des}}$  is significantly reduced with the Crane compensator. This phase error produces poor results when Franklin-Powell is used in place of the Crane compensator in a Neal-Smith analysis, see Figure 3.28.



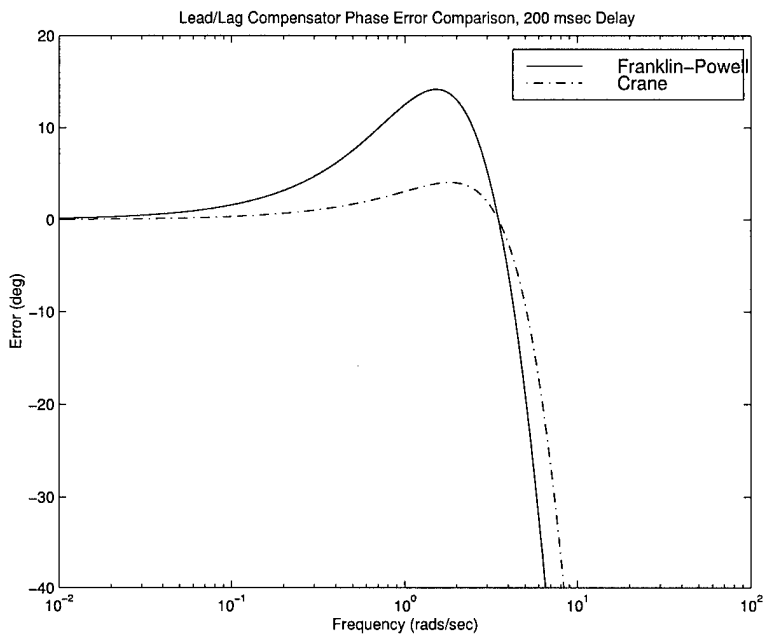


Figure 3.27 Lead/Lag Compensator Phase Error Comparison

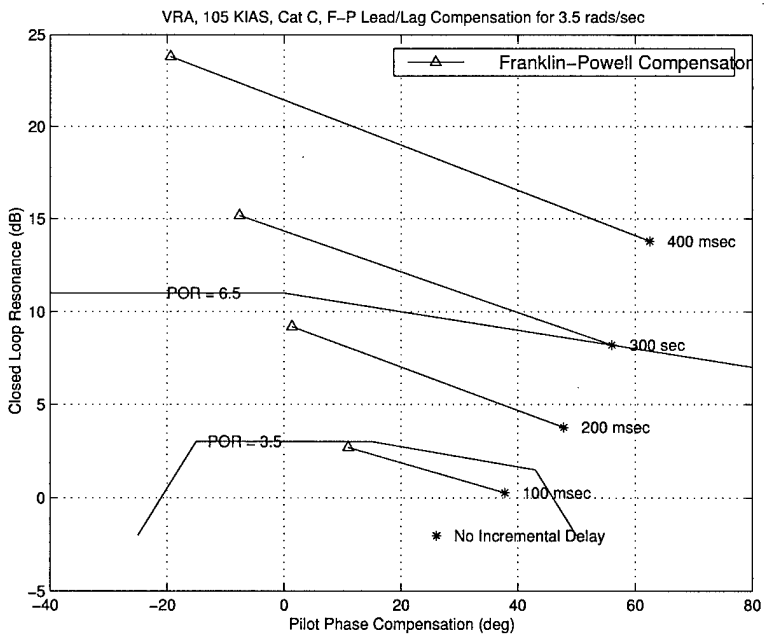


Figure 3.28 VRA, 105 KIAS Landing, Lead/Lag Compensation, Franklin-Powell

*3.2.1.2 Sensitivity to Gain.* The steady state gain of Lead/Lag compensators,  $K_d$ , tested by Crane in (12) was designed such that the gain of the entire compensator network was unity at the crossover frequency to minimize gain distortion around crossover. This was important in the Crane study due to the fact that pilots are more sensitive to gain distortion in this region and the studies focused on improving simulator performance. A compensation strategy that improved handling qualities at the expense of simulation fidelity was unacceptable. In the case of UAVs this may not be the case.

The pilot of a UAV will never sit in the cockpit and experience the “bare airframe” (or no delay, no compensation) handling qualities. He will instead be familiar only with the handling qualities experienced at the control station. As long as any gain distortion due to compensation does not adversely effect handling qualities, the UAV pilot most likely will not notice the difference having nothing other than the compensated aircraft dynamics as a basis for comparison.

In the Neal-Smith analysis the steady state gain is selected for proper crossover frequency. Any variation in compensator steady state gain will be offset by an opposite change in the Neal-Smith pilot gain. Thus the Neal-Smith technique is immune to gain effects and could not be used in gain sensitivity analysis.

Pilots have a fairly liberal “sweetspot” when it comes to gain selection. Extremes of too little and too much gain receive poor handling qualities ratings. However, pilots are very adaptive and will compensate for moderate gain variations with little effect on HQR.

*3.2.1.3 Sensitivity to Compensation Bandwidth Variations.* The bandwidth at which the Lead/Lag compensator is designed to compensate for the delay determines both the frequency at which phase error begins to increase substantially as well as the amount of gain distortion. It may be possible to select different compensation amounts for different tasks. However, delay compensation

would be more robust if the frequency at which phase error began to increase was constant and as high as practical. Figures 3.29 and 3.30 demonstrate that, as long as gain distortion does not adversely affect handling qualities, compensation for higher bandwidths will better negate the phase lag due to delay.

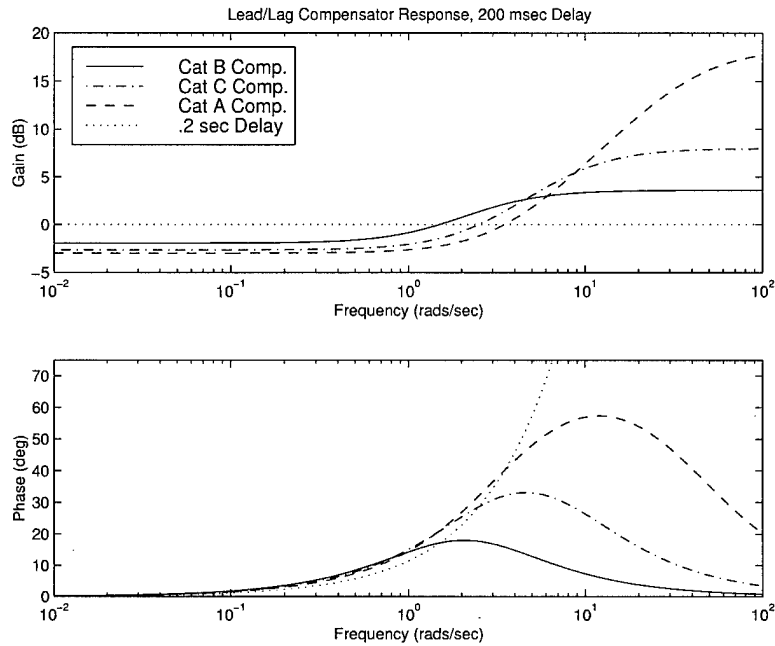


Figure 3.29 Lead/Lag Compensation at Varying  $\omega_c$

When Lead/Lag compensators designed for Cat A tasks were used in Cat C tasks, performance was found to increase. Comparing Figure 3.31 to Figure 3.22, one can see the improved performance. Unfortunately, attempting to compensate for delay at frequencies higher than 3.5 rads/sec displays the weakness of the Lead/lag compensation technique. As one seeks to compensate at higher frequencies, as well as longer delays, the maximum lead generated by the compensator increases as well. Gain distortion also increases. When compensating at 3.5 rads/sec, approximately 0.2 sec of delay is the maximum the Crane's technique can give and still maintain both pole and zero in the left half plane. The Matlab code written to generate the Lead/Lag compensator limits the pole to no greater than  $s = -70$ .

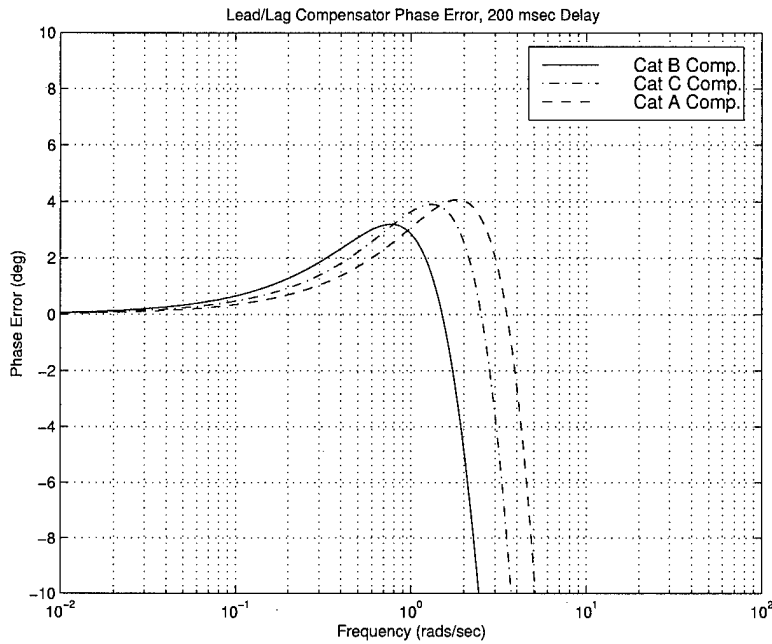


Figure 3.30 Phase error for Lead/Lag Compensation at Varying  $\omega_c$

3.2.1.4 *Sensitivity to Time Delay Variations.* In order for a delay compensation strategy to be of any use in operational UAVs it would need to be somewhat robust to variations in the amount of time delay in the control loop. While accurately determining the amount of delay present is certainly possible, it would be unrealistic to assume that the exact value was always known a priori. It would seem reasonable to assume that if the amount of time delay compensated was less than the actual time delay, the handling qualities would degrade from the fully compensated case, but it would be no worse than if the system had a small amount of extra delay. The real test comes when more delay has been compensated for than actually exists. Figures 3.32 and 3.33 demonstrate both situations.

The actual delay present is represented by the 200 msec pure delay. Bode plots of compensators designed for 100, 200, and 300 msec are compared against the actual delay. One can see that the compensator designed for 100 msec does not succeed in providing enough lead. It, however, has smaller gain distortion and does not provide too much lead below  $\omega_c$  which has been previously shown to decrease

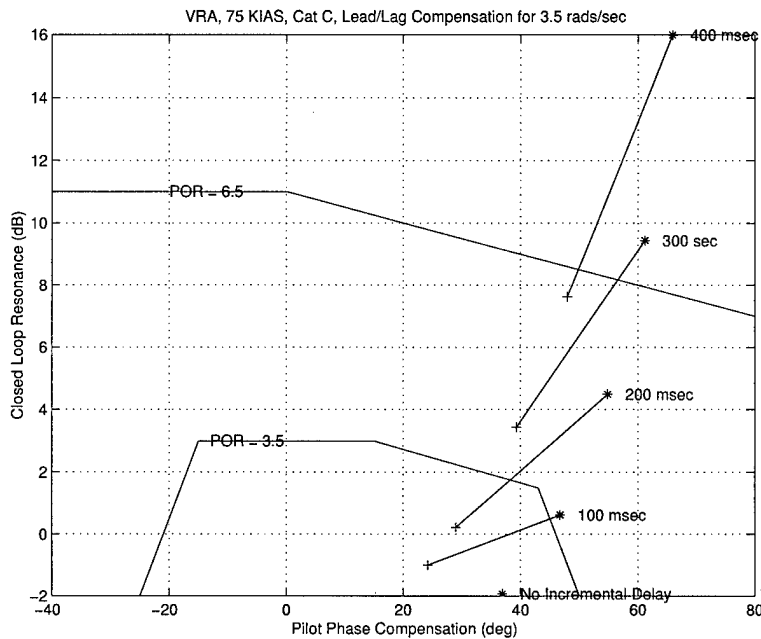


Figure 3.31 VRA, 105 KIAS Landing Task, Compensated for Cat A

performance. The 300 msec compensator, on the other hand, produces significant positive phase error as well as having more gain distortion than is necessary. Figure 3.34 shows Neal-Smith analysis for the VRA. Undercompensating results in improved handling qualities when compared to no compensation but does not provide optimum compensation. Overcompensating does not produce any instabilities and actually may improve handling qualities for small delays. Compensation for the 300 and 400 msec cases is already at the maximum, thus twice normal compensation coincides with normal compensation in these instances.

*3.2.2 Simulink Simulations.* Simulations were conducted to verify the results of the frequency domain methods as well as to study the effects of Lead/Lag compensation on gust rejection. The pilot model, Figure 3.35, used in the simulation was produced by the Neal-Smith analysis. It should be noted that pilot models produced by Neal-Smith tended to be pure lead compensators. An irrational transfer function was not compatible with Simulink and a fast pole at  $s = -20$  was added to rationalize the pilot model. The added dynamics were far enough above the pilot's

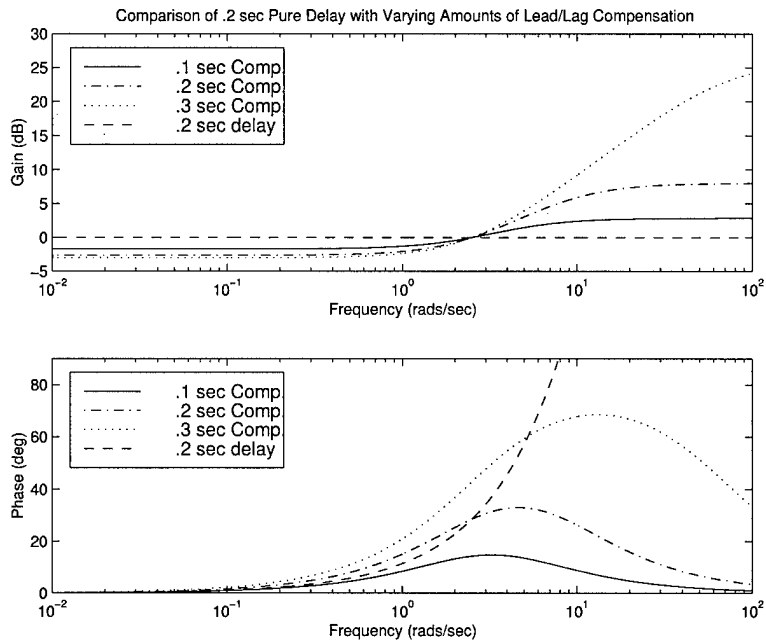


Figure 3.32 Comparison of Varying Amounts of Lead/Lag Compensation

compensation that they did not affect system behavior. The aircraft short period model, Figure 3.36, was modelled in state space in order to more easily inject the gust disturbance.

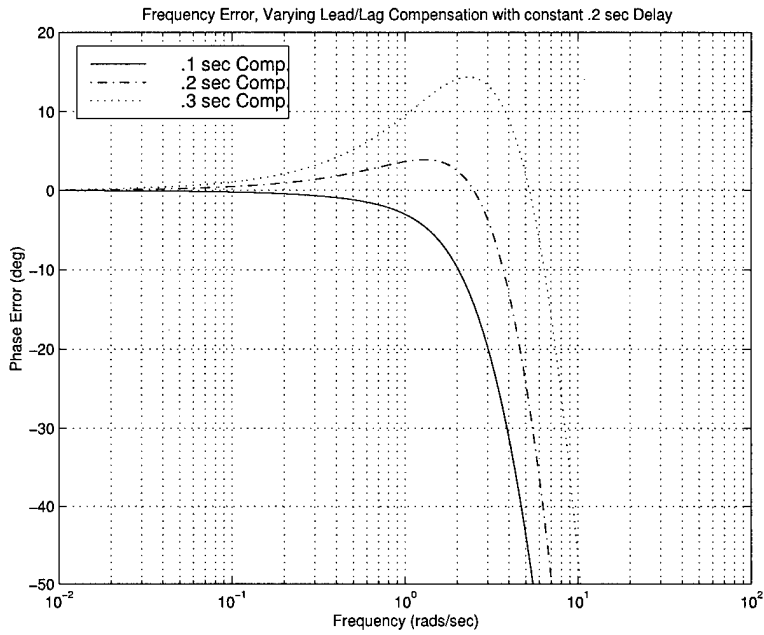


Figure 3.33 Phase Error of Varying Amounts of Lead/Lag Compensation

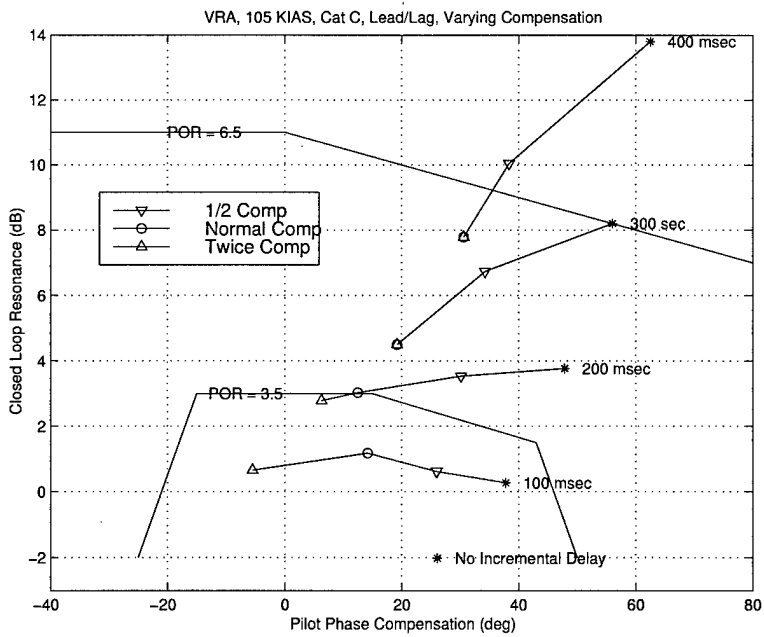


Figure 3.34 VRA, 105 KIAS Landing, Varying Amounts of Lead/Lag Compensation

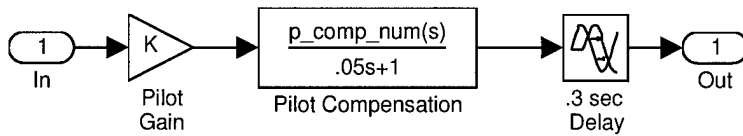


Figure 3.35 Pilot Model Used In Simulation

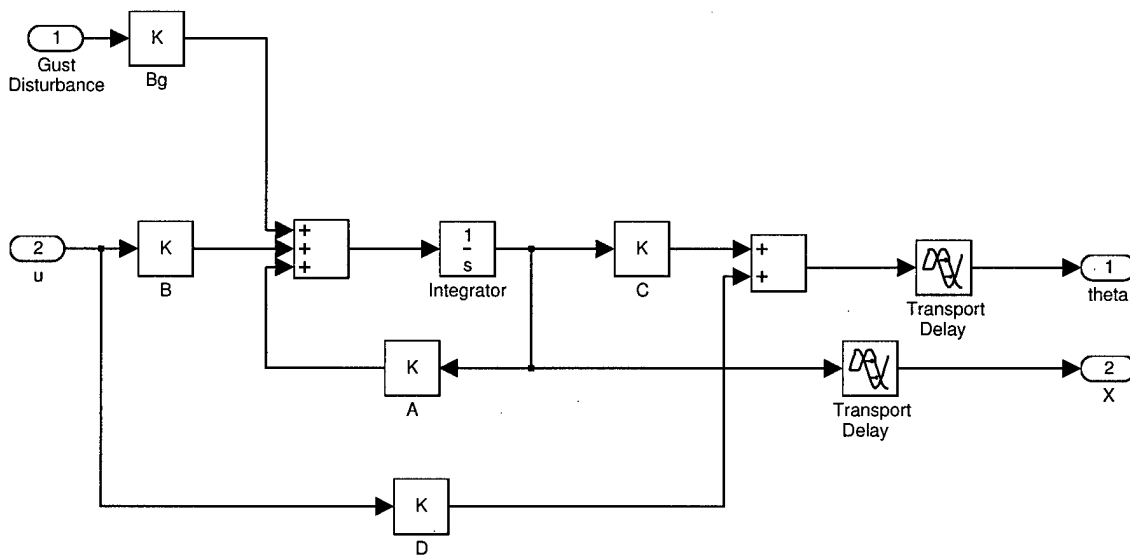


Figure 3.36 Aircraft Short Period Model



The vertical gust profile was a  $1 - \cos(\omega t)$  where  $\omega$  was 3.5 rads/sec. The maximum gust was 17.5 ft/sec, 10 percent of the VRA airspeed during landing at 105 KIAS. The tracking command used was a “smoothed step” input (the first half of the gust profile) of 10 degrees. Simulink model diagrams for the VRA tracking and gust rejection analysis are shown in Figures 3.37 and 3.38 respectively. The VRA 105 KIAS Landing dynamics were chosen as typical for analysis. F-8 DFBW SAS model analysis is presented for completeness in Appendix B.

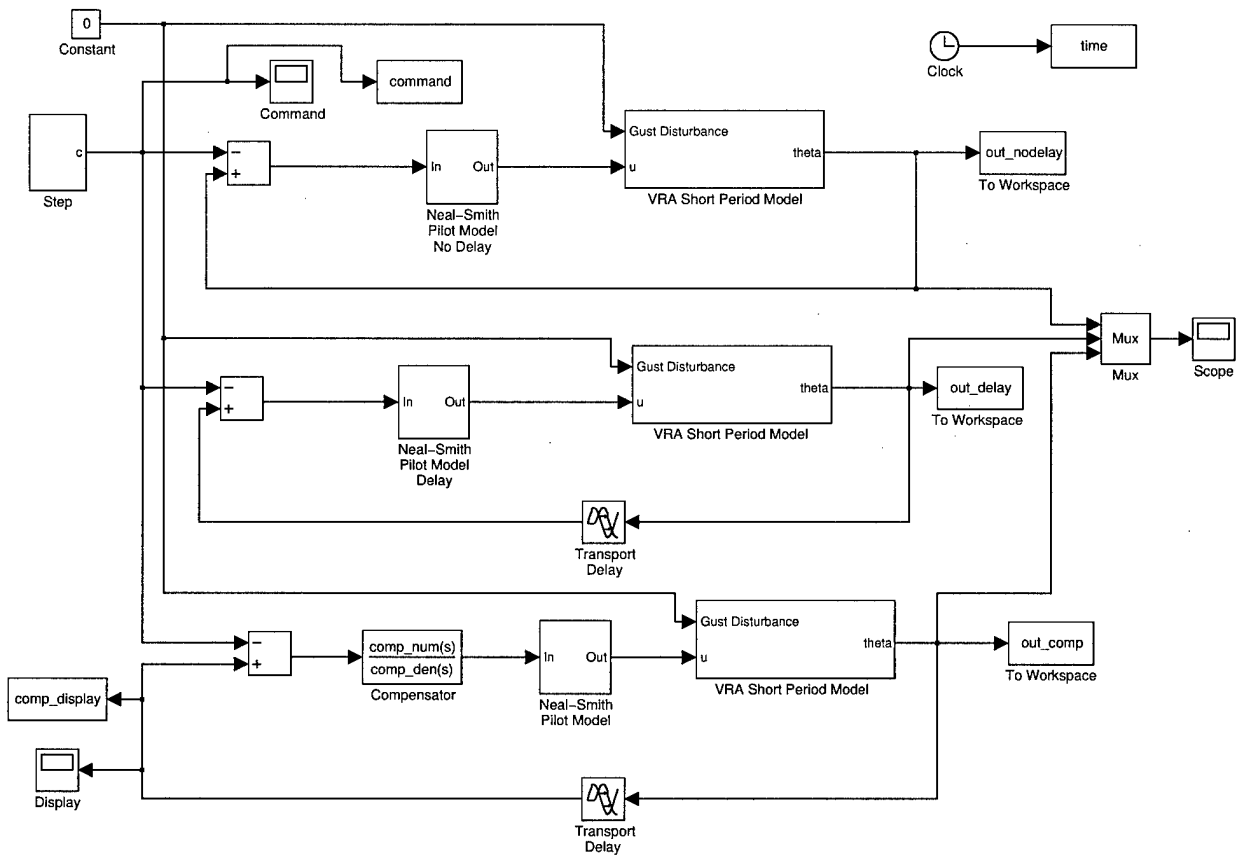


Figure 3.37 VRA Command Tracking Model

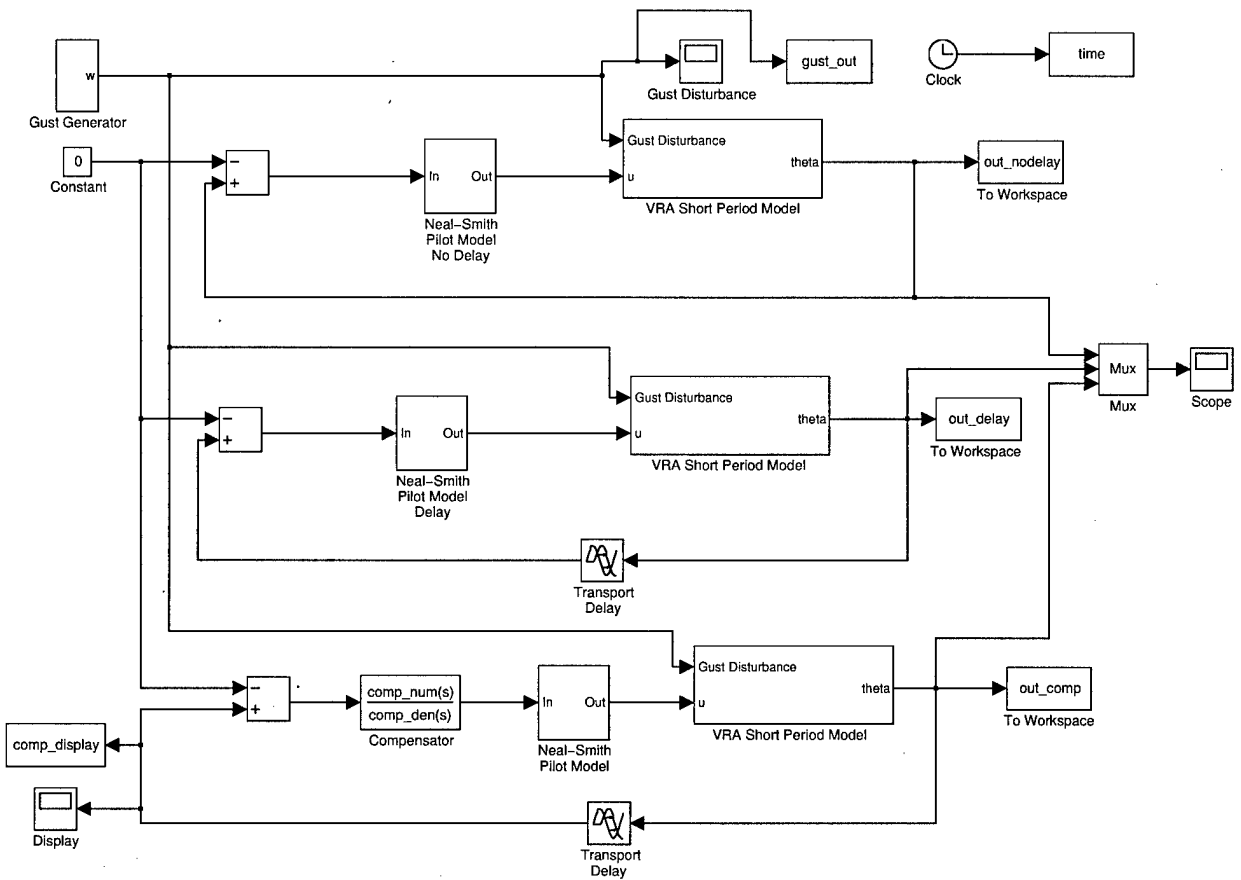


Figure 3.38 VRA Gust Rejection Model

Simulations for command tracking with feedback transport delays of 100, 200, 300, and 400 msec were run. Pitch angle output for each case is displayed in the following figures.

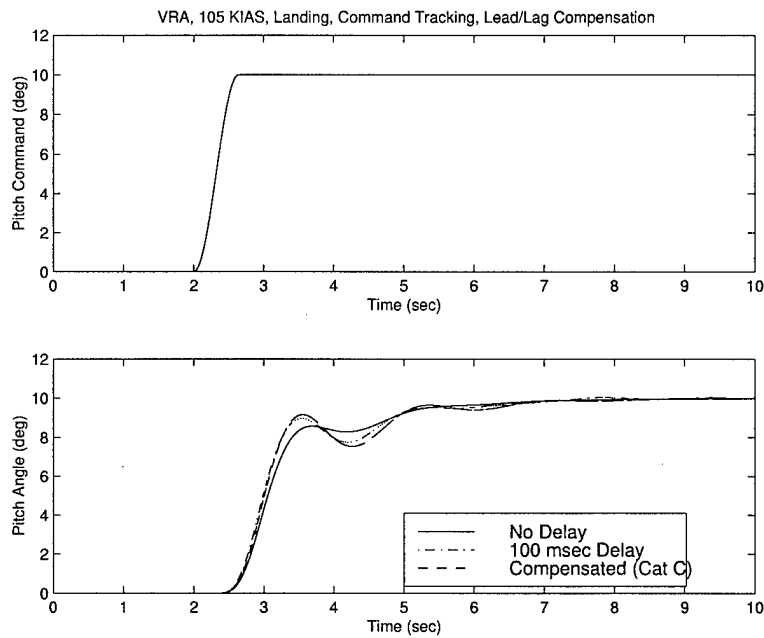


Figure 3.39 VRA Command Tracking, 100 msec Delay, Lead/Lag Compensation

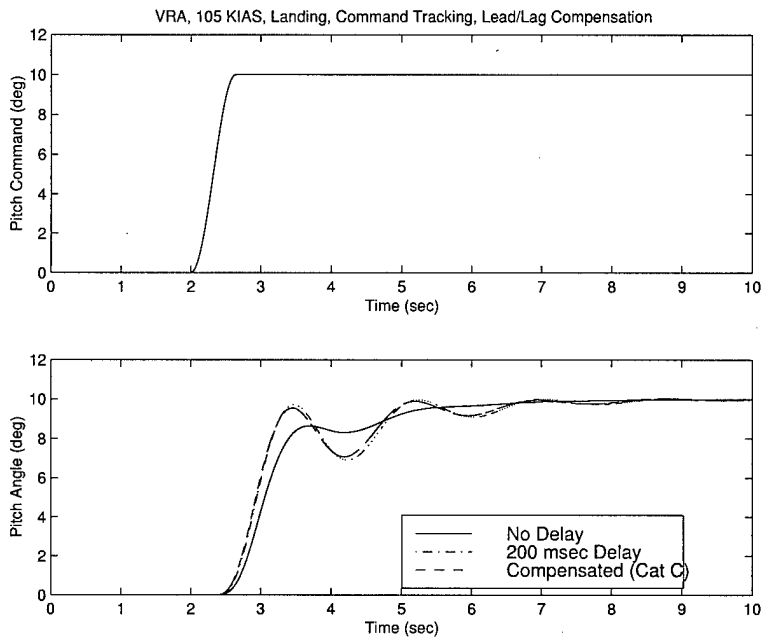


Figure 3.40 VRA Command Tracking, 200 msec Delay, Lead/Lag Compensation

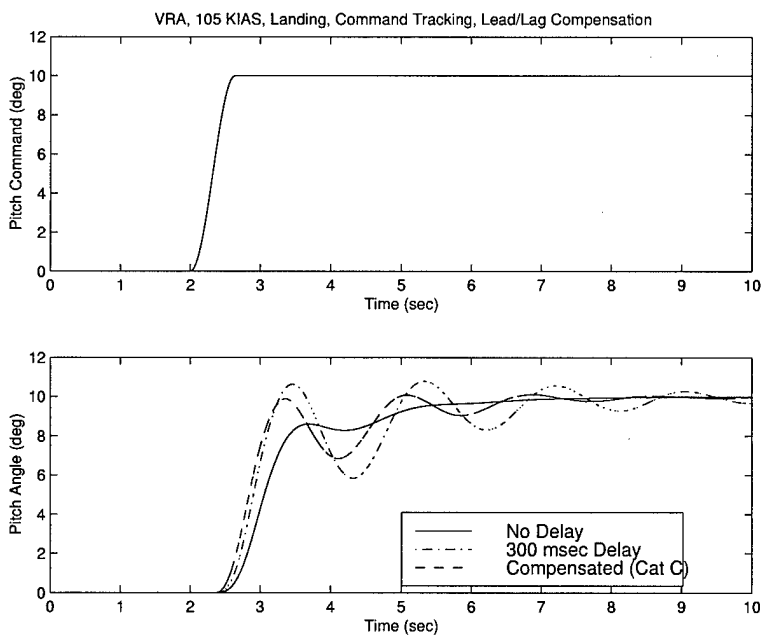


Figure 3.41 VRA Command Tracking, 300 msec Delay, Lead/Lag Compensation

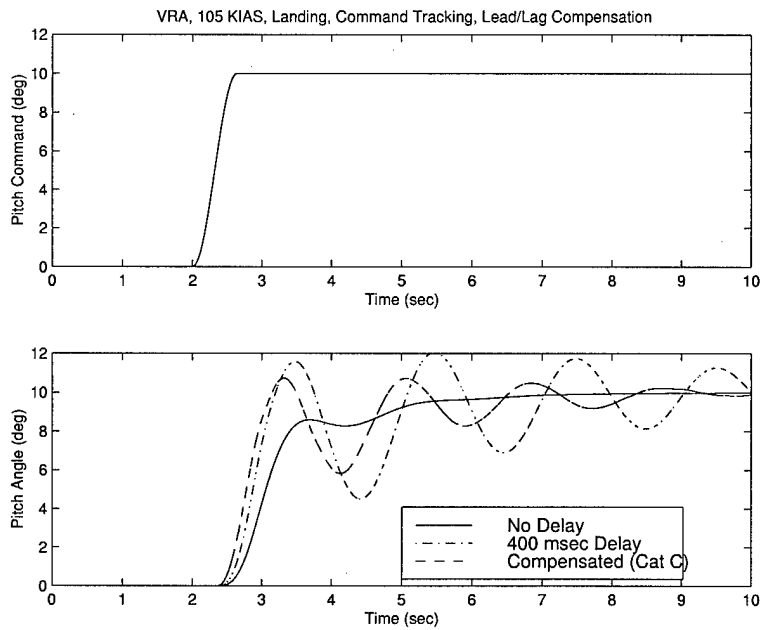


Figure 3.42 VRA Command Tracking, 400 msec Delay, Lead/Lag Compensation

Likewise simulations for gust rejection were run. Pitch angle output showed oscillations growing with increasing time delay similar to the command tracking examples in Figures 3.39 to 3.42. Pitch angle response for 400 msec delay was typical and is shown in the Figures 3.43.

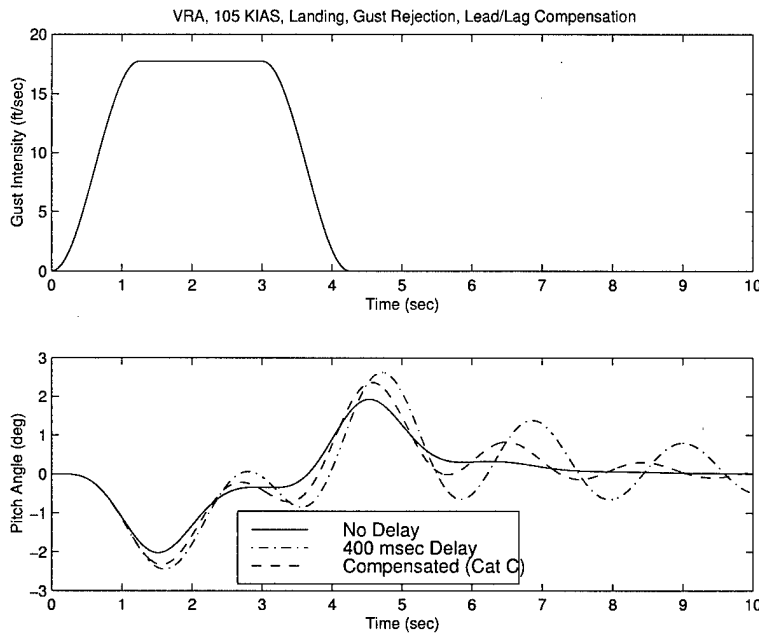


Figure 3.43 VRA Gust Rejection, 400 msec Delay, Lead/Lag Compensation

Since the pilot model used in the simulations was determined in the Neal-Smith analysis, one would expect there to be good agreement between the frequency domain and time domain evaluations of the compensation. This agreement is evident upon comparing Figures 3.39, 3.40, 3.41, and 3.42, to the closed loop resonance predicted in Figure 3.22. Since distributed time delays were used in the time domain simulation, the strong correlation between analysis methods confirms that lumping delays together for simpler frequency domain analysis is a valid technique.

### 3.3 State Predictor Compensation

*3.3.1 Compensator Design.* State Predictor compensation as discussed in chapter two and Equation 2.29 was applied to the F-8 DFBW data. Refer to

Figure 3.44 for a block diagram of the compensated system. In this diagram,  $\tilde{z}$  is

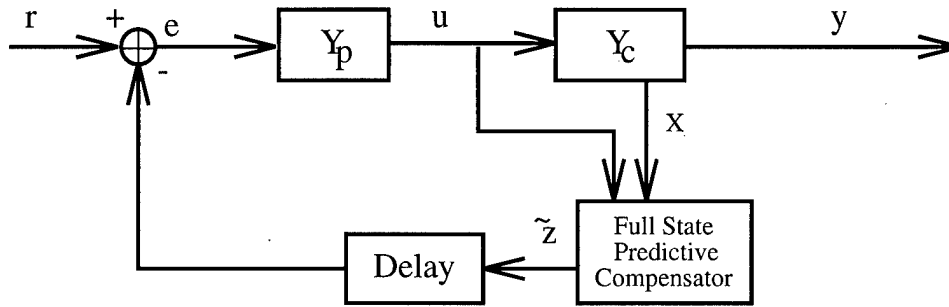


Figure 3.44 Full State Predictor Compensated System

the predicted output of the system  $\tau_d$  seconds into the future. When delayed by  $\tau_d$  seconds the signal becomes the predicted current, i.e. undelayed, output of the plant. This is the signal displayed to the pilot. The transfer function used in Bandwidth and Neal-Smith analysis was the transfer function from the pilot's output,  $u$ , to the error,  $e$ . When  $Y_c$  is presented in state space, see Figure 3.45, one can see the

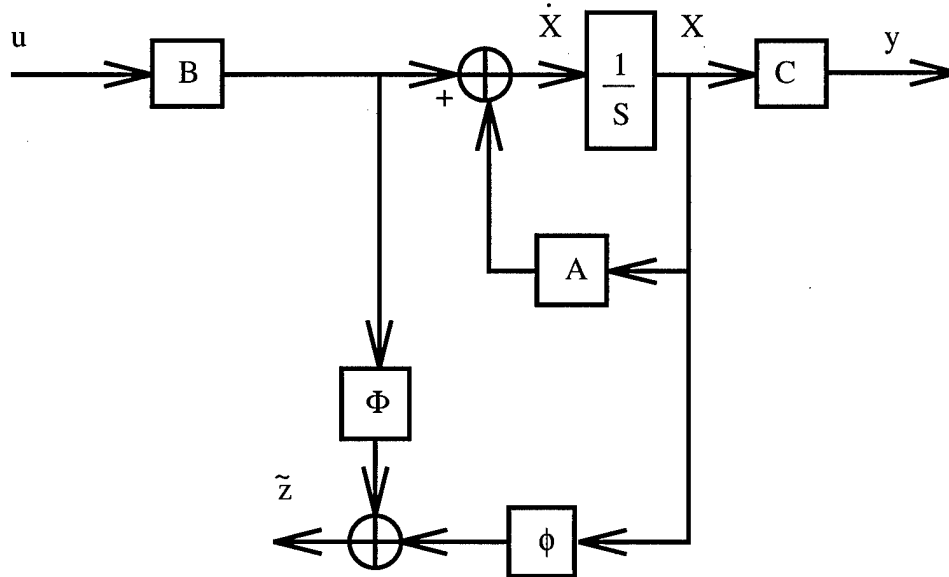


Figure 3.45 Full State Feedback Predictor Compensator

compensated system may be written in the classical presentation of a state space

system,

$$\dot{\mathbf{x}}(t) = \mathbf{A}\mathbf{x}(t) + \mathbf{B}u(t) \quad (3.5)$$

$$y(t) = \mathbf{C}\mathbf{x}(t) + \mathbf{D}u(t) \quad (3.6)$$

as

$$\dot{\mathbf{x}}(t) = \mathbf{A}\mathbf{x}(t) + \mathbf{B}u(t) \quad (3.7)$$

$$\tilde{z} = \mathbf{C}\phi\mathbf{x}(t) + \mathbf{C}\Phi\mathbf{B}u(t) \quad (3.8)$$

Thus a transfer function for the compensated system may be written

$$Y_{c_{comp}} = \hat{\mathbf{C}}(s\mathbf{I} - \mathbf{A})^{-1}\mathbf{B} + \hat{\mathbf{D}} \quad (3.9)$$

where  $\hat{\mathbf{C}} = \mathbf{C}\phi$  and  $\hat{\mathbf{D}} = \mathbf{C}\Phi\mathbf{B}$ ,  $\phi$  and  $\Phi$  are defined as

$$\phi = e^{\mathbf{A}(t-\tau)} \quad (3.10)$$

$$\Phi = \int_0^{\tau_d} \phi(t, \tau) d\tau \quad (3.11)$$

A closed form solution for  $\Phi$  is calculated by assuming that the input,  $u$ , remains constant throughout the delay interval. Sampling delays and incremental feedback delay were lumped together into a single system delay when calculating  $\phi$  and  $\Phi$ .

*3.3.2 Full State Feedback Predictor Results.* Bandwidth Criteria results, see Figures 3.46 and 3.47 show excellent success at restoring delay free handling qualities.

Neal-Smith Criteria results, see Figures 3.48 and 3.49, also show state predictor compensation essentially returning system performance to the no delay baseline.



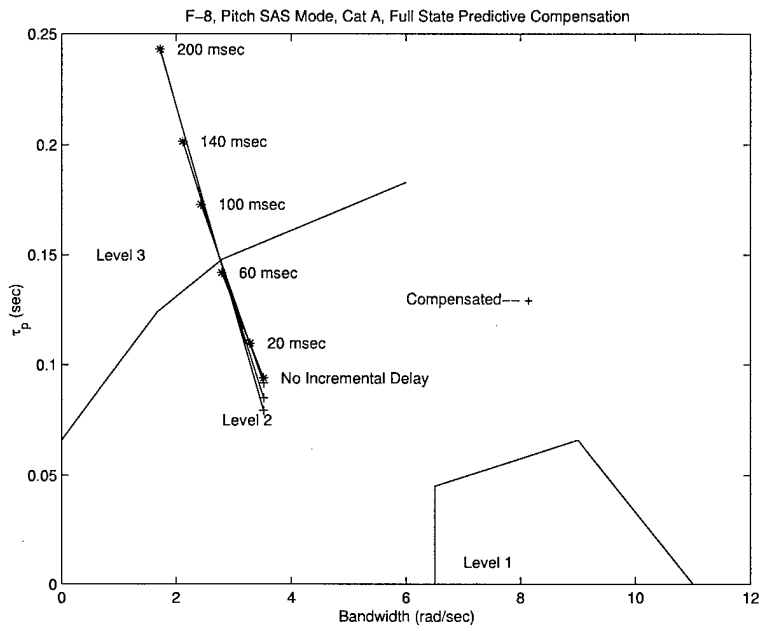


Figure 3.46 F-8 DFBW, Pitch SAS, State Predictor Compensation

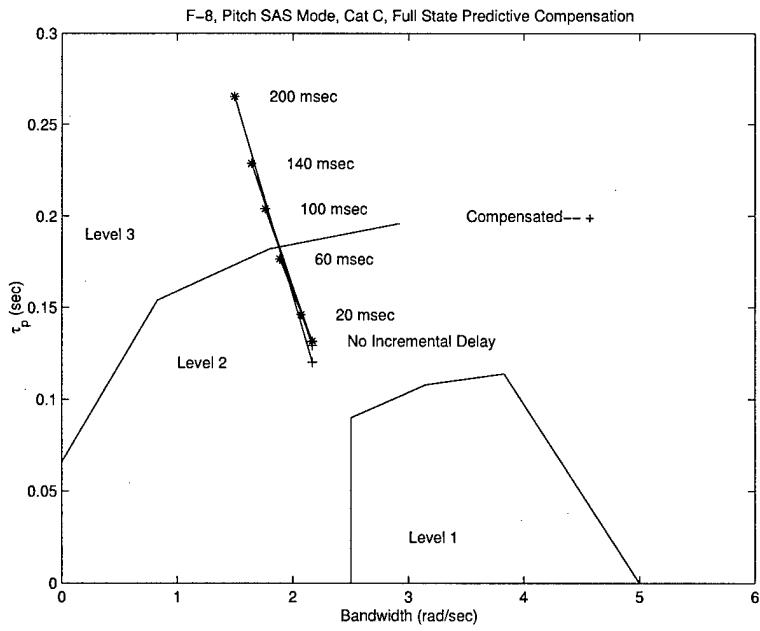


Figure 3.47 F-8 DFBW, Landing Task, Pitch SAS, State Predictor Compensation

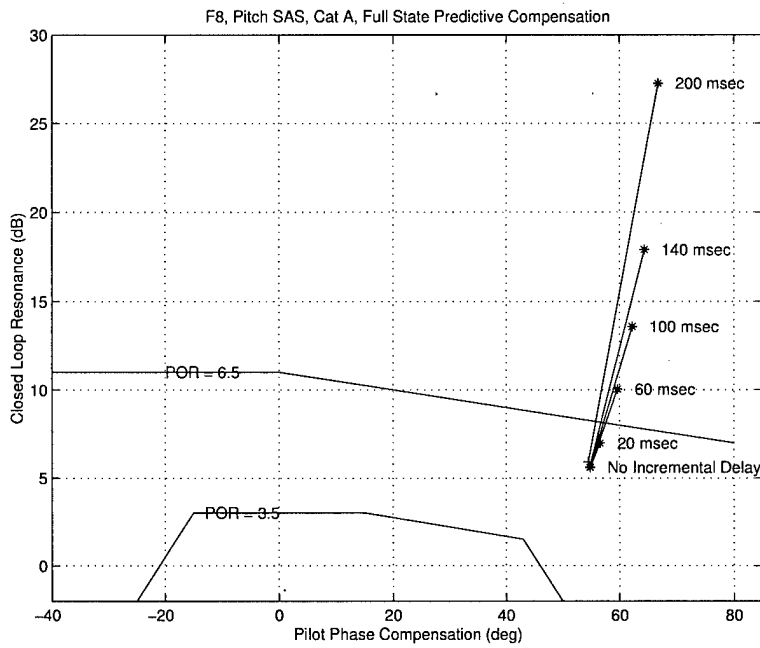


Figure 3.48 F-8 DFBW, Pitch SAS, State Predictor Compensation

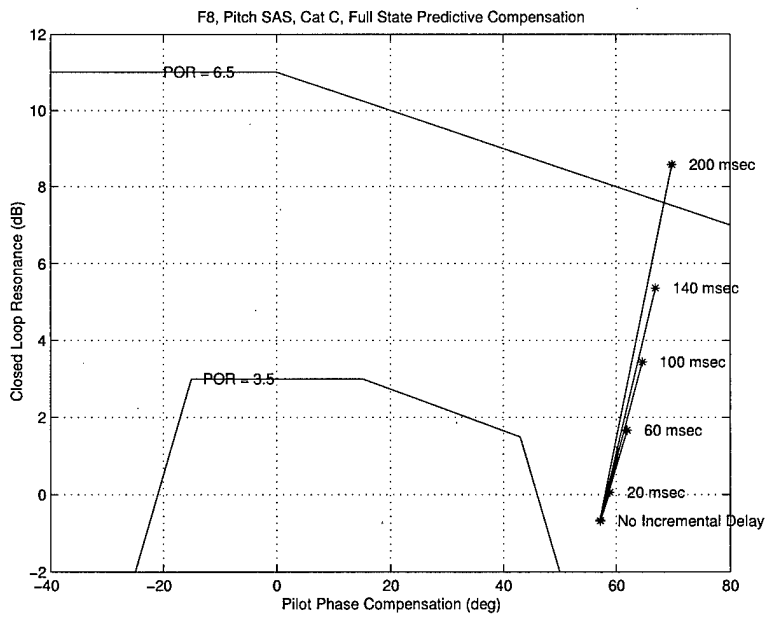


Figure 3.49 F-8 DFBW, Landing Task, Pitch SAS, State Predictor Compensation

State predictor compensation provided similar results in the case off the Princeton VRA. Figures 3.50 and 3.51 show that compensation returned HQR to the no delay case for smaller  $\tau_d$  and significantly improved for larger delays. Figures 3.52

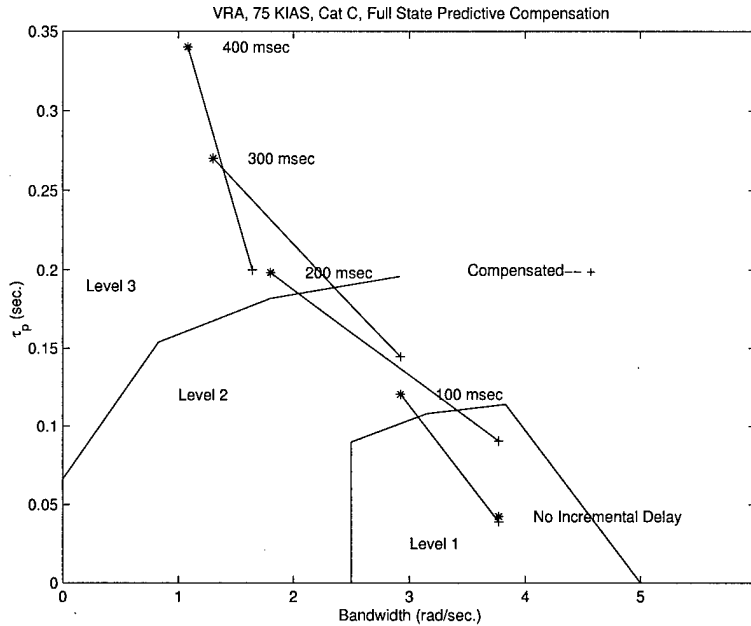


Figure 3.50 VRA, 75 KIAS Landing Task, State Predictor Compensation

and 3.53 again show similar recovery of handling qualities.

Full state compensation proved effective on the Utility UAV as well. Compensation returned HQ to the no delay case for small incremental time delays and greatly improved HQ for long time delays, see Figures 3.54 and 3.55.

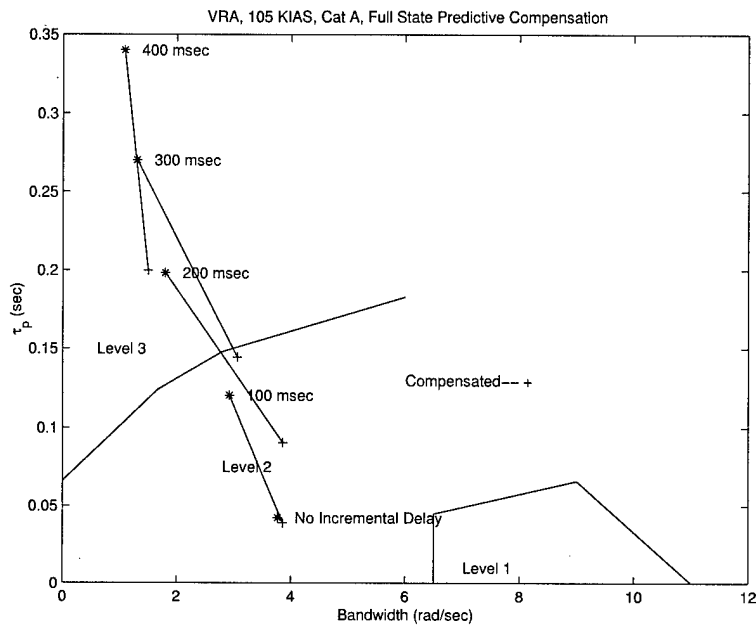


Figure 3.51 VRA, Formation Task, State Predictor Compensation

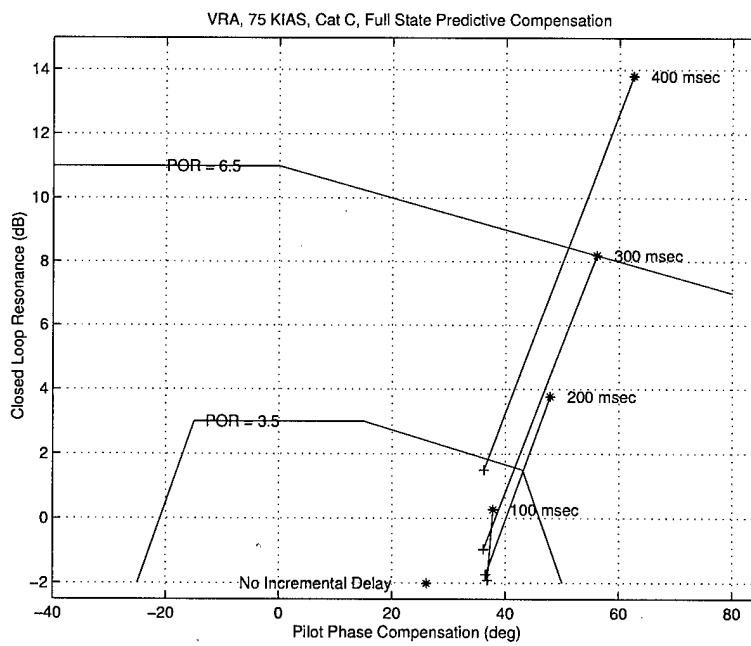


Figure 3.52 VRA, 75 KIAS Landing Task, State Predictor Compensation

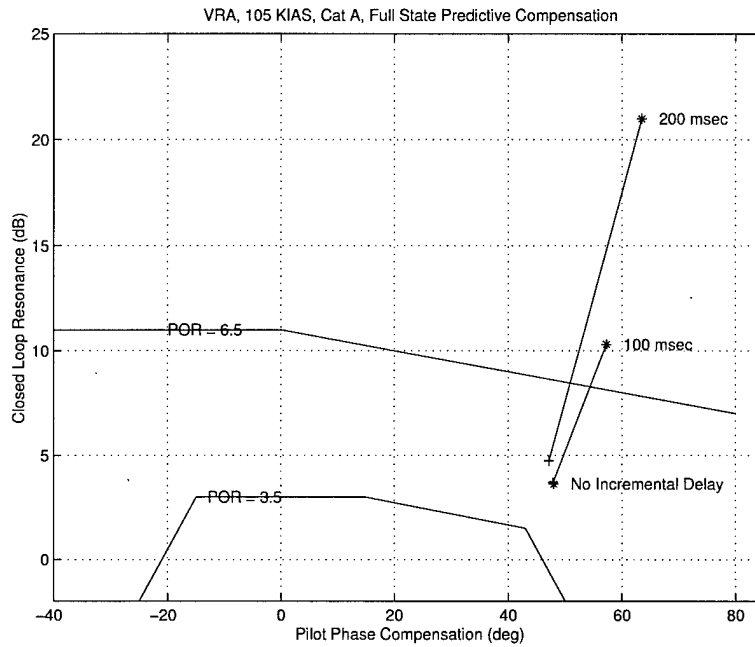


Figure 3.53 VRA, Formation Task, State Predictor Compensation

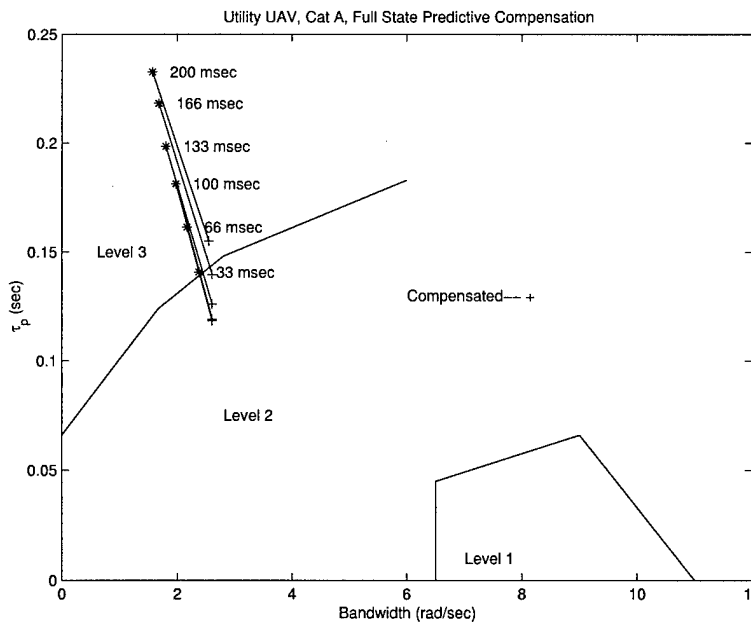


Figure 3.54 Utility UAV, Cat A Task, Full State Compensation, Bandwidth Criteria

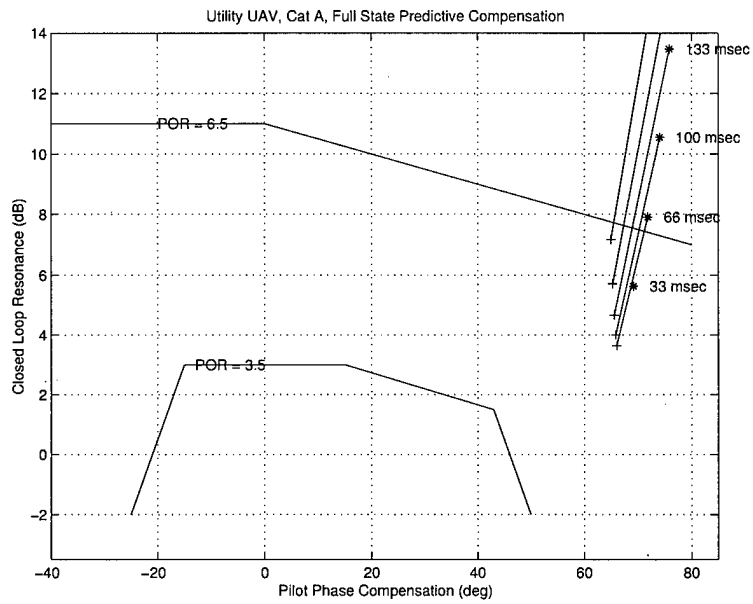


Figure 3.55 Utility UAV, Cat A Task, Full State Compensation, Neal-Smith Criteria

*3.3.3 State Predictor Compensator Analysis.* Like the Lead/Lag compensator, the state predictor is subject to some parameter variations. Since the state predictor is a model based technique, it is sensitive to uncertainties in the plant model. Sensitivity to time delay variations was again an issue. The determination of the actual time delay in the closed loop system could prove to be inaccurate and lead to improper compensation since the time delay,  $\tau_d$ , is used in calculating the  $\Phi$  matrix. Finally, since full state feedback is often impractical, output feedback based predictive compensation was examined.

*3.3.3.1 Sensitivity to Model Uncertainties.* The Neal-Smith analysis technique had proven to be the best indicator of the effects of delay on HQR and was chosen as the tool used to examine the sensitivity of the state predictor compensator to uncertainties in the plant. This was accomplished by forming the  $\phi$  and  $\Phi$  matrices with a perturbed  $\mathbf{A}$  matrix. The short period parameters,  $\omega_{n_{sp}}$ ,  $\zeta_{sp}$ ,  $T_{\theta_2}$ , and  $K_\theta$  of both the VRA and F-8 were perturbed by 50 percent in either direction. Neal-Smith analysis was accomplished for each case and plotted together to present a picture of the sensitivity to perturbation in each parameter. The results for the VRA are presented in Figures 3.56, 3.57, 3.58, and 3.59.

Results for the F-8 DFBW are displayed in Figures 3.60, 3.61, 3.62, and 3.63.

One can clearly see that the results are only mildly affected by a very large ( $\mp 50$  percent) perturbation. The handling qualities are still dramatically improved.

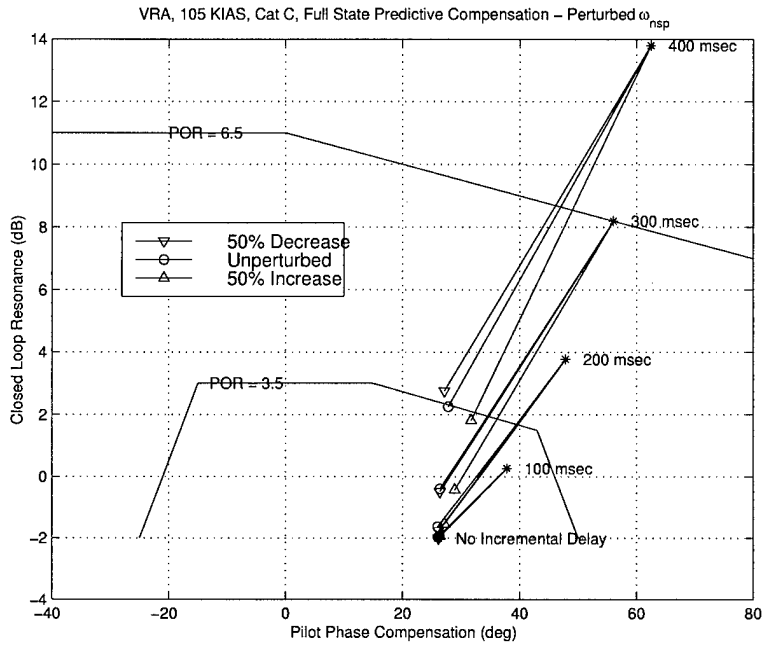


Figure 3.56 VRA, 105 KIAS Landing Task, Perturbed  $\omega_{nsp}$

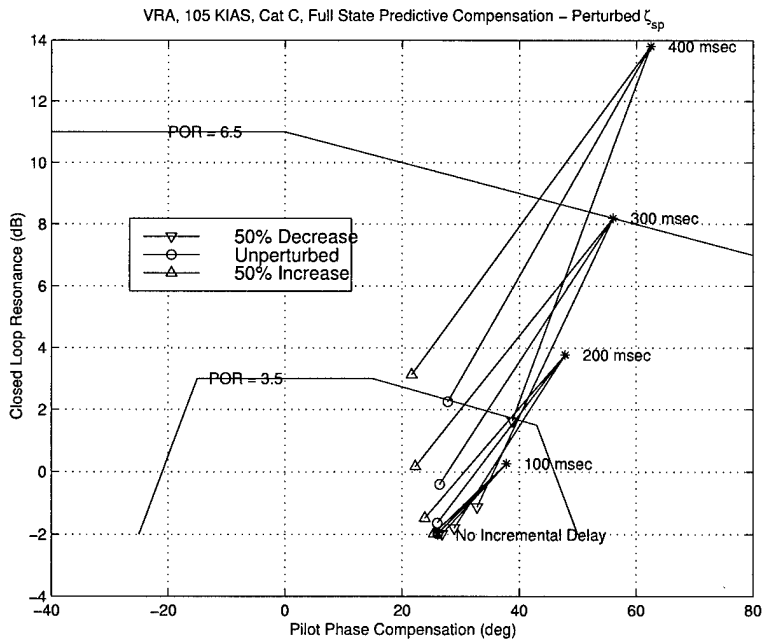


Figure 3.57 VRA, 105 KIAS Landing Task, Perturbed  $\zeta_{sp}$



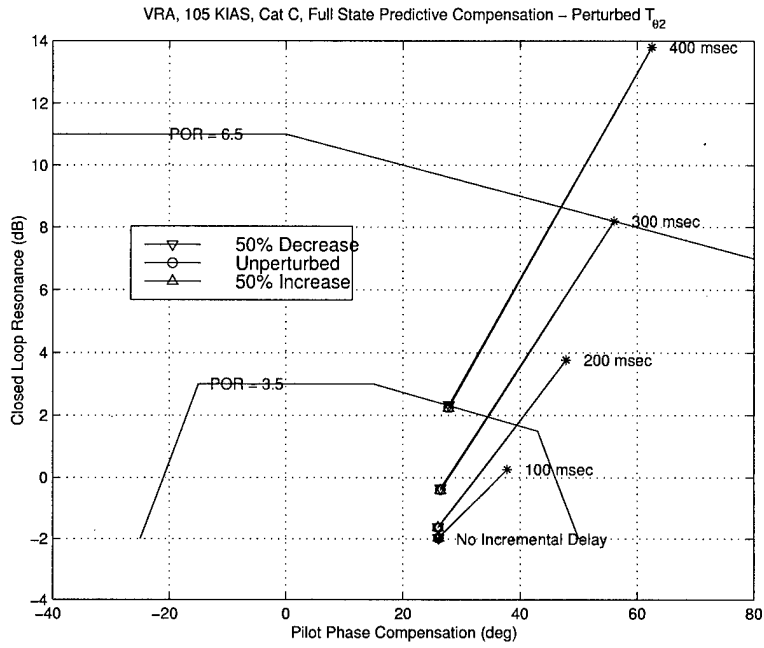


Figure 3.58 VRA, 105 KIAS Landing Task, Perturbed  $T_{\theta_2}$

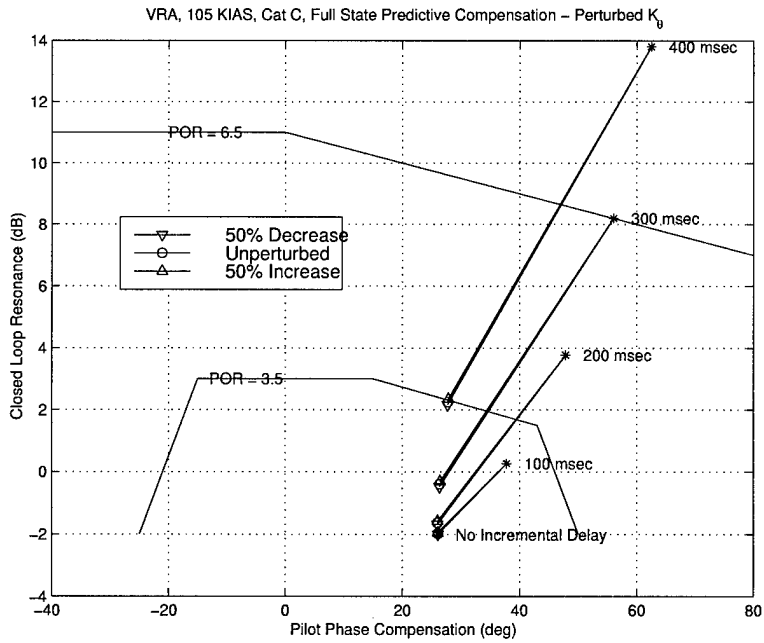


Figure 3.59 VRA, 105 KIAS Landing Task, Perturbed  $K_{\theta}$

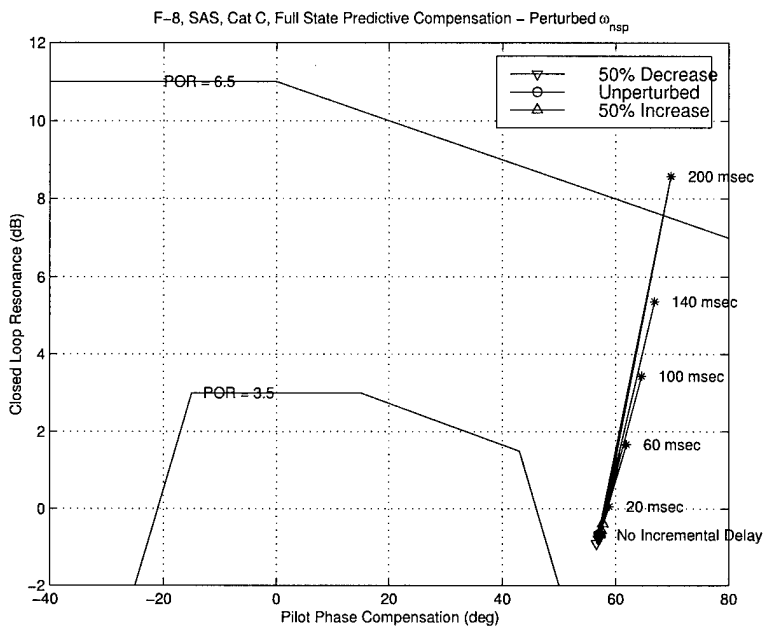


Figure 3.60 F-8 DFBW, Pitch SAS, Landing Task, Perturbed  $\omega_{nsp}$

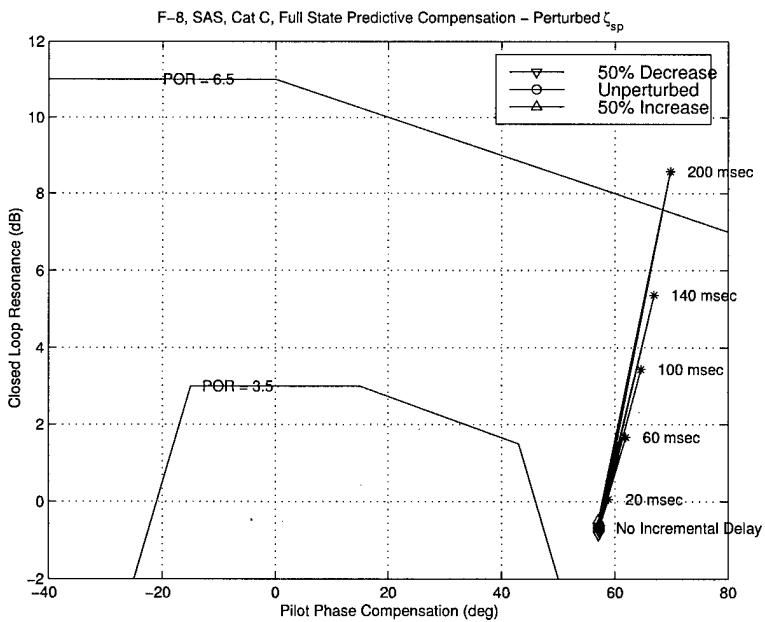


Figure 3.61 F-8 DFBW, Pitch SAS, Landing Task, Perturbed  $\zeta_{sp}$

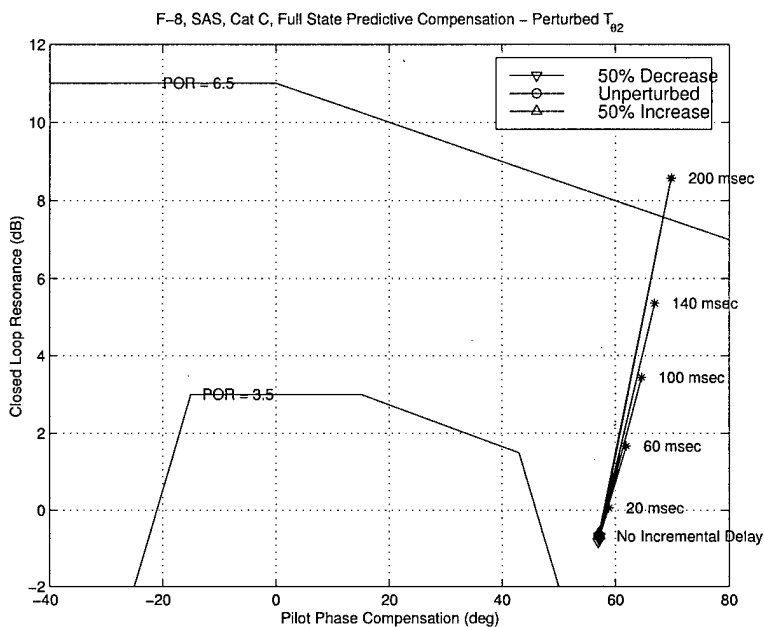


Figure 3.62 F-8 DFBW, Pitch SAS, Landing Task, Perturbed  $T_{\theta_2}$

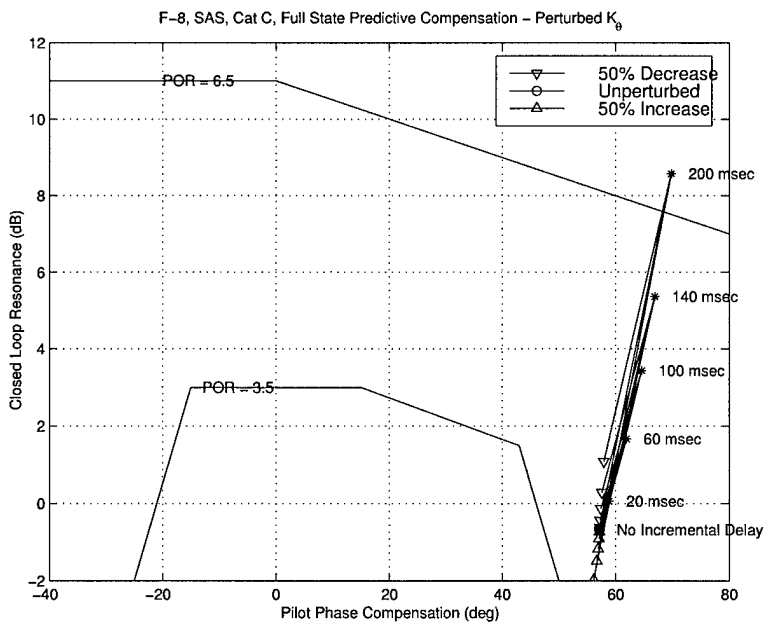


Figure 3.63 F-8 DFBW, Pitch SAS, Landing Task, Perturbed  $K_{\theta}$

3.3.3.2 *Sensitivity to Time Delay Variations.* Large variations in the amount of delay compensated were tested to determine the state predictor sensitivity to inaccurate knowledge of the actual delay present. Figure 3.64 demonstrates that, except for the extreme case of 400 msec delay with 800 msec compensation, the state predictor is quite robust to time delay uncertainty. Figure 3.65 provides 50 msec increments to better illustrate this point. The 300 msec delay, VRA at

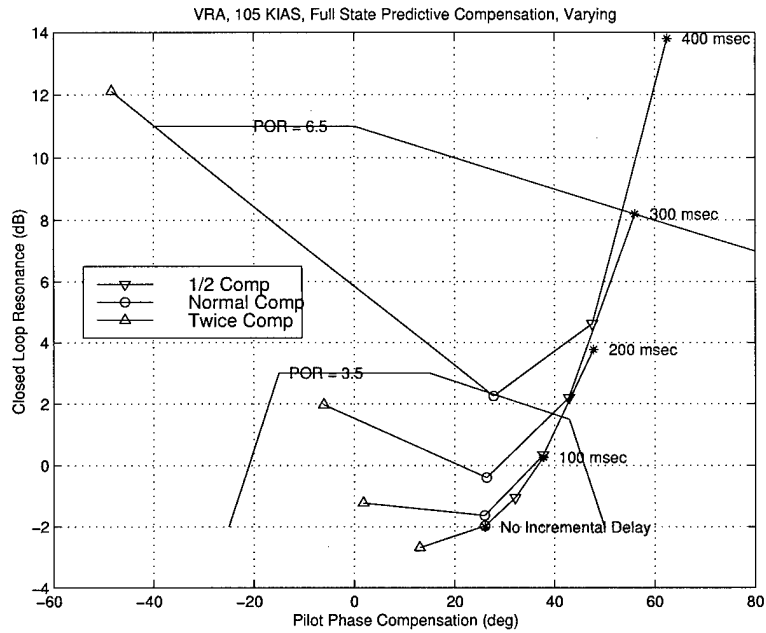


Figure 3.64 VRA, 105 KIAS, State Predictor Compensation, Varying Amounts

105 KIAS, Category C task demonstrates typical response. Compensation from 200 msec to 500 msec all produced Level 1 handling qualities contrasting sharply with the uncompensated case, borderline Level 3.

3.3.4 *Output Feedback Based Compensation.* Full state feedback is often unrealizable. In order to achieve it one must have access to and accurately measure every state in the plant. For this reason, output feedback is used along with an observer to recreate an estimate of the system state for use in feedback.

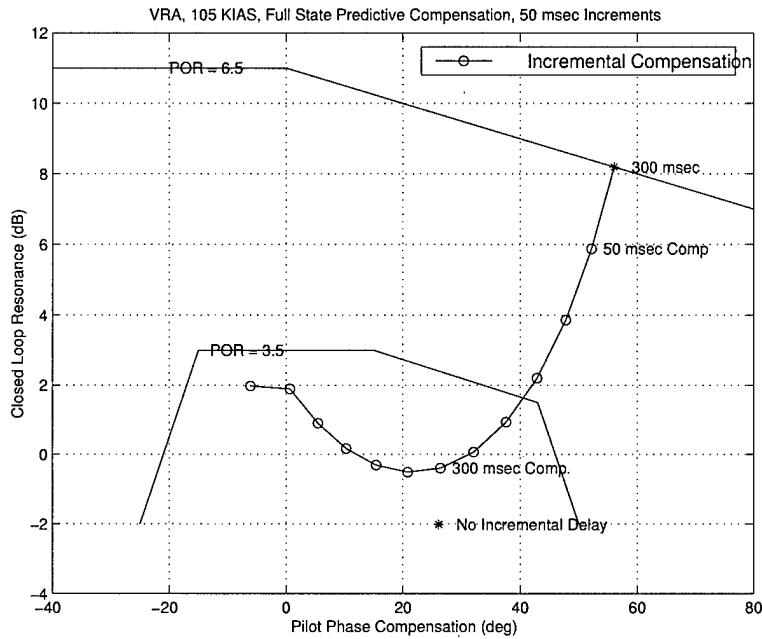


Figure 3.65 F-8, SAS, State Predictor Compensation, 50 msec Incremental Amounts

3.3.4.1 *Compensator design.* Design of the output feedback based state predictor compensator is similar to the full state predictor. Figure 3.66 shows the output feedback structure, while Figure 3.67 gives a more detailed picture of the design. A Luenberger observer is merged with the existing model of the plant. The

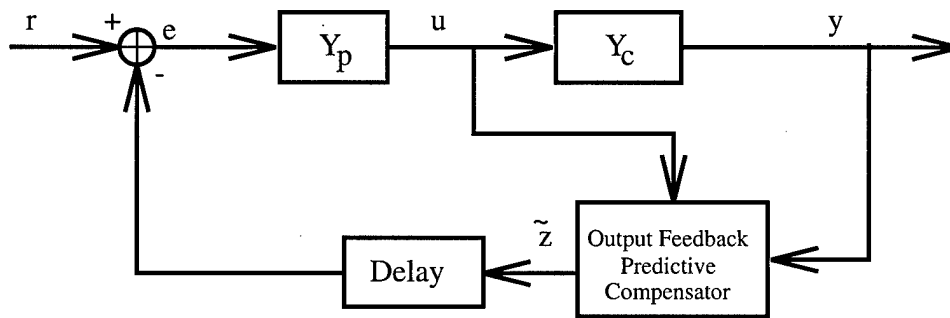


Figure 3.66 Output Feedback Based State Predictor System Diagram

matrix  $\phi$  now operates on the estimated states,  $\hat{x}$ . The transfer function for use in

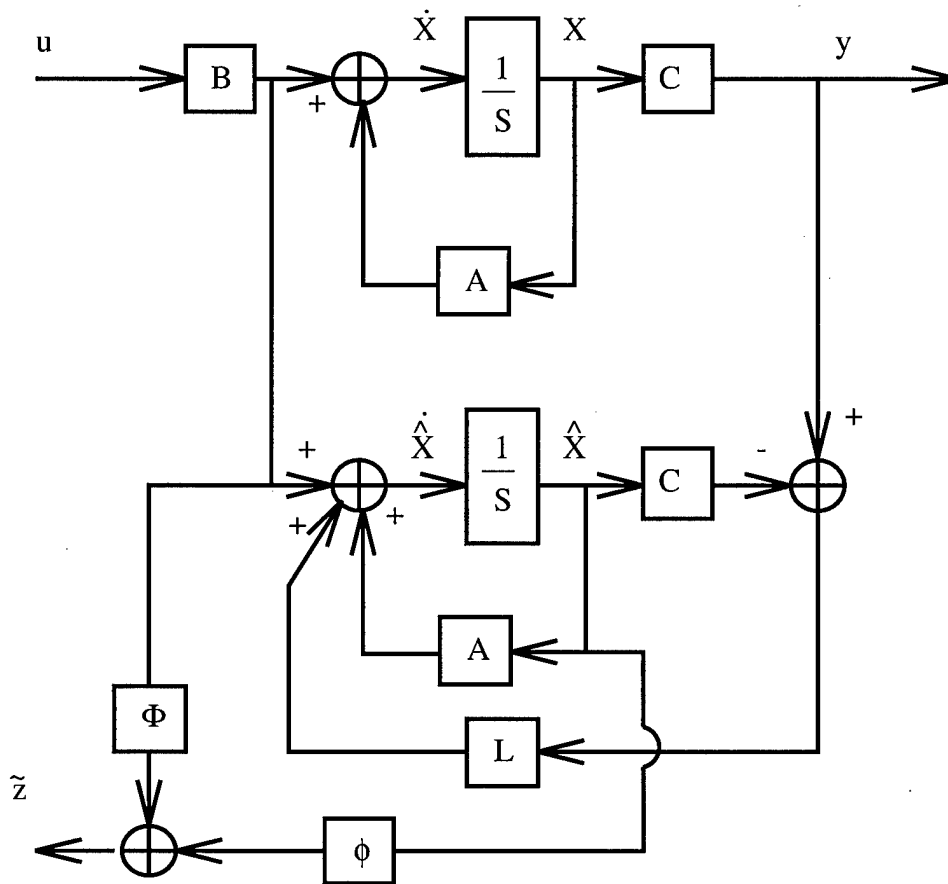


Figure 3.67 System Model with Luenberger Observer

frequency domain analysis is calculated from Equation 3.9 on the state space system

$$\begin{bmatrix} \dot{x} \\ \dot{\hat{x}} \end{bmatrix} = \begin{bmatrix} \mathbf{A} & 0 \\ \mathbf{LC} & \mathbf{A} - \mathbf{LC} \end{bmatrix} \begin{bmatrix} \mathbf{x} \\ \hat{\mathbf{x}} \end{bmatrix} + \begin{bmatrix} \mathbf{B} \\ \mathbf{B} \end{bmatrix} u \quad (3.12)$$

$$\tilde{z} = \begin{bmatrix} 0 & \mathbf{K}\phi \end{bmatrix} \begin{bmatrix} \mathbf{x} \\ \hat{\mathbf{x}} \end{bmatrix} + \mathbf{K}\Phi\mathbf{B}u \quad (3.13)$$

3.3.4.2 Output Feedback State Predictor Results. Figures 3.68, 3.69, and 3.70 display the results of Neal-Smith analysis the VRA and F-8 respectively. The 105 KIAS landing dynamics were chosen as typical for the VRA response; Pitch SAS mode demonstrated typical response for the F-8 DFBW.

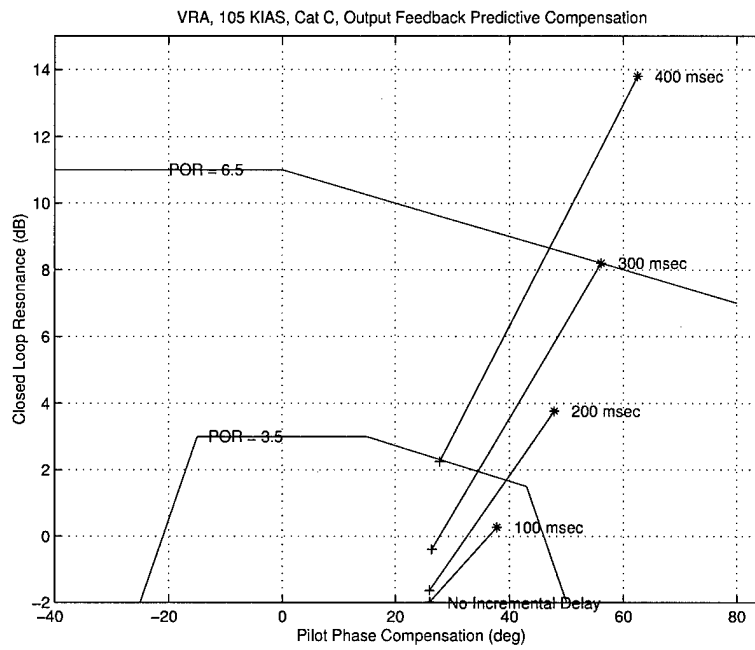


Figure 3.68 VRA, 105 KIAS Landing Task, Output Feedback State Predictor Compensation

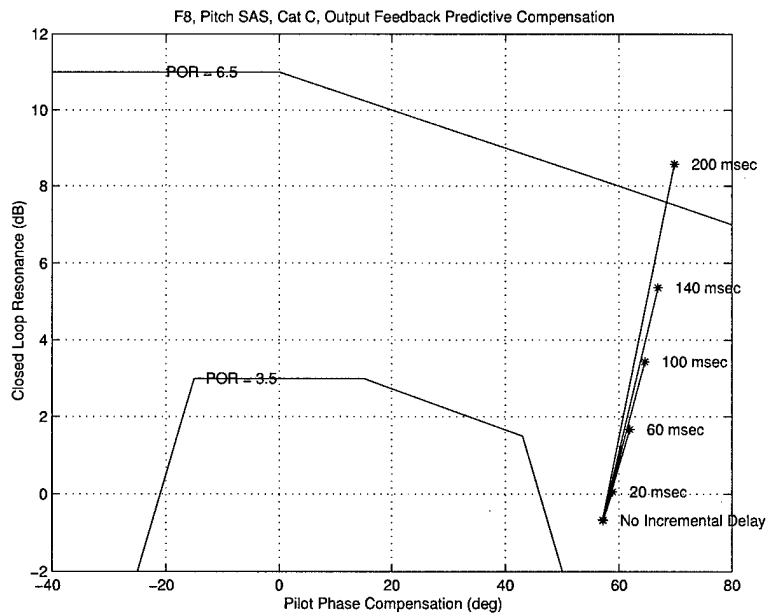


Figure 3.69 F-8, Pitch SAS, Landing Task, Output Feedback State Predictor Compensation

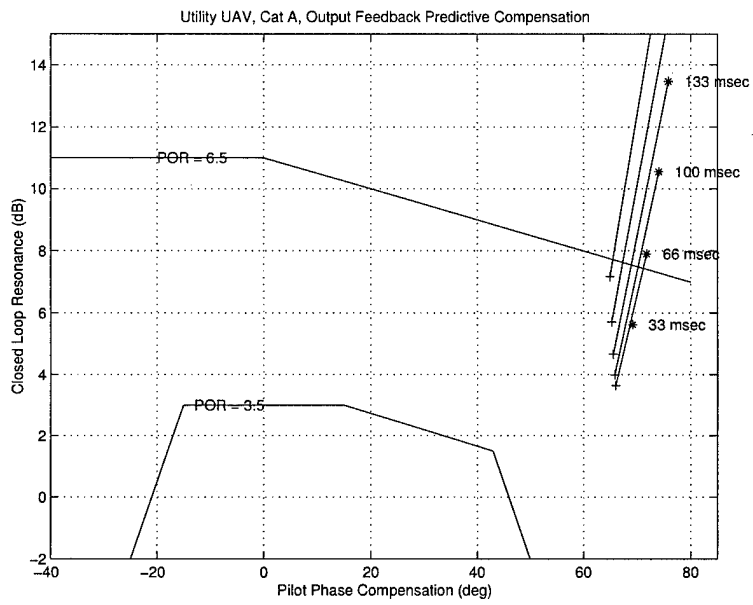


Figure 3.70 UAV, Cat A Task, Output Feedback State Predictor Compensation



Comparing these to Figures 3.52, 3.49, and 3.55 demonstrates that output feedback has negligible effect on frequency domain analysis; to explore the effects of output feedback properly it was necessary to compare the time domain responses in simulations.

*3.3.5 Simulink Model Simulations.* Simulations were conducted to verify the results of the frequency domain methods as well as to study the effects of state predictor compensation on gust rejection. As in the Lead/Lag Simulink analysis, the pilot model used in the simulation was produced by the Neal-Smith analysis. The aircraft short period and gust models remained unchanged from the earlier analysis.

Simulink model diagrams for the VRA tracking and gust rejection analysis are shown in Figures 3.71 and 3.72 respectively. The VRA 105 KIAS Landing dynamics were chosen as typical for analysis. F-8 DFBW SAS model analysis is presented for completeness in Appendix B.

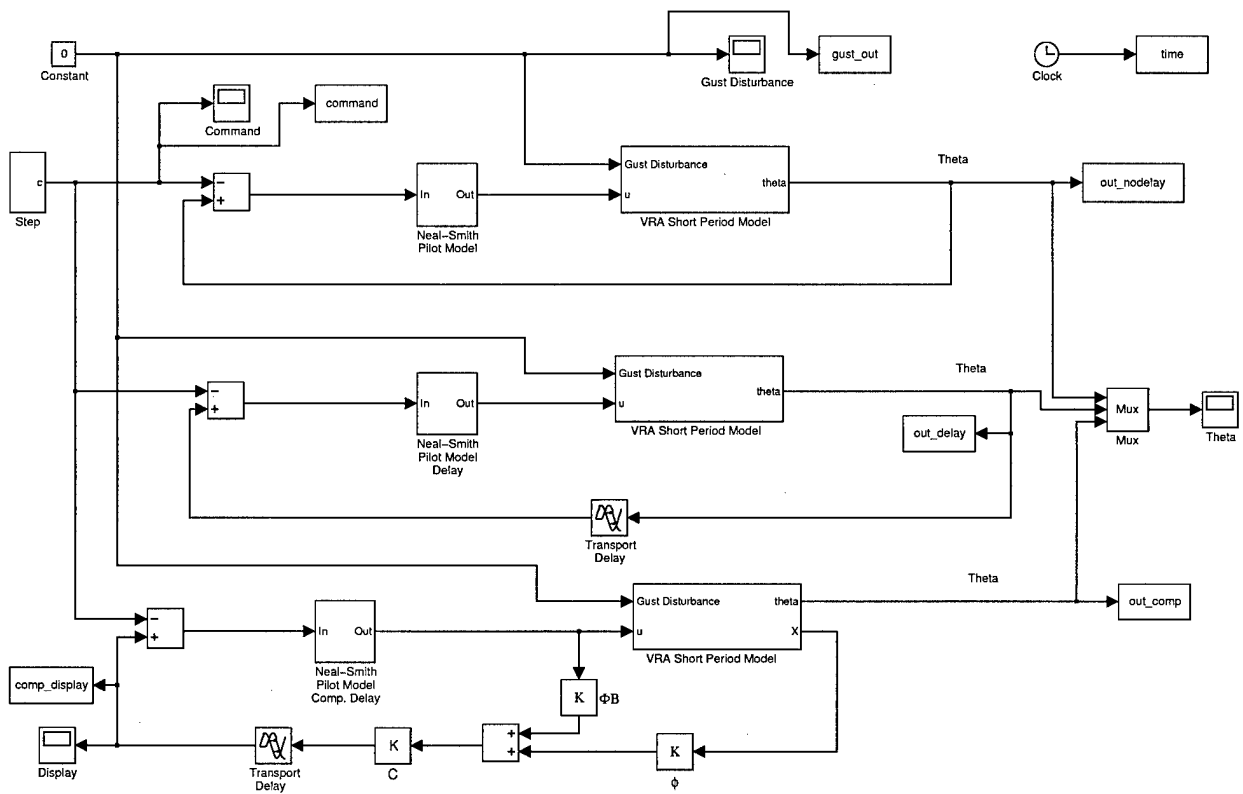


Figure 3.71 VRA Command Tracking Model, Full State Predictor Compensation

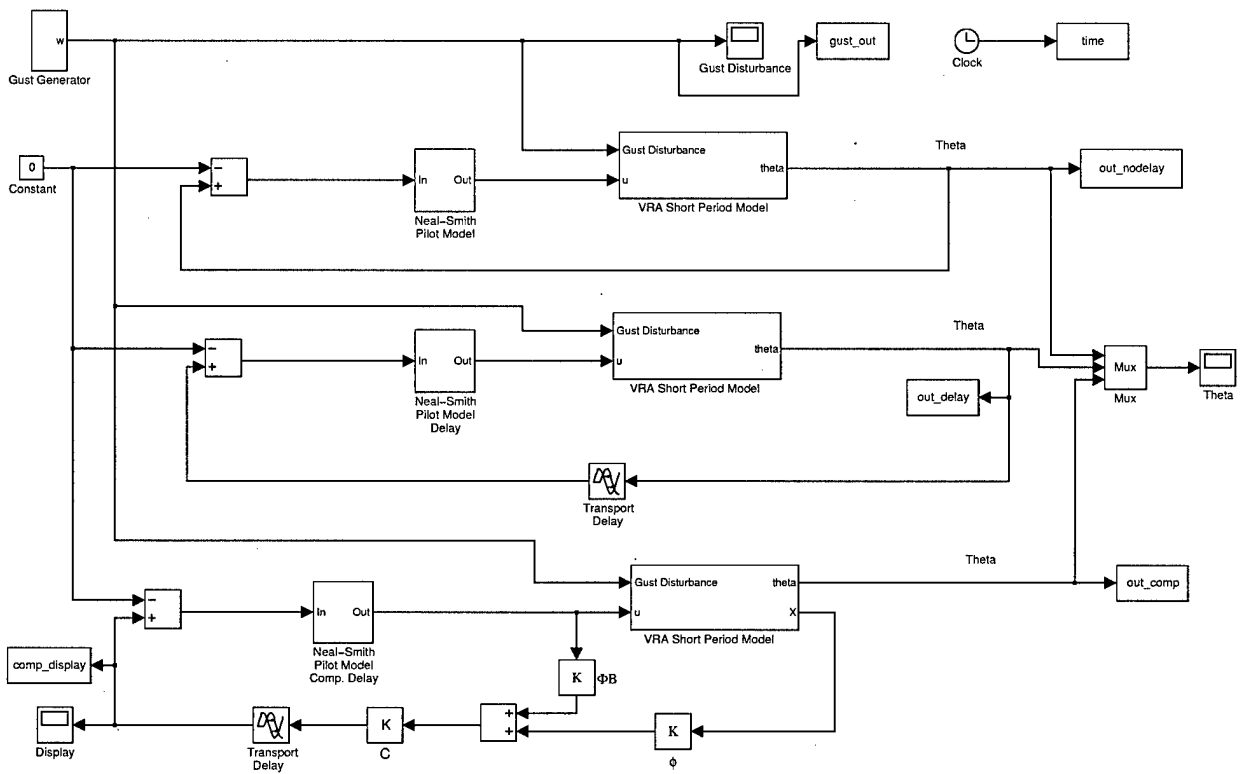


Figure 3.72 VRA Gust Rejection Model, Full State Predictor Compensation

Simulations for command tracking with feedback transport delays of 100, 200, 300, and 400 msec were run. Pitch angle output for each case is displayed in the following figures.

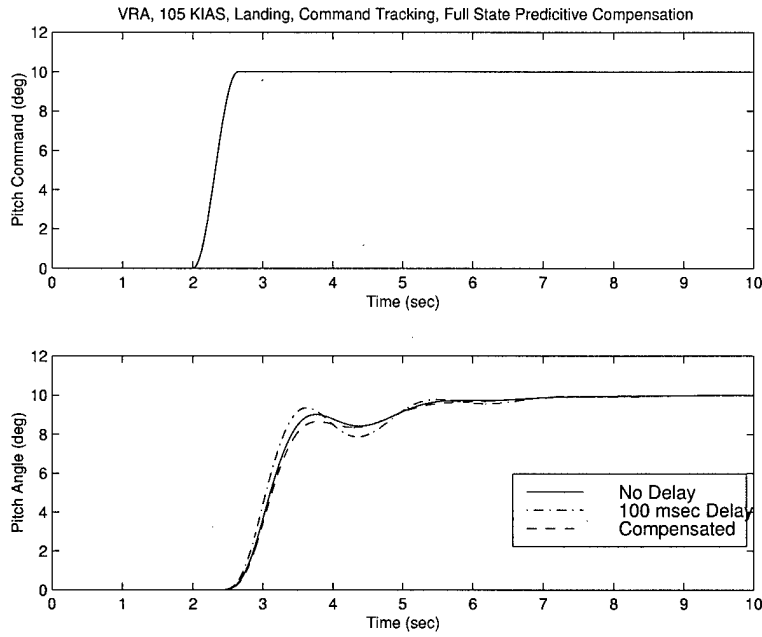


Figure 3.73 VRA Command Tracking, 100 msec Delay, Full State Predictive Compensation

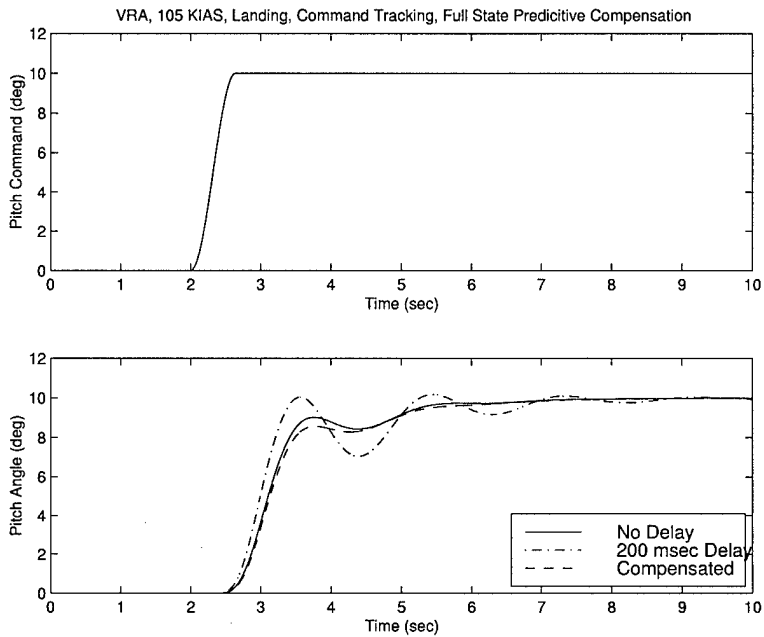


Figure 3.74 VRA Command Tracking, 200 msec Delay, Full State Predictive Compensation

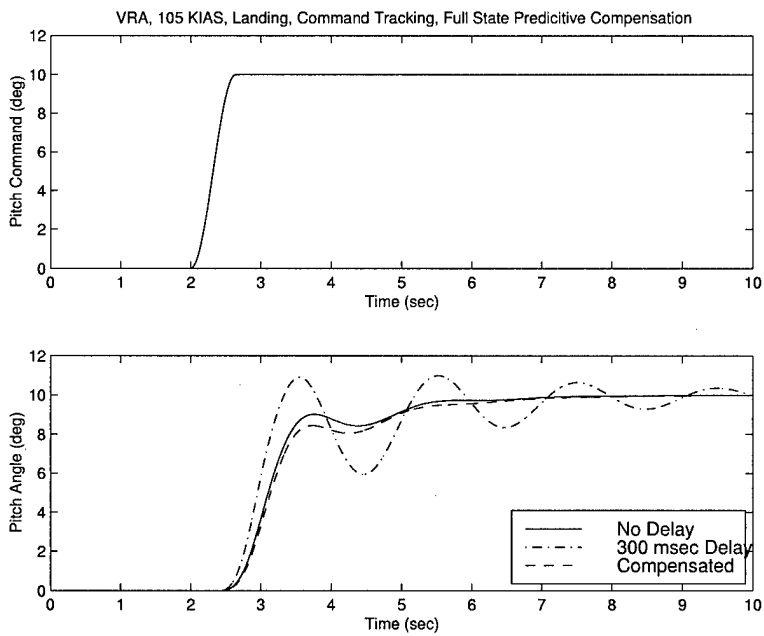


Figure 3.75 VRA Command Tracking, 300 msec Delay, Full State Predictive Compensation

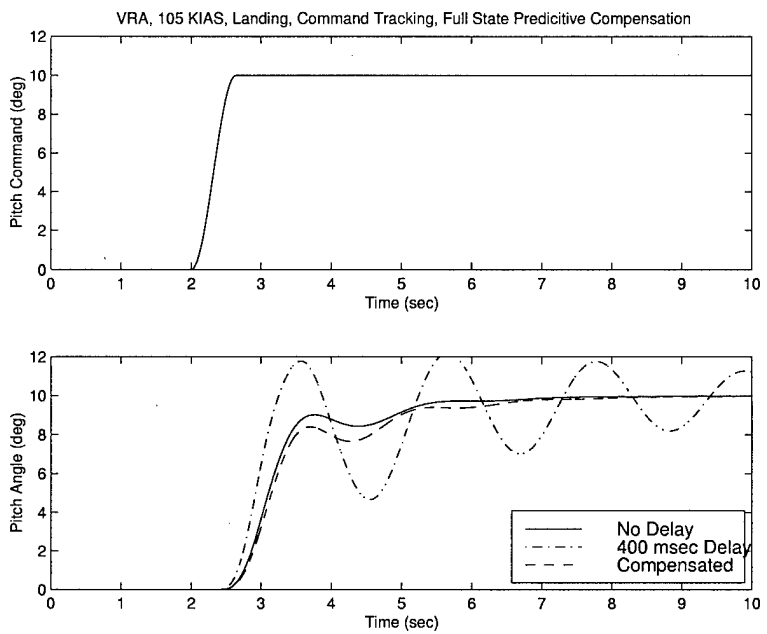


Figure 3.76 VRA Command Tracking, 400 msec Delay, Full State Predictive Compensation

It is clear from Figures 3.73, 3.74, 3.75, and 3.76, that the state predictor technique restores handling qualities. The assumption that the pilot's input remained constant over the delay interval made in order to obtain a closed form solution for  $\Phi$  was evidently valid for the input frequencies tested. Also of note is that the result of solving Equation 2.29 is the value of the output  $\tau_d$  seconds into the future. If this were actually occurring as theory would have, the pitch angle provided to the pilot by the state predictor compensator would be an exact copy of the undelayed output. This is essentially what the compensator is providing as seen in Figure 3.77.

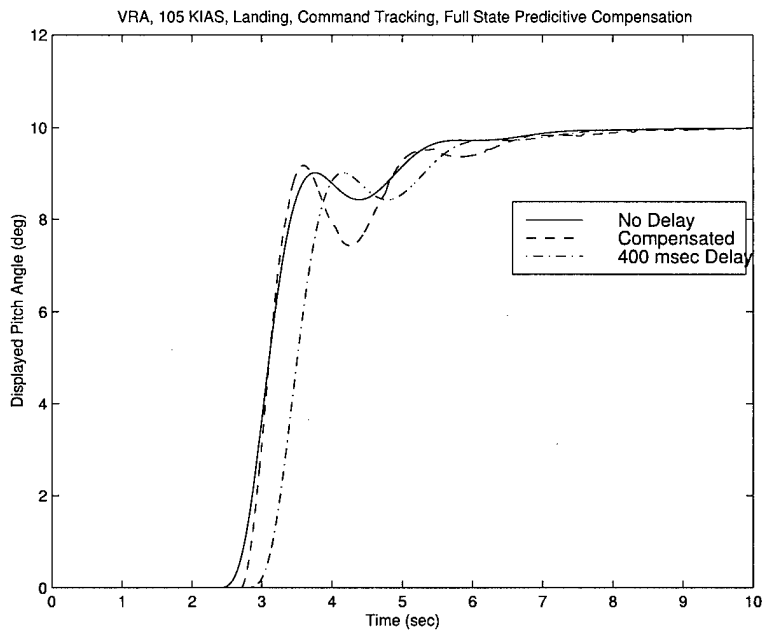


Figure 3.77 VRA Command Tracking, Displayed Pitch, 400 msec Delay, Full State Predictive Compensation

Likewise simulations for gust rejection were run. Pitch angle output for the 400 msec delay case is shown in Figure 3.78.

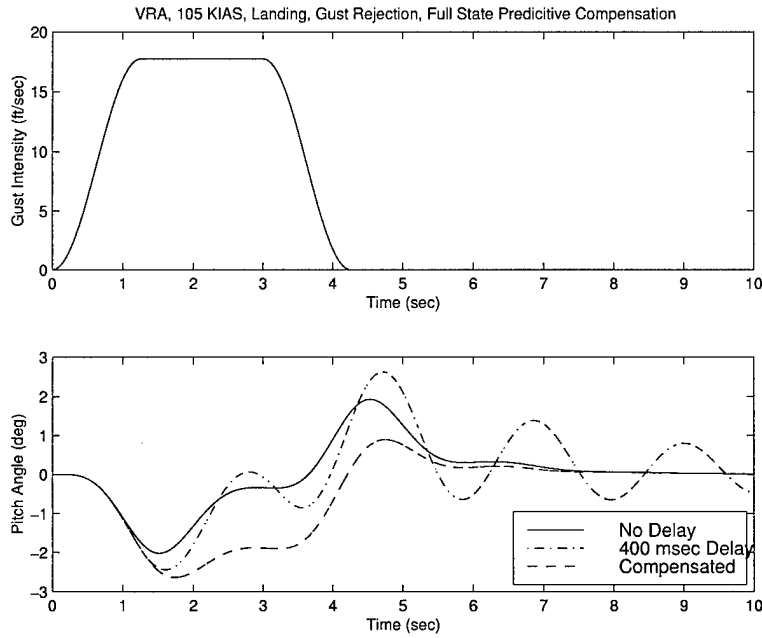


Figure 3.78 VRA Gust Rejection, 400 msec Delay, Full State Predictive Compensation



Gust rejection is one area where the state predictor compensator needs refinement. The state predictor is designed around the state transition matrix and the convolution integral which involves the pilot's input. In a gust rejection scenario, the pilot is not providing the input that is causing the system to respond nor is there a state in the model to provide the compensator with knowledge of the gust. This imperfect state knowledge combined with imperfect knowledge of the input results in the large steady state errors seen in pitch angle. The inability of the predictor to reject gust input would become a major concern during flight test.

As discussed previously, the transient observer error did not significantly influence frequency domain analysis techniques. Simulink models were constructed to test the effect of output feedback in the time domain. Model diagrams for the VRA tracking and gust rejection analysis are shown in Figures 3.79 and 3.80 respectively. The VRA 105 KIAS Landing dynamics were chosen as typical for analysis. F-8 DFBW SAS model analysis is presented for completeness in Appendix B.

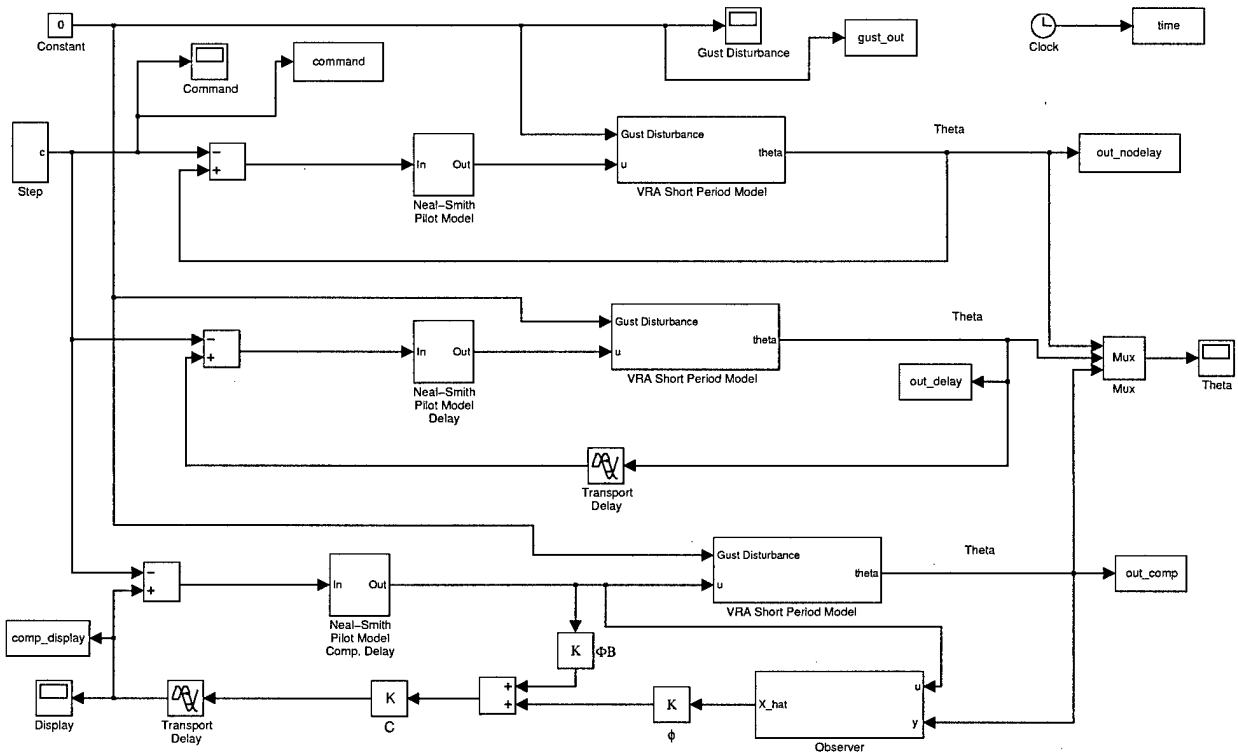


Figure 3.79 VRA Command Tracking Model, Output Feedback State Predictor Compensation

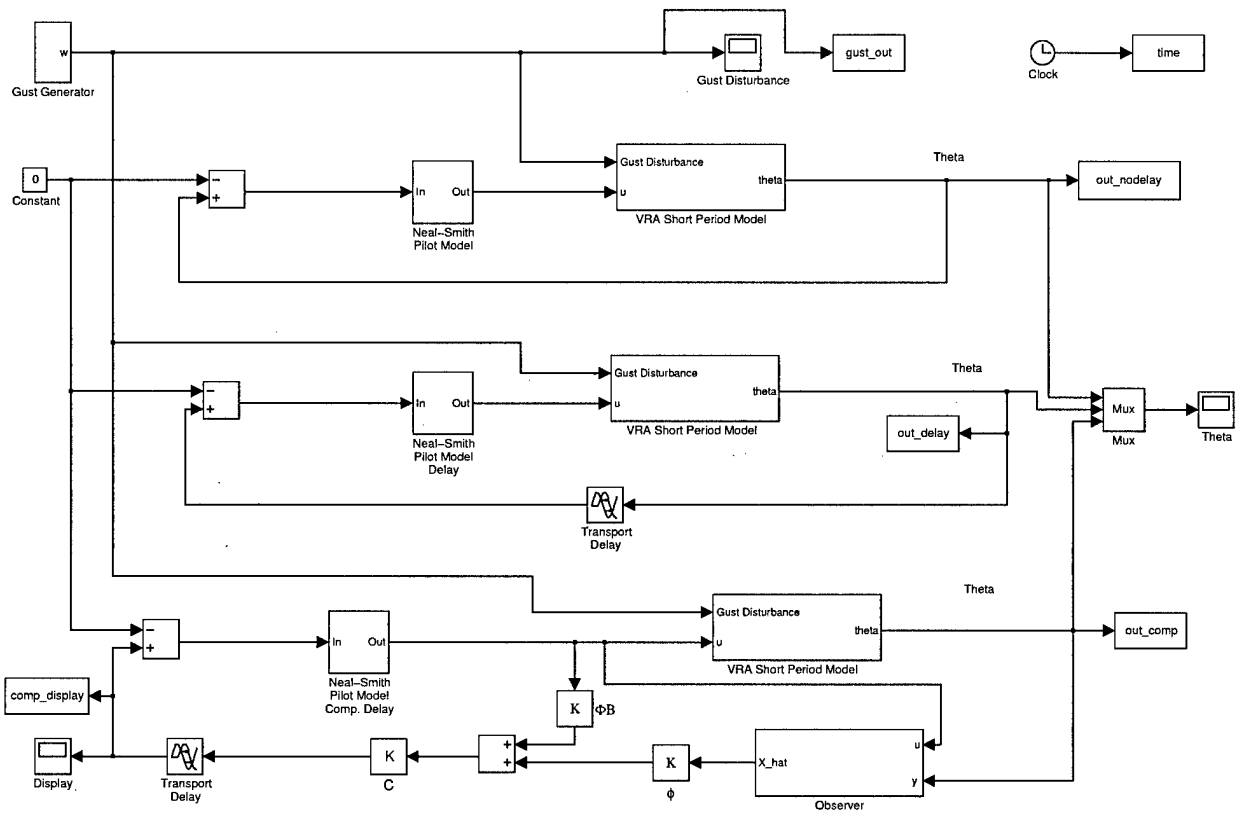


Figure 3.80 VRA Gust Rejection Model, Full Output Feedback State Predictor Compensation

Simulations for command tracking with feedback transport delays of 100, 200, 300, and 400 msec were run. Pitch angle output for the 400 msec delay case was typical and is presented in Figure 3.81.

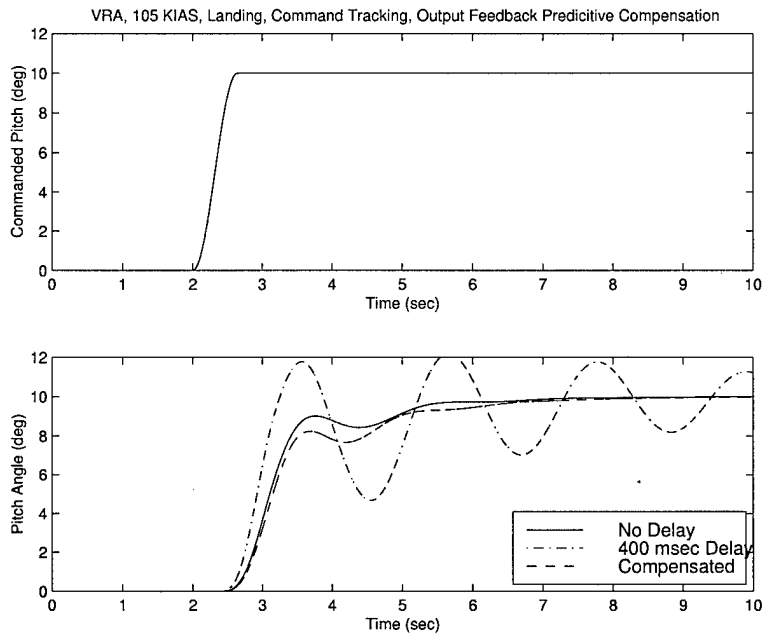


Figure 3.81 VRA Command Tracking, 400 msec Delay

It is clear from Figure 3.81, that the output feedback state predictor technique restores handling qualities almost as well as full state feedback. Pilot display is also essentially the same as the full state case, see Figure 3.82.

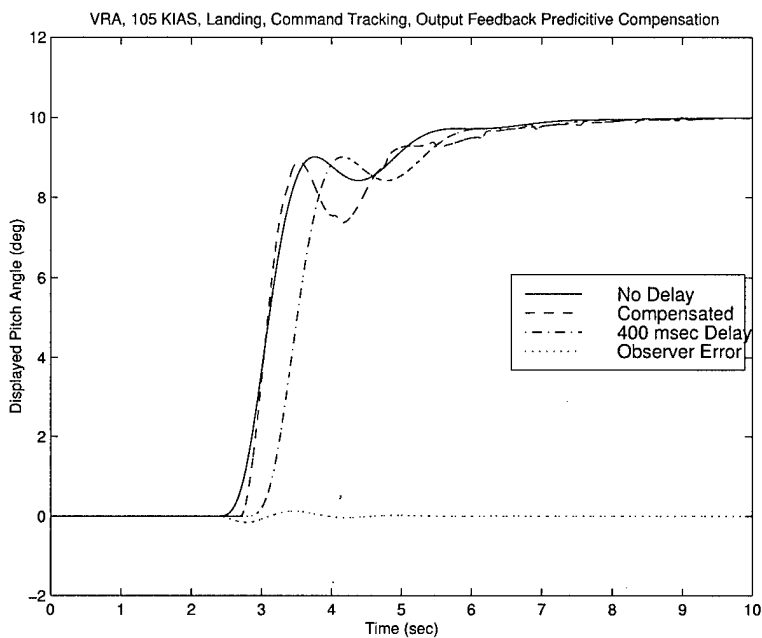


Figure 3.82 VRA Command Tracking, Displayed Pitch, 400 msec Delay

Gust rejection pitch angle output for for the 400 msec delay case is shown in Figure 3.83.

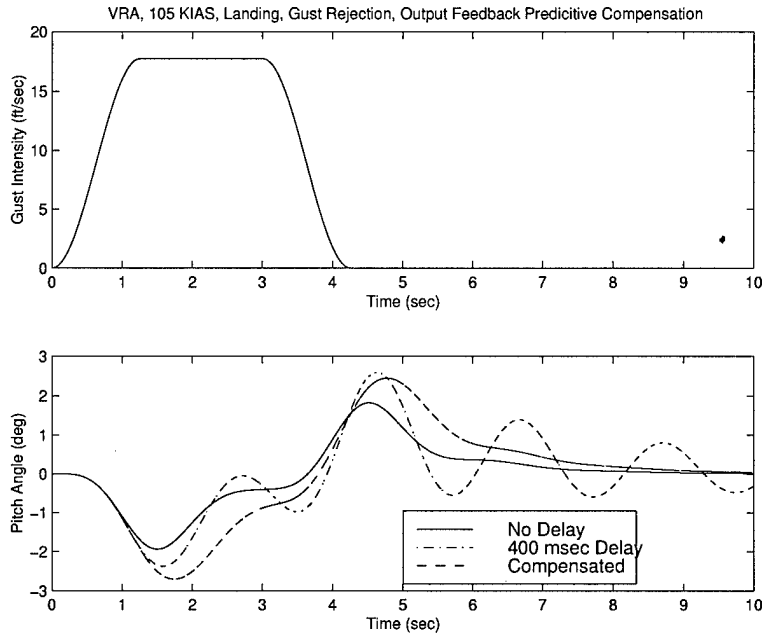


Figure 3.83 VRA Gust Rejection, 400 msec Delay

## IV. *Flight Test*

### 4.1 *Introduction*

The concept, scope, and methods used during the flight test of the model-based predictive algorithm discussed in Chapter III are presented in this section.

4.1.1 *General.* The overall objective of this flight test program was to determine the effects of additional time delay on UAV handling qualities and determine the extent to which the delay compensation algorithm developed in previous sections improved UAV handling qualities. Hand-held data were collected during pitch tracking tasks and consisted of research pilot comments, Cooper-Harper ratings (CHR), and Pilot-In-The-Loop Oscillation (PIO) Ratings (PIOR).

The UAV instrumentation system collected data regarding the error between commanded and predicted pitch (display error), and the error between commanded and actual UAV attitude (tracking error). Data were collected at various levels of additional time delay with and without delay compensation. These data were recorded and processed post-flight to extract handling qualities ratings and measure the performance of the pilot and compensation algorithm.

Testing was conducted by the USAF Test Pilot School (TPS) and the NASA Dryden Flight Research Center.

4.1.2 *Program Chronology.* The NASA Dryden Research Center Model Shop began the UAV modifications on 11 May 1999. Initial systems checkouts were on 4 August 1999. Parameter Identification (PID) sorties began on 18 Aug and ended on 24 Aug. A total of five PID sorties were flown. Final full systems checkout was completed on 31 August 1999. Software development by the Computer Sciences Corporation to implement the display delay, predictor algorithm, and data collection began in March 1999. Flight test began on 13 September 1999.

## 4.2 Model-Based Predictive Algorithm Design

The model-based predictor algorithm discussed in Chapters II and III was used to improve UAV handling qualities by providing a “quicken display” to help the pilot compensate for increased system time delay. The algorithm was based on small perturbations linearized about an equilibrium state ( $\alpha_0, \theta_0, V_0$ , et cetera). Using delayed aircraft data and the verified UAV aerodynamic model (Appendix G), the algorithm predicted the aircraft’s final state based on pilot input and current state. This allowed the pilot to rapidly see the effect of his input and determine future inputs based on this predicted final state.

Given a single input single output (SISO) system linearized about an equilibrium value, the small perturbation equations of motion may be represented in state space as:

$$\dot{\mathbf{x}}(t) = \mathbf{A}\mathbf{x}(t) + \mathbf{B}u(t) \quad (4.1)$$

$$y(t) = \mathbf{C}\mathbf{x}(t) + \mathbf{D}u(t) \quad (4.2)$$

where  $\mathbf{x}$  is the vector composed of system states,  $\mathbf{A}$  is the state transition matrix,  $u$  is the system input, and  $\mathbf{B}$  is the input matrix. The system output,  $y$ , is the state vector,  $\mathbf{x}$ , weighted by the output matrix,  $\mathbf{C}$ , added to the system input weighted by the feedforward matrix,  $\mathbf{D}$ . Using stick position,  $x_s$ , as input and pitch rate,  $q$ , as output variables, the system block diagram can be represented below in Figure 4.1.

The  $\mathbf{A}$ ,  $\mathbf{B}$ ,  $\mathbf{C}$  and  $\mathbf{D}$  matrices were determined from the aircraft flight parameters and stability derivatives determined during Parameter Identification flights (see Appendix G). Transforming to the Laplace domain and some matrix algebra reveal that the system transfer function from stick position to pitch rate,  $\frac{q}{x_s}$ , may be represented by the equation:



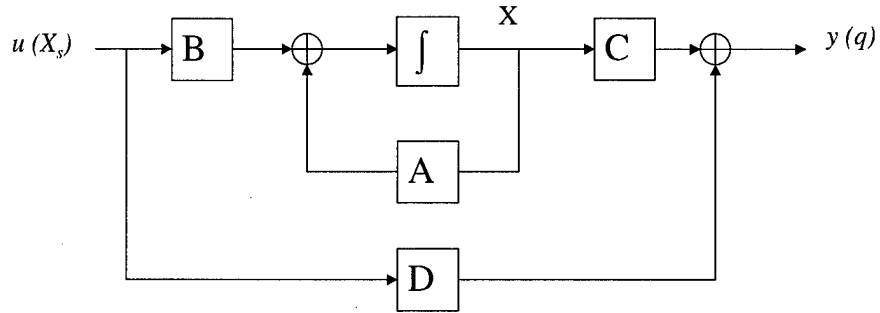


Figure 4.1 System Block Diagram

$$\frac{q}{x_s} = \mathbf{C} \cdot (s \cdot \mathbf{I} - \mathbf{A})^{-1} \cdot \mathbf{B} + \mathbf{D} \quad (4.3)$$

where  $\mathbf{I}$  is the identity matrix of the same dimensions as  $\mathbf{A}$ , and  $s$  is the Laplace operator. For the purposes of this test, a short period approximation was used to model the UAV time response to pilot inputs. The state space approximation for an aircraft short period mode may be written as:

$$\begin{bmatrix} \Delta \dot{\alpha} \\ \Delta \dot{q} \end{bmatrix} = \begin{bmatrix} \frac{Z_{\alpha}}{U_0} & 1 \\ M_{\alpha} + M_{\dot{\alpha}} \cdot \frac{Z_{\alpha}}{U_0} & M_q + M_{\dot{\alpha}} \end{bmatrix} \cdot \begin{bmatrix} \Delta \alpha \\ \Delta q \end{bmatrix} + \begin{bmatrix} \frac{Z_{\delta_e}}{U_0} \\ M_{\delta_e} + M_{\dot{\alpha}} \cdot \frac{Z_{\delta_e}}{U_0} \end{bmatrix} \cdot \Delta \delta_e \quad (4.4)$$

(4.5)

The aircraft state vector was composed of angle of attack,  $\alpha$ , and pitch rate,  $q$ . For the UAV used in this test, the system matrices were defined as follows:

$$\mathbf{A} = \begin{bmatrix} \frac{Z_\alpha}{U_0} & 1 \\ M_\alpha + M_{\dot{\alpha}} \cdot \frac{Z_\alpha}{U_0} & M_q + M_{\dot{\alpha}} \end{bmatrix} \quad (4.6)$$

$$\mathbf{B} = \begin{bmatrix} \frac{Z_{\delta_e}}{U_0} \\ M_{\delta_e} + M_{\dot{\alpha}} \cdot \frac{Z_{\delta_e}}{U_0} \end{bmatrix} \quad (4.7)$$

$$\mathbf{C} = \begin{bmatrix} 0 & 1 \end{bmatrix} \quad (4.8)$$

$$\mathbf{D} = \begin{bmatrix} 0 \end{bmatrix} \quad (4.9)$$

The dimensional stability derivatives,  $Z_\alpha$ ,  $M_\alpha$ , et cetera were calculated from the UAV flight parameters and aerodynamic characteristics discussed in Appendix G.  $U_0$  was the nominal airspeed around which the equations of motion were linearized. Elevator position was assumed to be related to stick position by a constant gain,  $K_G$ , determined from ground test.

The system state may be determined at any time given knowledge of the system's initial state and pilot control input history, see Equation 2.29. If  $[t, \tau]$  is chosen to be equal to the period of time delay  $\tau_d$  then  $x(t)$  will be the predicted state vector  $\tau_d$  seconds into the future. Knowledge of future elevator inputs  $u(t)$  is required to compute the convolution integral. However, if pilot input is assumed to remain constant over the time delay interval, a closed form solution is possible. Assuming constant pilot input over the time delay interval, the convolution integral in Equation 2.29 may be written as:

$$\mathbf{x}(t) = \phi(t, t_0)\mathbf{x}(t_0) + \mathbf{B}u(t_0) \int_{t_0}^t \phi(t, \tau) d\tau \quad (4.10)$$

Thus the estimated state vector at time  $t = (t_0 + \tau_D)$  is computed from:

$$\mathbf{x}(t_0 + \tau_d) = e^{\mathbf{A}\tau_d} \cdot \mathbf{x}(t_0) + \mathbf{B} \cdot \mathbf{A}^{-1} \cdot (e^{\mathbf{A}\tau_D} - \mathbf{I}) \cdot u(t_0) \quad (4.11)$$

making the substitution  $\phi = e^{\mathbf{A} \cdot (t-\tau)}$  and  $\Phi = \mathbf{A}^{-1} \cdot (e^{\mathbf{A} \cdot \tau_d} - \mathbf{I})$  we can rewrite Equation 4.11 as

$$\mathbf{x}(t_0 + \tau_d) = \phi \cdot \mathbf{x}(t_0) + \mathbf{B} \cdot \Phi \cdot \mathbf{u}(t_0) \quad (4.12)$$

Recalling the discussion in Section 3.3, a new block diagram may be drawn as follows,

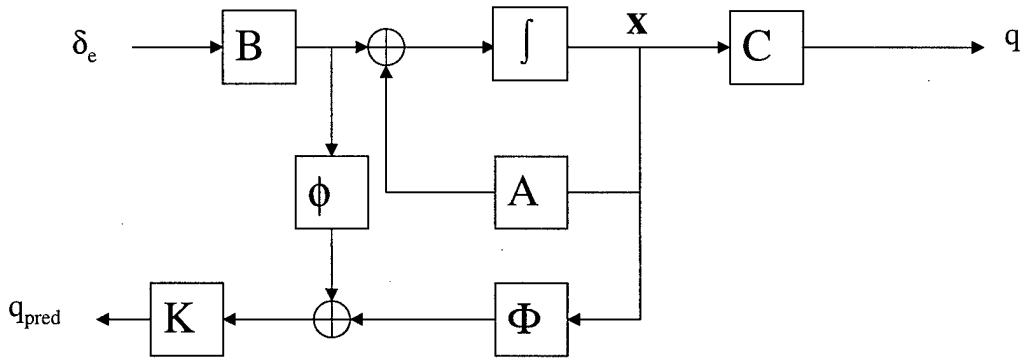


Figure 4.2 New System Block Diagram

If the output matrix  $\mathbf{K}$  is set equal to  $\mathbf{C}$ , the output will be the predicted pitch rate  $\tau_d$  seconds into the future. Thus, a new state space output equation may be written for the predicted pitch rate,  $q_{pred}$ ,

$$q_{pred} = \mathbf{C} \cdot \phi \cdot \mathbf{x} + \mathbf{C} \cdot \Phi \cdot \mathbf{B} \cdot \mathbf{K}_G \cdot x_s \quad (4.13)$$

The gain matrix  $\mathbf{C}\phi$  operates on the system states while the matrix  $\mathbf{C}\Phi\mathbf{B} \cdot \mathbf{K}_G$  applies a gain to the pilot station stick position,  $x_s$ . Gain matrices are computed for specific system dynamics and time delay interval using the formulas presented above.

The new output  $q_{pred}$  was integrated and displayed to the pilot as the predicted pitch response of the UAV.

UAV short period dynamics, pilot input, and the amount of time delay present in the control loop were used to calculate a predicted pitch reference signal. This signal was run through a washout filter discussed in the next section and mixed with the UAV out-front video for display to the pilot on the video monitor at the pilot station. A typical video frame is displayed in Figure 4.3. The notional Pilot/Display/UAV response to a commanded step input is shown in Figure 4.4 through Figure 4.9.

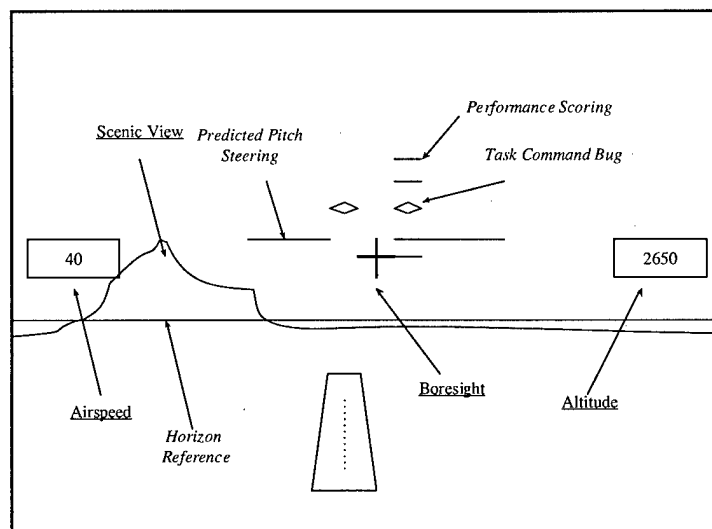


Figure 4.3 Typical UAV Video Frame

The UAV in straight and level flight prior to the commanded step input is illustrated in Figure 4.4. The pitch task bars commanding a four-degree step input are shown in Figure 4.5. In Figure 4.6, the predicted pitch steering bar begins moving up as the pilot makes an aft stick input to initiate the pitch capture. The pilot has captured the desired pitch change with the predicted pitch steering bar in Figure 4.7. The aircraft response begins to be perceived at the pilot station following the additional delay latency, Figure 4.8. Finally, the new pitch attitude is set and the

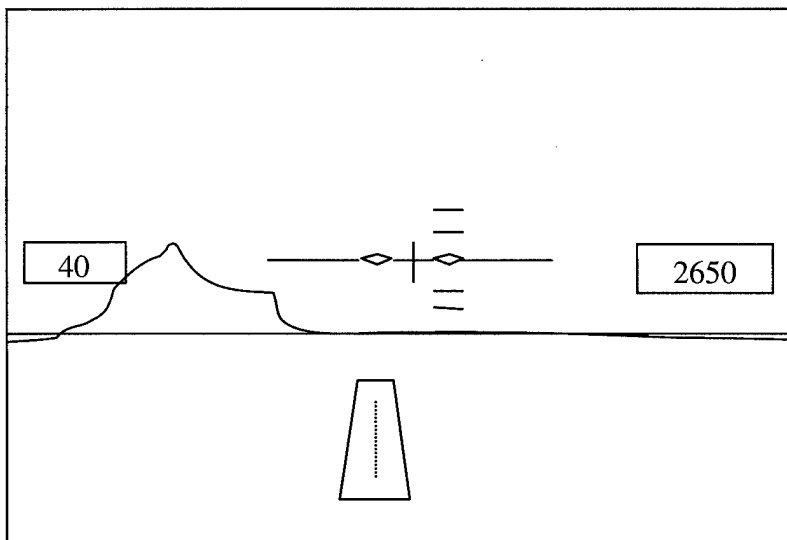


Figure 4.4 Straight and Level Flight

task and predicted pitch steering references are aligned with the aircraft boresight reference, Figure 4.9.

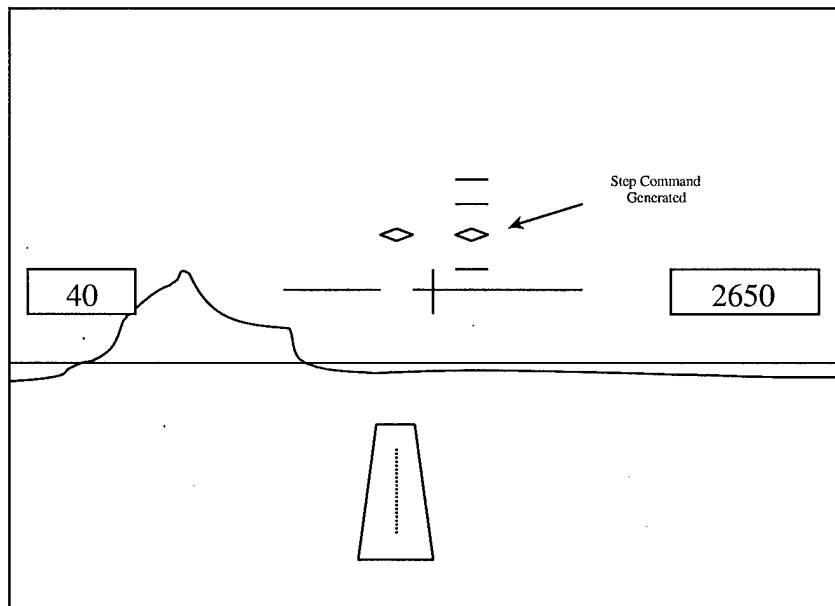


Figure 4.5 Pitch Capture Commanded

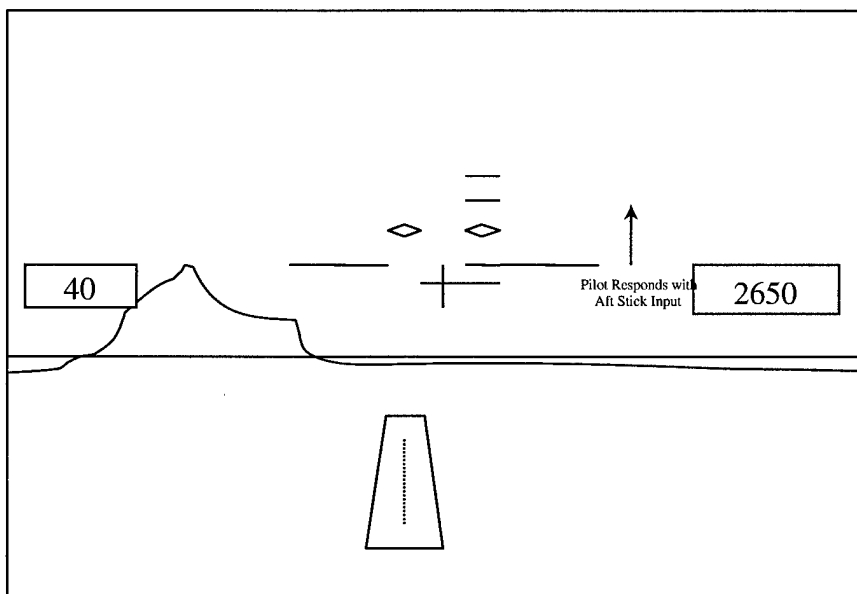


Figure 4.6 Predicted Pitch Response to Pilot Input

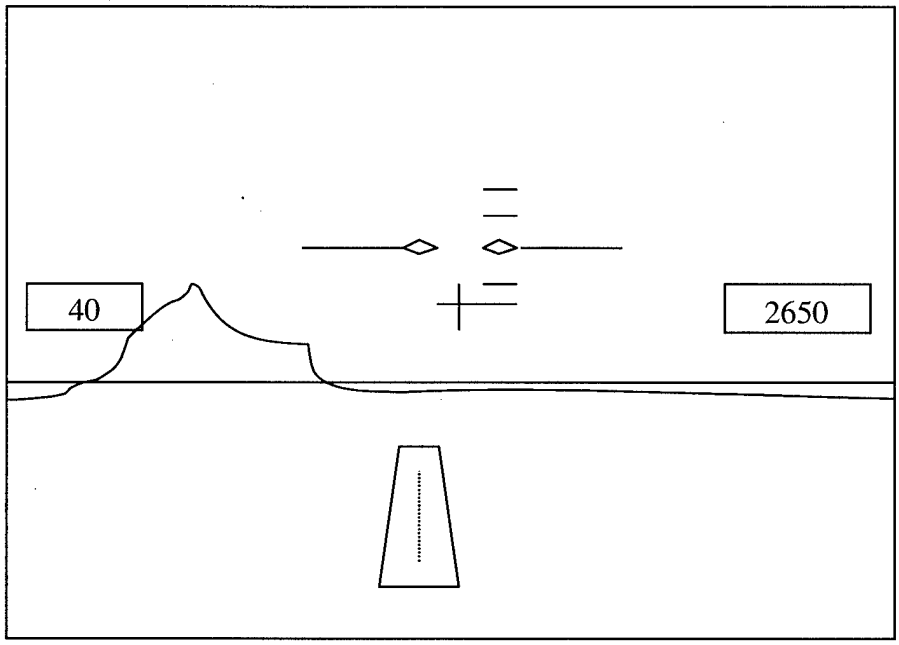


Figure 4.7 Predicted Pitch Capture

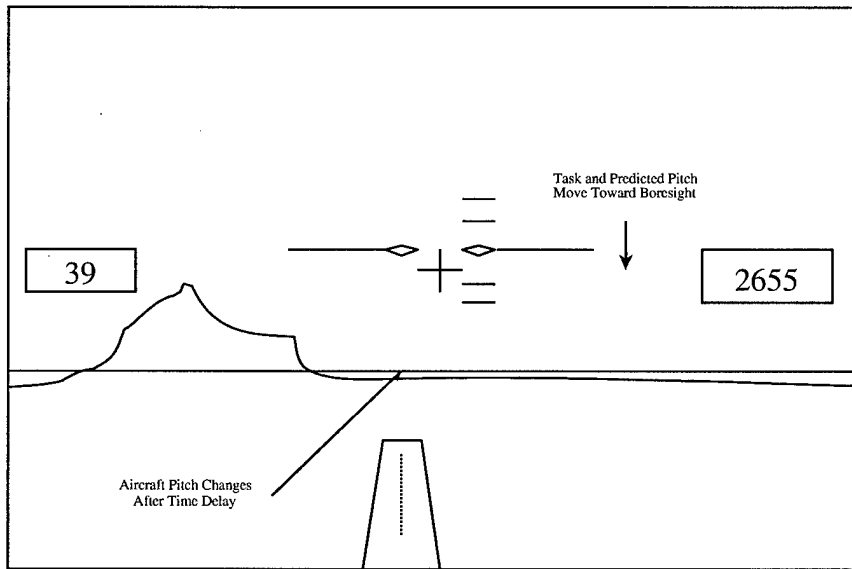


Figure 4.8 Delayed UAV Response

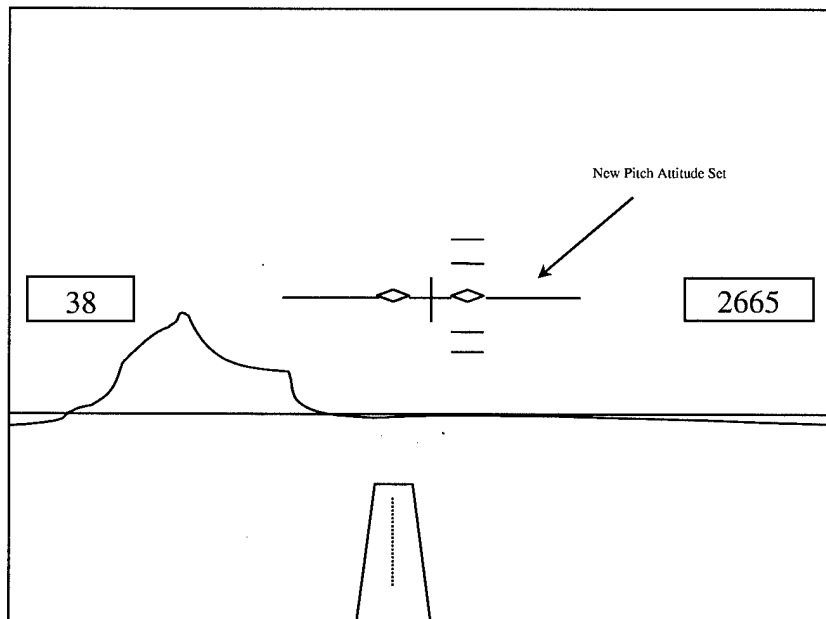


Figure 4.9 New Pitch Attitude Set



Early predictor test flights indicated that the predictive algorithm developed with a linear system model was sensitive to unmodeled nonlinearities. In the absence of pilot input, the predicted pitch should equal the actual pitch after the system time delay had elapsed. The test team found that this was not the case in most of the predictor test flights. Specifically, the predicted pitch would begin to deviate from the actual pitch due to unmodeled disturbances such as wind gusts. The test team also determined that the predicted pitch would acquire a growing offset from actual pitch when the pilot attempted to track ramp functions in the MIL-STD-1797A pitch tracking tasks.

*4.2.1 Deadband Modeling.* Simulations conducted using the Simulink™ real-time modeling capability in Matlab™ indicated that a deadband in the pitch rate response to elevator input resulted in a growing offset identical to that seen in flight test. Matlab™ simulations also showed that if the deadband was modeled appropriately in the predictive algorithm, the accuracy of the predictor could be recovered. Ground tests and one test flight were conducted to determine if such a deadband existed and quantify the deadband for inclusion in the pitch predictor algorithm.

Initial tests were conducted on the ground and determined that no measurable mechanical deadband existed between the pilot station stick position and the UAV elevator. The test team proceeded to inflight tests during which data were collected for small deflection pitch inputs. A deadband of 0.25 degrees elevator deflection was discovered. The deadband quantified in flight test was coded into the predictive algorithm in software. Subsequent flight tests showed improved ability of the predictor during ramp input tracking.

*4.2.2 Washout Filter Design.* Even with the deadband appropriately modeled, unmodeled nonlinearities and disturbances caused the predictive display to become disconnected with the actual pitch attitude. Similar results were seen in Chap-

ter III Simulink simulations where gust disturbances caused steady state offsets in predicted pitch. In order to rectify the problem, the test team decided to implement a washout filter that would cause the predicted pitch display to bias towards the actual pitch attitude. A single pole washout filter was proposed that incorporated a time constant large enough to allow the transient response of the predictor to be displayed while also negating steady state errors.

The predicted pitch was displayed to the pilot by the formula:

$$\theta_{pred_{display}} = \theta_B + \theta_{pred} - \theta_D \quad (4.14)$$

where  $\theta_D$  is the delayed UAV pitch attitude, and  $\theta_B$  is the boresight reference angle. The test team determined that the displayed predicted pitch should be washed out back to the boresight reference. Thus the difference becomes:

$$\theta_B - \theta_{pred_{display}} \rightarrow \theta_B - [\theta_B + \theta_{pred} - \theta_D] \rightarrow \theta_{pred} - \theta_D \quad (4.15)$$

The final quantity,  $(\theta_{pred} - \theta_D)$ , was determined to be the appropriate input for the washout filter. The new displayed parameter was the sum of the boresight reference and the output of the washout filter.

A single pole washout filter was designed of the form:

$$\frac{\theta_{OUT}}{\theta_{IN}} = \frac{K_B \cdot s}{s + a} \quad (4.16)$$

where  $K_B$  is the Bode gain,  $s$  is the Laplace operator, and  $a$  is the location of the pole giving a filter time constant of  $\frac{1}{a}$ . Filters using several different time constants were designed for flight test and the Bode gain ( $K_B$ ) was set to provide a unity filter gain. The filters were implemented in software using difference equations determined from the z-transform of the washout filter as follows:

$$\frac{\theta_{OUTD}}{\theta_{IN}} = \frac{K_B \cdot [1 - Z^{-1}]}{1 - A \cdot Z^{-1}} \quad (4.17)$$

One flight was flown to test the various time constants and select the one that gave the best steady state correlation with the actual pitch while providing the pilot with the best predictive display. The test team selected the filter with the one second time constant,  $A = .96754$  for a 30 hz sample rate, as the one that would be used in the flight test of the predictor.

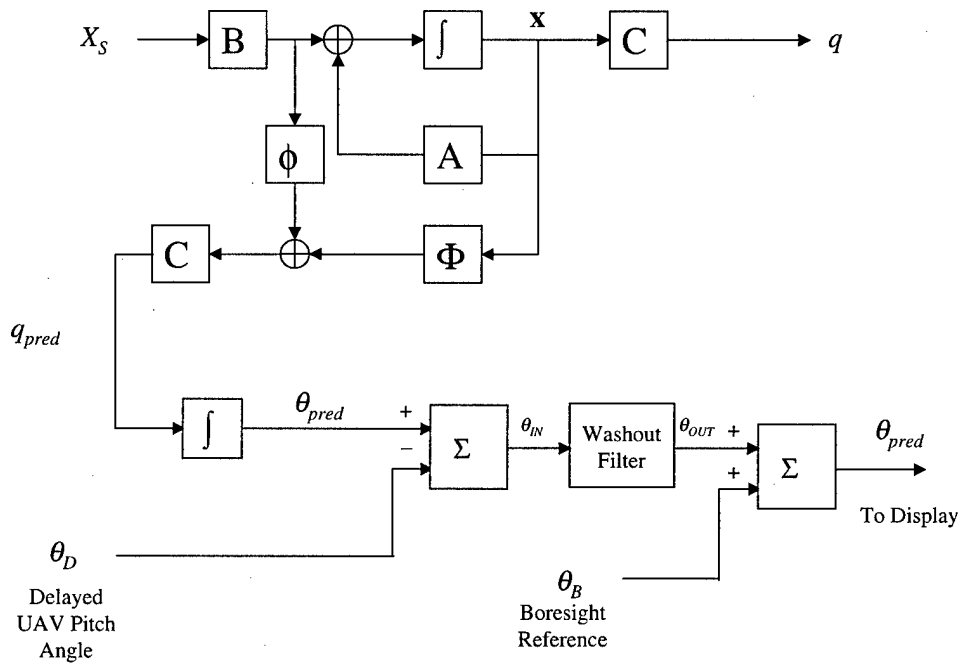


Figure 4.10 System Block Diagram with Washout Filter

### *4.3 Test Item Description*

The test item consisted of a NASA twin-engine Utility UAV, pilot control station, handheld radio controller, telemetry system, and computer workstation. The research pilot controlled the UAV from a pilot station consisting of a standard aircraft stick and throttle arrangement. Pilot stick inputs were fed to a radio-controlled aircraft transmitter unit, which was controlled by the NASA safety pilot. Aircraft response was fed through the telemetry system to the computer workstation. The pilot received feedback on aircraft response through a video monitor that displayed UAV out-front video, commanded task, and predicted pitch response cues generated by the computer workstation. For a detailed discussion of the UAV instrumentation and software data flow see Appendix C.

The test item was the NASA twin-engine Utility UAV and pilot station that is depicted graphically in Figure 4.11. The Research Pilot (RP) controlled the UAV from a pilot station consisting of a standard aircraft stick, and throttle arrangement. The pilot received feedback on aircraft flight performance via a video monitor that displayed UAV out-front video, commanded task, and predicted pitch response cues. Pilot stick inputs were fed to a commercially available Radio-Controlled (R/C) aircraft transmitter unit. Signals from the pilot station unit flowed to a similar R/C unit controlled by the NASA Safety Pilot (SP). The SP's R/C unit transmitted the RP's commands to the UAV on civilian R/C hobby aircraft frequencies. This arrangement allowed the SP to take control of the UAV with his R/C radio as necessary to ensure flight safety. UAV flight parameters were recorded by the onboard Data Acquisition System (DAS) and transmitted along with out-front UAV video to the NASA telemetry van. Video and individual data streams were recovered from the telemetry signal and provided via Ethernet to a Silicon Graphics workstation collocated with the pilot station. Predicted pitch attitude was calculated in software using the algorithm described in section 4.2. Software developed by Computer Sciences Corporation (CSC) generated the pitch tracking task and the predicted pitch

attitude displays. Tracking task and predicted pitch attitude displays were mixed into the existing UAV out-front video signal and presented to the RP at the pilot station. Pilot inputs along with actual and commanded aircraft attitude in addition to predicted and commanded pitch angle was recorded for later analysis.

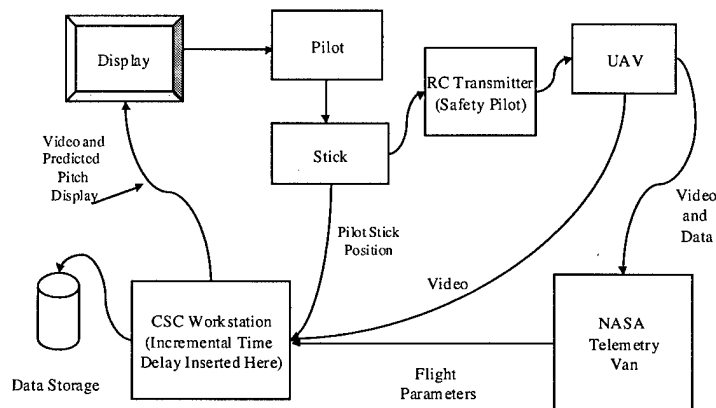


Figure 4.11 Block Diagram of Test Configuration

The test aircraft was a twin engine NASA Utility UAV modified with an on-board DAS, a pitot-static noseboom, and video data downlink as depicted in Figure 4.12. The UAV used standard civilian R/C aircraft radio equipment to provide flight control.

The telemetry system provided real-time downlink of three aircraft flight parameters: pitch rate ( $q$ ), angle of attack ( $\alpha$ ), and elevator position ( $\delta_e$ ). These data were sampled at 130 Hz, converted to 12 bit digital values, and placed on a Pulse Code Modulated (PCM) telemetry stream. The audio channel of the out-front UAV video was used to transmit the PCM data stream to the ground where it was received by the NASA telemetry van. The PCM data stream was stripped off the video signal and the data were recovered from the signal. Flight parameters were



Figure 4.12 NASA Utility UAV

then sent over an Ethernet connection to the computer workstation collocated with the pilot station. Target conditions were 40 KIAS and 500 ft AGL.

Pilot inputs (stick position) were sampled at 120 Hz and converted to 16 bit digital values. Stick position data were sent via an RS-232 connection to the computer workstation to be used in calculating the predicted pitch and recorded at 30 Hz for post-flight processing.

Two support vehicles, the NASA telemetry van and the NASA Model Shop van, were required for test operations at the Model Masters Field and are pictured in Figure 4.13.

The NASA telemetry van received the downlinked video and UAV flight parameters recorded by the onboard DAS. UAV flight data was received on the audio channel of the UAV video signal and decommutated into individual data streams. The outputs of the NASA telemetry van were an analog National Television System Committee (NTSC) video signal via standard cabling and digital UAV flight data via an Ethernet cable.



Figure 4.13 Have Reckon Support Vehicles

The NASA Model Shop van contained the pilot station and Silicon Graphics O<sub>2</sub> graphics workstation. The pilot station, as shown in Figure 4.14 consisted of a standard aircraft stick and throttle arrangement. The RP received feedback on aircraft flight performance via a video monitor that displayed UAV out-front video, commanded task, and predicted pitch response cues. Pilot stick inputs were fed to a commercially available R/C aircraft transmitter unit. The workstation received the video and digital data signals provided by the telemetry van. CSC software digitized the analog video signal and buffered it in memory. The additional time delay added to the closed loop Pilot/Display/UAV system was defined by the number of frames buffered. Predicted pitch attitude was calculated using algorithms discussed in section 4.2. The pitch tracking task and predicted pitch attitude displays were mixed into video signal and presented to the RP at the pilot station, Figure 4.15. Pilot inputs along with actual and commanded aircraft attitude in addition to predicted and commanded pitch angle were recorded for later analysis.

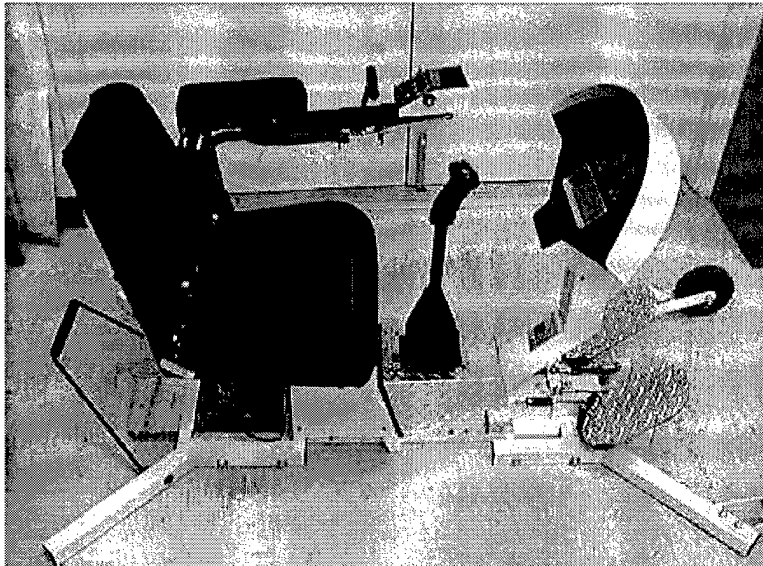


Figure 4.14 Pilot Station



Figure 4.15 Pilot Station With CSC Computer in Model Shop Van



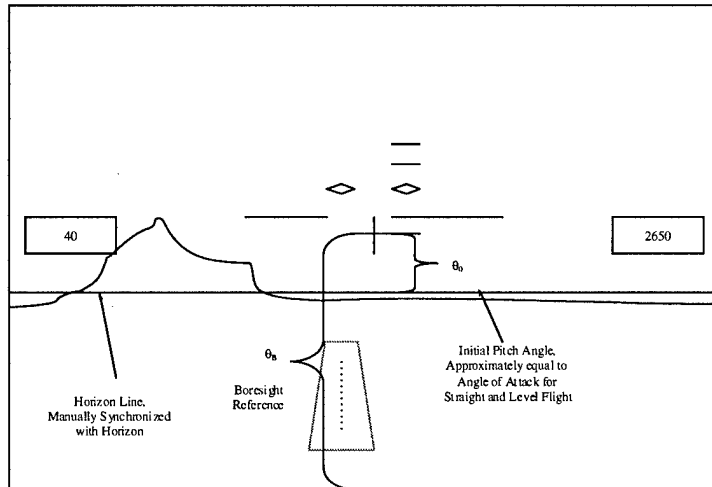


Figure 4.16 Reference Angles for CSC Display

A typical frame of UAV video is shown in Figure 4.3 on page 4-6. Items identified by underlined descriptors were present on the video signal downlinked from the UAV. Italicized descriptors identify data mixed onto the video signal in the workstation.

Specific reference angles for the pitch tracking task, predicted response, and error calculations are identified in Figure 4.16. NASA Model Shop personnel determined that the field of view of the out-front UAV video camera was 37 degrees. Once the video was digitized, this translated to roughly 13 video pixels per degree.

#### 4.4 Test Objectives

The general test objective was to determine the improvement, if any, in UAV handling qualities when using the model-based predictive algorithm to compensate for system time delay. The specific test objectives in support of the general test objective were as follows:

1. Characterize the effects of time delay on UAV handling qualities.

2. Determine the improvement in UAV handling qualities attained by using a model-based predictive compensation technique for additional time delay.
3. Conduct a limited evaluation of the predictive compensation algorithm sensitivity to uncertainty in the aerodynamic model of the UAV and total system time delay.

#### *4.5 Test and Execution*

*4.5.1 General.* Flight testing was conducted at the Air Force Flight Test Center (AFFTC), Edwards AFB, California, from 13 September 1999 to 19 October 1999 at the Model Masters Field on Rosamond Lakebed. It consisted of 16 test days and 62 data sorties with each flight lasting approximately twenty minutes for a total of 18.6 flight hours. Testing was divided into three phases by specific test objective. For the first objective, the test team determined the baseline handling qualities of the UAV using a pitch tracking task and six different additional time delays ranging from 33 to 200 millisecond (msec) in increments of 33 msec. During the second objective, the model-based predictive algorithm was enabled and the handling qualities of the UAV for the same additional time delays as the first test phase were determined. During the third and final phase, a limited evaluation of the sensitivity of the algorithm to uncertainties in the UAV aerodynamic properties and total system time delay was performed. This was accomplished by perturbing the aerodynamic stability derivatives and the compensated additional time delays used when calculating predictor parameters. There were six research pilots for this test program. Pilots and associated flight experience are listed in Table D.1 in Appendix D, page D-1.

#### *4.5.2 Test Procedures.*

*4.5.2.1 Modeling and Simulation.* The test team used the USAF Test Pilot School's Flying Qualities (TPS FQ) simulator to examine the effects of

delay on pilot control strategies, define appropriate pitch tracking tasks, and predict the maximum additional time delay for the baseline UAV,  $\tau_{d_{max}}$ . In order to make the TPS FQ simulator capable of duplicating the UAV handling qualities, baseline system time delay in addition to verified aerodynamic parameters were required. The baseline system time delay of the UAV system was approximately 183 msec (see Appendix G, Section G.2 for further discussion). Verified UAV aerodynamic model parameters were determined during the parameter identification phase of the system checkouts. Refer to Appendix G for these parameters. Finally, the stick feel springs were changed to match the stick force gradient on the UAV pilot station. Once this was accomplished, the RSmith handling qualities criteria (49) implemented in the RSmith32 computer program (1) predicted a Cooper-Harper rating of 5.5 for the baseline configuration. The test team used this RSmith prediction as a starting point for determining appropriate pitch tracking tasks as well as desired and adequate criteria.

The test team used the TPS FQ simulator to examine both a sum of sines and MIL-STD-1797A discrete pitch tracking tasks for use during the flight test. The sum of sines made it difficult for the pilot to assess performance since the error caused by the task was difficult to separate from either disturbances or pilot input. As a result, the discrete pitch tracking tasks were chosen for this evaluation. Both ninety second discrete pitch tracking tasks were flown during the simulator evaluation; however, the tasks were divided into two forty-five second segments for use in the flight test.

*4.5.2.2 Inflight Procedures.* For each test sortie, the RP and Test Conductor (TC) were located in the Model Shop van at the pilot station and the computer workstation. The SP was on the lakebed and was responsible for the safe flight of the UAV. NASA personnel were in the telemetry van ensuring the continued integrity of the flight data. The RP, TC, and SP were within 10 feet of one another to enable verbal communication. Flight test sorties were conducted as follows. The SP performed the UAV takeoff. When safely up and away, the SP placed the UAV on a

straight and level flight path with sufficient airspace for a minimum of 30 seconds of data collection. The TC input the test configuration into the workstation and briefed the test point. The SP transferred longitudinal control to the RP who then performed Phase 1/2 Handling Qualities (HQ) evaluations. Phase 1 HQ evaluations consisted of open and semi-closed loop maneuvers (i.e., pitch captures and gentle maneuvering). Phase 2 HQ evaluations required aggressive and assiduous tracking of the pitch task bars striving consistently for zero error with no pilot compensation. At the end of the pass, the SP turned the UAV and set it up for the Phase 3 HQ evaluations. Phase 3 HQ evaluations required the RP to track one of the three pitch tracking tasks selected at random while maintaining desired performance using normal pilot compensation techniques. After two 30 to 45 second passes of Phase 3 evaluation were complete, the TC recorded the RP's comments, Cooper-Harper ratings (see Figure 2.6 on page 2-7 for definition), and PIO ratings, Figure 4.17. The TC input the next test point into the workstation and the above process was repeated. After all test points were complete or the sortie time expired (approximately 20 minutes), the SP landed the UAV. Once the UAV was on the ground, the test team checked the battery voltage and system status and refueled the UAV for the next sortie. Data passes were limited to less than 45 seconds in order to maintain visual contact with the UAV.

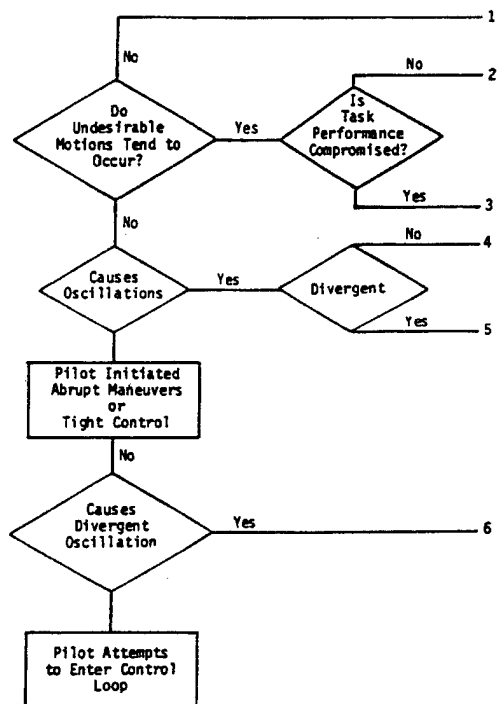


Figure 4.17 Pilot-In-The-Loop Oscillation Rating Scale

4.5.2.3 *Baseline UAV Handling Qualities.* The purpose of Objective One testing was to characterize the effects of time delay on UAV handling qualities by first establishing the maximum tolerable additional time delay and then characterizing the handling qualities of the UAV at various increments of time delay up to the maximum additional. To determine the maximum tolerable additional time delay, each RP evaluated the UAV's PIO susceptibility as the time delay increased in increments of 33 msec using the scale in Figure 4.17. The maximum additional time delay,  $\tau_{d_{max}}$ , was defined as the additional time delay that three of the six RPs gave a PIO rating of 5 or higher. Once the maximum additional time delay was known, the test team completed the randomized test matrix shown in Table D.2, Appendix D, page D-1. Pilot comments and ratings were collected for each test point.

Midway through completion of the Objective One test matrix, the test procedures were altered. The test team intended to minimize pilot bias in Cooper-Harper ratings by using a randomized test matrix with the RP unaware of the additional time delay inserted into the control loop. While this removed any conscious pilot bias, it added a dimension that had not been considered in the test planning. A quick look at the data from the first two RPs showed an interesting dynamic: pilot performance on a test point was affected by the amount of additional time delay on the prior test point. While pilots generally displayed adequate performance on the "known" or warm-up baseline configuration (33 msec delay), they would perform poorly on a baseline configuration test point if it followed a test point involving large additional time delays. Likewise, while pilots performed poorly on test points with very long additional time delays, they would perform notably better on subsequent long delay test points. It became apparent that pilots were quickly adapting to the additional time delay and were adopting control strategies for the best performance in the face of that delay. However, previously adopted control strategies were affecting subsequent test points. Discussions with Mr. David Mitchell (Hoh Aeronautics),

a recognized expert in the field of handling qualities, revealed that this phenomenon had been encountered in previous research.

Test procedures were changed to negate as much of this effect as possible. The RP flew a warm-up with a 33 msec additional time delay. Immediately after, the RP flew with a 200 msec additional time delay. This was to provide the RP with known best (33 msec) and worst (200 msec) case configurations. The RP would then fly the test points assigned in the order defined in the test matrix. However, the RP was given the best case configuration of 33 msec delay whenever the randomized test matrix called for a large change in additional time delay between test points. The TC was responsible for injecting the best case configurations and told the RP that he or she was seeing the base case configuration. The TC was able to inject the best case configuration at random and as necessary to prevent the RP from gaining any knowledge of what the next additional time delay was likely to be. This procedure effectively "reset" the pilot's control strategies and allowed a more accurate assessment of additional time delay effects on performance and workload. The RPs reaccomplished their previous sorties to ensure that all data were collected using the same method. Although effective in improving data quality, this method cut the number of test points per sortie in half. Thus, the number of sorties to determine the baseline UAV handling qualities was almost twice the number originally planned.

*4.5.2.4 Improvement of UAV Handling Qualities using Model-Based Predictive Compensation.* The purpose of the second objective was to determine the improvement in UAV Handling Qualities attained using a model-based predictive compensation technique by first establishing the maximum additional time delay and then characterizing the handling qualities of the UAV at the same additional time delays investigated in the first objective. The addition of the washout filter described in Section 4.2.2, page 4-11, changed the dynamics of the predictor at large additional time delays. Thus, the maximum additional time delay was set at 400

msec. Each RP flew test points at 200, 300 and 400 msec additional time delay prior to beginning a test matrix designed to provide head-to-head comparison of the compensated and uncompensated configurations. The test points flown to determine the compensated UAV handling qualities are listed in Table D.3, Appendix D, page D-2.

During this test phase, the test team noted that the RPs found very little difference in predictive display handling qualities at different additional time delays. This eliminated the need for injecting best case configuration test points to reset pilot compensation strategies.

#### *4.5.2.5 Sensitivity of Model-Based Predictive Compensation Algorithm.*

The purpose of the third objective was to perform a limited evaluation of the sensitivity of the model-based predictive compensation algorithm to uncertainty in the aerodynamic model of the UAV and in total system time delay. Aerodynamic model uncertainty was simulated by altering the stability derivatives by  $\pm 20\%$  as shown in Table D.4, Appendix D, page D-2. Time delay uncertainty was simulated by changing the amount of additional time delay compensated for by  $\pm 33\%$  in the compensation algorithm and keeping the additional time delay constant at 100 msec as shown in Table D.5, Appendix D, page D-3. For each sortie, the RP started with a 100 msec additional time delay using the predictor compensation algorithm before beginning the test point matrices.



## V. *Flight Test Results and Analysis*

### 5.1 *Baseline UAV Handling Qualities*

The first phase of the flight test program sought to characterize the effects of time delay on the Utility UAV handling qualities. These results would then serve as a “baseline” against which predictor flight test data could be compared.

*5.1.1 Modeling and Simulation.* The test team used the USAF Test Pilot School’s Flying Qualities (TPS FQ) simulator to examine the effects of delay on pilot control strategies, define appropriate pitch tracking tasks, and predict the maximum additional time delay,  $\tau_{d_{max}}$ , for the baseline UAV.

Each RP flew the UAV dynamics on the TPS FQ simulator with increasing amounts of additional time delay before and after flight testing the UAV. RPs flew the additional time delays specified in Table 5.1.1. Pilot comments and performance as well as PIO ratings were recorded. The test team found that total system delays of between 500 and 550 msec resulted in PIO ratings of 5. Table 5.1.1 summarizes the PIO ratings as a function of additional time delay. Each RP returned to the simulator after the flight testing was complete to validate the learning curve. Statistical tests (see Appendix F) confirmed that PIO ratings were the same before and after flight testing with 90% confidence. Thus it was assumed that no significant learning curve biased flight test results.

*5.1.2 Flight Test.* As had been done in the simulator, each RP flew the baseline UAV through a series of increasing additional time delays until they gave the configuration a PIO rating of 5. The maximum additional time delay was determined in accordance with the test plan (55) as that additional time delay for which three of the six RPs gave a PIO rating of 5. The maximum additional time delay for the

Table 5.1 Flying Qualities Simulator PIO Ratings

RP	$\tau_d$ (msec)	100	200	300	350	400	450	500	550	600
1	Session 1	2	3	3	4	4	4	4	5	X
	Session 2	2	3	3	3	4	4	5	X	X
2	Session 1	X	X	X	X	X	X	X	X	X
	Session 2	2	4	4	4	4	4	4	5	X
3	Session 1	2	3	3	4	4	4	4	5	X
	Session 2	X	X	X	X	X	X	X	X	X
4	Session 1	2	3	4	4	4	4	4	5	X
	Session 2	2	3	3	3	4	4	4	4	5
5	Session 1	1	2	2	2	3	3	5	X	X
	Session 2	2	2	2	4	4	5	X	X	X
6	Session 1	2	2	3	4	4	4	4	5	X
	Session 2	2	3	3	3	4	5	X	X	X

baseline UAV was determined to be 189 msec. The inherent system time delay of 183 msec combined with the 189 msec additional time delay gave a total system time delay of approximately 372 msec; 26% less than the simulator predicted value.

While the test team was establishing the baseline maximum additional time delay, pilot performance was recorded for use in determining desired and adequate scoring criteria. Pilot performance was scored in real time to provide the RP with an aid in making appropriate Cooper-Harper ratings. Since no mission representative criteria were available, the test team chose available criteria from MIL-STD-1797A (14). Desired and adequate criteria were set at 5 mils and 10 mils respectively. Actual pilot performance for the baseline configuration was generally above 50% in the adequate range. The test team used the RSmith criteria prediction that the baseline UAV was a Cooper-Harper 5.5 and using this as a starting point, defined desired and adequate performance as 50% of the time in the appropriate range.

With the maximum additional time delay and desired/adequate criteria defined, the test team began the test point matrix defined in Table D.2 in Appendix D on page D-1. The four pitch tracking tasks initially used were derived from the

MIL-STD-1797A discrete pitch tracking tasks. The two 90 second tasks defined in the MIL-STD were each divided in half to yield four 45 second tasks named 1A, 1B, 2A, and 2B. The tasks were considered equally difficult; however, task 1B proved to be much easier since the more difficult portion of the task occurred in the last 15 seconds. Since the average data pass was 38 seconds, the more difficult portion of the task was essentially cut off. The test team discarded task 1B and proceeded with only three tasks. Test points were reaccomplished as necessary.

The results of the uncompensated flight testing formed the baseline to which the results from the predictor flight test were compared and are included in the plots in the following sections. Data specific to the first objective may be found in Appendix E. Pilot comments and ratings are included in Table E.1 through E.6 on pages E-1 to E-4. The baseline UAV was a Level 2 aircraft for additional time delays from 22 msec to 122 msec. Above these additional time delays, the UAV was a Level 3 aircraft.

During the analysis of these results, the test team discovered that actual additional time delays differed from the additional time delays discussed in the test plan (55). The first frame of additional time delay was actually 22 msec instead of the 33 msec initially assumed. Thus, while subsequent time delays were still in increments of 33 msec, they were offset by 11 msec. All of the data figures are based on the actual additional time delays. Discussions of test points flown will be based on those in the test plan.

## *5.2 Improvement of UAV Handling Qualities using Model-Based Predictive Compensation*

The second phase of flight testing was to determine the improvement in UAV Handling Qualities attained by using the model-based predictive compensation technique for additional time delay.

*5.2.1 Modeling and Simulation.* Early predictor test flights indicated that the predictive algorithm developed with a linear system model was sensitive to unmodeled nonlinearities. In the absence of pilot input, the predicted pitch should equal the actual pitch after the system time delay had elapsed. The test team found that this was not the case in most of the early predictor test flights. Specifically, the predicted pitch would begin to deviate from the actual pitch due to unmodeled disturbances such as wind gusts. The test team also determined that the predicted pitch would acquire a growing offset from actual pitch when the pilot attempted to track ramp functions in the MIL-STD-1797A pitch tracking tasks.

Simulink<sup>TM</sup> models of the compensated predictor UAV system run in Matlab<sup>TM</sup> suggested that a deadband was responsible for the growing offset during ramp input tracking. The flight test hardware was examined and no mechanical deadband was observed between pilot input and elevator position. It was possible that an aerodynamic deadband existed since small elevator deflections, less than 0.25 degrees, elicited no aircraft response during a flight test sortie flown to specifically quantify dead band effects. The Simulink<sup>TM</sup> model was used to confirm that once the deadband was appropriately modeled in the predictor software, the deadband effects on predictor performance were significantly reduced. However, the addition of deadband modeling did not entirely account for the unmodeled effects observed during flight test. Since the predictor algorithm was derived from the equations of motion linearized about a trim condition, any external disturbance to the trim condition (i.e. turbulence and wind gusts) would result in the predicted pitch attitude deviating from the actual pitch attitude. Model infidelities and integration algorithm error would have similar effects. Deviations from the linear model were accounted for with the addition of a washout filter designed to bias the predicted pitch to the actual pitch with a one second time constant. Section 4.2.2 on page 4-11 details the design, implementation, and flight test of the washout filter and deadband compensation.

The addition of the washout filter limited the maximum additional time delays that could be tested with the predictor enabled. For the one second time constant selected, 63% of the prediction was washed out at one second. Thus, as the additional time delay increased, the pilot would begin to see the dynamics of the washout filter rather than the predictor. This effect was most noticeable above 389 msec; therefore, the maximum additional time delay tested with the predictor algorithm was set at 389 msec. All six RPs flew one 389 msec additional time delay test point in addition to the test matrix from the first objective.

*5.2.2 Flight Test.* The test team RPs flew the test point matrix outlined in Table D.3 on page D-2 in Appendix D. Increasing additional time delay did not appreciably affect the handling qualities of the predictor. This allowed the test team to progress through the test points without the time consuming process of injecting best case configuration points between test points as was required in the first objective. Pilot comments and ratings are in Tables E.7 to E.12 on pages E-5 to E-10 in Appendix E. Comparisons were made between the baseline and compensated configurations using maximum additional time delay, Cooper-Harper ratings, PIO ratings, root mean square tracking error (RMSTE), and root mean square display error (RMSDE). The Cooper-Harper and PIO rating definitions are in Figure 2.6 and 4.17, respectively. RMSTE was a measure of how well the boresight of the UAV was tracking the pitch task bars. RMSDE was a measure of how well the pilot made the predicted pitch attitude, determined by the model-based predictor compensation algorithm, track the task bars. Comparisons between the two configurations were developed using the data analysis methods detailed in Appendix F. Overall, UAV handling qualities improved with respect to maximum additional time delay and Cooper-Harper ratings; however, there was no statistical improvement in PIO ratings or pilot performance (i.e. RMSTE).

5.2.2.1 *Maximum Additional Time Delay.* With the compensation enabled, the maximum additional time delay of 389 msec was double that of the uncompensated system with 189 msec of maximum additional time delay. This shows a substantial improvement; however, the quality of that improvement was also of interest. The average Cooper-Harper rating for the predictor compensated UAV with an additional 189 msec delay was 4.8. The average Cooper-Harper rating for the 389 msec test point was 5.3. Thus, even at 389 msec of additional time delay, the UAV was still a Level 2 aircraft. The raw data used to develop these averages are in Tables E.7 to E.12, Appendix E. Looking at the raw data for the 189 msec additional time delay using the compensation algorithm, six out of six RPs rated the UAV as Level 2 with Cooper-Harper ratings ranging from 4 to 5. At 389 msec, five out of six RPs rated the compensated UAV as Level 2 with Cooper-Harper ratings ranging from 4 to 7. These results contrast sharply with the baseline maximum additional time delay of 189 msec: five out of six RPs rated the baseline UAV as Level 3. Not only did the compensation double the maximum additional time delay, it also showed a one level handling qualities improvement of the UAV from the baseline configuration.

Additionally, pilots did not show a tendency to PIO at 389 msec when using the predictor. Initial set up of the test point required the RP to fly the UAV without the compensation algorithm enabled. RPs noted that PIOs were easily entered; however, once compensation was enabled, there were no PIO tendencies. PIO ratings at the maximum additional time delay for the compensated configuration ranged from 3 to 4.

5.2.2.2 *Cooper-Harper Ratings.* When using the model-based predictor compensation, the Cooper-Harper ratings improved over the baseline configuration in two distinct ways. First, a one-to-one comparison of baseline results with predictor compensated results showed that the algorithm improved Cooper-Harper

ratings. Second, with the compensation enabled, Cooper-Harper ratings dependence on additional time delay was significantly diminished.

The average Cooper-Harper ratings for the two configurations are depicted in Figure 5.1 with 90% confidence intervals and in Figure 5.2 with minimums and maximums. Looking at the figures and comparing ratings for each additional time delay; the Cooper-Harper ratings improved in both an average and statistical sense with the predictor enabled. Thus, the pilot experienced a significantly reduced workload when using the predictive compensation algorithm. Comments in Tables E.7 to E.12 further support these conclusions. RP 3 commented on high workload during the 100 msec Objective 1 test point. Once the predictor compensation algorithm was enabled, the pilot commented that his compensation was moderate. RP5 noted that good performance was easier to attain with the compensation enabled.

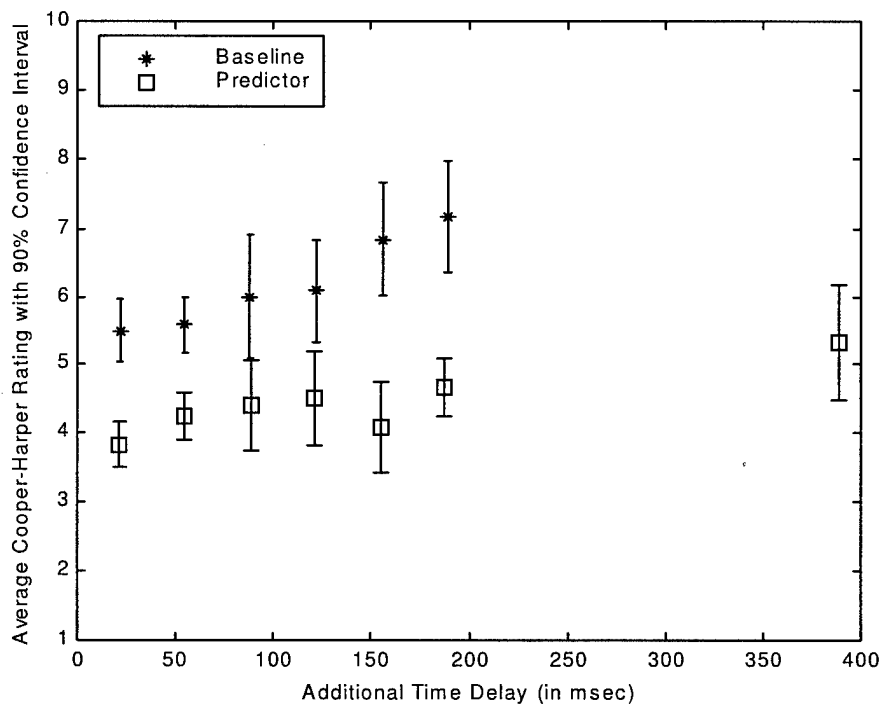


Figure 5.1 Average Cooper-Harper Rating with 90% Confidence Interval

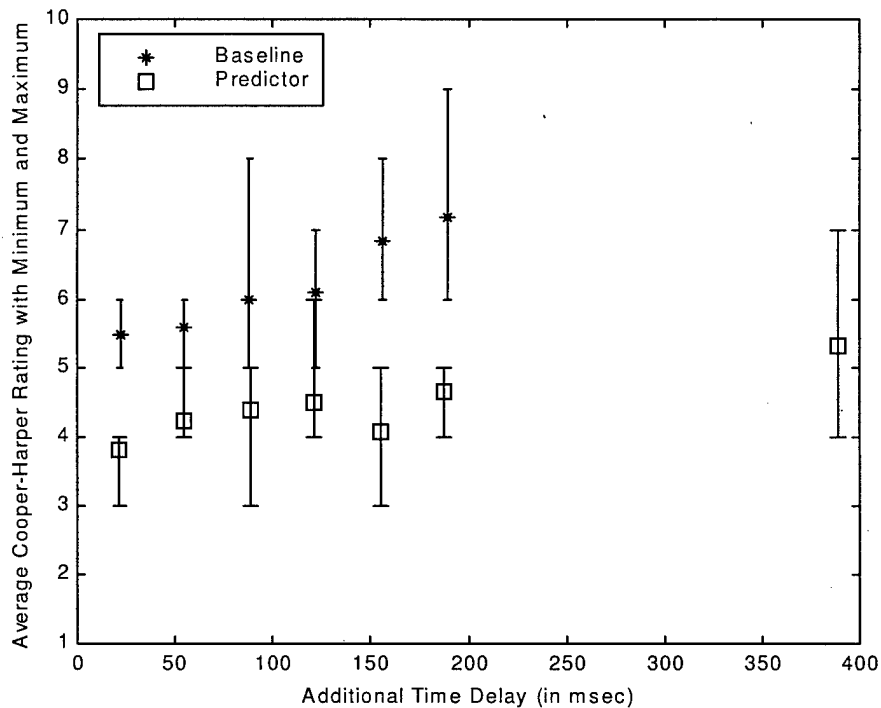


Figure 5.2 Average Cooper-Harper Rating with Minimum and Maximum

The second improvement characteristic was that Cooper-Harper ratings became less a function of additional time delay when the compensation algorithm was enabled. Looking again at Figure 5.1 and Figure 5.2, the Cooper-Harper ratings for the baseline configuration substantially degraded with additional time delay. Once the compensation was enabled, this degradation in Cooper-Harper ratings with respect to additional time delay was not as substantial, and the pilot did not have to drastically alter his or her workload or compensation techniques with increasing additional time delay.

*5.2.2.3 Pilot-in-the-Loop Oscillation Ratings.* PIO ratings were also used to determine if the predictor algorithm improved the handling qualities of the UAV. There was no statistically significant improvement in PIO ratings; however,



the dependence of PIO ratings with respect to additional time delay decreased when the compensation was enabled.

The average PIO ratings with 90% confidence intervals are plotted as a function of additional time delay in Figure 5.3 and in Figure 5.4 with minimums and maximums. Except for the 122 and 189 msec test points, there was no clear statistical improvement in the PIO ratings. This conclusion was further substantiated by comparing the pilot ratings and comments in Tables E.7 to E.12 on pages E-5 to E-10 in Appendix E. For the baseline configuration, the PIO ratings at 189 msec ranged from 3 - 5. For the predictor compensated configuration, the PIO ratings ranged from 3 to 4 at 189 and 389 msec. The significant conclusion to be drawn was that in spite of the fact that the predictor compensated maximum additional time delay was nearly double that of the baseline, 389 msec of additional time delay still did not cause a PIO (i.e., PIO rating of 6).

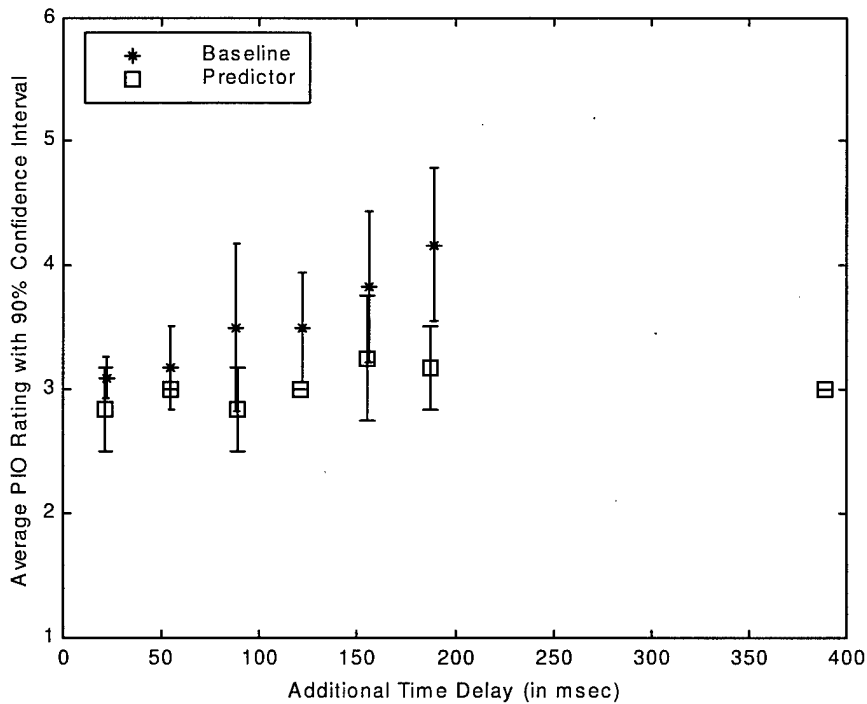


Figure 5.3 Average PIO Rating with 90% Confidence Interval

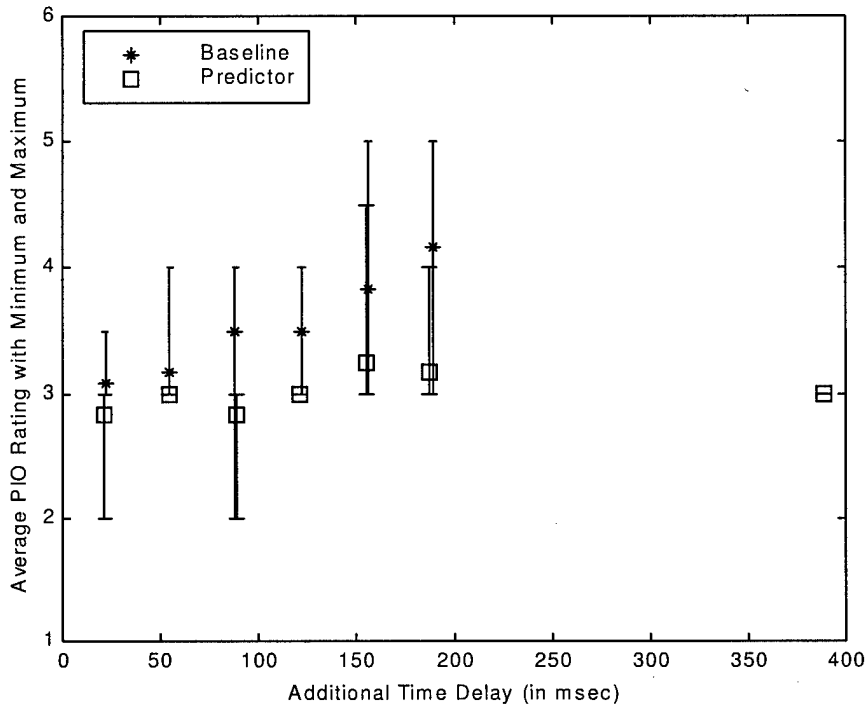


Figure 5.4 Average PIO Rating with Minimum and Maximum

While the PIO ratings did not statistically improve from the baseline, they were less a function of additional time delay and a general trend toward improvement can be observed. For the baseline configuration, there was a marked degradation in PIO ratings as the additional time delay increased. For the compensated configuration, the PIO ratings were fairly constant describing a trend toward improvement over the baseline configuration.

With the improvement in the Cooper-Harper ratings for the compensated configuration, the lack of improvement in the PIO ratings required some additional analysis. This seeming lack of improvement may be the difference between the two rating scales. PIO ratings were based on the pilot's perception of aircraft response. Cooper-Harper ratings were based on pilot workload (to include compensation) and performance. The predictor was created to simulate UAV response and remove the additional time delay. If the predictor were implemented correctly, PIO ratings

would be fairly constant across the range of additional time delays. Looking at the PIO ratings in Figure 5.3 and Figure 5.4, the predictor performed as expected. It removed the additional time delay (as evidenced by the fairly flat curve), but it maintained the aircraft response since there was no significant improvement in PIO ratings. The trend toward improvement, however, was present and may have been more pronounced if the baseline test vehicle were Level 1 with no additional time delay.

*5.2.2.4 Root Mean Square Tracking and Display Errors.* There were three primary results from this portion of the investigation. First, time delay compensation had no effect on RMSTE. Second, pilots were able to track the task bars more accurately with the predicted pitch bars as measured by the RMSDE. Third, the predictor compensation algorithm did not predict aircraft pitch response accurately enough to improve overall pilot/display/UAV system performance.

The time delay compensation did not degrade RMSTE. The average RMSTE with 90% confidence intervals are plotted as a function of additional time delay in Figure 5.5 and with minimums and maximums in Figure 5.6. There was no statistical change in performance between the two configurations. However, simulations done in Chapter III predicted a clear improvement in tracking error as the predictor eliminated lightly damped PIO. The flight test results, therefore, were somewhat unexpected. Many individual test points showed a notable reduction in oscillations and a corresponding improvement in performance. However, most test points showed steady state pitch angle offsets which greatly increased RMSTE. Section 5.4 contains a detailed analysis of steady state predictor error.

The RMSDE was a measure of how well the RP was able to make the predictor bars track the pitch task bars on the pilot display. The average RMSDE and the average RMSTE, both with 90% confidence intervals, are plotted as a function of additional time delay in Figure 5.7 and with minimums and maximums in Figure 5.8.

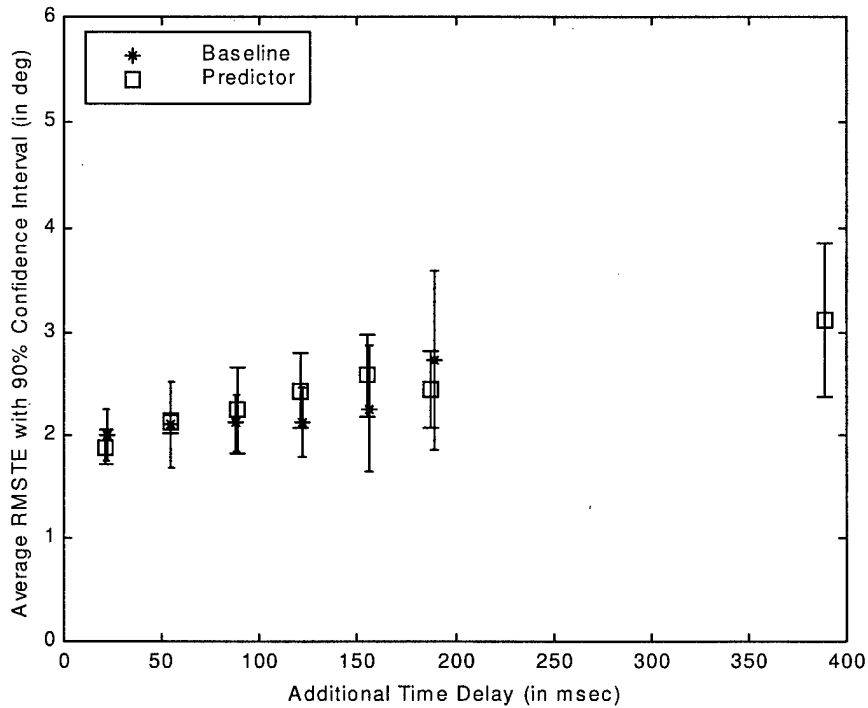


Figure 5.5 Average Root Mean Square Tracking Error with 90% Confidence Interval

Except for 122 msec, pilot performance using the predictor bars was better than boresight tracking performance for both the baseline and compensated configuration.

The RMSTE for the compensated configuration was a combination of pilot error and predictor error. Referring to the definitions in Figure F.1 on page F-3, it may be seen that if the predicted pitch were equal to the actual pitch when adjusted for additional time delay, the RMSTE and RMSDE would be equivalent. Additionally, if the predictor accurately modeled the UAV response, the compensated RMSTE would closely match the RMSDE. Looking again at Figures 5.1 and 5.5, it is clear that the predicted response did not forecast the actual UAV accurately enough to reduce both workload and improve task performance. This was most likely due to external disturbances or errors in the linear model.

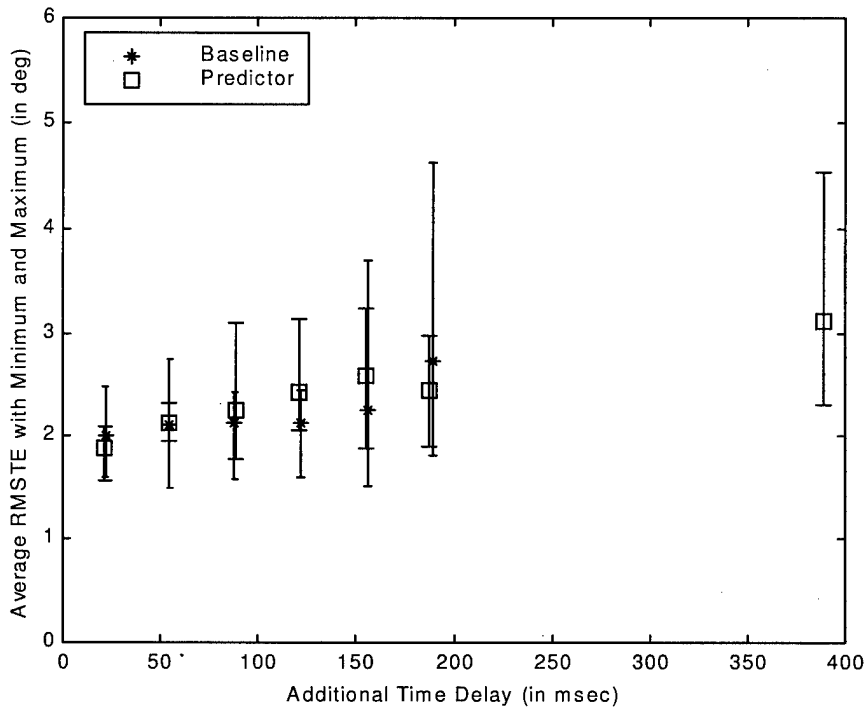


Figure 5.6 Average Root Mean Square Tracking Error with Minimum and Maximum

Analysis and simulation conducted after the flight test program was complete revealed that improvements in predictor performance were possible. This analysis is discussed in detail in Section 5.5.

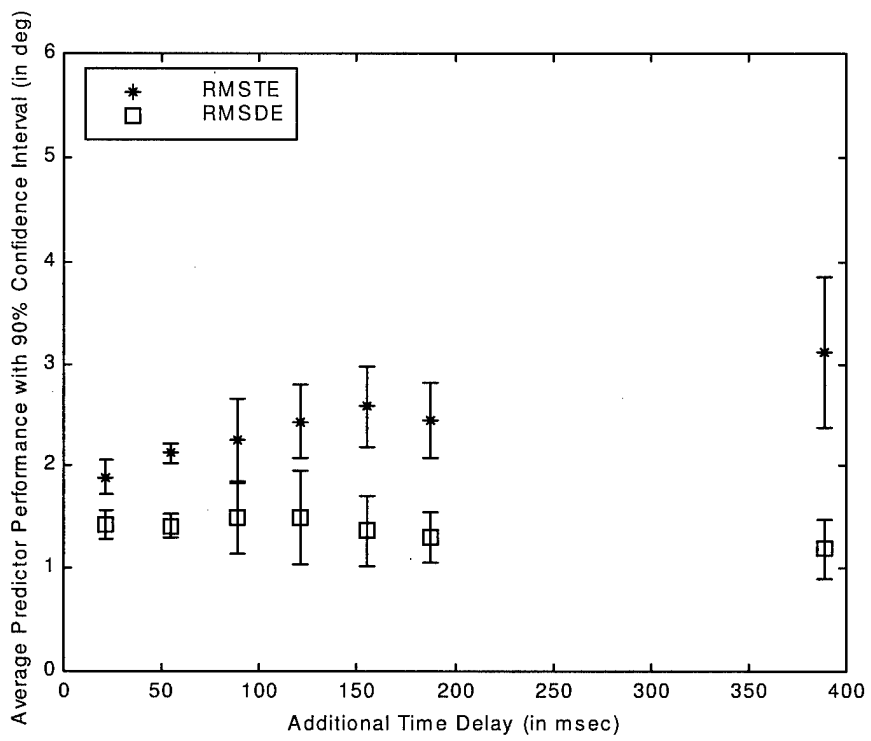


Figure 5.7 Average Predictor Performance with 90% Confidence Interval

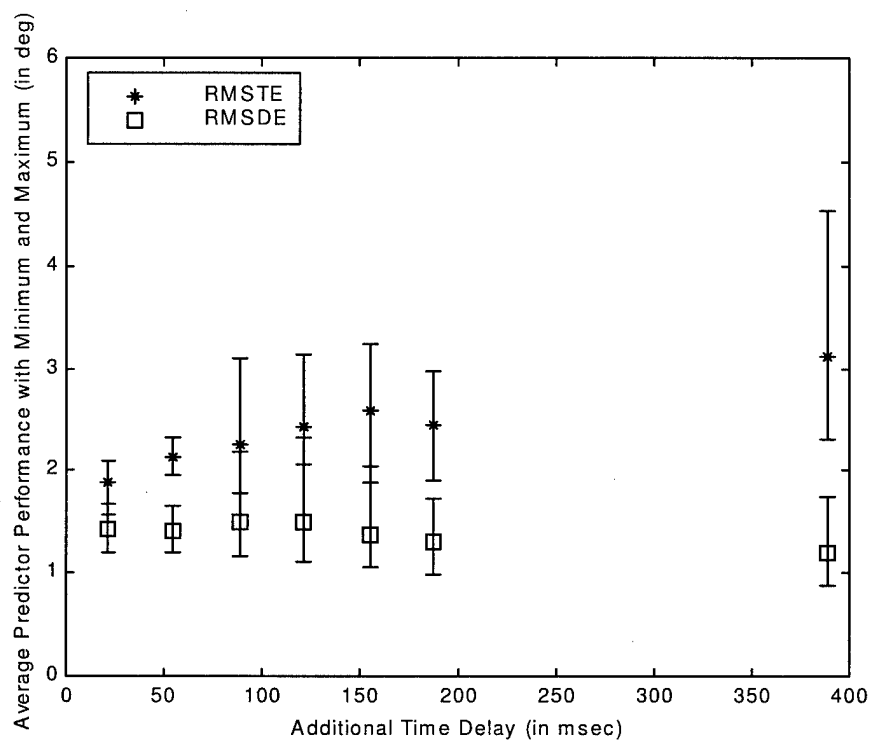


Figure 5.8 Average Predictor Performance with Minimum and Maximum

### 5.3 Sensitivity of Model-Based Predictive Compensation Algorithm

The purpose of this segment of the flight test program was to conduct a limited evaluation of the model-based predictive compensation algorithm sensitivity to uncertainty in the UAV aerodynamic model and total system time delay.

*5.3.1 Modeling and Simulation.* The test team used the TPS FQ simulator to perform a limited evaluation of the UAV handling qualities sensitivity to stability derivative variations. This evaluation was conducted in order to determine stability derivative candidates for variation in the third objective. The assumption was made that a parameter variation in a stability derivative that significantly impacted UAV handling qualities in the simulator would similarly impact the predictor handling qualities during flight test. The test team determined that variations in  $C_{L_{\delta_e}}$  and  $C_{L_{\alpha}}$  had little effect on handling qualities. These parameters were not considered for the sensitivity analysis. Parameters that did have a large effect were  $C_{M_{\alpha}}$ ,  $C_{M_q}$ , and  $C_{M_{\delta_e}}$ . These parameters were varied by  $\pm 20\%$  as shown in Tables D.4 and D.5 on page D-2, Appendix D.

*5.3.2 Flight Test.* Program delays due to issues discussed in the previous sections caused the test team to enter the third phase with the sub-optimal test matrices in Tables D.4 and D.5. The test team considered variations in candidate stability derivatives of  $\pm 20\%$  and variations in additional time delay of  $\pm 33$  msec. Actual additional time delay for all test points was 88 msec. Stability derivative parameter variations for each test point were applied to the aerodynamic model from which the predictive display was derived. The predictor was not appreciably affected by uncertainty in the aerodynamic parameters and time delays tested. The stability derivative that most affected pilot comments and ratings was  $C_{M_{\alpha}}$ . The stability derivative that most affected performance was  $C_{M_q}$ . Time delay uncertainty had a statistically insignificant impact on pilot comments, ratings, and performance.



The robustness of the predictor algorithm to model variations in this flight test program reflects well on the operational utility of the predictor. A pilot flying an operational UAV mission would likely find any changes in vehicle flying qualities caused by time delay or model uncertainties objectionable. Total system time delay is likely to vary during a UAV mission especially using OTH communication relays. If the predictive display compensated UAV flying qualities change from moment to moment as system latencies vary; pilot workload is likely to be increased as the pilot struggles to shift control strategies. Even with “gain scheduling” of aerodynamic model parameters for changing flight conditions, uncertainties are likely to exist. The flight test results show the compensated UAV handling qualities were essentially unaffected by model and time delay uncertainties. Operational pilots using the predictive compensation technique will be presented with predictable handling qualities throughout the mission profile.

*5.3.2.1 Stability Derivative Uncertainty.* As mentioned above, the stability derivatives examined during the sensitivity analysis were  $C_{M_\alpha}$ ,  $C_{M_q}$ , and  $C_{M_{\delta_e}}$ . Pilot comments and ratings were not sufficient to clearly determine factor effects. To help determine what effects were significant, the test team used the Response Surface Methodology (RSM) approach described in Appendix F. Using this approach, the stability derivative that had the most effect on pilot comments and ratings was  $C_{M_\alpha}$ . The stability derivative that had the most effect on pilot performance was  $C_{M_q}$ .

Looking at pilot comments in Tables E.13 to E.15 on pages E-11 to E-13 in Appendix E, it was difficult to draw conclusions regarding the specific configurations. For example, when all three stability derivatives were increased by 20%, RP comments were contradictory. Two RPs commented on undershoots while the third found overshoots. One found the configuration more predictable; another did not. This was likely due to different control strategies adopted to compensate for changes in the predictor response. The PIO ratings for all three RPs were 3 with Cooper-

Harper ratings ranging from 4 to 5. The same comment inconsistencies were found when all three derivatives were reduced by 20%. Two RPs commented on overshoots; another said it undershot. Two RPs said there was no difference from the baseline; another said it was better. PIO ratings ranged from 2 to 3 and Cooper-Harper ratings ranged from 3 to 5. Raw data were not sufficient to determine significant effects and factors.

The RSM approach described in Appendix F was used with the ratings, RMSTE, and RMSDE to determine the significant stability derivatives. The RSM determined that Cooper-Harper and PIO ratings were most affected by  $C_{M_\alpha}$ ; RMSTE and RMSDE were most affected by  $C_{M_q}$ .

The stability derivative's effect on predictor performance can be explained by looking at the model the predictor used to determine the pitch response of the UAV to a given pilot input. Referring to Section 4.2, the mathematical derivation of the predictive display reveals that the predicted pitch attitude is derived from the system state, which includes  $C_{M_\alpha}$ ,  $C_{M_q}$ , and  $C_{M_{\delta_e}}$  and the amount of time delay,  $\tau_d$ . Variations in  $C_{M_\alpha}$  and  $C_{M_q}$  predominantly affect the short period response of the predictor. Variations in  $C_{M_{\delta_e}}$  are reflected predominantly in the overall system gain.

Given the effect of  $C_{M_\alpha}$  and  $C_{M_q}$  on the predictor's short period response, the observed differences in pilot opinion and performance in the face of these parameter variations may be explained. The washout filter passed higher frequency dynamics such as the short period response characteristics. Thus changes in the short period flying qualities of the UAV induced by stability derivative parameter variation were passed directly to the pilot.

A variation in the static stability parameter  $C_{M_\alpha}$  resulted in a change of the system's natural frequency and a mismatch between the speed of the predictive response and the actual response. This mismatch in response times was not found to increase overall system tracking error during flight test. RPs were accustomed to the predictive display leading the UAV response and were not particularly sensitive

to small variations in the lead generated by the display. While system performance was not degraded in this case, an increase in pilot workload was indicated by a decrease in average Cooper-Harper rating.

In the case of an increase in the system damping parameter  $C_{M_q}$  the pilot saw a more heavily damped, sluggish predictor and was likely to over control the system resulting in a decrease in overall performance. This was reflected in flight test data.

Pilots are able to compensate for system gain variations. With this in mind, the fact that RP comments and workload were not significantly affected by variations in  $C_{M_{\delta_e}}$  was understandable. Nevertheless, a variation in the predictive display gain should have negative effects on tracking performance as a pilot input causes a smaller or larger predictor response than appropriate. However, the addition of the washout filter described in Section 4.2.2 added a new dynamic to the predictor. Specifically, the washout filter significantly attenuated low frequency contributions to the overall predictor response, such as a gain variation. Examination of the Bode magnitude response of the washout filter implemented for the flight test, Figure 5.9, shows that steady state terms were virtually eliminated. Thus the negligible effects of  $C_{M_{\delta_e}}$  variation were not surprising.

*5.3.2.2 Time Delay Uncertainty.* Time delay uncertainty did not significantly affect pilot ratings and performance. This result was determined using both a classical statistical methodology as well as the RSM approach described in Appendix F. Classical statistical methodology showed that the time delay uncertainty had no effect on Cooper-Harper and PIO ratings. Time delay uncertainty also did not affect RMSTE or RMSDE. RSM results were similar to the classical results in that time delay did not affect Cooper-Harper ratings, RMSTE, and RMSTE. Further discussions regarding this analysis and the resulting RSM models can be found in Appendix F.

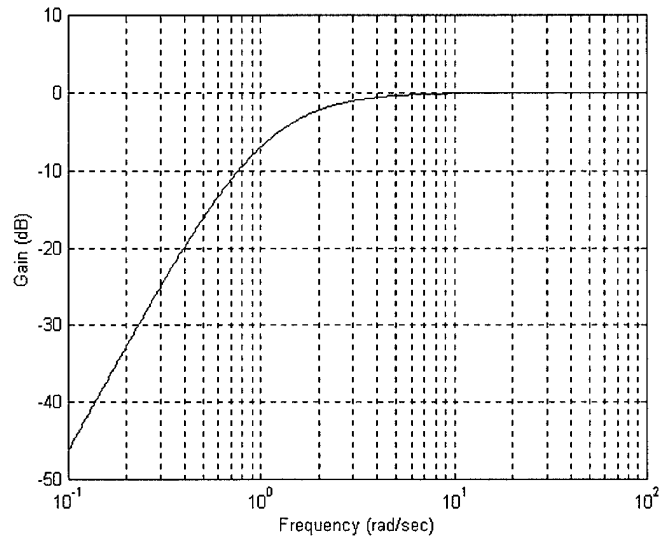


Figure 5.9 Bode Magnitude Response of Washout Filter

The predicted UAV pitch response was determined using the system state space model and the system time delay. Pilot inputs were passed through a gain determined by the system states integrated over the time delay. Thus, the amount of time delay and hence time delay uncertainties affect the gains placed on the pilot input. As stated above, pilots were able to compensate for system gain variations. Thus, the negligible effects of time delay uncertainty were not surprising.

The limited sensitivity analysis performed in this flight test revealed a slight variation in predictor handling qualities with parameter variations in the aerodynamic model. This variation, however, was not large enough to be operationally significant. The parameter variations examined in this test were  $\pm 20\%$  for the stability derivatives and  $\pm 33\%$  for additional time delay. These variations were on the low end of the traditional 20 to 40% expected errors in predicted stability derivatives. If predictive compensation were to be employed on UAV designs with unverified aerodynamics, additional flight testing would be necessary to ensure that no significant handling qualities “cliffs” exist with model parameter variations of as much as 40%.

Additional flight test should be conducted to explore the impact of larger model and time delay uncertainties on the predictive display handling qualities.

#### 5.4 *Flight Test Time Histories*

Even though the statistical analysis of the flight test data did not show a significant improvement in performance with the predictive display, many individual test points showed a notable reduction in oscillations and a corresponding improvement in performance. However, many test points showed considerable steady state offsets which greatly increased RMSTE. The time history for test point 1214 is displayed in Figure 5.10. Test point identification numbers are of the form *WXYZ*; *W* is the flight test objective number, *X* is the specific Measure of Performance (MOP), see Appendix F for description, *Y* identifies the RP that flew the point, and *Z* is the order that the RP flew the test point in the test matrices, see Appendix D. Other information regarding the test point, such as RMSDE and RMSTE, can be found in Appendix E and Appendix F by using the information coded into the test point identification number.

A comparison of the uncompensated data in Figure 5.10 to the compensated data in Figure 5.11 reveals both an improvement in performance and the presence of a steady state offset. The improvement in performance is clear, particularly in ramp tracking. However, a one degree steady state offset begins to develop at the beginning of the ramp tracking and can clearly be seen after approximately 30 seconds into the task. The RMSDE data show the pilot is accurately tracking the command with the predictor bars. The actual pitch attitude, however, is offset by approximately one degree. The offset is more clear when comparing Figure 5.12 to 5.13 and Figure 5.14 to 5.15. When no offset is encountered, the actual pitch follows the predicted pitch nicely, (reference Figures 5.16 and 5.17).

An extreme example of a steady state offset can be observed at the maximum allowable compensated time delay of 389 msec, Figure 5.18. The UAV was uncontrol-

lable at this delay with no compensation, thus no data is available for comparison. However, the nearly four degree steady state offset is obvious.

The wide variation in RPs, see Table D.1 on page D-1, provided a variety of control strategies. The performance improvement seen by a "high gain" RP using the predictive display is evident in Figures 5.19 and 5.20.

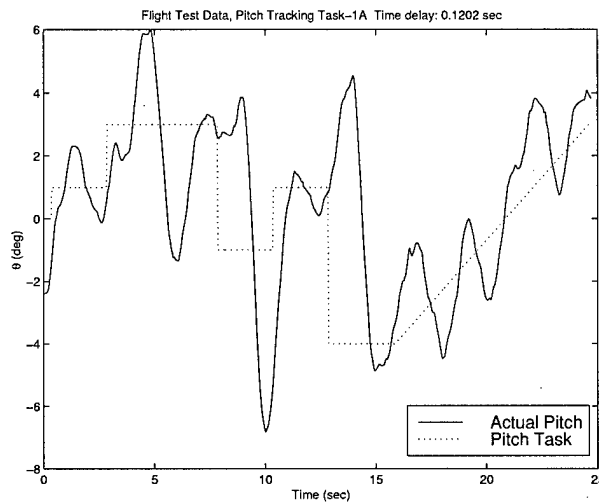


Figure 5.10 Flight Test Data, Test Point 1214, 120 msec Additional Delay, Baseline

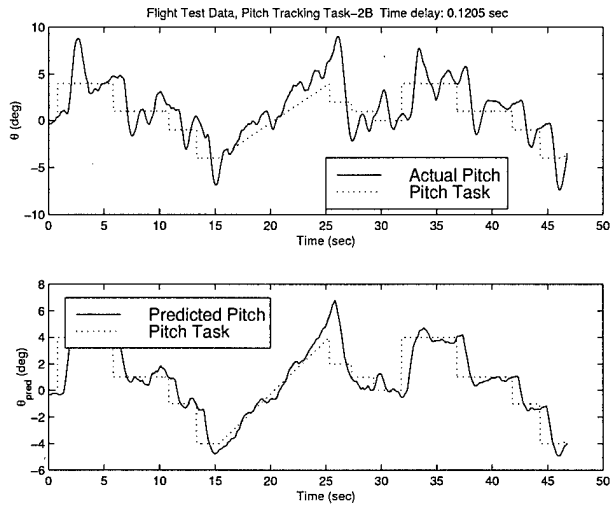


Figure 5.11 Flight Test Data, Test Point 2213, 120 msec Additional Delay, Predictive Compensation

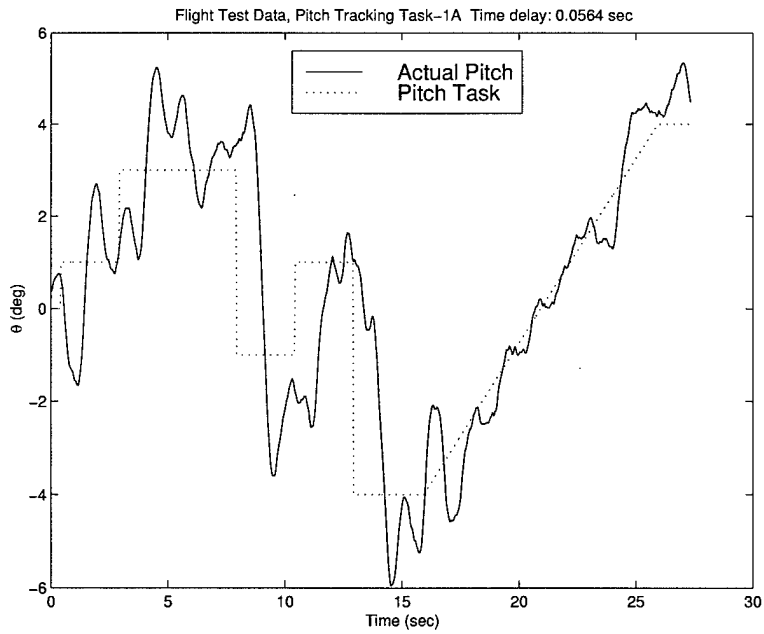


Figure 5.12 Flight Test Data, Test Point 1221, 55 msec Additional Delay, Baseline

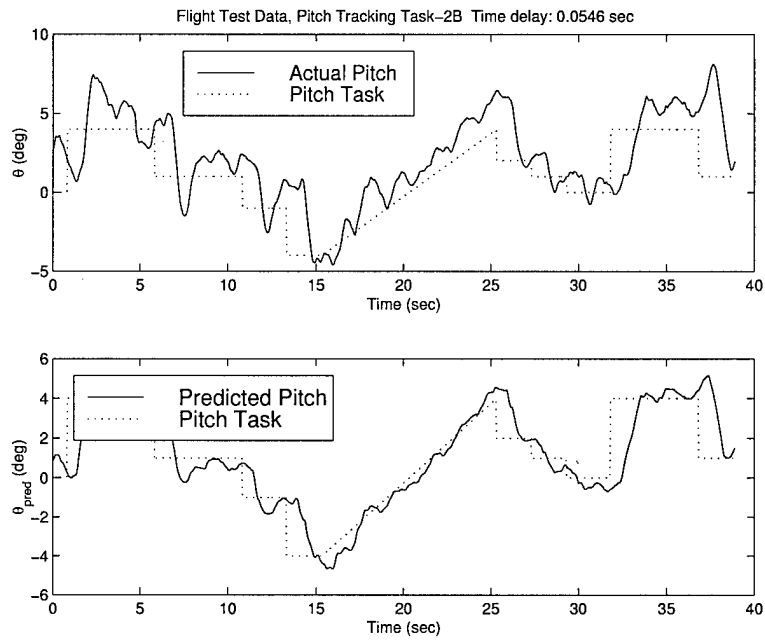


Figure 5.13 Flight Test Data, Test Point 2223, 55 msec Additional Delay, Predictive Compensation

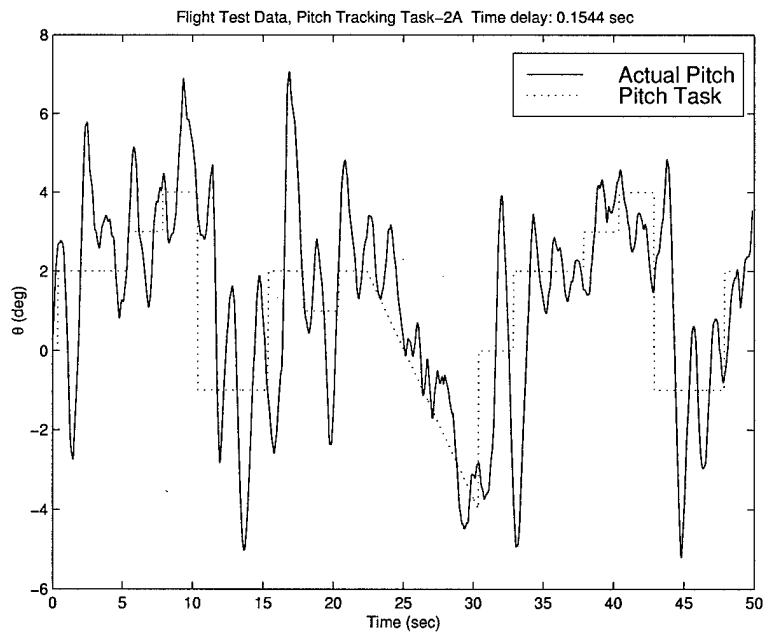


Figure 5.14 Flight Test Data, Test Point 1235, 154 msec Additional Delay, Baseline



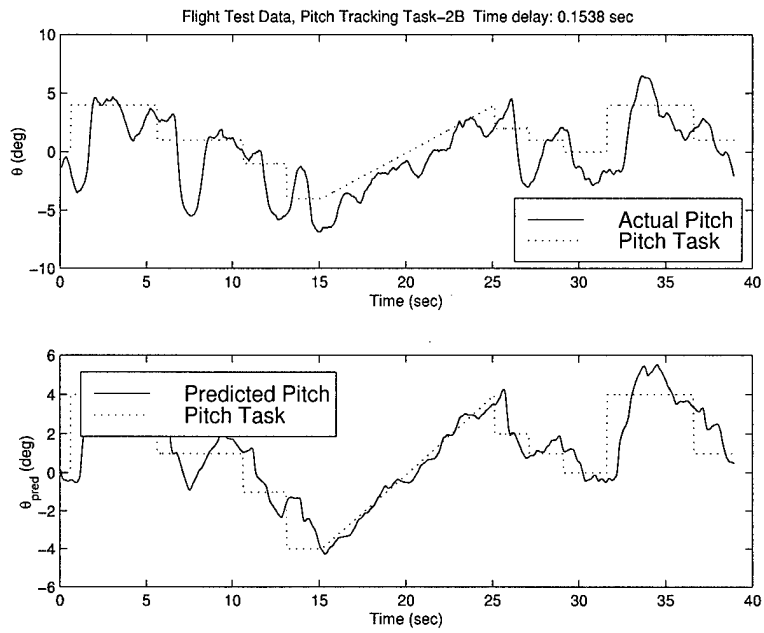


Figure 5.15 Flight Test Data, Test Point 2234, 154 msec Additional Delay, Predictive Compensation

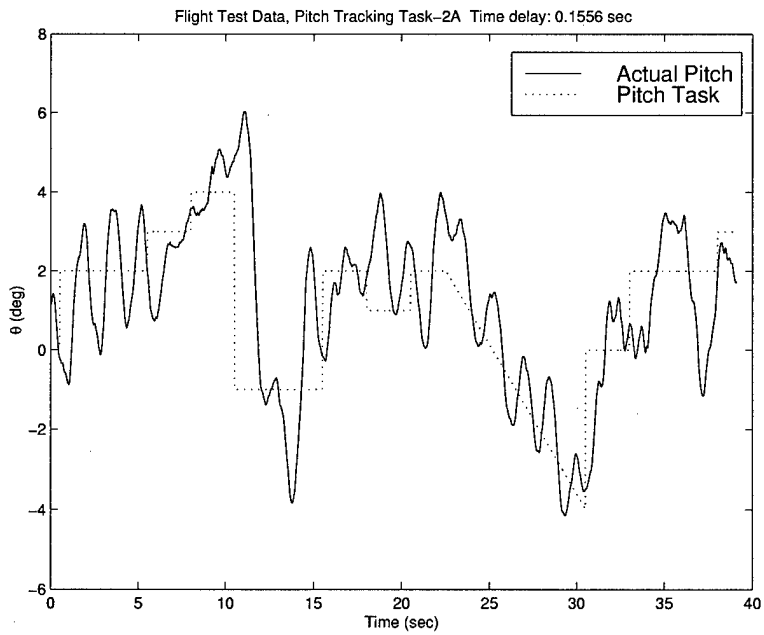


Figure 5.16 Flight Test Data, Test Point 1222, 156 msec Additional Delay, Baseline

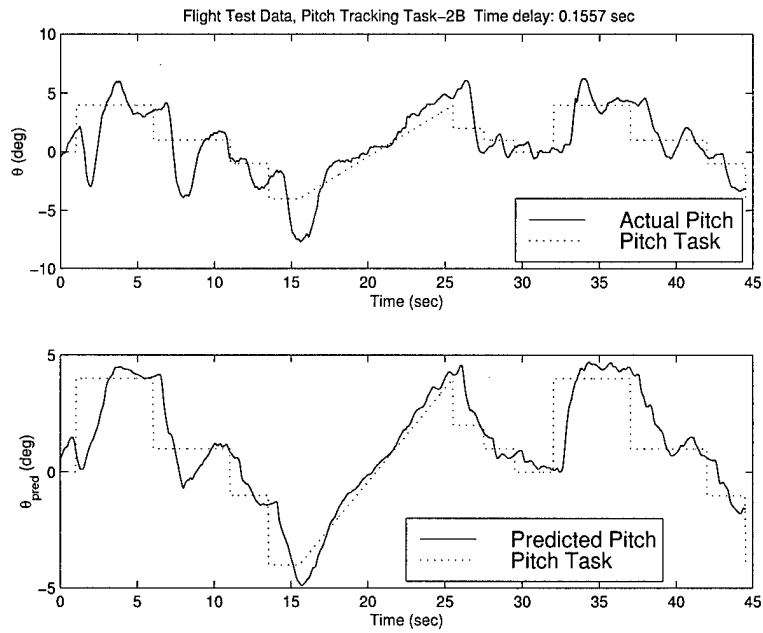


Figure 5.17 Flight Test Data, Test Point 2226, 156 msec Additional Delay, Predictive Compensation

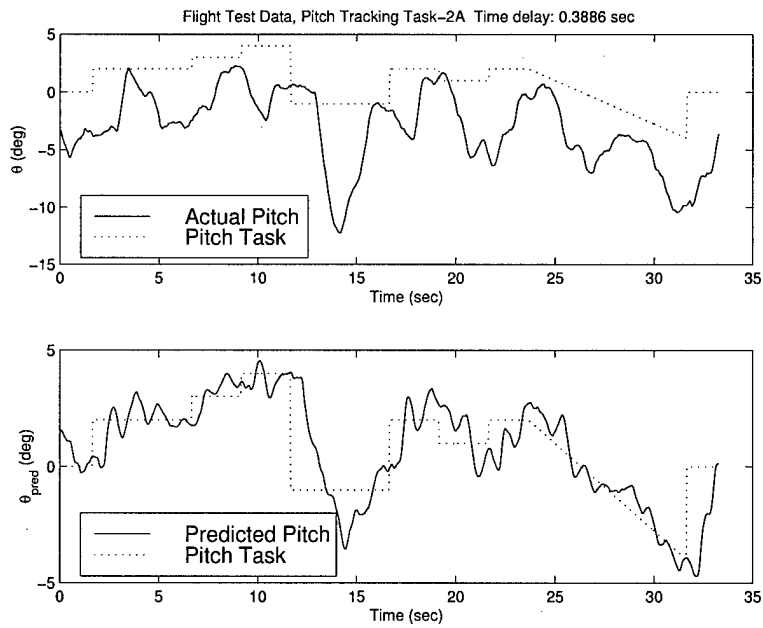


Figure 5.18 Flight Test Data, Test Point 2221, 389 msec Additional Delay, Predictive Compensation

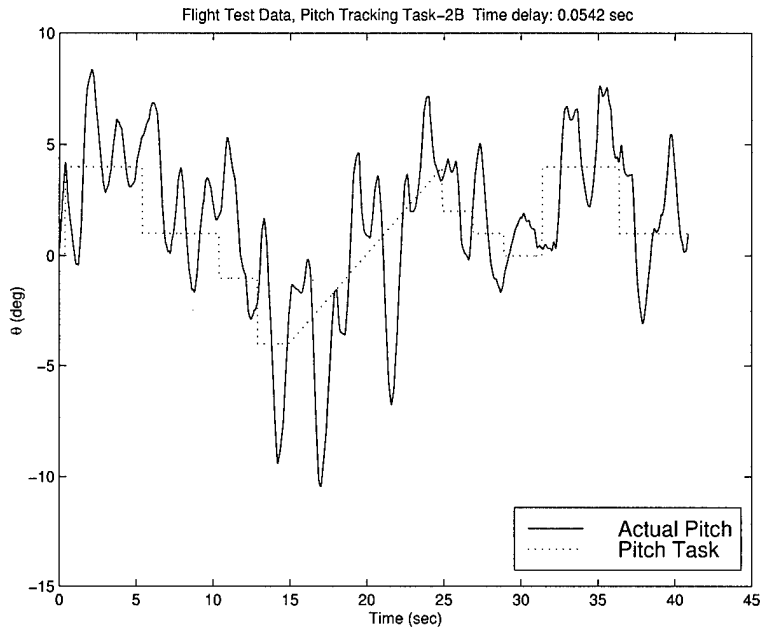


Figure 5.19 Flight Test Data, Test Point 1245, 55 msec Additional Delay, Baseline

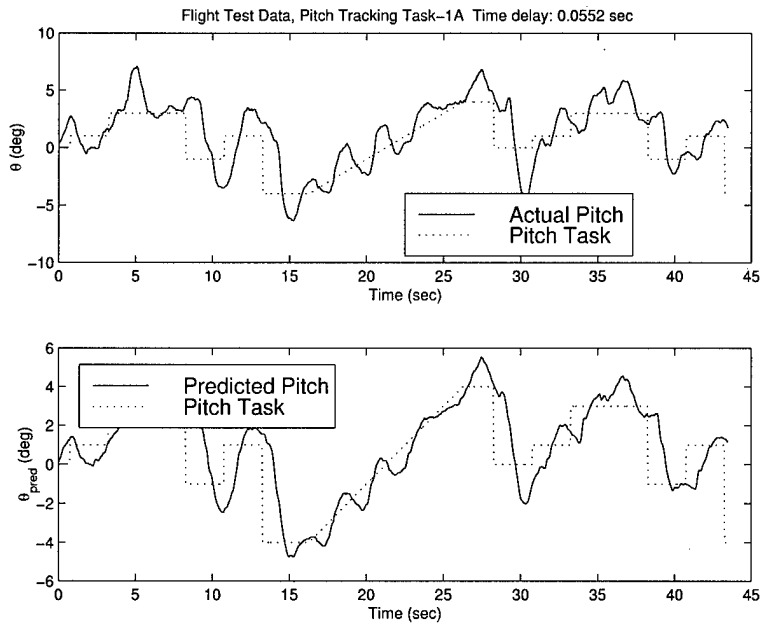


Figure 5.20 Flight Test Data, Test Point 2246, 55 msec Additional Delay, Predictive Compensation

Flight test results and pilot comments clearly showed that the predictive display significantly reduced the pilot's workload and improved performance in many cases. Nonlinear behavior of the UAV, integration error, and atmospheric disturbances combined to reduce the accuracy of the model-based algorithm's pitch prediction. When the predicted pitch became offset from the actual pitch, RMSTE increased significantly such that the overall results of the flight test showed no improvement in tracking performance. Further analysis was required to develop performance enhancing improvements to the predictive display algorithm.

### 5.5 *Post Flight Test Analysis*

Experience gained during flight test permitted a more complete analysis of the predictor algorithm's behavior. Knowing flight test verified predictor response to unmodeled effects and gust disturbances provided insight into how the predictor algorithm could be improved.

*5.5.1 UAV Mathematical Models.* Additional analysis began by creating more detailed Simulink<sup>TM</sup> models of the UAV/Display system. An updated UAV Simulink<sup>TM</sup> model including the elevator travel limits as well as deadband is shown in Figure 5.21. A model duplicating the predictor algorithm as flight tested, (Figures 5.22 and 5.23), was created in the attempt to duplicate deadband and gust disturbance effects observed in flight test. Measurement noise was included to make the models match the flight test environment as closely as possible. Additional models, (Figures 5.24, 5.25, and 5.27), with upgraded predictor algorithms were created to test various predictor enhancements.

Three enhanced predictor algorithms were tested in simulation. The first, Figure 5.24, included the UAV pitch attitude,  $\theta$ , in the telemetry stream. The UAV state space model was expanded from two to three states,  $\alpha$ ,  $q$ , and  $\theta$ , and the predictive algorithm gain matrices,  $\phi$  and  $\Phi$ , were derived from the augmented state

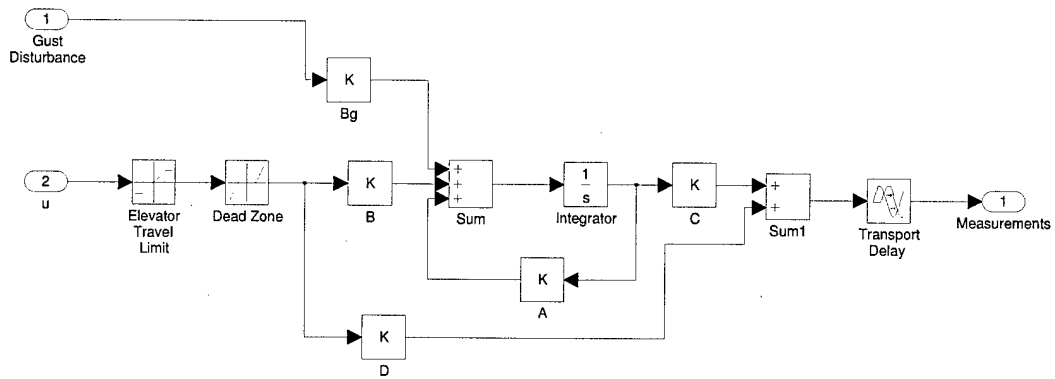


Figure 5.21 Utility UAV Simulink Model

space model. No filtering was done on the feedback signals; measurement noise was passed directly to the algorithm.

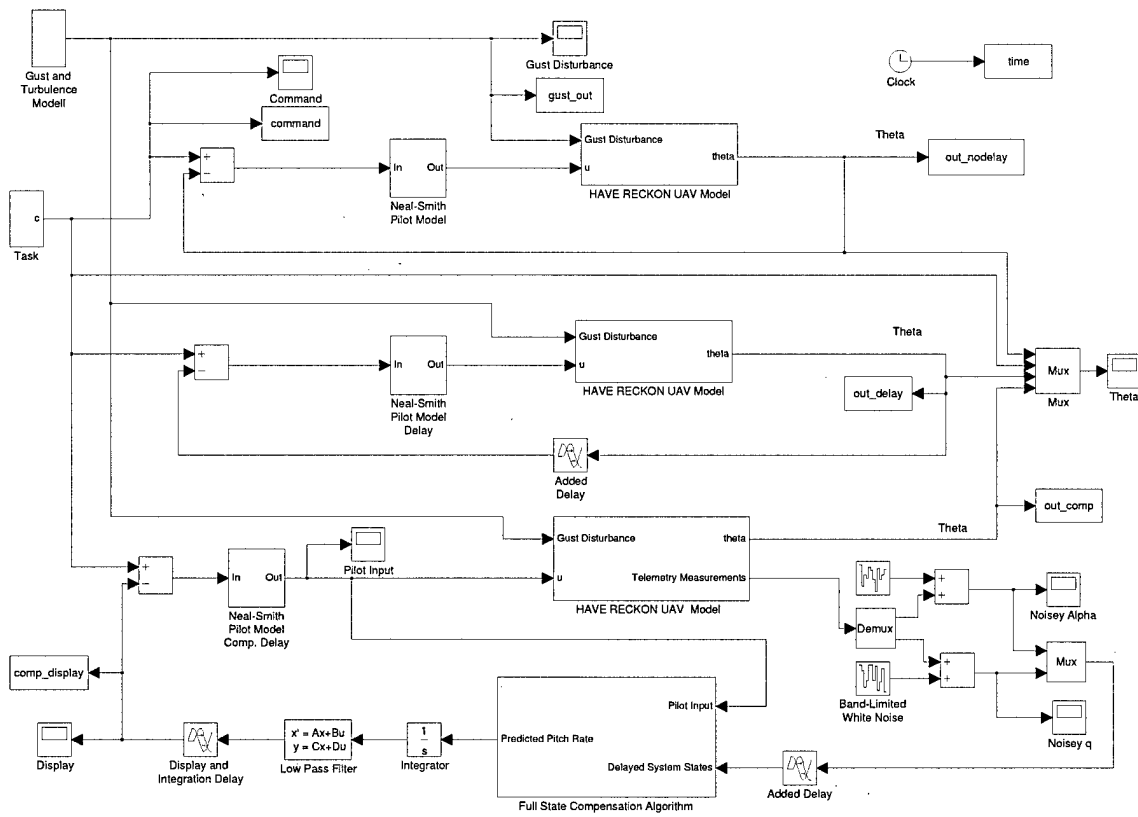


Figure 5.22  $\alpha$  and  $q$  Feedback Compensation Simulink Model

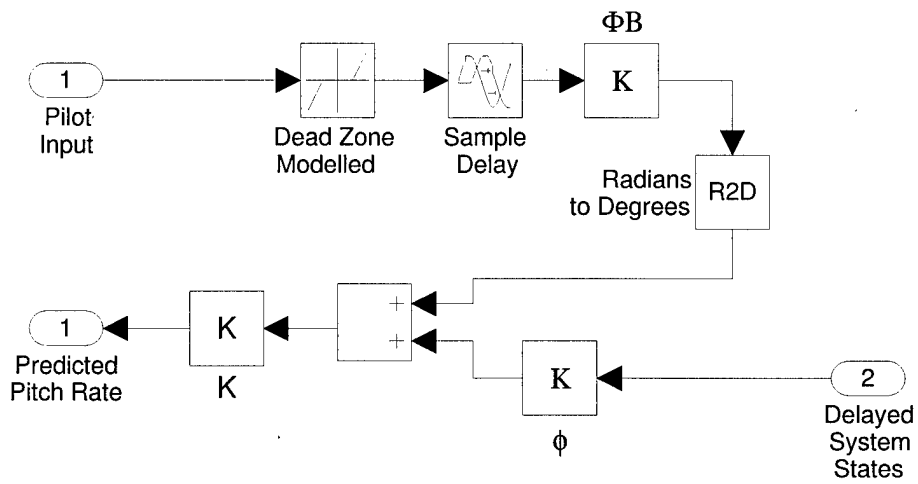


Figure 5.23  $\alpha$  and  $q$  Feedback Compensation Simulink Algorithm Model

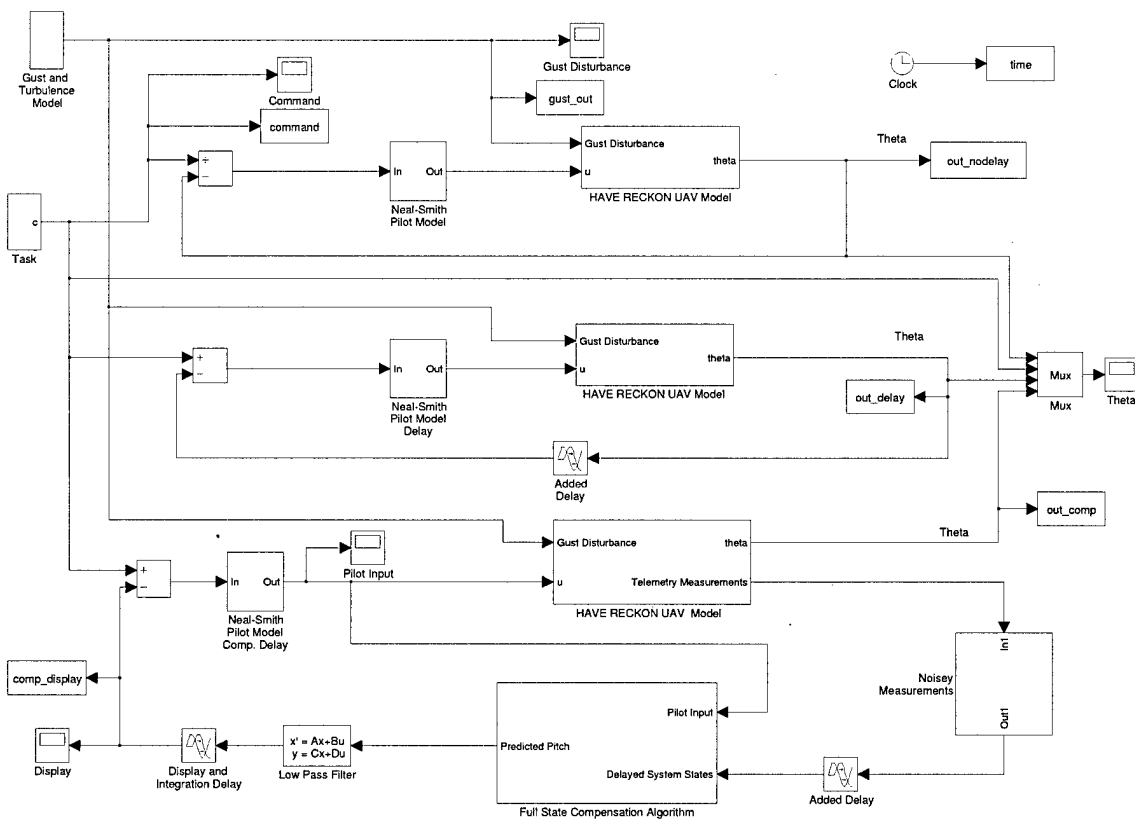


Figure 5.24  $\alpha$ ,  $q$ , and  $\theta$  Feedback Compensation Simulink Model



The second model, Figure 5.25, incorporated only  $\theta$  in the telemetry stream. A complete state vector was provided by a Kalman filter using output feedback,  $\theta$ , and pilot input to mathematically derive an optimal estimate of all three states, (depicted in Figure 5.26).

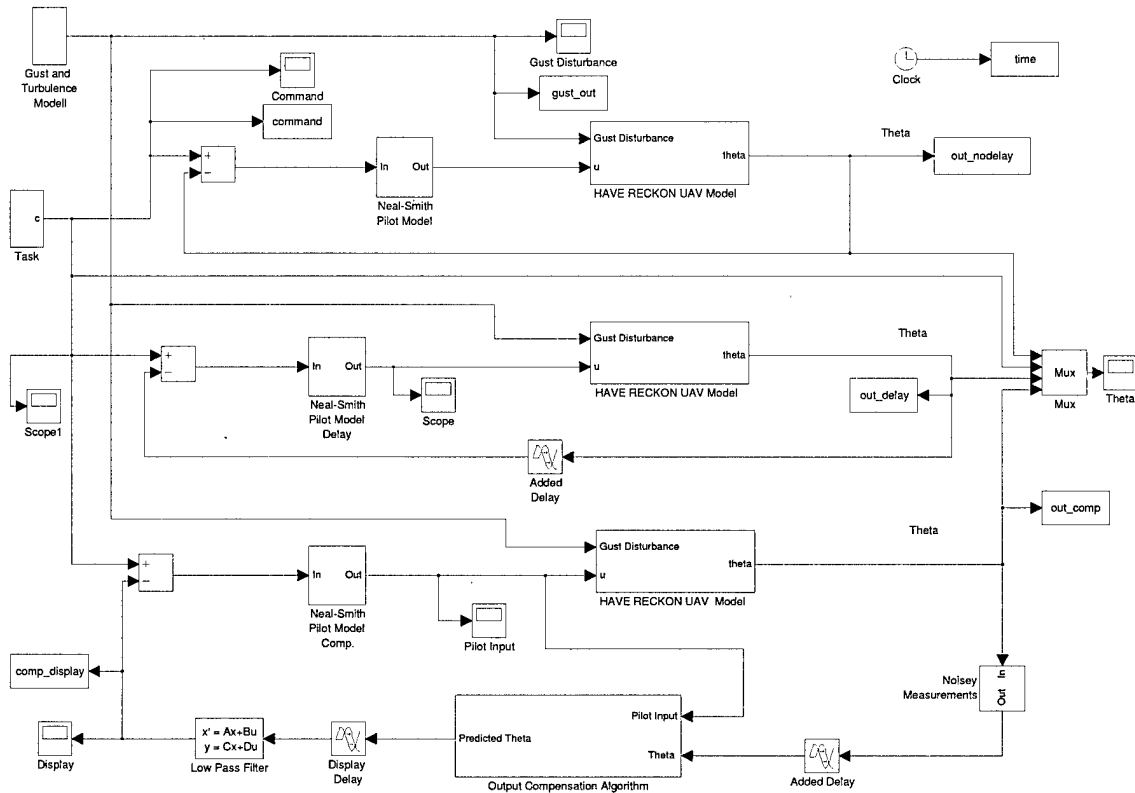


Figure 5.25  $\theta$  Feedback with Kalman Filter Compensation Simulink Model

The final model, Figure 5.27 involved full state feedback,  $\alpha$ ,  $q$ , and  $\theta$ , and a Kalman filter to provide an optimal estimate of the states based on the three noisy measurements and the pilot input.

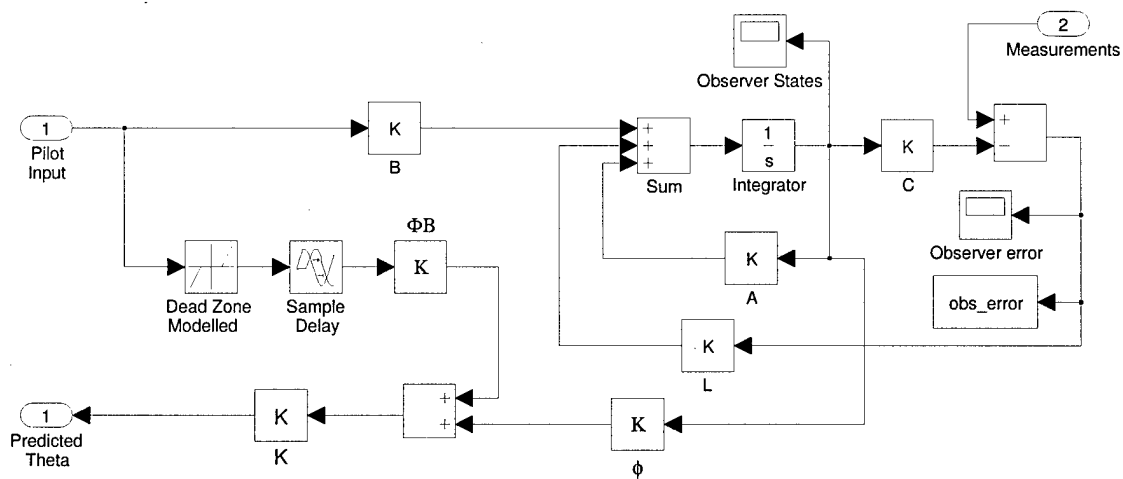


Figure 5.26 Kalman Filter Compensation Algorithm

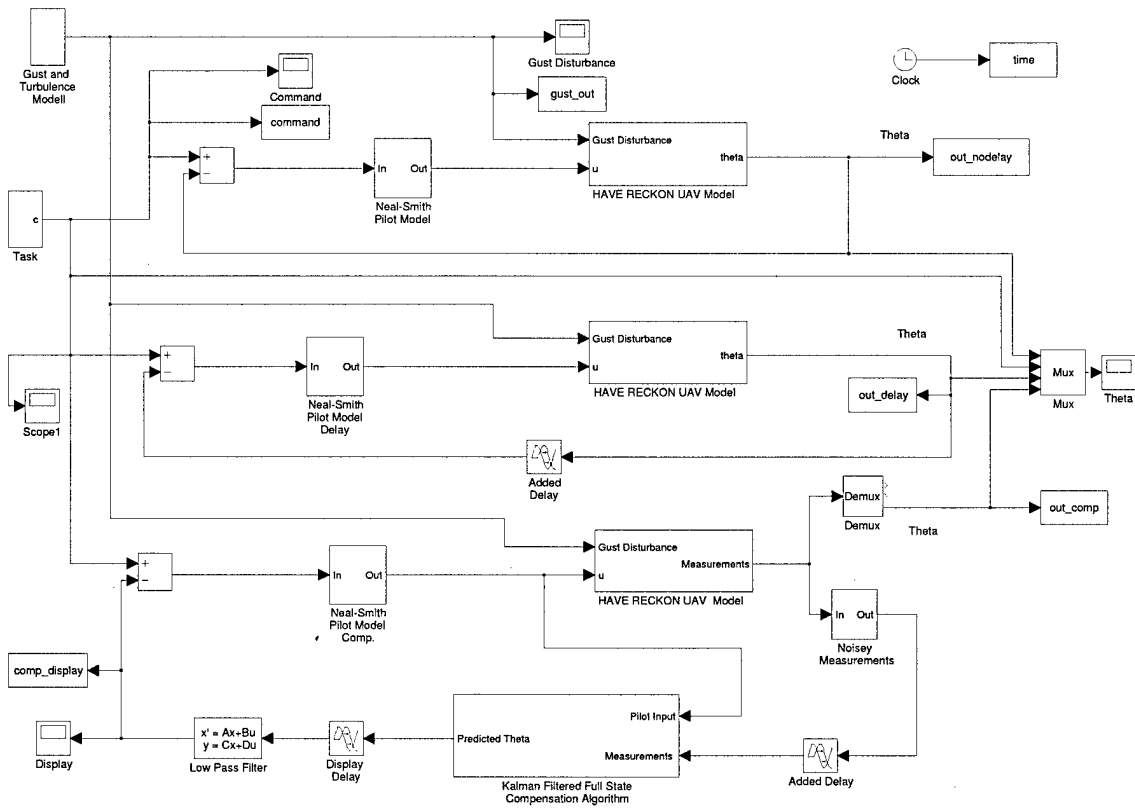


Figure 5.27 Kalman Filtered  $\alpha$ ,  $q$ , and  $\theta$  Feedback Compensation Simulink Model

5.5.2 *Atmospheric Disturbances.* Flight testing was conducted during the hours just after sunrise in order to minimize the effects of wind and turbulence. However, some atmospheric disturbances were encountered during most of the test points. An accurate model of the gust disturbances was essential to the creation of high fidelity mathematical simulations. Atmospheric turbulence was modelled by the Boeing linear filter presented in MIL-STD-1797. Zero mean Gaussian white noise was fed into the filter in Equation 5.1

$$w_g(s) = \frac{(s + .38(\frac{V}{L}))(s + 7.7(\frac{V}{L}))}{(s + .48(\frac{V}{L}))(s + 1.22(\frac{V}{L}))(s + 11.1(\frac{V}{L}))} \quad (5.1)$$

where  $L$  is 500 ft., the nominal test altitude, and  $V$  is the test airspeed of 69.7 ft/sec. The output of the filter provided a realization of the Von Karman turbulence spectrum discussed in MIL-STD-1797 (14). A  $1 - \cos x$  shaped discrete gust peaking

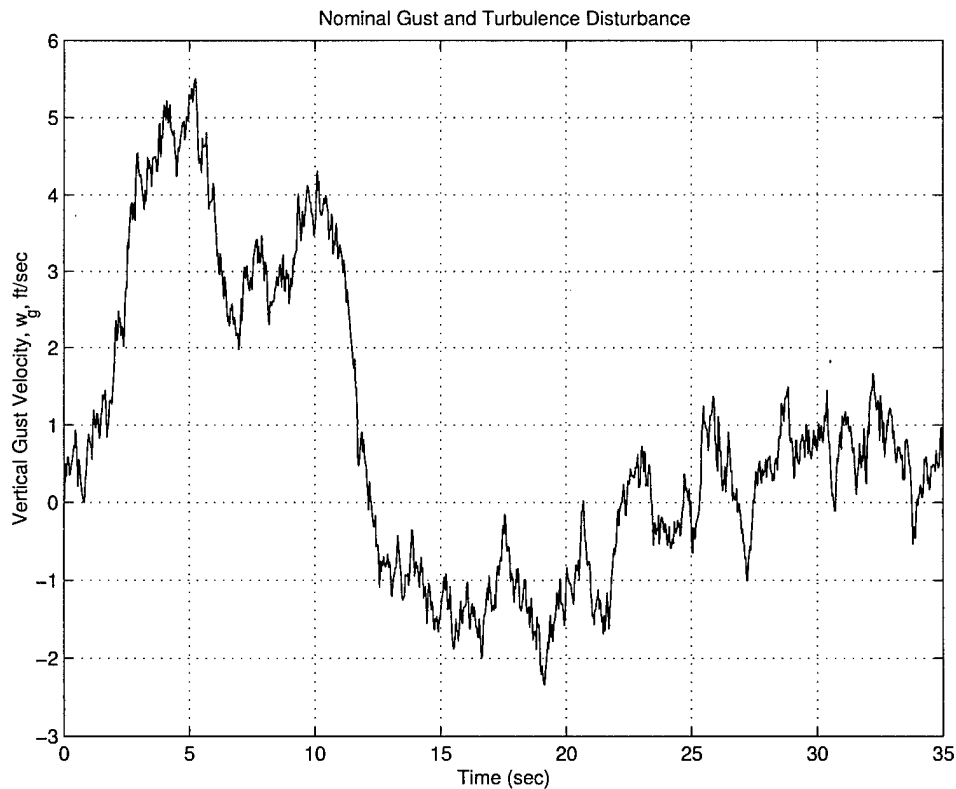


Figure 5.28 Nominal Turbulence and Gust Disturbance

at 4 ft/sec was added to the filter output thereby generating the disturbance signal shown in Figure 5.28. The gust disturbance was injected into the UAV state space model in Simulink<sup>TM</sup> as depicted in Figure 5.21.

*5.5.3 Kalman Filter Design.* A Kalman filter is an integral part of two of the additional Simulink models created for this analysis. Some discussion regarding the filter design is warranted.

The state space system with gust disturbances and measurement noise can be represented by the following equation

$$\dot{x} = \mathbf{A}x + \mathbf{B}u + \mathbf{B}_g w_g \quad (5.2)$$

$$\dot{z} = \mathbf{A}_z z + \mathbf{B}_z w \quad (5.3)$$

$$w_g = \mathbf{C}_z z + \mathbf{D}_z w \quad (5.4)$$

$$y = \mathbf{C}x + \mathbf{D}u + v \quad (5.5)$$

where  $w$  is the zero mean Gaussian white noise exciting the turbulence filter,  $u$  is the pilot input,  $y$  is the UAV state space model output,  $v$  is measurement white noise,  $z$  is the turbulence filter system state vector, and  $\mathbf{A}_z$ ,  $\mathbf{B}_z$ ,  $\mathbf{C}_z$  and  $\mathbf{D}_z$  represent the turbulence filter state space model. Assuming no direct feed forward terms,  $\mathbf{D} = \mathbf{D}_z = 0$ , the entire system may be represented in state space by

$$\begin{bmatrix} \dot{x} \\ \dot{z} \end{bmatrix} = \begin{bmatrix} \mathbf{A} & \mathbf{B}_g \mathbf{C}_z \\ 0 & \mathbf{A}_z \end{bmatrix} \begin{bmatrix} x \\ z \end{bmatrix} + \begin{bmatrix} \mathbf{B} \\ 0 \end{bmatrix} u + \begin{bmatrix} 0 \\ \mathbf{B}_z \end{bmatrix} w \quad (5.6)$$

$$y = [\mathbf{C} \quad 0] \begin{bmatrix} x \\ z \end{bmatrix} + v \quad (5.7)$$

where the inputs are known,  $u$ , and white noise,  $w$ .

The optimal observer gain  $L$  used in the Kalman observer model, Figure 5.26, is determined from

$$\mathbf{L} = \mathbf{P}\mathbf{C}^T\mathbf{R}^{-1} \quad (5.8)$$

where  $P$  is the steady state error covariance determined from the algebraic Riccati equation

$$0 = \mathbf{A}\mathbf{P} + \mathbf{P}\mathbf{A}^T + \mathbf{G}\mathbf{Q}\mathbf{G}^T - \mathbf{P}\mathbf{C}^T\mathbf{R}^{-1}\mathbf{C}\mathbf{P} \quad (5.9)$$

and noise spectral densities  $\mathbf{Q} = E\{ww^T\}$  and  $\mathbf{R} = E\{vv^T\}$ .  $\mathbf{Q}$  and  $\mathbf{R}$  were chosen as

$$\mathbf{Q} = \begin{bmatrix} .01 & 0 \\ 0 & .01 \end{bmatrix} \quad (5.10)$$

$$\mathbf{R} = \begin{bmatrix} \frac{1}{30} & 0 & 0 \\ 0 & \frac{1}{20} & 0 \\ 0 & 0 & \frac{1}{30} \end{bmatrix} \quad (5.11)$$

*5.5.4 Simulation Error.* Simulations were run on all four models for the additional time delays encountered in the flight test program. The 133 msec additional delay results were chosen as typical for analysis. When the state variables available during flight test,  $\alpha$  and  $q$ , were the only state information used in the predictive algorithm, the Simulink<sup>TM</sup> modeled predictor behaved in a similar fashion to the algorithm used in flight test. Specifically, gust disturbances caused large steady state errors in the predictor response, Figure 5.29. However, if  $\theta$  was added to the telemetry stream and the predictor algorithm was augmented to include the pitch angle, steady state offset was reduced into the noise, Figure 5.30. The most successful algorithm employed  $\alpha$ ,  $q$ , and  $\theta$  feedback along with a Kalman filter to provide an optimal estimate of the system states from the noisy measurements and pilot input,

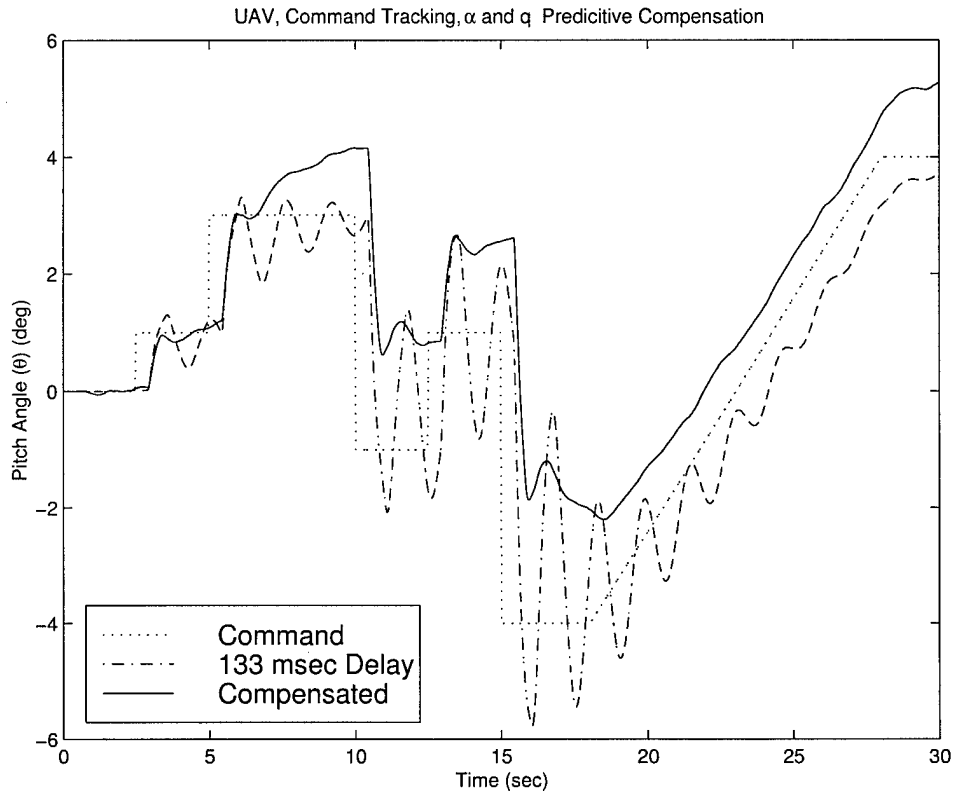


Figure 5.29 Simulation Time History, 133 msec Additional Delay,  $\alpha$  and  $q$  Feedback Compensation

Figure 5.31. Output feedback with a Kalman estimator worked nearly as well as the full state feedback. This has operational implications in that full state feedback may not be available do to problems instrumenting operational UAVs. Pitch attitude will always be in the telemetry stream and available for use in the Kalman estimator. Simulation error for each model and the entire range of time delays flight tested are provided in Tables 5.2 to 5.5, and graphically depicted in Figures 5.32 and 5.33.

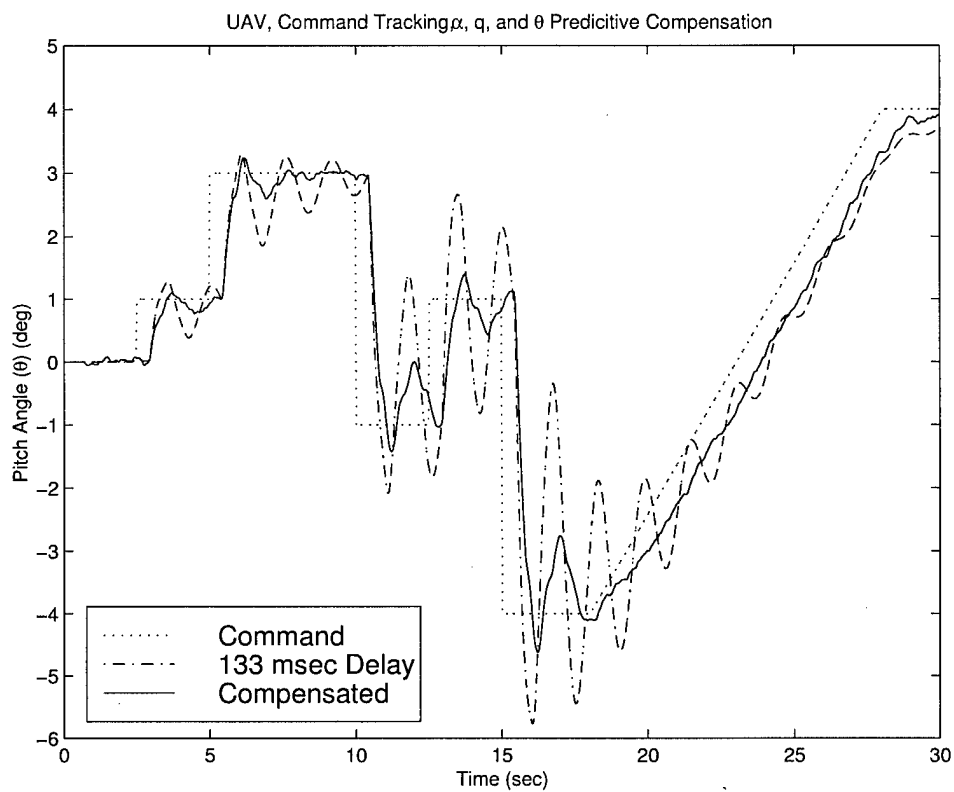


Figure 5.30 Simulation Time History, 133 msec Additional Delay,  $\alpha$ ,  $q$ , and  $\theta$  Feedback Compensation



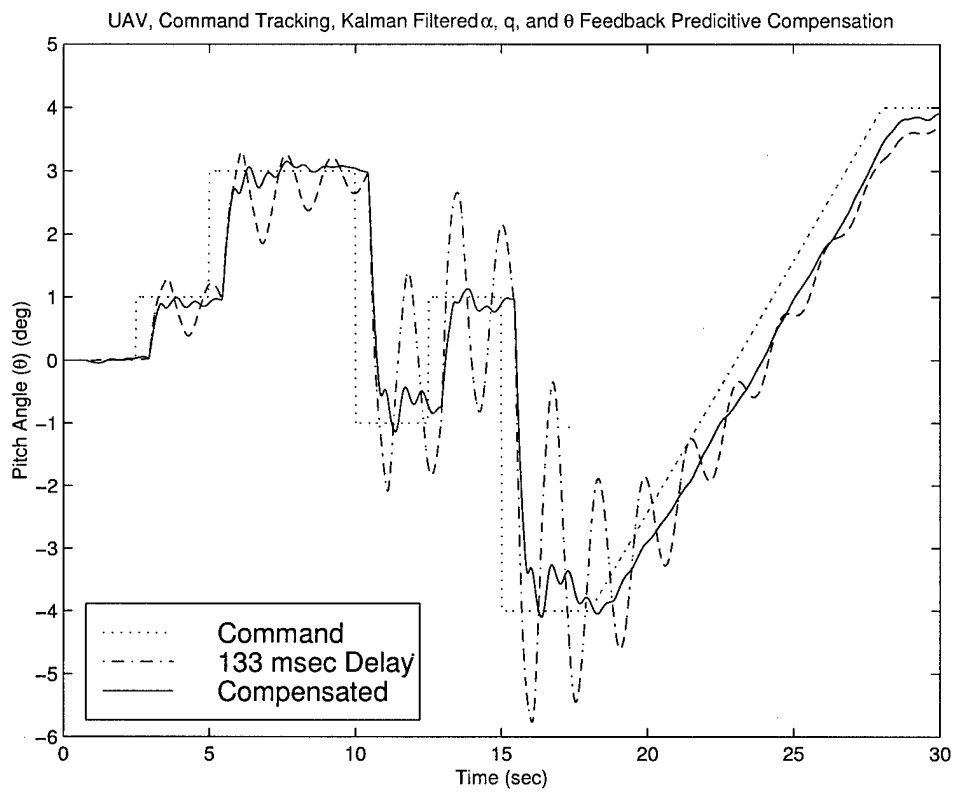


Figure 5.31 Simulation Time History, 133 msec Additional Delay, Kalman Filtered  $\alpha$ ,  $q$ , and  $\theta$  Feedback Compensation

Table 5.2 Simulation Results,  $\alpha$  and  $q$  Feedback Compensation

Additional Delay (msec)	RMS Error	RMS Error, Compensated
33	.9979	1.4879
66	1.0278	1.5878
100	1.0967	1.6214
133	1.2265	1.6606
166	1.4339	1.5633
200	1.7586	1.5035

Table 5.3 Simulation Results,  $\alpha$ ,  $q$ , and  $\theta$  Feedback Compensation

Additional Delay (msec)	RMS Error	RMS Error, Compensated
33	.9979	1.0168
66	1.0280	1.0118
100	1.0970	1.0035
133	1.2271	.9943
166	1.4349	.9882
200	1.7602	.9975

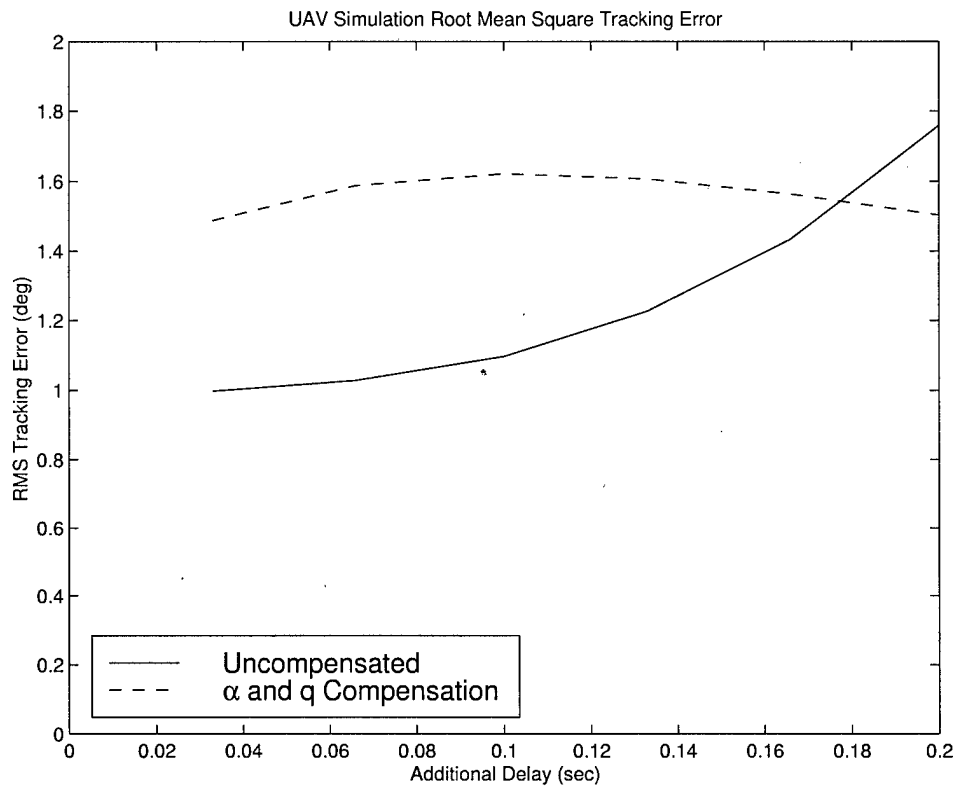


Figure 5.32 Simulation Results,  $\alpha$  and  $q$  Feedback Compensation

Table 5.4 Simulation Results,  $\theta$  Feedback with Kalman Filter Compensation

Additional Delay (msec)	RMS Error	RMS Error, Compensated
33	.9979	.9762
66	1.0280	.9813
100	1.0970	.9909
133	1.2271	1.0033
166	1.4349	1.0181
200	1.7602	1.0361

Table 5.5 Simulation Results, Kalman Filtered  $\alpha$ ,  $q$ , and  $\theta$  Feedback Compensation

Additional Delay (msec)	RMS Error	RMS Error, Compensated
33	.9979	.9688
66	1.0280	.9624
100	1.0970	.9592
133	1.2271	.9608
166	1.4349	.9700
200	1.7602	.9972

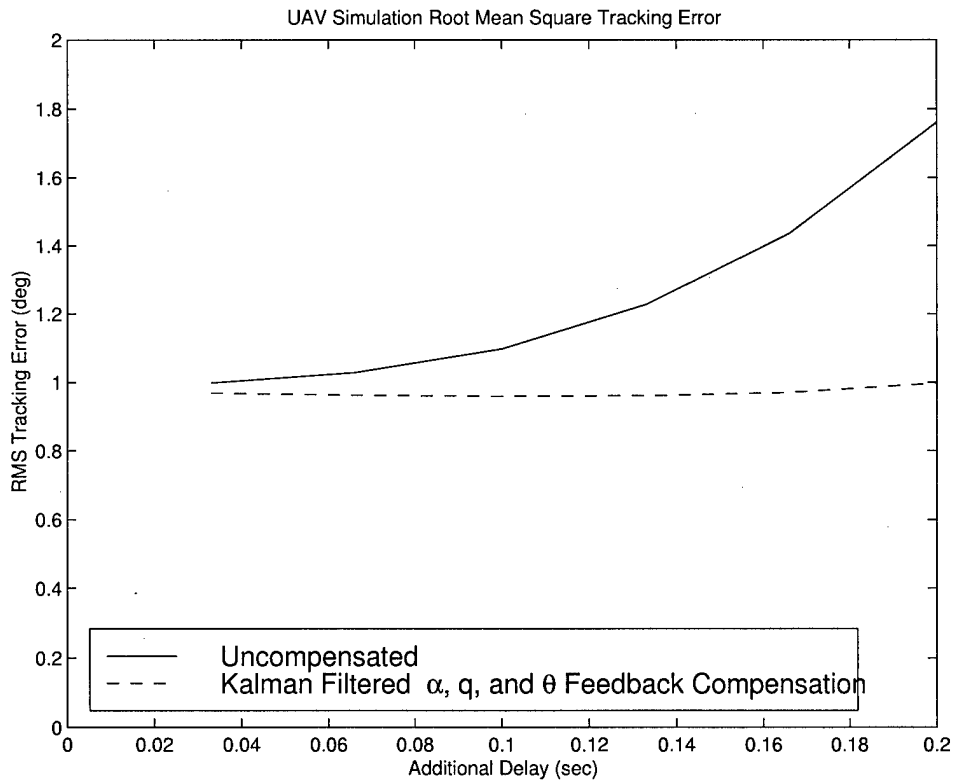


Figure 5.33 Simulation Results, Kalman Filtered  $\alpha$ ,  $q$ , and  $\theta$  Feedback Compensation

## *VI. Conclusions and Recommendations for Further Research*

This research investigated control loop time delay and its effect on UAV handling qualities. The characteristics of time delay systems were discussed with a focus on how transport delay affects human control behavior and aircraft handling qualities. Current methods for estimating test pilot rating of handling qualities from a mathematical model of the aircraft were presented and discussed within the context of application on a UAV, and compensation techniques to improve handling qualities were developed and analyzed. One technique was selected and successfully flight tested on a UAV.

Three different types of predictive techniques, the Bandwidth criteria, Neal-Smith criteria, and the Bacon-Schmidt technique, were evaluated using time delay study data from two available data sets. The Bandwidth and Neal-Smith techniques showed success in predicting handling qualities rating degradation as time delay increased. Ratings from predictive techniques more closely matched ratings assigned during flight test when the inflight task closely matched established bandwidth criteria.

Compensation techniques to reduce the effects of transport delay were investigated and implemented for simulation. A classical Lead/Lag filter and a model-based algorithm were evaluated. Bandwidth and Neal-Smith criteria were used to measure the efficacy of each technique in the frequency domain. Simulink™ simulations were conducted to evaluate time domain performance. The model-based predictive algorithm was the most effective at reducing the effects of the additional delay in both frequency and time domain analysis and was selected for evaluation in flight test.

Flight test data revealed the model-based predictive algorithm was able to compensate for increased system time delays and improve UAV handling qualities. With the predictor enabled, pilot workload decreased while overall system perfor-

mance and aircraft response remained the same. Larger additional time delays could be flown with essentially the same pilot comments and ratings as those for lower additional time delays.

Time delay compensation improved Cooper-Harper ratings and doubled the maximum additional time delay from the baseline configuration. Pilots noted a significant decrease in workload and required compensation which increased pilot comfort when flying the maximum additional time delays. The dependence of Cooper-Harper and pilot-in-the-loop oscillations ratings on additional time delay diminished once the predictor was enabled. There was no statistically significant improvement in PIO ratings or root mean square tracking error when using the model-based predictor compensation. However, pilot performance improved when measured by root mean square display error. Test results show that pilots were able to fly the predictive display precisely. The differences between the RMSDE and RMSTE for the compensated UAV system were most likely due to inadequacies in the linear model used to generate the predictive display or unmodeled disturbances such as wind gusts and turbulence.

Parameter variations in amount of additional time delay compensated did not result in degraded handling qualities. There was no significant difference in pilot opinion or performance for additional time delay uncertainties of  $\pm 33\%$ . Likewise, parameter variations in the UAV aerodynamic model used to generate the predictive display did not result in any instability or objectionable handling qualities. However, parameter variations of  $\pm 20\%$  in longitudinal stability derivatives did produce statistically significant changes in both pilot opinion and performance. Cooper-Harper and PIO ratings were most affected by changes in  $C_{M_\alpha}$ . Pilot performance, RMSTE and RMSDE was most affected by  $C_{M_q}$ . These changes were small and not considered operationally significant. Operational pilots using the predictive compensation technique will likely be presented with predictable handling qualities throughout the

mission profile. However, additional flight testing will be necessary to ensure that no significant handling qualities “cliffs” exist with larger model parameter variations.

Further analysis of UAV flight test data and further simulations revealed that, while not accomplished in this research due to instrumentation limitations of the flight test vehicle, including UAV pitch attitude in the feedback signal greatly increased the gust rejection capability of the model-based predictive algorithm. Algorithm accuracy, which was a problem during flight test for this research, was improved to the point of restoring system tracking performance to equal that of the system with no additional time delay.

Future research should focus on implementing the improved predictor algorithm in pitch and adding a flight path and lateral/directional axis predictor. It is the firm belief of the author that a UAV equipped with a three axis and flight path predictor could perform all mission tasks and be successfully landed with substantial time delay in the control loop. With compensation techniques developed and investigated in this thesis, future UAV operators will be able to employ UAVs from anywhere in the world thus increasing the flexibility of this already versatile platform.

## Appendix A. Experimental Data

### A.1 F-8 DFBW

The data extracted from the studies (7)(4)(6) accomplished on the NASA DFBW F-8 aircraft was in the form of non-dimensional stability derivatives and needed to be converted into transfer function form to be compatible with the Handling Qualities Toolbox(16). Data from Berry (6),

$$\text{Weight} = 20,000 \text{ lb}$$

$$\text{Mass (m)} = 621.12 \text{ slugs}$$

$$\text{Wing Area(S)} = 375 \text{ ft}^2$$

$$\text{Wingspan(b)} = 35.67 \text{ ft}$$

$$\text{Chord } (\bar{c}) = 11.8 \text{ ft}$$

$$I_y = 87,490 \text{ ft} - \text{lb/s}^2$$

$$C_{L_{\dot{\alpha}}} = 3.7/\text{rad}$$

$$C_{L_{\delta_e}} = .57/\text{rad}$$

$$C_{m_q} = -6$$

$$C_{m_{\dot{\alpha}}} = -.5/\text{rad}$$

$$C_{m_{\alpha}} = -.42$$

$$C_{m_{\delta_e}} = -.8$$

Actuator Characteristics:

$$\text{Secondary Actuator} - \frac{15876}{s+176s+15876}$$

$$\text{Power Actuator} - \frac{12.5}{s+12.5}$$

Flight Control Characteristics:

$$\text{Prefilter(SAS, Pitch Direct)} - \frac{12}{s+12}$$

$$\text{Prefilter(ISAS)} - \frac{50}{s+50}$$

$$\text{q feedback washout} - \frac{1}{s+1}$$



Values for dynamic pressure ranged from 100 to 270 psi. Flight tests were conducted on several landing tasks and an up-and-away formation flying task intended to simulate air-to-air refueling. Average true airspeed during the landing approach was calculated at 337.05 ft/sec resulting in a dynamic pressure,  $Q$ , of 130.65 psf at sea level. The formation flying task altitude was not given. It was assumed to take place at 290 KIAS at an altitude of 20,000 ft; typical airspeed and altitude for a receiver fighter aircraft to be holding during inflight refueling. These values resulted in a dynamic pressure of 277 psf, approximately the given upper value for dynamic pressure during the tests.

The F-8 employed non-linear stick shaping following the formula,

$$Output = 0.35 * input + .45 * input * |input| \quad (A.1)$$

Analysis with the Handling Qualities Tool Box required a linearized approximation of the stick shaping. This was accomplished by selecting a linear gain of 0.65 which provided a least squares fit between  $\mp 1cm$ . This value was chosen to match performance between the author's Simulink models, see figures A.1 and A.2 and the actual F-8 DFBW aircraft simulated pitch step response (54).

Calculation of the F-8 airframe  $\frac{\theta}{\delta_e}$  transfer function from the stability derivatives followed from Nelson(42). The denominator of the short period approximation is calculated from,

$$\Delta_{sp} = s^2 - (M_q + M_{\dot{\alpha}} + \frac{Z_{\alpha}}{u_0})s + \frac{Z_{\alpha}M_q}{u_0} - M_{\alpha} \quad (A.2)$$

and the numerator from,

$$N_{sp} = (M_{\delta_e} + \frac{M_{\dot{\alpha}}Z_{\delta_e}}{u_0})s + (\frac{M_{\alpha}Z_{\delta_e} - M_{\delta_e}Z_{\alpha}}{u_0}) \quad (A.3)$$

Table A.1 F-8 Short Period Parameters

Airspeed	Altitude	$\omega_{n_{sp}}$	$\zeta_{sp}$	$T_{\theta_2}$	$K_{\theta}$
377.05 (ft/sec)	Sea Level	1.976	.407	1.276	5.280
290 KIAS	20,000	2.776	.313	1.183	11.20

where,

$$M_q = C_{m_q} \frac{\bar{c}}{2u_0} (QS\bar{c})/I_y \quad (A.4)$$

$$M_{\dot{\alpha}} = C_{m_{\dot{\alpha}}} \frac{QS\bar{c}^2}{2u_0 I_y} \quad (A.5)$$

$$Z_{\alpha} = \frac{-(C_{L_{\alpha}} + C_{D_0})QS}{m} \quad (A.6)$$

$$M_{\alpha} = C_{m_{\alpha}} \frac{(QS\bar{c})}{I_y} \quad (A.7)$$

$$M_{\delta_e} = C_{m_{\delta_e}} \frac{(QS\bar{c})}{I_y} \quad (A.8)$$

$$Z_{\delta_e} = -C_{L_{\delta_e}} \frac{(QS)}{m} \quad (A.9)$$

$$(A.10)$$

The results of the F-8 calculations are given in Table A.1

Pilot opinion ratings were gathered for landings and simulated aerial refueling at digital delays of 20, 60, 100, 140, and 200 ms. Different flight control augmentation schemes were also tested. These included Pitch Direct, SAS, Improved SAS (ISAS), CAS, and Improved CAS (ICAS). Modes examined in this thesis included pitch direct, SAS, and ISAS.

#### A.2 Princeton Variable-Response Research Aircraft (VRA)

The Princeton study(53) provided airframe dynamics in the form of literal factors,  $M_{\delta_e}$ ,  $\omega_{n_{sp}}$ ,  $\zeta_{sp}$ , and  $n_{z_{\alpha}}$ .

Airspeed (KIAS)	$M_{\delta_e}$	$\omega_{n_{sp}}$	$\zeta_{sp}$	$n_{z\alpha}$
75	-6.4	2.60	.77	5.04
86	-8.4	2.95	.75	7.39
105	-12.5	3.54	.71	11.02

Pilot opinion data was collected for several types of landings at varying airspeeds as well as a tracking at altitude task.

Task	Airspeed(KIAS)
Tracking	105
Normal Landing	75
Carrier Landing	105
Carrier Landing	86

It was necessary to derive transfer function representations at each of the airspeed data points for analysis. Calculation of the short period approximation denominator,  $\Delta_{sp}$ , follows quickly,

$$\Delta_{sp} = s^2 + 2\zeta_{sp}\omega_{n_{sp}}s + \omega_{n_{sp}}^2 \quad (\text{A.11})$$

Calculation of the numerator,  $N_{sp}$ , from equation A.3 required dimensional stability derivatives which were not explicitly provided. However, using the relationship between  $T_{\theta_2}$  and  $n_{z\alpha}$ ,

$$T_{\theta_2} = \frac{u_0}{g} \frac{1}{n_{z\alpha}} \quad (\text{A.12})$$

The ratio of the numerator factors from equation A.3 is provided. Additionally, the short period approximation for  $\omega_{n_{sp}}$  and  $\zeta_{sp}$  may be calculated from,

$$\omega_{n_{sp}} = \left( \frac{Z_\alpha M_q}{u_0} - M_\alpha \right)^{\frac{1}{2}} \quad (\text{A.13})$$

$$\zeta_{sp} = \frac{-(M_q + M_{\dot{\alpha}} + \frac{Z_{\dot{\alpha}}}{u_0})}{2\omega_{n_{sp}}} \quad (\text{A.14})$$

Calculation of these values made it necessary to find the set of dimensional stability derivatives that match in an optimal fashion  $\omega_{n_{sp}}$ ,  $\zeta_{sp}$ , and  $T_{\theta_2}$  with the literal factors provided.

The Princeton VRA is a Navion modified with a digital flight control system which may be programmed to provide variable response characteristics. The variable response features of the aircraft were not used in this study and the basic aircraft flight characteristics are those of the bare Navion airframe. Using Navion stability derivatives from Nelson(42) as an initial value, a Nelder-Mead algorithm was used to find stability derivatives that minimized the following cost function,

$$J = (\omega_{\hat{n}_{sp}} - \omega_{n_{sp}})^2 + 18(\zeta_{\hat{sp}} - \zeta_{sp})^2 + 36(\hat{T}_{\theta_2} - T_{\theta_2})^2 \quad (\text{A.15})$$

where  $\omega_{\hat{n}_{sp}}$ ,  $\zeta_{\hat{sp}}$ , and  $\hat{T}_{\theta_2}$  are the literal factors calculated from the current iteration's values for the stability derivatives. The weights were chosen to give each term approximately equal effect on the cost function. Landing approaches were assumed to occur at sea level and used standard atmosphere density while the tracking at altitude was assumed to occur at 15,000 ft. No altitude for this task was given in the Princeton paper. The resulting short period LOES transfer function parameters are listed in table A.2.

Airspeed (KIAS)	Altitude	$\omega_{n_{sp}}$	$\zeta_{sp}$	$T_{\theta_2}$	$K_{\theta}$
75	Sea Level	2.60	.77	.7805	6.322
86	Sea Level	2.95	.75	.6103	8.300
105	Sea Level	3.54	.71	.4998	12.34
105	15,000	3.54	.71	.6296	12.40

The Matlab code used for the calculations follows.

```

% navion.m
% ~/thesis/navion.m
%
% Calculate stability derivatives based on values for Navion
% in Nelson and use them as a starting place to find stability
% derivative values that result in an optimal match with the
% literal factors cited in Princeton VRA study.
%
% stab_dir(1) = M_q;
% stab_dir(2) = M_alpha_dot;
% stab_dir(3) = Z_alpha; 4.44 .05
% stab_dir(4) = M_alpha;
% stab_dir(5) = Z_delta_e;
%
% Flight Parameters from paper
% [A/S (kias) Mdeltae Omega_sp Zeta_sp N_z_alpha]
data(1,:)=[75 -6.4 2.60 .77 5.04];
data(2,:)=[86 -8.4 2.95 .75 7.39];
data(3,:)=[105 -12.5 3.54 .71 11.02];
%
U = data(index,1); %KIAS
M_delta_e = data(index,2);
Wn_sp_data = data(index,3);
zeta_sp_data = data(index,4);
n_alpha = data(index,5);
%
% Navion data from Nelson
%
nm_in_feet = 6080;
hr_in_sec = 3600;
U = U*(nm_in_feet/hr_in_sec);
S = 184;
b = 33.4;
c_bar = 5.7;

```

```

W = 2750;
m = 2750/32.2;
I_y = 3000;
%
% Landing approaches at sea level
%
rho = .0023769;
% Use when calculating up-and-away at 15,000
%rho = .0014962;
%U = U/((.63)^.5);
Q = (1/2)*rho*U^2;
disp(sprintf('U = %f ft/sec, Q = %f',U,Q))
%
C_m_q = -9.96;
C_m_alpha_dot = -4.36;
C_m_alpha = -.683;
C_z_delta_e = -.355;
%
M_q = C_m_q*(c_bar/(2*U))*(Q*S*c_bar)/I_y;
M_alpha_dot = U*(C_m_alpha_dot*(c_bar/(2*U))*(Q*S*c_bar)/(U*I_y));
Z_alpha = -U*(4.44 + .05)*Q*S/(m*U);
M_alpha = U*(C_m_alpha*Q*S*c_bar/(U*I_y));
Z_delta_e = C_z_delta_e*Q*S/m;
disp(sprintf('\nInitial guess (data from Nelson):\nM_q = %f\t M_alpha_dot = %f',M_q,M_alpha_dot))
disp(sprintf('Z_alpha = %f\t M_alpha = %f\t Z_delta_e = %f',Z_alpha,M_alpha,Z_delta_e))

T_theta_2 = (U/32.2)/n_alpha;
Wn_sp = (M_q*Z_alpha/U - M_alpha)^(1/2);
zeta_sp = -(M_q + M_alpha_dot + Z_alpha/U)/(2*Wn_sp);
T_theta_2_est = (M_delta_e + M_alpha_dot*Z_delta_e/U)/(M_alpha*Z_delta_e/U - %
M_delta_e*Z_alpha/U);
disp(sprintf('\nResults in Literal Factors (short period approx.): \nWn_sp = %f\t zeta_sp = %f\t %
T_theta_2 = %f',Wn_sp,zeta_sp,T_theta_2_est))

```

```

stab_dir(1) = M_q;
stab_dir(2) = M_alpha_dot;
stab_dir(3) = Z_alpha;
stab_dir(4) = M_alpha;
stab_dir(5) = Z_delta_e;

x = fmins('pcost',stab_dir,[],[],data,index);

M_q = x(1);
M_alpha_dot = x(2);
Z_alpha = x(3);
M_alpha = x(4);
Z_delta_e = x(5);

disp(sprintf('\nOptimal stability derivatives:\nM_q = %f\t M_alpha_dot = %f',M_q,M_alpha_dot))
disp(sprintf('Z_alpha = %f\t M_alpha = %f\t Z_delta_e = %f',Z_alpha,M_alpha,Z_delta_e))
Wn_sp = (M_q*Z_alpha/U - M_alpha)^(1/2);
zeta_sp = -(M_q + M_alpha_dot + Z_alpha/U)/(2*Wn_sp);
T_theta_2_est = (M_delta_e + M_alpha_dot*Z_delta_e/U)/(M_alpha*Z_delta_e/U - M_delta_e*Z_alpha/U);
disp(sprintf('\nResults in Literal Factors (short period approx.): \nWn_sp = %f\t zeta_sp = %f\t T_theta_2 = %f',Wn_sp,zeta_sp,T_theta_2_est))

num = [(M_delta_e + M_alpha_dot*Z_delta_e/U) (M_alpha*Z_delta_e/U - M_delta_e*Z_alpha/U)]
den = [1 2*zeta_sp*Wn_sp Wn_sp^2 0]

function out = pcost(stab_dir,data,index)
% pcost.m
% Computes cost function to find optimal solution for
% Navion stability derivatives.
% stab_dir(1) = M_q;
% stab_dir(2) = M_alpha_dot;
% stab_dir(3) = Z_alpha;

```

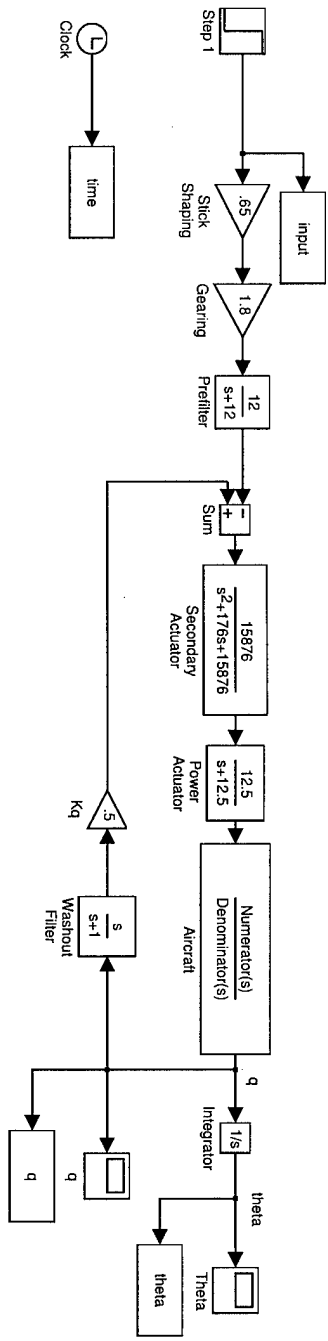
```

% stab_dir(4) = M_alpha;
% stab_dir(5) = Z_delta_e;
%
M_q = stab_dir(1);
M_alpha_dot = stab_dir(2);
Z_alpha = stab_dir(3);
M_alpha = stab_dir(4);
Z_delta_e = stab_dir(5);
%
% Flight Parameters from paper
U = data(index,1); %KIAS
M_delta_e = data(index,2);
Wn_sp_data = data(index,3);
zeta_sp_data = data(index,4);
n_alpha = data(index,5);
%
nm_in_feet = 6080;
hr_in_sec = 3600;
U = U*(nm_in_feet/hr_in_sec);
% Use when calculating up-and-away at 15,000
% U = U/((.63)^.5);
Wn_sp = (M_q*Z_alpha/U - M_alpha)^(1/2);
zeta_sp = -(M_q + M_alpha_dot + Z_alpha/U)/(2*Wn_sp);
%
% Calculate actual T_theta_2 from data given
%
T_theta_2 = (U/32.2)/n_alpha;%
%
T_theta_2_est = (M_delta_e + M_alpha_dot*Z_delta_e/U)/(M_alpha*Z_delta_e/U - %
M_delta_e*Z_alpha/U);
%
% Compute cost Function
%
out = (Wn_sp_data - Wn_sp)^2 + 18*(zeta_sp_data - zeta_sp)^2 + 36*(T_theta_2 - T_theta_2_est)^2;

```







F-8 SAS Simulink Model  
 (~\thesis\8\_sas.mdl)

Figure A.1 F-8 SAS Simulink Model

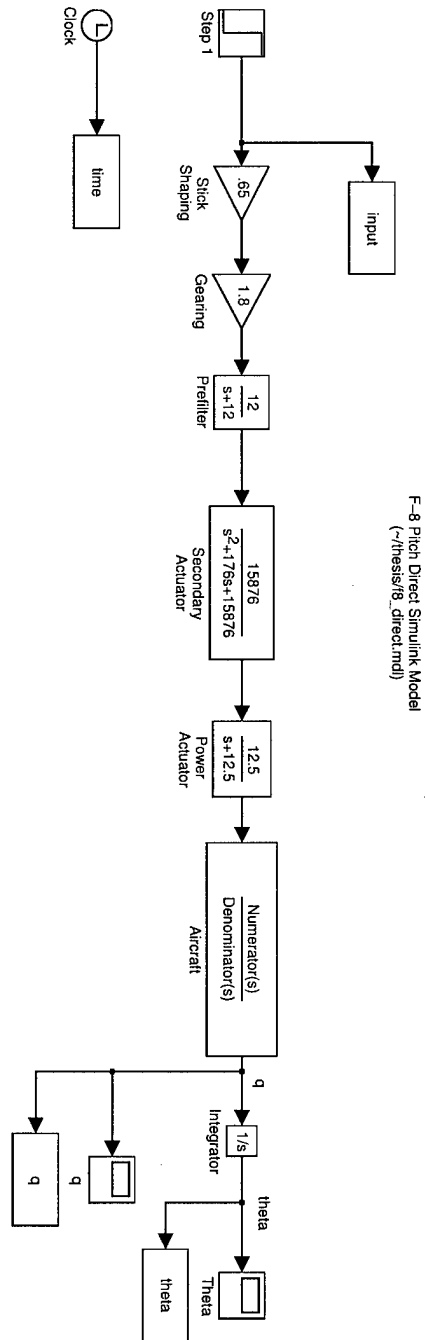


Figure A.2 F-8 Pitch Direct Simulink Model

## Appendix B. Additional Simulation Results

### B.1 F-8 DFBW, Lead/Lag Compensation

The F-8 DFBW data was modelled in the same manner as the VRA in Chapter 3. Results for the Lead/Lag Compensator command tracking are presented below,

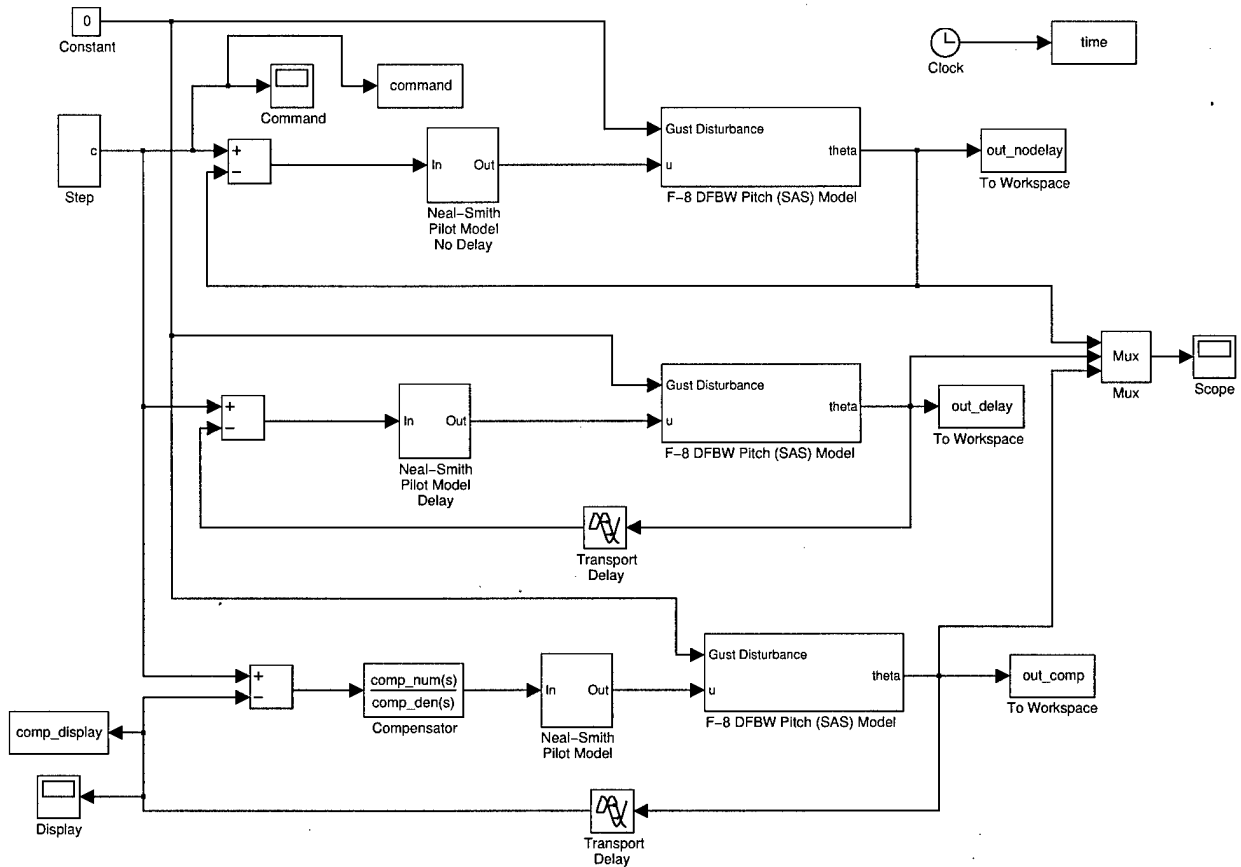


Figure B.1 F-8 DFBW Command Tracking Model

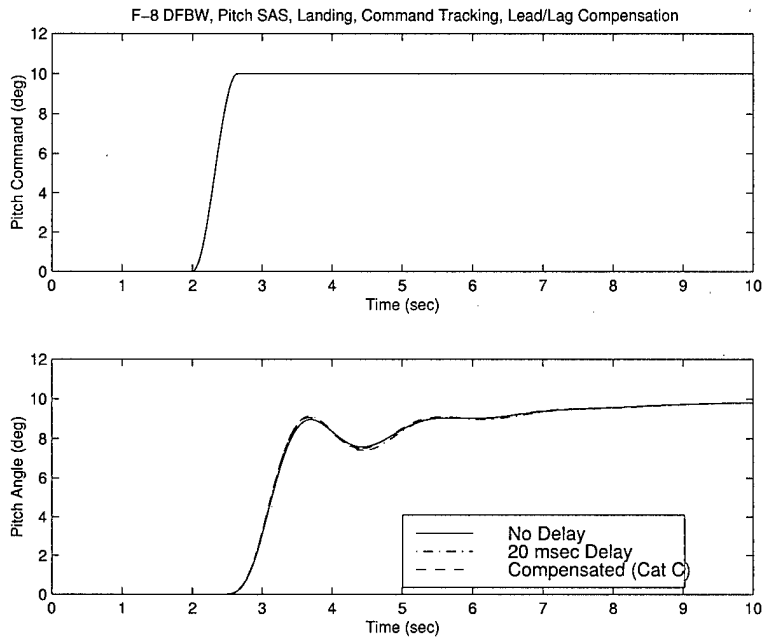


Figure B.2 F-8 DFBW Command Tracking, 20 msec Delay, Lead/Lag Compensation

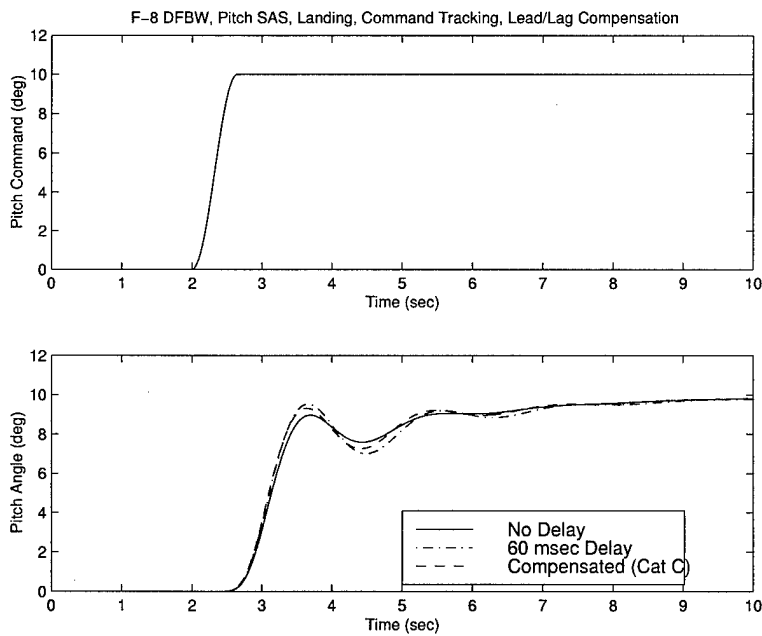


Figure B.3 F-8 DFBW Command Tracking, 60 msec Delay, Lead/Lag Compensation

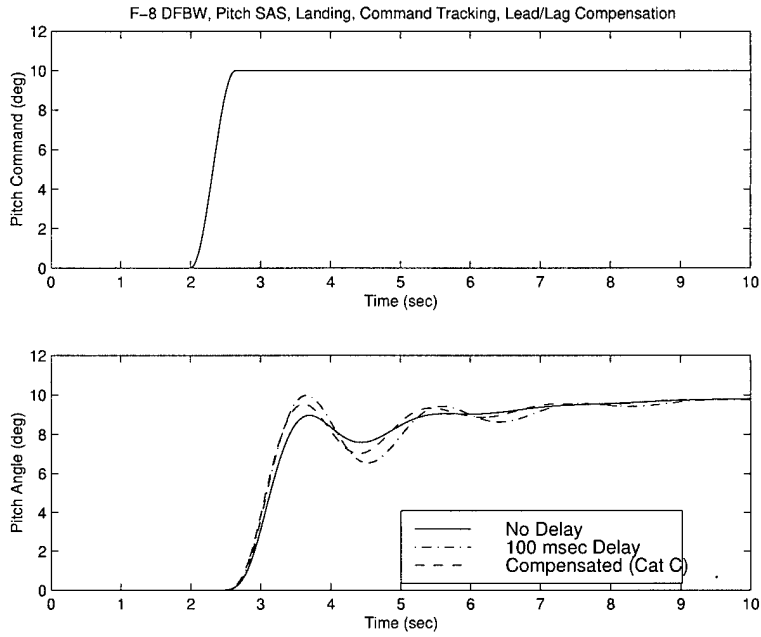


Figure B.4 F-8 DFBW Command Tracking, 100 msec Delay, Lead/Lag Compensation

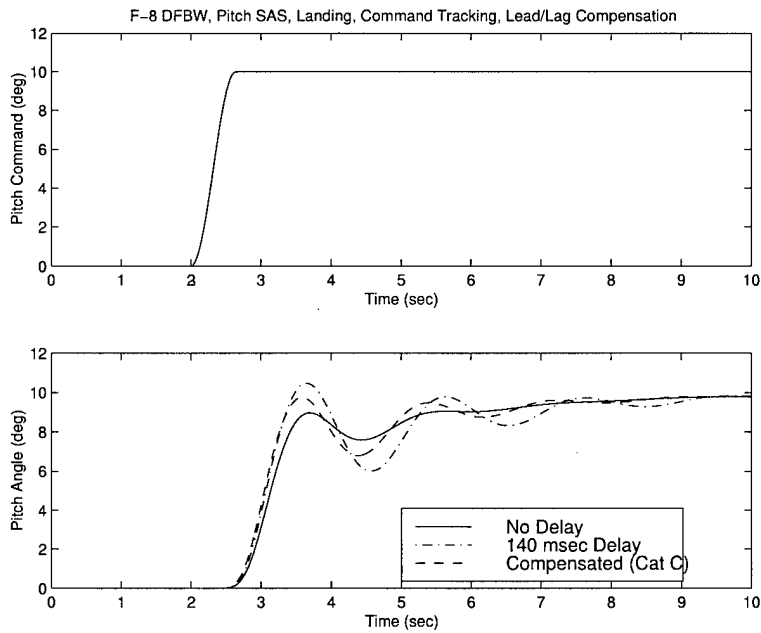


Figure B.5 F-8 DFBW Command Tracking, 140 msec Delay, Lead/Lag Compensation

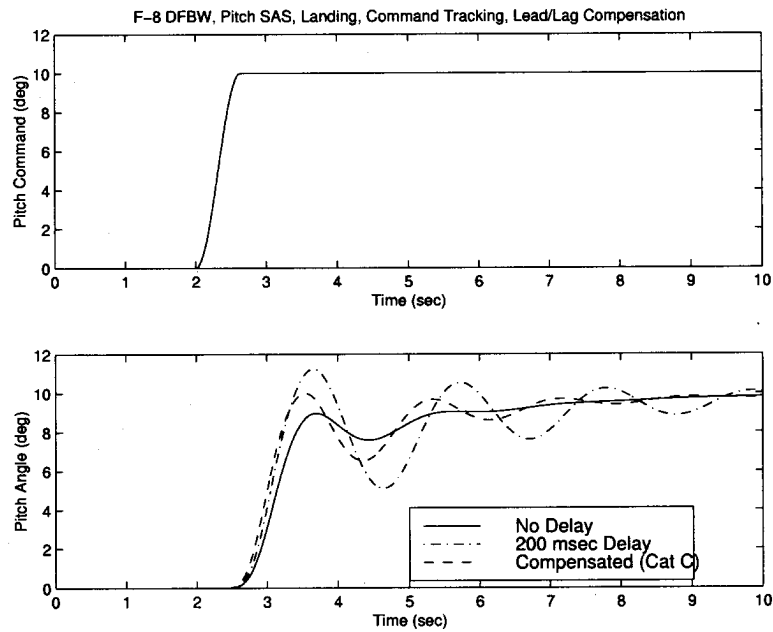


Figure B.6 F-8 DFBW Command Tracking, 200 msec Delay, Lead/Lag Compensation

B.2 F-8, Full State Predictor Compensation

Results for the Full State Predictor Compensator command tracking are presented below,

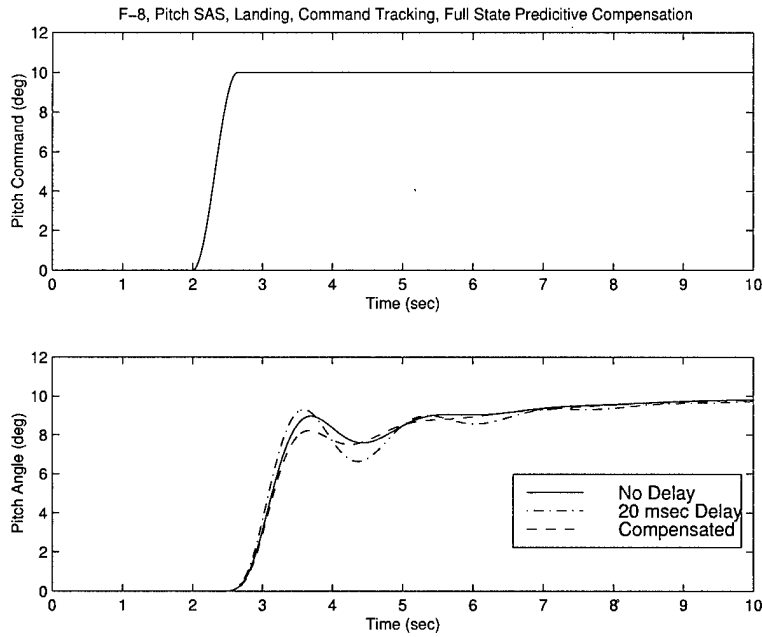


Figure B.7 F-8 DFBW Command Tracking, 20 msec Delay, Full State Predictive Compensation



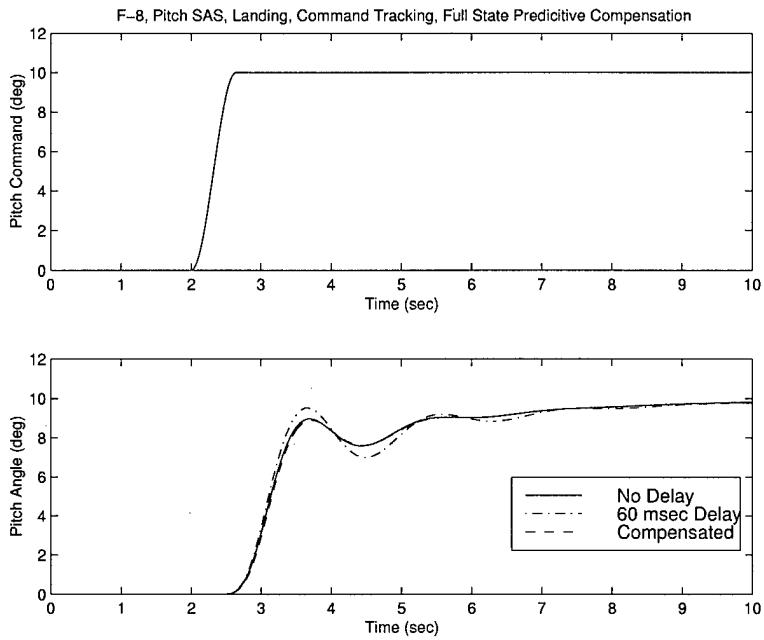


Figure B.8 F-8 DFBW Command Tracking, 60 msec Delay, Full State Predictive Compensation

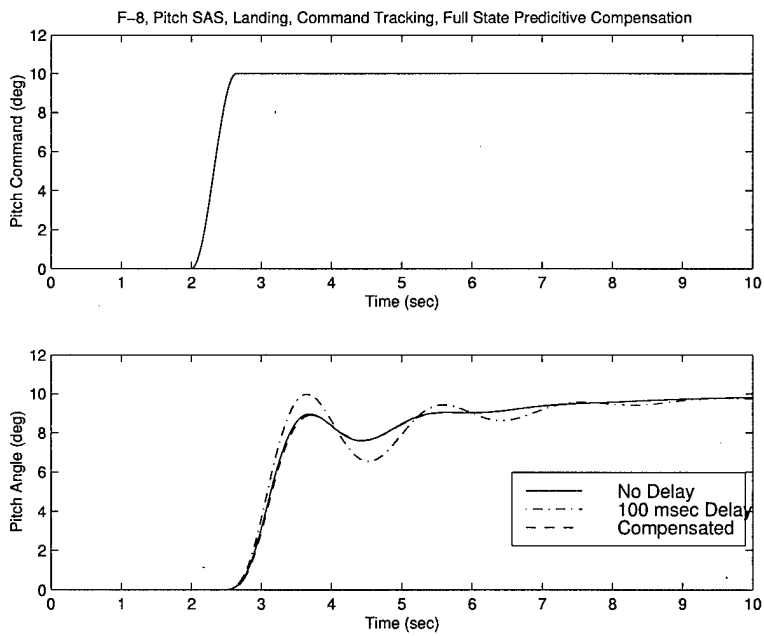


Figure B.9 F-8 DFBW Command Tracking, 100 msec Delay, Full State Predictive Compensation

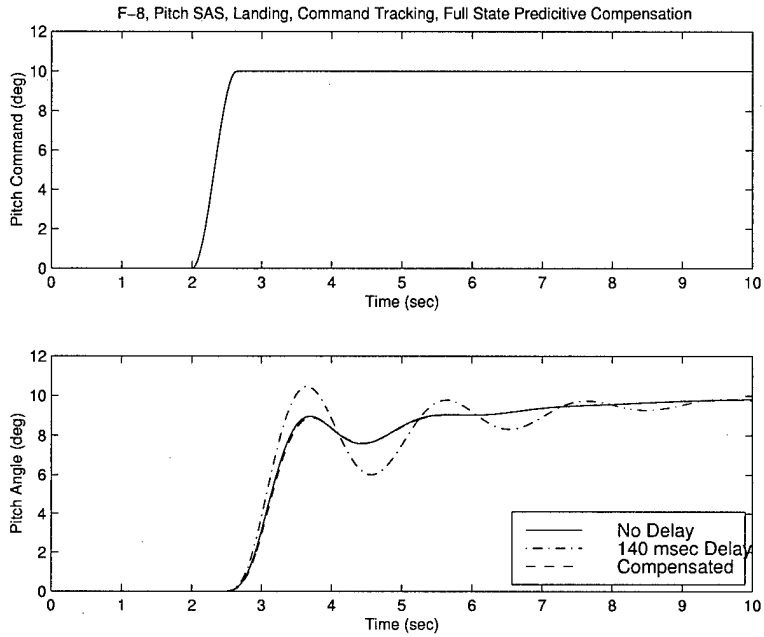


Figure B.10 F-8 DFBW Command Tracking, 140 msec Delay, Full State Predictive Compensation

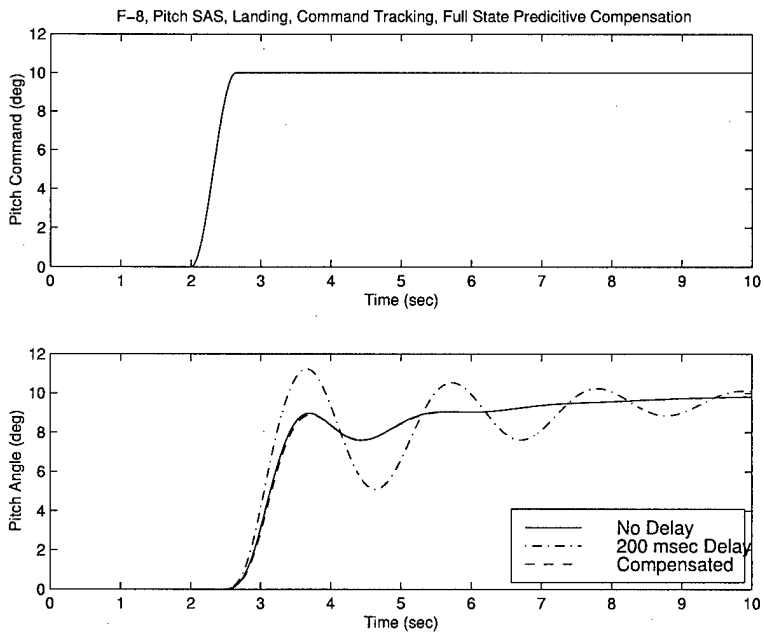


Figure B.11 F-8 DFBW Command Tracking, 200 msec Delay, Full State Predictive Compensation

### B.3 F-8, Output Feedback State Predictor Compensation

Results for the Output Feedback State Predictor Compensator command tracking are presented below,

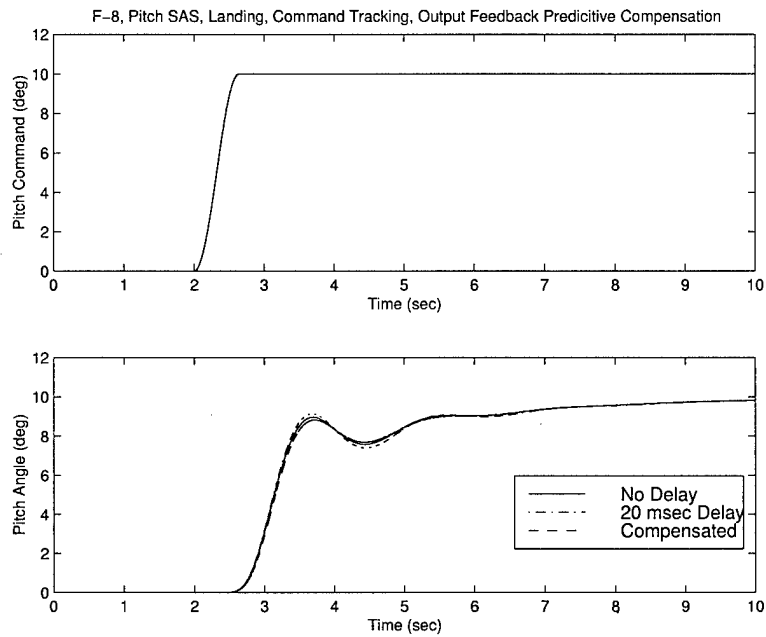


Figure B.12 F-8 DFBW Command Tracking, Output Feedback, 20 msec Delay

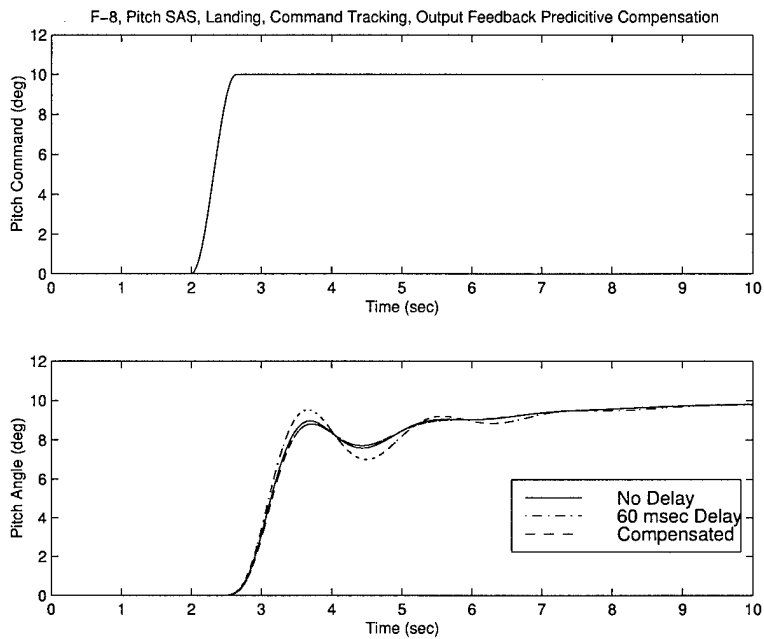


Figure B.13 F-8 DFBW Command Tracking, Output Feedback, 60 msec Delay

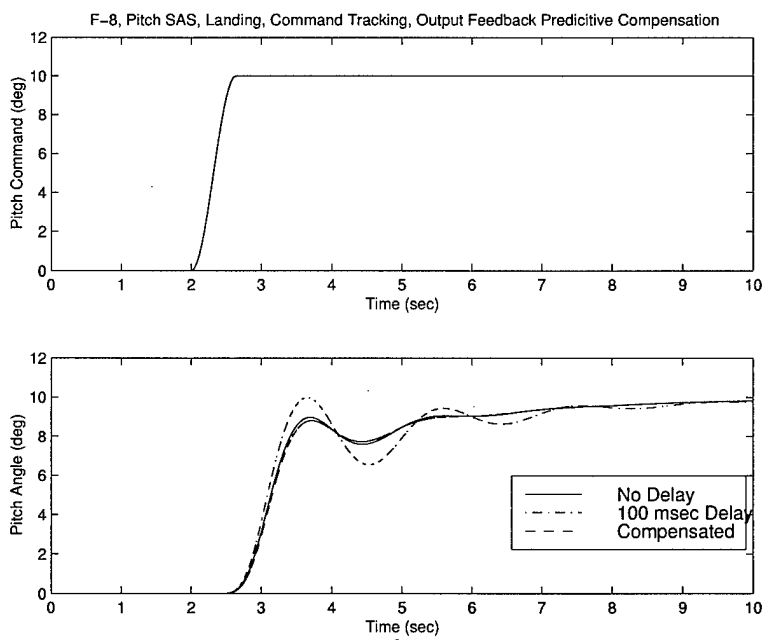


Figure B.14 F-8 DFBW Command Tracking, Output Feedback, 100 msec Delay

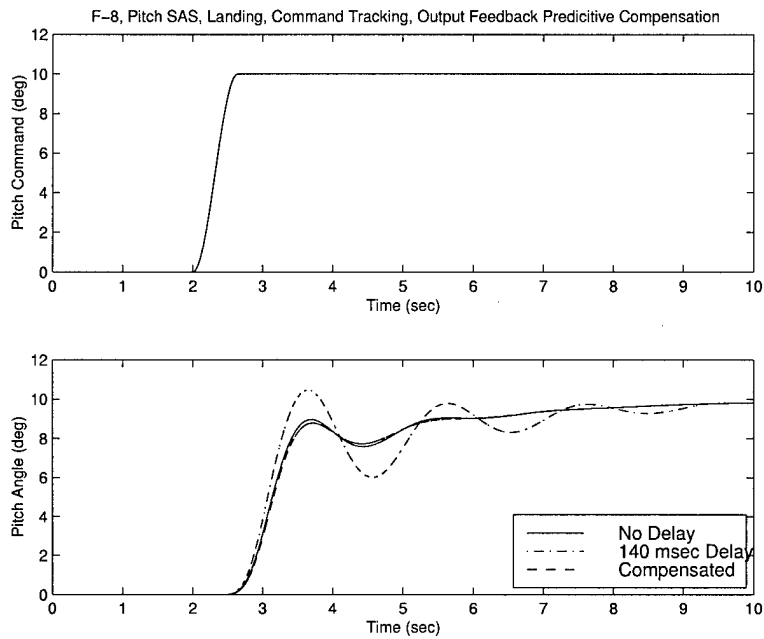


Figure B.15 F-8 DFBW Command Tracking, Output Feedback, 140 msec Delay

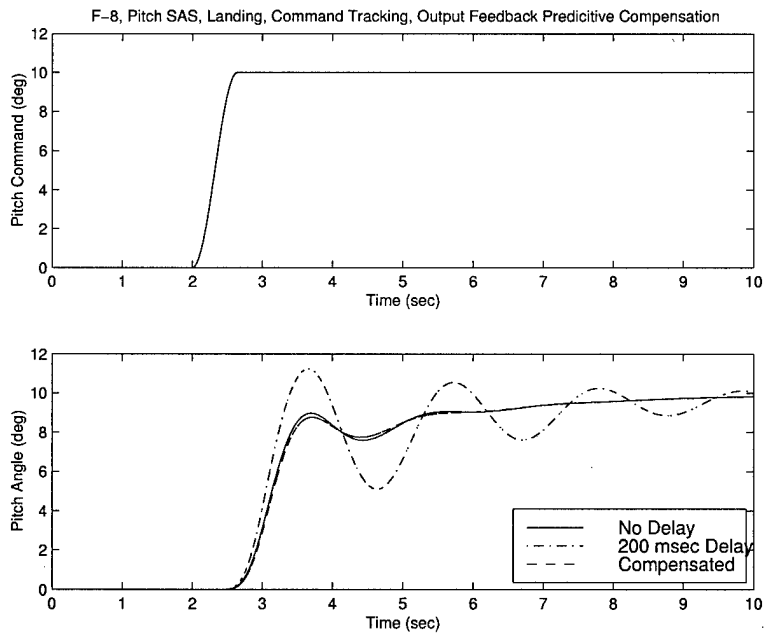


Figure B.16 F-8 DFBW Command Tracking, Output Feedback, 200 msec Delay

### *Appendix C. Instrumentation*

The instrumentation system requirements, the responsibilities, and hook-ups to support the Utility UAV flight test program are described in this appendix. Since the workstation software and derived data were an important facet of this test effort, the computational flow and data flow are also described.

#### *C.1 Parameter List*

<b>Parameter Name</b>	<b>Location</b>	<b>Units</b>	<b>Resolution</b>	<b>Sample Rate</b>	<b>Remarks</b>
pitch rate, $q$	UAV	deg/sec	24 Bit	130 Hz	Recorded at 30 Hz
angle of at- tack, $\alpha$	UAV	deg	24 Bit	130 Hz	Recorded at 30 Hz
Elevator position, $\delta_e$	UAV	deg	24 Bit	130 Hz	Recorded at 30 Hz
initial pitch, $\theta_0$	CSC	deg	32 Bit	Each test point	Recorded at sync
delayed pitch, $\theta_D$	CSC	deg	32 Bit	30 Hz	Integrated Pitch rate
task pitch, $\theta_T$	CSC	deg	32 Bit	30 Hz	
predicted pitch, $\theta_{pred}$	CSC	deg	32 Bit	30 Hz	
stick posi- tion, $x_S$	Pilot Station	deg	16 Bit	120 Hz	Recorded at 30 Hz

## C.2 Utility UAV Flight Data

Calculation of the predicted pitch required knowledge of the UAV short period flight parameters. UAV out-front video was provided by a color television camera mounted in the nose of the aircraft, see Figure 4.12. The Utility UAV onboard data acquisition system is schematically represented in Figure C.1.

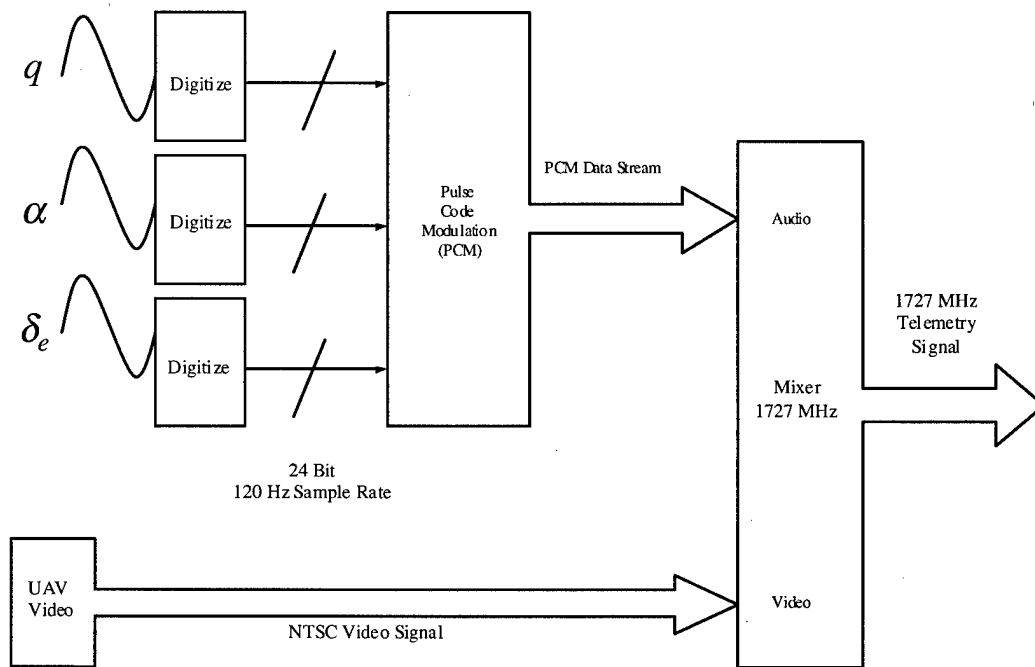


Figure C.1 UAV Onboard Data Acquisition System

UAV altitude and airspeed were derived from a calibrated pitot-static system and numerical indications were mixed onto the video signal prior to transmission to the telemetry receiver. Onboard UAV instrumentation measured pitch rate,  $q$ , angle of attack,  $\alpha$ , and elevator position,  $\delta_e$ . These parameters were sampled at 120 hz using a 24 bit analog-to-digital conversion. Prefiltering was accomplished using a third order Butterworth filter with corner frequency set at 15 hz. Filtering was done

to reduce aircraft body vibration noise in the pitch rate sensor signal. The corner frequency of 15 hz was selected to provide anti-aliasing as the signals were ultimately sampled by the SGI workstation at 30 hz. Filtered data were placed on a pulse code modulated data stream and mixed onto the audio channel of the video stream. The video signal was received by the NASA telemetry van, Figure 4.13, where the audio (data) channel was stripped off the video signal and the individual short period parameters decommutated. The NASA telemetry van provided the video channel in standard NTSC format over a shielded cable and the UAV short period parameters over Ethernet to the CSC workstation at the pilot station.

### *C.3 Pilot Station*

The pilot station control stick was instrumented to provide pilot input data to the predictive display algorithm. The control stick was instrumented to measure longitudinal displacement,  $x_S$ . Data were sampled at 120 hz with 16 bit accuracy and provided to the SGI workstation over an RS-232C standard datalink.

### *C.4 SGI Workstation*

The SGI workstation and software designed by Computer Sciences Corporation (CSC) was used to provide a programmable system delay, calculate UAV pitch attitude, and calculate predicted pitch attitude. The software also recorded all data for later analysis. SGI workstation data flow is depicted in Figure C.3.

*C.4.1 Delay.* Video was received from the NASA telemetry van, digitized, and stored in a buffer for a user selectable number of frames. This provided the test team with a method for precisely defining additional time delay. After each frame was digitized, the CSC software sampled the UAV short period parameters provided on the Ethernet link from the telemetry van. Pitch rate was integrated using a trapezoidal rule integration routine and current pitch rate,  $q$ , pitch attitude,  $\theta$ , angle of attack,  $\alpha$ , and elevator position,  $\delta_e$ , were tagged to the appropriate frame



of video and stored in the delay buffer. Video frames and the associated data block were stored in the buffer for the number of video frames necessary to achieve the selected additional delay.

*C.4.2 Display.* Predicted pitch attitude was then calculated from Equation 4.13 using the delayed data block and current pilot input data. The CSC software made use of the trim values of  $\alpha$ ,  $q$ , and  $x_S$  recorded during a trim shot at the beginning of the data run when calculating  $\Delta\alpha$ ,  $\Delta q$ , and  $\Delta u$  ( $u$  being  $x_S$ ). The initial pitch angle,  $\theta_0$ , was the difference between the boresight reference and the horizon line which was manually synchronized with the actual horizon during the initial trim shot. Figure C.2 details the various displayed data and the equations used to calculate them.

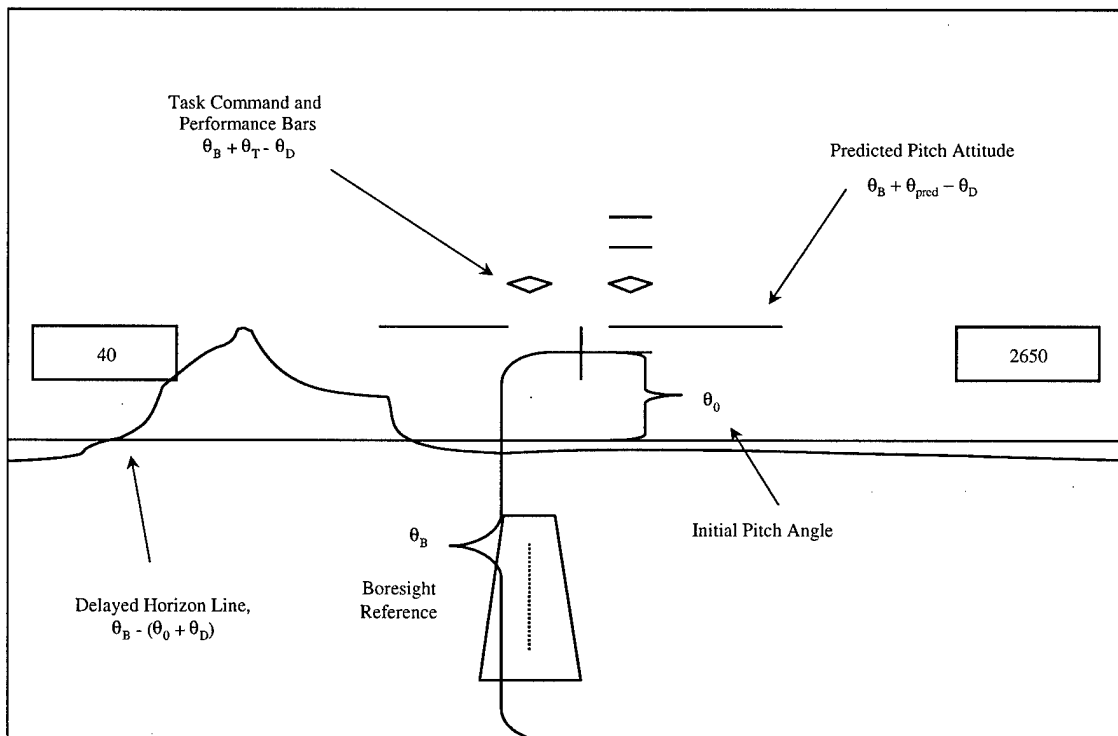


Figure C.2 Frame of Video With Displayed Data

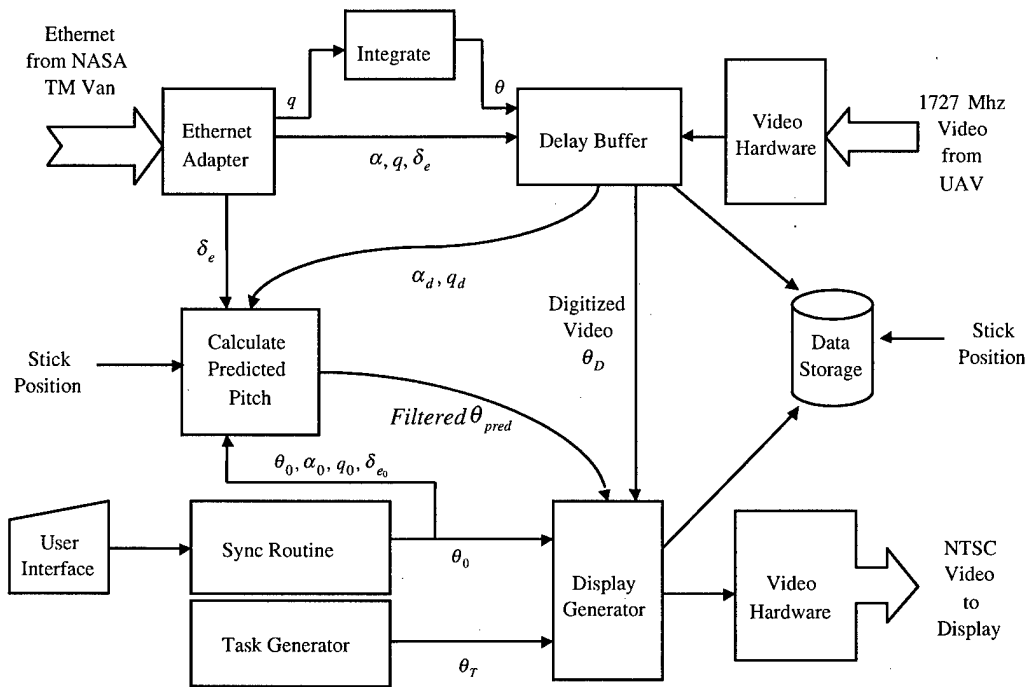


Figure C.3 Computer Workstation Data Flow Diagram

An overview of the computer workstation software computational flow is provided Figure C.4 through C.6.

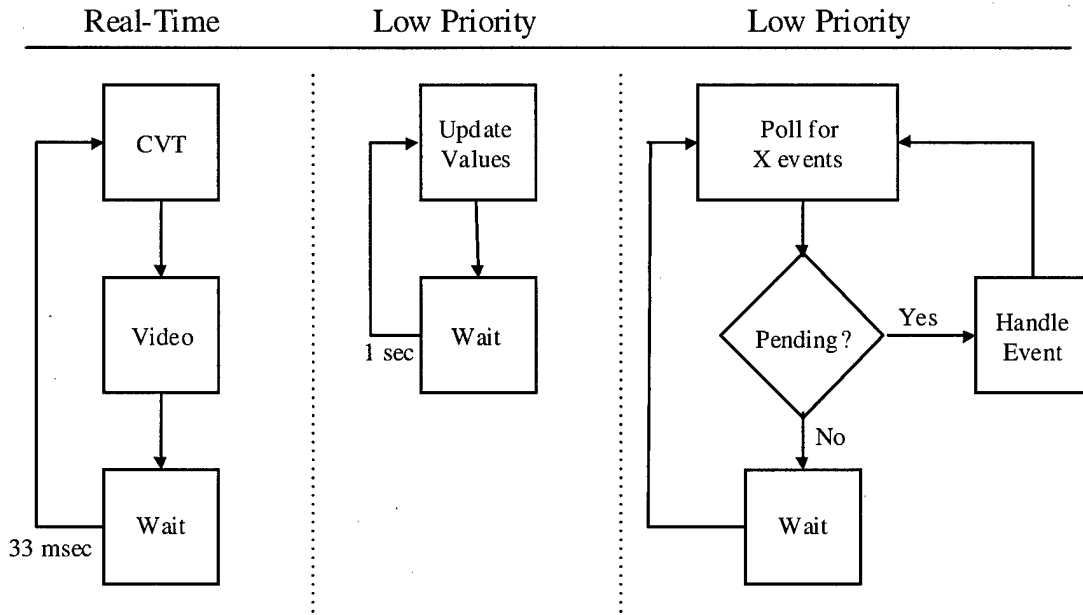


Figure C.4 Computer Workstation Top-Level Threads of Execution

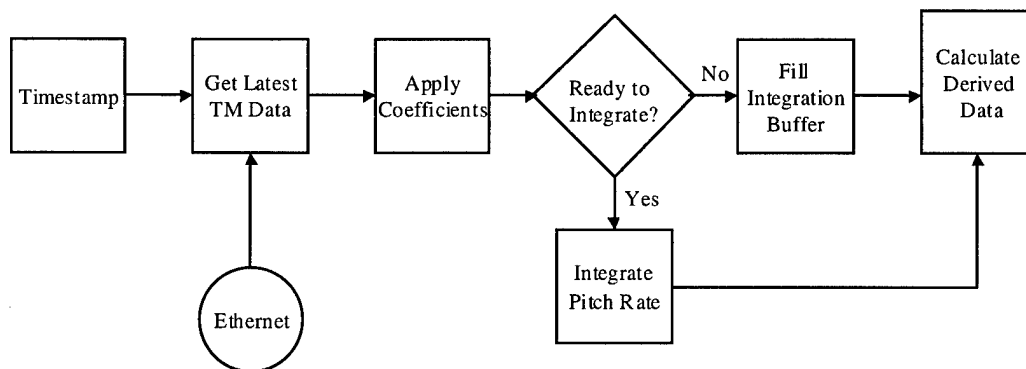


Figure C.5 Computer Workstation Update Current Variable Table (CVT)

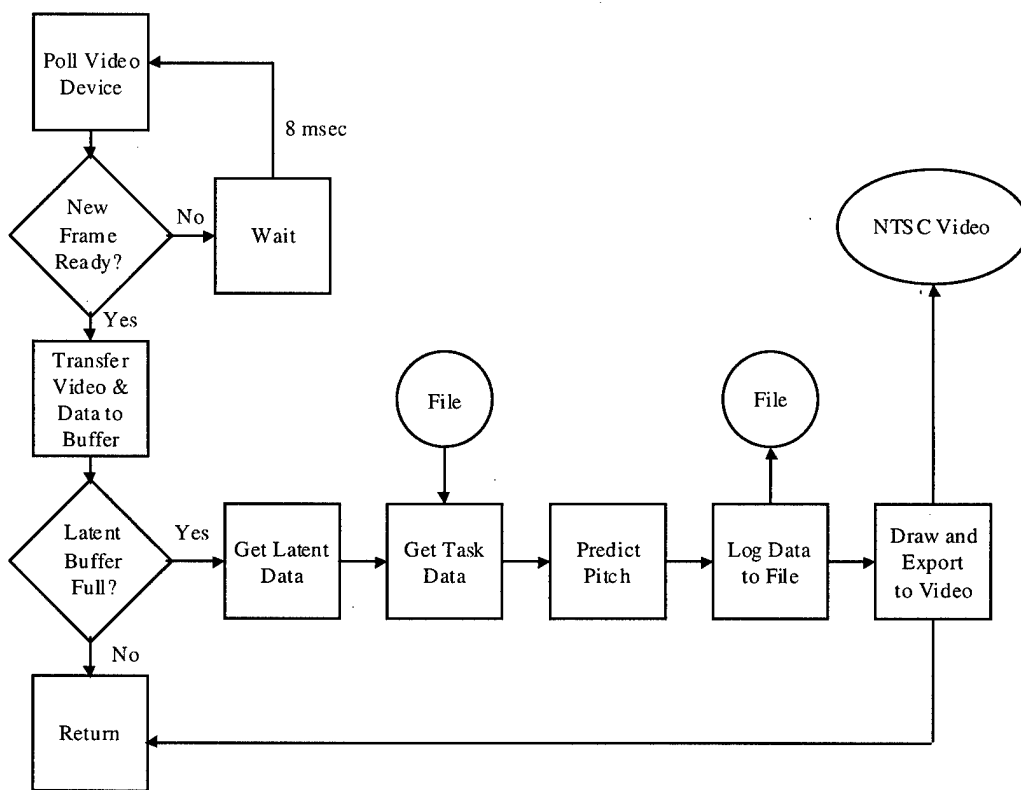


Figure C.6 Computer Workstation Video Processing

*Appendix D. Test Point Matrices*

Table D.1 Research Pilots

<b>RP</b>	<b>NAME</b>	<b>POSITION</b>	<b>FLYING EXPERIENCE</b>
1	Maj Andrew J. Thurling	Test Pilot Student	1,500 hours
2	Lt Col Kevin Ford	Test Pilot	2,400 hours
3	Lt Col Dana Purifoy	Test Pilot	4,500 hours
4	Capt Andrew J. Adams	FTE Student	65 Private Pilot hours
5	Capt Shahnaz M. Punjani	FTE Student	None
6	Capt Kelly A. Greene	FTE Student	160 Private Pilot hours

Table D.2 Objective 1 Test Matrix- Baseline UAV Handling Qualities

$\tau_d$ (msec)	<b>RP1</b>	<b>RP2</b>	<b>RP3</b>	<b>RP4</b>	<b>RP5</b>	<b>RP6</b>
33	2	6	3	4	3	6
66	6	1	2	5	2	2
100	4	3	4	3	4	5
133	5	5	6	1	5	1
166	1	2	5	6	1	3
200	3	4	1	2	6	4

Note: Numbers refer to order in which the pilots flew the test points.

Table D.3 Objective 2 Test Matrix- Predictor Handling Qualities

$\tau_d$ (msec)	RP1	RP2	RP3	RP4	RP5	RP6
33.33	2	6	3	4	3	6
66.67	6	1	2	5	2	2
100	4	3	4	3	4	5
133.33	5	5	6	1	5	1
166.67	1	2	5	6	1	3
200	3	4	1	2	6	4
400	*	*	*	*	*	*

Note: \* - Pilots flew the 400 msec delay as a "worst case" warmup prior to beginning test point matrix.

Note: The numbers refer to the order in which the pilots flew the test points.

Table D.4 Objective 3 Test Matrix - Aerodynamic Sensitivity ( $\tau_d = 100$  msec)

RP	$C_{M_\alpha}$	$C_{M_q}$	$C_{M_{\delta_e}}$
1	-20%	-20%	+20%
1	+20%	-20%	-20%
1	-20%	+20%	-20%
1	+20%	+20%	+20%
2	-20%	+20%	-20%
2	+20%	-20%	-20%
2	+20%	+20%	+20%
2	-20%	-20%	+20%
3	+20%	-20%	-20%
3	-20%	+20%	-20%
3	+20%	+20%	+20%
3	-20%	-20%	+20%

RP	$C_{M_\alpha}$	$C_{M_q}$	$C_{M_{\delta_e}}$
4	-20%	-20%	-20%
4	-20%	+20%	+20%
4	+20%	+20%	-20%
4	+20%	-20%	+20%
5	+20%	-20%	+20%
5	-20%	+20%	+20%
5	-20%	-20%	-20%
5	+20%	+20%	-20%
6	-20%	-20%	-20%
6	+20%	-20%	+20%
6	+20%	+20%	-20%
6	-20%	+20%	+20%

Table D.5 Objective 3 Test Matrix - Time Delay Uncertainty

<b>RP</b>	$\tau_{true}$ (msec)	$\tau_{comp}$ (msec)
1	100	67
1	100	133
2	100	133
2	100	67
3	100	67
3	100	133

<b>RP</b>	$\tau_{true}$ (msec)	$\tau_{comp}$ (msec)
4	100	133
4	100	67
5	100	67
5	100	133
6	100	133
6	100	67



*Appendix E. Pilot Comments and Ratings*

Table E.1 Objective 1 - Baseline Handling Qualities, MOP 2 - Research Pilot 1, Comments and Ratings

<b>Research Pilot 1</b>						
$\tau_d$	<b>TASK</b>	<b>CHR</b>	<b>PIOR</b>	<b>%D</b>	<b>%A</b>	<b>Pilot Comments</b>
33	2B	6	3	25	46	Very Predictable. Low workload.
67	2B	5	3	31.2	55.9	Fairly predictable. Little more work than baseline delay.
100	2A	8	4	16	34	Difficult to do task, just staying in the loop. 4-5 Overshoots for pitch capture
133	1A	7	4	22	47	More predictable than last test point (200ms delay)
167	1A	8	4	22	42	4-5 Overshoots. Bordering on PIOR 5.
200	2A	9	5	16	31	Difficult to stay in loop. Terminated Phase 3 early.

Table E.2 Objective 1 - Baseline Handling Qualities, MOP 2 - Research Pilot 2, Comments and Ratings

Research Pilot 2						
$\tau_d$	TASK	CHR	PIOR	%D	%A	Pilot Comments
33	1A	6	3.5	31.7	57.1	1-2 overshoots to get desired.
67	1A	5	3	26.4	48.7	Barely getting adequate. A little looser than baseline
100	2B	6	4	28.3	50.2	Tend to oscillate on captures, but not divergent.
133	2A	5	3	37.2	61.3	Feels easier to control (compared to 200ms). Some oscillations.
167	2A	6	3	32.2	58.2	Oscillations about adequate (not really tracking).
200	1A	7	4	26.8	50	Overshoots-tougher to get adequate; oscillations about adequate.

Table E.3 Objective 1 - Baseline Handling Qualities, MOP 2 - Research Pilot 3, Comments and Ratings

Research Pilot 3						
$\tau_d$	TASK	CHR	PIOR	%D	%A	Pilot Comments
33	2A	6	3	23.2	44.6	More overshoots than baseline/workload higher (task tended to raise nose).
67	2B	5.5	3	33.8	56.6	Some delay, not as big as baseline. Workload high. 1-2 overshoots for desired.
100	1A	6	4	17.6	37.2	Delay more noticeable. Workload high. Large pitch captures drive near CHR 7 type overshoots.
133	2B	6.5	4	23.7	39.2	Delay high, performance down. 2(+) overshoots to stay with task (not gross).
167	2A	7	4	26.6	49.9	Bigger delays and overshoots. Hard to predict. Large pitch capture requires 3-4 overshoots.
200	2A	6	3	17.8	40	Maximum workload, task performance compromised to maintain control.

Table E.4 Objective 1 - Baseline Handling Qualities, MOP 2 - Research Pilot 4, Comments and Ratings

Research Pilot 4						
$\tau_d$	TASK	CHR	PIOR	%D	%A	Pilot Comments
33	1A	6	3	22	40	Delay not as noticeable (as 100ms). Aircraft is responsive; "pretty tight"
67	2A	6	3	15	29	Similar oscillations to baseline.
100	2A	6	4	25	56	Smaller oscillations than last test point (200ms). One overshoot.
133	2A	6	3	25.7	40.9	Annoying oscillations. One large overshoot to get desired. Not worst case delay.
167	1A	6	4	25	45	Oscillations outside of adequate.
200	1A	7	4	10	22	Large oscillations/overshoots (bounded).

Table E.5 Objective 1 - Baseline Handling Qualities, MOP 2 - Research Pilot 5, Comments and Ratings

Research Pilot 5						
$\tau_d$	TASK	CHR	PIOR	%D	%A	Pilot Comments
33	1A	5	3	19.1	40.4	Minor overshoots, but controllable. Better than last test point (66ms).
67	1A	7	4	17	32.8	Overshoots are controllable. Compensating by taking input out early.
100	2B	5	3	9.4	20.4	More overshoots than baseline. Still feel "with" the aircraft.
133	2A	7	4	6.3	14.8	Degraded aircraft noticeable. Performance not as good as last test point (100ms)
167	2A	8	5	9.8	17.8	Considerable compensation; 2-3 overshoots. Task compromised to maintain control.
200	1A	7	4	6.3	12.7	Definite degradation; terminated early. "Looks funky" (buffet/turbulence?)

Table E.6 Objective 1 - Baseline Handling Qualities, MOP 2 - Research Pilot 6, Comments and Ratings

Research Pilot 6						
$\tau_d$	TASK	CHR	PIOR	%D	%A	Pilot Comments
33	2A	5	3	20	44.4	Low workload, easy to perform task.
67	1A	6	4	20	40.2	Pitch capture causes 2-3 overshoots to get desired.
100	2B	5	2	24.9	43.3	Overshoots noticeable, but not large.
133	1A	5	3	26	44.6	Better performance, better aircraft than last test point (200ms)
167	1A	6	3	19.8	34.9	Overshoots not as large as last test point (67ms).
200	2A	7	5	23.1	43.3	Overshoots just to get adequate. PIO divergent..

Table E.7 Objective 2 - Predictor Handling Qualities, MOP 2 - Research Pilot 1, Comments and Ratings

Research Pilot 1				
$\tau_d$	TASK	CHR	PIOR	Pilot Comments
33	1A	4	3	Few oscillations, staying in desired.
67	1A	4	3	One overshoot then staying in desired. Feels like the simulator.
100	2A	3	2	Can feel effect of deadband. Jitter noticed (due to wind)
133	2B	4	3	One overshoot to capture, then staying in desired.
167	2B	3.5	3	One overshoot to get adequate. Using less stick deflection, less aggressive.
200	2B	4	3	One overshoot to capture, then desired. Can't be too aggressive. Can't tell the difference between this point and last test point (166ms).
400	2B	6	3	Undershoot tendency due to washout filter. So much delay in predictor that I want to look at the "real world". Oscillations in predicted display to get adequate.

Table E.8 Objective 2 - Predictor Handling Qualities, MOP 2 - Research Pilot 2, Comments and Ratings

Research Pilot 2				
$\tau_d$	TASK	CHR	PIOR	Pilot Comments
33	1A	4	3	Desired performance easy; bobble inside desired.
67	2B	4	3	Overshoots within adequate; undesired motions affect performance. Workload high to get desired.
100	2A	5	3	No oscillations. Not entirely desired performance.
133	1A	4	3	Undershooting but not oscillating. Overshoots are larger in amplitude than last test point (66ms).
167	2B	4	3	Undershoots result in an overshoot (capture short, then overcompensate).
200	2A	4	3	Overshoot, then a step input to get desired.
400	2B	4	3	Barely getting desired. Small oscillations about neutral. Undershoots due to rapid response of predictor.

Table E.9 Objective 2 - Predictor Handling Qualities, MOP 2 - Research Pilot 3, Comments and Ratings

Research Pilot 3				
$\tau_d$	TASK	CHR	PIOR	Pilot Comments
33	2A	4	3	Good captures. Performance is a high desired, workload moderate. "Strong level 2" aircraft (CHR4). Undesired motions caused performance to go down.
67	2A	4	3	Two steps (undershoot, then correction) for large captures. Control is tighter/better than previous test point (100ms).
100	1A	4	3	Desired with moderate compensation. Bobble, but no oscillations. Deadbeat on small steps. Compensation moderate.
133	2A	6	3	Maintaining adequate, in and out of desired. "Hint" of oscillation in large steps, but didn't drive oscillation.
167	2B	5	3	More bobble noticeable. Undershoots now becoming a "true" overshoot. Workload is higher; adequate is easy ("solid CHR 5"). Ramp task gets desired, but steps are only adequate.
200	2B	5	3	Delay is noticeable, no oscillations. Two steps or one overshoot in pitch capture. "Pushing along" behind the ramp task. Gray area CHR 4/5 because workload is high, performance is lower than baseline.
400	2B	5	3	Adequate easy, desired attainable. "Well, that's nice" (after aggressive pitch capture). Would be CHR 4, but want more performance. Prior to task, significant oscillations, during task there were none.

Table E.10 Objective 2 - Predictor Handling Qualities, MOP 2 - Research Pilot 4, Comments and Ratings

Research Pilot 4				
$\tau_d$	TASK	CHR	PIOR	Pilot Comments
33	2A	4	3	Overshoots are smaller in amplitude than last test point (133ms).
67	1A	5	3	Undershoots on small steps, small overshoot on large steps. Performance not completely desired. Easier to fly predictor tasks than the original (no predictor) tasks.
100	2B	5	3	Did not get desired performance (CHR 5). Not much different from last test point (67ms).
133	2B	4	3	One overshoot. Can keep up with the ramp task, but captures cause undershoot then overshoot. Better performance than last test point (100ms).
167	2A	4	3	Small pitch captures are easy with no overshoots; large steps cause larger overshoots. Mostly desired performance.
200	2B	5	3	Sense a little delay. Performance was good, but not desired. Aggressive captures with one overshoot; ramp task is easier.
400	2A	5	3	Doesn't feel solid. Nearly desired, but noticeable motions degrade performance.



Table E.11 Objective 2 - Predictor Handling Qualities, MOP 2 - Research Pilot 5, Comments and Ratings

Research Pilot 5				
$\tau_d$	TASK	CHR	PIOR	Pilot Comments
33	2B	4	3	No overshoots. Almost desired best performance so far (test point #5). Feels better, but undesired motions still affect performance.
67	2B	4.5	3	Small overshoots, not desired performance. Still, I like this aircraft.
100	1A	5	3	Little difference between this test point and others (test point #6). Can fly aggressively and large pitch captures are controllable.
133	1A	5	3	Not much different than last two test points (200ms/167ms). Adequate, but not desired. Good performance is much easier with predictor than without.
167	2A	5	3	1-2 overshoots to get within adequate bars. Overshoots smaller than last test point (400ms).
200	2B	5	3	Adequate, but not desired. Feels better than last test point (167ms), but still CHR 5.
400	1A	7	4	Not very controllable. Have to lead input and then put back in opposite direction.

Table E.12 Objective 2 - Predictor Handling Qualities, MOP 2 - Research Pilot 6, Comments and Ratings

<b>Research Pilot 6</b>				
$\tau_d$	<b>TASK</b>	<b>CHR</b>	<b>PIOR</b>	<b>Pilot Comments</b>
33	2A	3	2	Feels like a level 1 aircraft. Little bobbles, but still getting performance.
67	2A	4	3	Feels like you can get desired easily. Much easier to fly predictor task than with no predictor.
100	1A	4.5	3	One overshoot, but always inside adequate bars. Undesired oscillations compromised performance. Not as good as last test point (33ms).
133	2A	4	3	Desired performance required moderate work, especially to prevent overshoots.
167	2B	3	4.5	Overshoots caused excursions outside of the adequate bars.
200	1A	5	4	Feeling a little out of control. Less predictable. Overshoots are bigger in amplitude than last test point (167ms).
400	2A	5	3	Predictor performance is definitely degraded. Overshoots are larger in amplitude than last test point (200ms).

Table E.13 Objective 3 - Sensitivity Analysis, MOP 1 - Aerodynamic Sensitivity

$C_{M_\alpha} = -20\%$ , $C_{M_q} = -20\%$ , $C_{M_{\delta_e}} = +20\%$				
RP	RUN	CHR	PIOR	Pilot Comments
1	1	3	2	Predictor more sensitive. Overshoots not as large. Performance is better than baseline.
2	4	3	3	Easier to capture than previous (TP3). Less overshoots; easier to stop. Always in adequate, mostly desired.
3	4	5	3	Adequate is possible; more oscillatory. Jittery, 1-2 overshoots. Workload high.
$C_{M_\alpha} = +20\%$ , $C_{M_q} = -20\%$ , $C_{M_{\delta_e}} = -20\%$				
RP	RUN	CHR	PIOR	Pilot Comments
1	2	5	3	Predictor is sluggish/more lag. Undesired motions. Not desired performance.
2	2	5	3	Overshoots not as bad as last test point (TP1). Few more oscillations; harder to nail it.
3	1	4	3	Able to make reasonable steps with small overshoots. A little better than baseline. Some undesired motion, but bounded.
$C_{M_\alpha} = -20\%$ , $C_{M_q} = +20\%$ , $C_{M_{\delta_e}} = -20\%$				
RP	RUN	CHR	PIOR	Pilot Comments
1	3	4	2	Not very different from baseline (working a little harder). Able to maintain desired with one overshoot.
2	1	4	3	Not much different from baseline. Little bit of overshoot.
3	2	5	3	Larger jumps in display; response difficult to track. Jitter and larger overshoots for large steps. Worse than last test point (TP1)

Table E.14 Objective 3 - Sensitivity Analysis, MOP 1 - Aerodynamic Sensitivity cont.

$C_{M_\alpha} = + 20\%, C_{M_q} = + 20\%, C_{M_{\delta_e}} = + 20\%$				
RP	RUN	CHR	PIOR	Pilot Comments
1	4	4	3	Undershoots, less overshoots. Small motions are less predictable. Can get "in synch" with undesired motions.
2	3	5	3	Did not like it. Initial response is slow; under shoots. Had to force it.
3	3	4	3	Pulling overshoots-a little more predictable. Large pitch captures get desired. Fewer undesired motions.
$C_{M_\alpha} = - 20\%, C_{M_q} = - 20\%, C_{M_{\delta_e}} = - 20\%$				
RP	RUN	CHR	PIOR	Pilot Comments
4	1	3	2	Pretty responsive, fairly predictable. Undershoots "slide in". Better than baseline.
5	3	5	3	Don't see any difference from baseline. Definite overshoots.
6	1	5	3	Not desired. Can't tell difference from baseline. Undesirable motions, but no oscillations. Overshoots, jittery.
$C_{M_\alpha} = - 20\%, C_{M_q} = + 20\%, C_{M_{\delta_e}} = + 20\%$				
RP	RUN	CHR	PIOR	Pilot Comments
4	2	4	3	Undershoots less predictable; more under-shoots.
5	2	6	3	Overshoots, unpredictable. Felt like I was flying something different from baseline.
6	4	5	3	More solid, more predictable. Goes right where you want it to go.

Table E.15 Objective 3 - Sensitivity Analysis, MOP 1 - Aerodynamic Sensitivity cont.

$C_{M_\alpha} = + 20\%$ , $C_{M_q} = + 20\%$ , $C_{M_{\delta_e}} = - 20\%$				
RP	RUN	CHR	PIOR	Pilot Comments
4	3	6	4	Sluggish, less precise. Slides past where you want it to stop. Oscillations within adequate. Notable lag.
5	4	6	3	Compensation requires taking out input as soon as you put it in. Very hands off.
6	3	5	4	Initial delay, initial response is slow. Change from baseline too small to notice.
$C_{M_\alpha} = + 20\%$ , $C_{M_q} = - 20\%$ , $C_{M_{\delta_e}} = + 20\%$				
RP	RUN	CHR	PIOR	Pilot Comments
4	4	5	3	Crisp, responsive-almost "snappy". Less predictable.
5	1	5	3	Some compensation-leads to undershoots.
6	2	5	4	More jittery; undesirable oscillations. Adequate; hard to get desired.

Table E.16 Objective 3 - Sensitivity Analysis, MOP 2 - Time Delay Sensitivity

Research Pilot 1					
RUN	$\tau_{true}$ (msec)	$\tau_{comp}$ (msec)	CHR	PIOR	Pilot Comments
5	100	67	4	2	Predictor is smoother, but not sluggish.
6	100	133	4	3	Predictable in small and large captures. More sensitive within desired; undesirable motions.
Research Pilot 2					
RUN	$\tau_{true}$ (msec)	$\tau_{comp}$ (msec)	CHR	PIOR	Pilot Comments
5	100	133	4	3	Tendency to undershoot.
6	100	67	5	3	Adequate, can't sustain desired. More tendency to overshoot; prefer the undershoot in previous test point (TP5).
Research Pilot 3					
RUN	$\tau_{true}$ (msec)	$\tau_{comp}$ (msec)	CHR	PIOR	Pilot Comments
5	100	67	5	3	Precision not as great; not easy to predict and end up sliding through. Lead compensation did not work as well as baseline.
6	100	133	4	3	Undershoot, then drift to desired. Lead compensation techniques are impacted. Less objectionable than previous (TP5); easier to compensate.

Table E.17 Objective 3 - Sensitivity Analysis, MOP 2 - Time Delay Sensitivity cont.

Research Pilot 4					
RUN	$\tau_{true}$ (msec)	$\tau_{comp}$ (msec)	CHR	PIOR	Pilot Comments
5	100	133	5	3	Less predictable. Oscillations within adequate.
6	100	67	5	3	Better performance. Undershoots to "slide in" to desired. Predictable with one overshoot on large captures.
Research Pilot 5					
RUN	$\tau_{true}$ (msec)	$\tau_{comp}$ (msec)	CHR	PIOR	Pilot Comments
5	100	67	7	3	Takes more stick input to get same response; more deadband. Larger overshoots.
6	100	133	7	3	Need to put in a lot of stick. Have to lead response by putting in opposite stick. Liked previous test point better (TP5).
Research Pilot 6					
RUN	$\tau_{true}$ (msec)	$\tau_{comp}$ (msec)	CHR	PIOR	Pilot Comments
5	100	133	4	2	Liked that aircraft better than baseline.
6	100	67	5.5	4	Overshoots from putting in too much and going past task. Oscillations divergent. Liked previous test point better (TP5).

## *Appendix F. Data Analysis Methods*

### *F.1 Required Data*

The following data elements were required for data analysis:

- Pilot Comments and ratings
- Unmanned Aerial Vehicle (UAV) Flight Parameters:
  1. Pitch rate,  $q$
  2. Angle of attack,  $\alpha$
  3. Elevator position,  $\delta_e$
- Calculated or Derived Data:
  1. Commanded tracking task,  $\theta_T$
  2. UAV pitch angle from integrating pitch rate,  $\theta_D$
  3. Predicted pitch angle,  $\theta_{pred}$
  4. Initial pitch attitude,  $\theta_0$

Other data required:

- Pilot stick position,  $x_S$

Data from all sources were stored at 30 samples per second by the computer workstation. Data in engineering units were saved to an ASCII file in a format compatible with the Matlab<sup>TM</sup>; software package. Matlab<sup>TM</sup>; was used to reduce the data and produce the final data products.



## F.2 Data Analysis

*F.2.1 Baseline UAV Handling Qualities.* Characterize the effects of time delay on UAV handling qualities. The Measures of Performance (MOPs) were:

1. Maximum Additional Time Delay: Determine the maximum additional time delay for the uncompensated UAV.
2. Pilot Comments and Ratings: Evaluate UAV handling qualities by collecting pilot comments and ratings for a series of additional time delays.
3. Root Mean Square Tracking Error: Determine the root mean square tracking error (RMSTE) during the pitch tracking task.

For MOP 1, pilot-in-the-loop oscillation ratings using the PIO rating scale in Figure 4.17 were collected. For MOP 2, data required were pilot comments and ratings using the Cooper-Harper scale in Figure 2.6. Additional data collected for MOP 2 were PIO ratings. For MOP 3, data required were research pilot (RP) commanded and actual UAV pitch.

Tracking error for MOP 3 was the difference between the task command and the boresight reference. Figure F.1 presents the display symbology and requisite calculations. Thus, if the pilot were able to precisely control the actual delayed pitch attitude ( $\theta_D$ ) to match the commanded task ( $\theta_T$ ), the resulting error was zero. The commanded pitch task was generated in the computer workstation and was composed of segments of the discrete pitch tracking task defined in MIL-STD-1797A.

Equation F.1 was used to calculate the RMSTE:

$$\sigma_{track} = (\theta_T - \theta_D)_{RMS} \quad (F.1)$$

*F.2.2 Statistical Methodologies.* Two methodologies were used for data analysis:

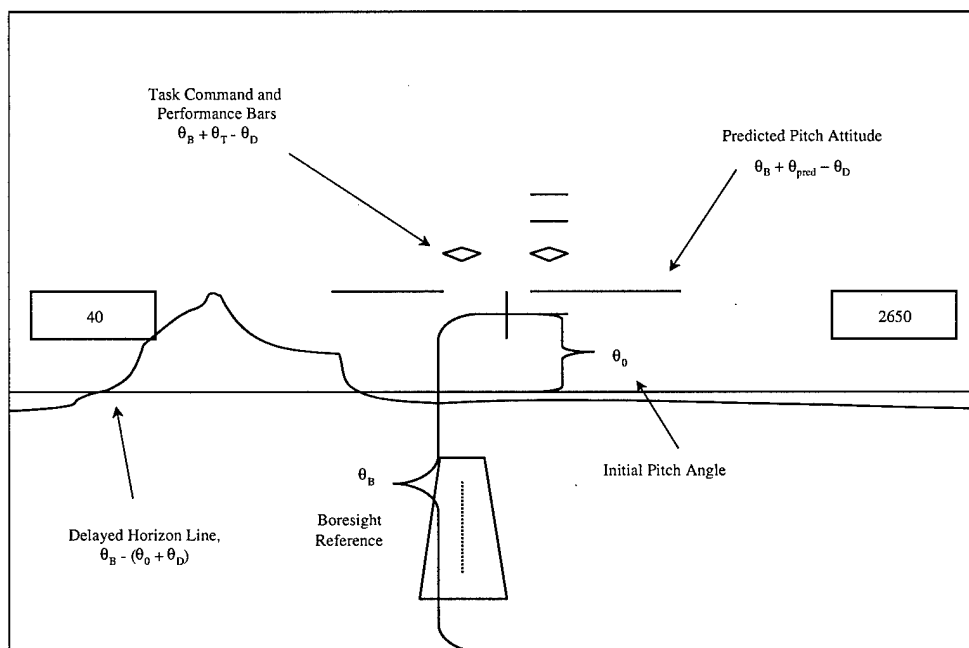


Figure F.1 Display Symbology Definitions

Table F.1 Baseline Maximum Additional Time Delay Data

RP	1	2	3	4	5	6
$\tau_{d,max}$ (msec)	200	166	266	266	200	233

1. Classical statistical approach
2. Response surface methodology (RSM) approach

*F.2.2.1 Classical Statistical Approach.* The data collected for Objective 1, MOP1 are listed in Table F.1 where  $\tau_{d,max}$  is the maximum additional time delay in milliseconds (msec).

The descriptive statistics for Objective 1, MOP 1 are listed in Table F.2 where FTE is flight test engineer. Descriptive statistics are used throughout this appendix where  $N$  is the sample size, MEAN is the sample mean, MIN is the sample minimum, MAX is the sample maximum, STD is the sample standard deviation, LOWER CI is

Table F.2 Baseline Maximum Additional Time Delay Descriptive Statistics

GROUP	N	MEAN	MIN	MAX	STD	LOWER CI	UPPER CI
RP	6	221.8333	166	266	40.2414	188.7300	254.9367
FTE	3	233.0000	200	266	33.0000	177.3665	288.6335
Pilot	3	210.6667	166	266	50.8462	124.9470	296.3863

Note: All times in msec.

the lower bound of the 90% confidence interval on the population mean, and UPPER CI is the upper bound of the 90% confidence interval on the population mean. All confidence levels are 90% Throughout this thesis.

A student's *t*-test was performed to determine if the baseline maximum additional time delay for pilots was different than that for FTEs. The student's *t*-tests performed throughout this thesis assume that the variances for the two populations are unknown and unequal. Analysis revealed that the FTE  $\tau_{d,max}$  was equal to the pilot  $\tau_{d,max}$  with 90% confidence.

The data collected for Objective 1, MOP 2 and MOP 3 are listed in Table F.3 where  $\tau_d$  is the planned additional time delay,  $\tau_{d,true}$  is the time delay actually achieved, PIOR is pilot-in-the-loop oscillation rating, and CHR is Cooper-Harper rating.

The descriptive statistics for Objective 1, MOP 2 are listed in Table F.4 and Table F.5. The descriptive statistics for Objective 1, MOP 3 are listed in Table F.6.

The classical statistical approach used the  $\chi^2$  test and the student's *t*-test that assumes unknown and unequal population variances. For a more detailed discussion of the statistical methods used during data analysis, see the Have Reckon Final Test Report(56). The  $\chi^2$  tests determined that *overall* there was no significant difference between pilots and FTEs for the baseline PIO ratings, Cooper-Harper ratings, and RMSTE with 90% confidence. The student's *t*-tests determined that baseline Cooper-Harper ratings were different among pilots and FTEs at 33 msec and

Table F.3 Objective One, Processed Baseline Data

$\tau_d$ (msec)	$\tau_{d,true}$ (msec)	RP	TASK	DATE	PIOR	CHR	RMSTE (in deg)
33	19.1	1	1A	9/29/99	3	6	1.6033
33	22.6	2	1A	10/7/99	3.5	6	2.0740
33	22.2	3	2A	10/4/99	3	6	2.0695
33	23	4	2A	9/29/99	3	5	2.4850
33	23.6	5	2A	9/30/99	3	5	1.7921
33	20.7	6	1A	9/30/99	3	5	2.0600
67	55	1	2B	9/29/99	3	5	1.5000
67	53.7	2	1A	10/7/99	3	5	1.7194
67	54.5	3	2B	10/4/99	3	5.5	1.8642
67	56.3	4	2B	10/4/99	3	6	2.7385
67	56.6	5	1A	10/5/99	3	6	2.6882
67	53.5	6	2A	10/7/99	4	6	2.1086
100	86.4	1	2A	9/29/99	4	8	2.2455
100	89.3	2	2B	10/7/99	4	6	1.8739
100	86.6	3	1A	10/4/99	4	6	2.4338
100	88.5	4	2B	10/13/99	4	6	1.5890
100	88.6	5	2B	9/30/99	3	5	2.4234
100	89	6	2B	9/30/99	2	5	2.1664
133	123.8	1	1A	9/29/99	4	7	2.4487
133	120.4	2	2A	10/7/99	3	5	1.6035
133	121.7	3	2B	10/4/99	4	6.5	2.3678
133	123.9	4	2A	10/5/99	3	6	2.2538
133	120.8	5	2A	10/14/99	4	7	1.6311
133	120.8	6	1A	10/7/99	3	5	2.4514
167	156.5	1	1A	9/29/99	4	8	2.2295
167	156.3	2	2A	10/7/99	3	6	1.5069
167	156	3	2A	10/4/99	4	7	1.9478
167	155.5	4	1A	10/13/99	4	6	2.1406
167	158.6	5	2B	10/5/99	5	8	3.6963
167	155.3	6	1A	9/30/99	3	6	2.0414
200	189	1	2B	9/29/99	5	9	3.0193
200	189.1	2	1A	10/7/99	4	7	1.8100
200	189.5	3	2A	10/4/99	3	6	2.2679
200	190	4	1A	9/29/99	4	7	1.8238
200	189.5	5	1A	9/28/99	4	7	4.6077
200	190.2	6	1A	10/7/99	5	7	2.7994

Table F.4 Baseline PIO Rating Descriptive Statistics

GROUP	$\tau_d$ (msec)	<i>N</i>	MEAN	MIN	MAX	STD	LOWER CI	UPPER CI
RP	33	6	3.0833	3	3.5	0.2041	2.9154	3.2513
	67	6	3.1667	3	4	0.4082	2.8308	3.5025
	100	6	3.5000	2	4	0.8367	2.8117	4.1883
	133	6	3.5000	3	4	0.5477	3.0494	3.9506
	167	6	3.8333	3	5	0.7528	3.2141	4.4526
	200	6	4.1667	3	5	0.7528	3.5474	4.7859
FTE	33	3	3.0000	3	3	0.0000	3.0000	3.0000
	67	3	3.3333	3	4	0.5774	2.3600	4.3067
	100	3	3.0000	2	4	1.0000	1.3141	4.6859
	133	3	3.3333	3	4	0.5774	2.3600	4.3067
	167	3	4.0000	3	5	1.0000	2.3141	5.6859
	200	3	4.3333	4	5	0.5774	3.3600	5.3067
Pilot	33	3	3.1667	3	3.5	0.2887	2.6800	3.6533
	67	3	3.0000	3	3	0.0000	3.0000	3.0000
	100	3	4.0000	4	4	0.0000	4.0000	4.0000
	133	3	3.6667	3	4	0.5774	2.6933	4.6400
	167	3	3.6667	3	4	0.5774	2.6933	4.6400
	200	3	4.0000	3	5	1.0000	2.3141	5.6859

Table F.5 Baseline Cooper-Harper Rating Descriptive Statistics

GROUP	$\tau_d$ (msec)	N	MEAN	MIN	MAX	STD	LOWER CI	UPPER CI
RP	33	6	5.5000	5	6	0.5477	5.0494	5.9506
	67	6	5.5833	5	6	0.4916	5.1789	5.9877
	100	6	6.0000	5	8	1.0954	5.0989	6.9011
	133	6	6.0833	5	7	0.9174	5.3286	6.8380
	167	6	6.8333	6	8	0.9832	6.0245	7.6421
	200	6	7.1667	6	9	0.9832	6.3579	7.9755
FTE	33	3	5.0000	5	5	0.0000	5.0000	5.0000
	67	3	6.0000	6	6	0.0000	6.0000	6.0000
	100	3	5.3333	5	6	0.5774	4.3600	6.3067
	133	3	6.0000	5	7	1.0000	4.3141	7.6859
	167	3	6.6667	6	8	1.1547	4.7200	8.6133
	200	3	7.0000	7	7	0.0000	7.0000	7.0000
Pilot	33	3	6.0000	6	6	0.0000	6.0000	6.0000
	67	3	5.1667	5	5.5	0.2887	4.6800	5.6533
	100	3	6.6667	6	8	1.1547	4.7200	8.6133
	133	3	6.1667	5	7	1.0408	4.4120	7.9214
	167	3	7.0000	6	8	1.0000	5.3141	8.6859
	200	3	7.3333	6	9	1.5275	4.7581	9.9085

Table F.6 Baseline Root Mean Square Tracking Error Descriptive Statistics

<b>GROUP</b>	$\tau_d$ (msec)	<i>N</i>	<b>MEAN</b>	<b>MIN</b>	<b>MAX</b>	<b>STD</b>	<b>LOWER CI</b>	<b>UPPER CI</b>
RP	33	6	2.0140	1.6033	2.4850	0.2995	1.7676	2.2604
	67	6	2.1032	1.5000	2.7385	0.5127	1.6814	2.5249
	100	6	2.1220	1.5890	2.4338	0.3319	1.8489	2.3950
	133	6	2.1261	1.6035	2.4514	0.4007	1.7964	2.4557
	167	6	2.2604	1.5069	3.6963	0.7471	1.6459	2.8750
	200	6	2.7213	1.8100	4.6077	1.0483	1.8590	3.5837
FTE	33	3	2.1124	1.7921	2.4850	0.3494	1.5234	2.7014
	67	3	2.5118	2.1086	2.7385	0.3501	1.9216	3.1019
	100	3	2.0596	1.5890	2.4234	0.4273	1.3392	2.7800
	133	3	2.1121	1.6311	2.4514	0.4281	1.3904	2.8338
	167	3	2.6261	2.0414	3.6963	0.9281	1.0614	4.1908
	200	3	3.0770	1.8238	4.6077	1.4126	0.6956	5.4584
Pilot	33	3	1.9156	1.6033	2.0740	0.2705	1.4596	2.3716
	67	3	1.6946	1.5000	1.8642	0.1834	1.3854	2.0037
	100	3	2.1844	1.8739	2.4338	0.2849	1.7042	2.6647
	133	3	2.1400	1.6035	2.4487	0.4664	1.3537	2.9263
	167	3	1.8948	1.5069	2.2295	0.3642	1.2807	2.5088
	200	3	2.3657	1.8100	3.0193	0.6106	1.3364	3.3950

Table F.7 Flying Qualities Simulator PIO Ratings

RP	$\tau_d$ (msec)	100	200	300	350	400	450	500	550	600
1	Session 1 PIOR	2	3	3	4	4	4	4	5	X
	Session 2 PIOR	2	3	3	3	4	4	5	X	X
2	Session 1 PIOR	X	X	X	X	X	X	X	X	X
	Session 2 PIOR	2	4	4	4	4	4	4	5	X
3	Session 1 PIOR	2	3	3	4	4	4	4	5	X
	Session 2 PIOR	X	X	X	X	X	X	X	X	X
4	Session 1 PIOR	2	3	4	4	4	4	4	5	X
	Session 2 PIOR	2	3	3	3	4	4	4	4	5
5	Session 1 PIOR	1	2	2	2	3	3	5	X	X
	Session 2 PIOR	2	2	2	4	4	5	X	X	X
6	Session 1 PIOR	2	2	3	4	4	4	4	5	X
	Session 2 PIOR	2	3	3	3	4	5	X	X	X

at 67 msec of time delay. The student's  $t$ -tests also determined that baseline RMSTE was different among pilots and FTEs at 67 msec. Though there were some significant differences for baseline Cooper-Harper ratings and RMSTE at smaller time delays, these differences were not enough to cause an overall significant difference between pilots and FTEs.

*F.2.2.2 Response Surface Methods.* A Response Surface Methodology (RSM) analysis was conducted to verify the student's  $t$ -test results. The RSM also concluded that there was no statistical difference between FTE and Pilot ratings and performance. For a complete discussion of the RSM results, see the final test report(56).

*F.2.3 Learning Curve Validation.* The Flying Qualities simulator at the United States Air Force Test Pilot School (TPS) was used to validate the learning curve of the RPs. The data collected to validate learning curve are listed in Table F.7. The descriptive statistics for validated the learning curve are listed in Table F.8. In order to determine is there were any learning curve effects, a  $\chi^2$  test and the student's  $t$ test was performed. The  $\chi^2$  tests determined that *overall* there was



Table F.8 Flying Qualities Simulator PIO Ratings Descriptive Statistics

SESSION	$\tau_d$ (msec)	N	MEAN	MIN	MAX	STD	LOWER CI	UPPER CI
1	100	5	1.8000	1	2	0.4472	1.3736	2.2264
	200	5	2.6000	2	3	0.5477	2.0778	3.1222
	300	5	3.0000	2	4	0.7071	2.3258	3.6742
	350	5	3.6000	2	4	0.8944	2.7472	4.4528
	400	5	3.8000	3	4	0.4472	3.3736	4.2264
	450	5	3.8000	3	4	0.4472	3.3736	4.2264
	500	5	4.2000	4	5	0.4472	3.7736	4.6264
	550	5	5.0000	5	5	0.0000	5.0000	5.0000
2	600	5	5.0000	5	5	0.0000	5.0000	5.0000
	100	5	2.0000	2	2	0.0000	2.0000	2.0000
	200	5	3.0000	2	4	0.7071	2.3258	3.6742
	300	5	3.0000	2	4	0.7071	2.3258	3.6742
	350	5	3.4000	3	4	0.5477	2.8778	3.9222
	400	5	4.0000	4	4	0.0000	4.0000	4.0000
	450	5	4.4000	4	5	0.5477	3.8778	4.9222
	500	5	4.6000	4	5	0.5477	4.0778	5.1222
550	5	4.8000	4	5	0.4472	4.3736	5.2264	
600	5	5.0000	5	5	0.0000	5.0000	5.0000	

no significant learning curve for simulator PIO ratings with 90% confidence. The student's *t*-tests determined that simulator PIO ratings were different between the two sessions at 450 msec of time delay. Though there was one significant differences for simulator PIO ratings at 450 msec of time delays, this difference was not enough to cause an overall significant difference between sessions. As such, there was no significant learning curve.

### *F.3 Improvements of UAV Handling Qualities Using Model-Based Predictive Compensation*

Determine the improvement in UAV handling qualities attained using the predictive display. The MOPs were:

1. Maximum additional Time Delay: Determine the maximum additional time delay for the compensated UAV.
2. Pilot Comments and Ratings: Evaluate UAV handling qualities by collecting pilot comments and ratings for a series of additional time delays.
3. RMSTE: Determine the RMSTE during the pitch tracking task.
4. RMSDE: Determine the RMSDE during the pitch tracking task.

For MOP 1, PIO ratings using the PIO rating scale in Figure 4.17 were collected. For MOP 2, data required were pilot comments and ratings using the Cooper-Harper scale in Figure 2.6 and the PIO rating scale in Figure 4.17. For MOPs 3 and 4, data required were RP commanded and actual UAV pitch.

*F.3.1 Data Reduction.* Figure F.1 presents the display symbology and requisite calculations. Display error for MOP 3 was the difference between the predicted pitch reference and the task command. Thus, if the pilot were able to precisely control the predicted pitch attitude ( $\theta_{pred}$ ) to match the commanded task ( $\theta_T$ ), the resulting error was zero. The commanded task was generated in the computer work-

station and was composed of segments of the discrete pitch tracking task defined in MIL-STD-1797A.

The following equation was used to calculate the RMSDE:

$$\sigma_{display} = (\theta_T - \theta_{pred})_{RMS} \quad (F.2)$$

Tracking error for MOP 4 was the difference between the task command and the actual aircraft pitch attitude adjusted for time delay, see Equation F.1. Thus, if the actual pitch attitude,  $\theta_D$ , (adjusted for time delay) matched the commanded pitch attitude,  $\theta_T$ , the resulting error was zero. Essentially, the error due solely to the imposed time displacement between the two data streams should not be counted as system error.

*F.3.2 Statistical Methodologies.* Classical statistics were used for data analysis. The data collected for Objective 2, MOP 2 through MOP 4 are listed in Table F.9. The descriptive statistics for Objective 2, MOP 2 are listed in Table F.11 and Table F.12. Descriptive statistics for Objective 2, MOP 3 and 4 are listed in Table F.13 and Table F.14 respectively.

Analysis was performed to determine if FTEs and Pilots could be grouped together in subsequent analysis. The  $\chi^2$  tests determined that *overall* there was no significant difference between pilots and FTEs for the predictor PIO ratings, Cooper-Harper ratings, RMSTE, and RMSDE with 90% confidence. The student's *t*-tests determined that predictor RMSDE was different among pilots and FTEs at 167 msec of additional time delay. The student's *t*-tests also determined that predictor RMSDE was different among pilots and FTEs at the following levels of additional time delay: 167 msec, 200 msec, and 400 msec. Though there were some significant differences for predictor RMSTE and RMSDE at larger additional time delays, these

Table F.9 Predictor Data

$\tau_d$ (msec)	$\tau_{d,true}$ (msec)	RP	TASK	DATE	PIOR	CHR	RMSTE (deg)	RMSDE (deg)
33	22.7	1	1A	10/7/99	3	4	2.0686	1.4724
33	21.8	2	2A	10/8/99	3	4	1.5643	1.1941
33	21	3	2A	10/8/99	3	4	1.8992	1.3826
33	19.9	4	2A	10/12/99	3	4	1.7364	1.2702
33	22.5	5	2B	10/12/99	3	4	2.0872	1.6667
33	22.3	6	2A	10/7/99	2	3	1.9865	1.5217
67	56.5	1	1A	10/7/99	3	4	2.1058	1.4179
67	54.6	2	2B	10/8/99	3	4	2.1080	1.1934
67	55.1	3	2A	10/8/99	3	4	2.3183	1.4410
67	52.7	4	1A	10/12/99	3	5	1.9529	1.3475
67	53.4	5	2B	10/12/99	3	4.5	2.2004	1.6481
67	56.3	6	2A	10/7/99	3	4	2.0472	1.4474
100	89	1	2A	10/7/99	2	3	1.8848	1.1951
100	88.7	2	2A	10/8/99	3	5	1.7854	1.1597
100	87	3	2A	10/8/99	3	4	2.2556	1.3038
100	88.4	4	2B	10/12/99	3	5	1.9109	1.2760
100	87.8	5	2A	10/12/99	3	5	3.0968	2.1737
100	89.9	6	1A	10/7/99	3	4.5	2.5290	1.8706
133	121.7	1	2B	10/7/99	3	4	2.1009	1.1407
133	120.8	2	1A	10/8/99	3	4	2.0615	1.1148
133	120.7	3	2A	10/8/99	3	6	2.3377	1.2032
133	116.7	4	2B	10/12/99	3	4	2.1510	1.1046
133	122.1	5	1A	10/12/99	3	5	3.1399	2.3194
133	124.9	6	1A	10/7/99	3	4	2.8047	2.1018
167	156.4	1	2B	10/7/99	3	3.5	2.4449	1.0592
167	155.9	2	2B	10/8/99	3	4	1.8814	1.0492
167	148.9	3	2B	10/8/99	3	5	2.4014	1.0582
167	155.8	4	2A	10/12/99	3	4	2.4633	1.2987
167	156.5	5	2A	10/12/99	3	5	3.2334	2.0375
167	155.7	6	2B	10/7/99	4.5	3	3.0463	1.7174

Table F.10 Predictor Data, cont.

$\tau_d$ (msec)	$\tau_{d,true}$ (msec)	RP	TASK	DATE	PIOR	CHR	RMSTE (deg)	RMSDE (deg)
200	187.6	1	2B	10/7/99	3	4	2.0373	0.9770
200	187.5	2	2A	10/8/99	3	4	1.9072	1.1079
200	188.8	3	2B	10/8/99	3	5	2.6930	1.1465
200	187.3	4	2B	10/12/99	3	5	2.2220	1.2124
200	189.8	5	2A	10/12/99	3	5	2.9779	1.6049
200	185.9	6	1A	10/7/99	4	5	2.8206	1.7228
400	388.4	1	2B	10/7/99	3	6	2.5075	0.8861
400	388.7	2	2A	10/8/99	3	4	4.5303	0.9097
400	388	3	2A	10/8/99	3	5	2.3027	0.9036
400	387.7	4	2A	10/12/99	3	5	2.7996	1.2232
400	389.8	5	2A	10/19/99	3	7	3.9455	1.7357
400	389.1	6	2B	10/7/99	3	5	2.6185	1.4860

differences were not enough to cause an overall significant difference between pilots and FTEs.

Using Pilots and FTEs as one group, analysis was performed to determine if the predictor produced better tracking performance and decreased research pilot workload. Both  $\chi^2$  and student's *t*-tests determined that *overall* there was no significant difference between the baseline and predictor configurations for PIO ratings and RMSTE with 90% confidence. Both  $\chi^2$  and student's *t*-tests determined that *overall* there was a significant difference between the baseline and predictor configurations for Cooper-Harper ratings with 90% confidence. Additionally, the student's *t*-tests determined that there was a significant difference between the baseline and predictor configurations for PIO ratings with 90% confidence for following levels of additional time delay tested: 133 msec and 200 msec.

Table F.11 Predictor PIO Rating Descriptive Statistics

GROUP	$\tau_d$ (msec)	N	MEAN	MIN	MAX	STD	LOWER CI	UPPER CI
RP	33	6	2.8333	2	3	0.4082	2.4975	3.1692
	67	6	3.0000	3	3	0.0000	3.0000	3.0000
	100	6	2.8333	2	3	0.4082	2.4975	3.1692
	133	6	3.0000	3	3	0.0000	3.0000	3.0000
	167	6	3.2500	3	4.5	0.6124	2.7462	3.7538
	200	6	3.1667	3	4	0.4082	2.8308	3.5025
	400	6	3.0000	3	3	0.0000	3.0000	3.0000
FTE	33	3	2.6667	2	3	0.5774	1.6933	3.6400
	67	3	3.0000	3	3	0.0000	3.0000	3.0000
	100	3	3.0000	3	3	0.0000	3.0000	3.0000
	133	3	3.0000	3	3	0.0000	3.0000	3.0000
	167	3	3.5000	3	4.5	0.8660	2.0400	4.9600
	200	3	3.3333	3	4	0.5774	2.3600	4.3067
	400	3	3.0000	3	3	0.0000	3.0000	3.0000
Pilot	33	3	3.0000	3	3	0.0000	3.0000	3.0000
	67	3	3.0000	3	3	0.0000	3.0000	3.0000
	100	3	2.6667	2	3	0.5774	1.6933	3.6400
	133	3	3.0000	3	3	0.0000	3.0000	3.0000
	167	3	3.0000	3	3	0.0000	3.0000	3.0000
	200	3	3.0000	3	3	0.0000	3.0000	3.0000
	400	3	3.0000	3	3	0.0000	3.0000	3.0000

Table F.12 Predictor Cooper-Harper Rating Descriptive Statistics

GROUP	$\tau_d$ (msec)	<i>N</i>	MEAN	MIN	MAX	STD	LOWER CI	UPPER CI
RP	33	6	3.8333	3	4	0.4082	3.4975	4.1692
	67	6	4.2500	4	5	0.4183	3.9059	4.5941
	100	6	4.4167	3	5	0.8010	3.7577	5.0756
	133	6	4.5000	4	6	0.8367	3.8117	5.1883
	167	6	4.0833	3	5	0.8010	3.4244	4.7423
	200	6	4.6667	4	5	0.5164	4.2419	5.0915
	400	6	5.3333	4	7	1.0328	4.4837	6.1829
FTE	33	3	3.6667	3	4	0.5774	2.6933	4.6400
	67	3	4.5000	4	5	0.5000	3.6571	5.3429
	100	3	4.8333	4.5	5	0.2887	4.3467	5.3200
	133	3	4.3333	4	5	0.5774	3.3600	5.3067
	167	3	4.0000	3	5	1.0000	2.3141	5.6859
	200	3	5.0000	5	5	0.0000	5.0000	5.0000
	400	3	5.6667	5	7	1.1547	3.7200	7.6133
Pilot	33	3	4.0000	4	4	0.0000	4.0000	4.0000
	67	3	4.0000	4	4	0.0000	4.0000	4.0000
	100	3	4.0000	3	5	1.0000	2.3141	5.6859
	133	3	4.6667	4	6	1.1547	2.7200	6.6133
	167	3	4.1667	3.5	5	0.7638	2.8791	5.4543
	200	3	4.3333	4	5	0.5774	3.3600	5.3067
	400	3	5.0000	4	6	1.0000	3.3141	6.6859

Table F.13 Predictor Root Mean Square Tracking Error Descriptive Statistics

GROUP	$\tau_d$ (msec)	N	MEAN	MIN	MAX	STD	LOWER CI	UPPER CI
RP	33	6	1.8904	1.5643	2.0872	0.2049	1.7218	2.0589
	67	6	2.1221	1.9529	2.3183	0.1260	2.0185	2.2258
	100	6	2.2437	1.7854	3.0968	0.5018	1.8310	2.6565
	133	6	2.4326	2.0615	3.1399	0.4415	2.0694	2.7958
	167	6	2.5785	1.8814	3.2334	0.4891	2.1761	2.9808
	200	6	2.4430	1.9072	2.9779	0.4454	2.0766	2.8093
	400	6	3.1173	2.3027	4.5303	0.9020	2.3754	3.8593
FTE	33	3	1.9367	1.7364	2.0872	0.1806	1.6322	2.2412
	67	3	2.0669	1.9529	2.2004	0.1249	1.8562	2.2775
	100	3	2.5122	1.9109	3.0968	0.5931	1.5123	3.5122
	133	3	2.6985	2.1510	3.1399	0.5029	1.8507	3.5463
	167	3	2.9143	2.4633	3.2334	0.4017	2.2372	3.5915
	200	3	2.6735	2.2220	2.9779	0.3988	2.0011	3.3459
	400	3	3.1212	2.6185	3.9455	0.7196	1.9080	4.3344
Pilot	33	3	1.8440	1.5643	2.0686	0.2566	1.4113	2.2767
	67	3	2.1774	2.1058	2.3183	0.1221	1.9716	2.3832
	100	3	1.9752	1.7854	2.2556	0.2478	1.5574	2.3930
	133	3	2.1667	2.0615	2.3377	0.1494	1.9148	2.4186
	167	3	2.2426	1.8814	2.4449	0.3135	1.7140	2.7711
	200	3	2.2125	1.9072	2.6930	0.4212	1.5024	2.9225
	400	3	3.1135	2.3027	4.5303	1.2312	1.0378	5.1892



Table F.14 Predictor Root Mean Square Display Error Descriptive Statistics

GROUP	$\tau_d$ (msec)	<i>N</i>	MEAN	MIN	MAX	STD	LOWER CI	UPPER CI
RP	33	6	1.4179	1.1941	1.6667	0.1725	1.2760	1.5599
	67	6	1.4159	1.1934	1.6481	0.1481	1.2940	1.5377
	100	6	1.4965	1.1597	2.1737	0.4216	1.1497	1.8433
	133	6	1.4974	1.1046	2.3194	0.5578	1.0386	1.9562
	167	6	1.3700	1.0492	2.0375	0.4167	1.0273	1.7128
	200	6	1.2953	0.9770	1.7228	0.2980	1.0501	1.5404
	400	6	1.1907	0.8861	1.7357	0.3576	0.8965	1.4849
FTE	33	3	1.4862	1.2702	1.6667	0.2006	1.1480	1.8244
	67	3	1.4810	1.3475	1.6481	0.1531	1.2229	1.7391
	100	3	1.7734	1.2760	2.1737	0.4567	1.0035	2.5433
	133	3	1.8419	1.1046	2.3194	0.6477	0.7499	2.9340
	167	3	1.6845	1.2987	2.0375	0.3705	1.0599	2.3092
	200	3	1.5134	1.2124	1.7228	0.2672	1.0629	1.9639
	400	3	1.4816	1.2232	1.7357	0.2563	1.0495	1.9137
Pilot	33	3	1.3497	1.1941	1.4724	0.1421	1.1102	1.5892
	67	3	1.3508	1.1934	1.4410	0.1368	1.1202	1.5813
	100	3	1.2195	1.1597	1.3038	0.0751	1.0929	1.3462
	133	3	1.1529	1.1148	1.2032	0.0455	1.0763	1.2295
	167	3	1.0555	1.0492	1.0592	0.0055	1.0462	1.0649
	200	3	1.0771	0.9770	1.1465	0.0888	0.9274	1.2269
	400	3	0.8998	0.8861	0.9097	0.0122	0.8792	0.9205

#### *F.4 Sensitivity of the Model-Based Predictive Compensation Algorithm*

Evaluate the limited sensitivity of the model-based predictive compensation algorithm to uncertainty in the aerodynamic model of the UAV and total system time delay. The MOPs were:

1. Aerodynamic Model Uncertainty: Characterize the sensitivity of the delay compensated Pilot/Display/UAV system to aerodynamic uncertainties of  $\pm 20\%$ .
2. Time Delay Magnitude Uncertainty: Characterize the sensitivity of the delay compensated Pilot/Display/UAV system to time delay magnitude uncertainties of  $\pm 33\%$ .

Data required for both MOPs were pilot comments and Cooper-Harper ratings. Additional data collected for analysis included PIO ratings, RMSTE, and RMSDE.

*F.4.1 Statistical Methodologies* . The RSM approach was used for Objective 3, MOP 1 data analysis. Two methodologies were used for Objective 3, MOP 2 data analysis:

1. Classical statistical approach
2. RSM approach

*F.4.1.1 Classical Statistical Approach* . The data collected for Objective 3, MOP 2 are listed in Table F.15. The descriptive statistics for Objective 3, MOP 2 are listed in Table F.16 through Table F.19.

The classical statistical approach used the student's *t*-test for analysis. The  $\chi^2$  test was not used since  $T = 3$  (three time delay uncertainties tested) and the  $\chi^2$  needs  $T \geq 5$ . The student's *t*-tests determined that for each time delay uncertainty there was no significant difference between pilots and FTEs for the PIO ratings, Cooper-Harper ratings, RMSTE, and RMSDE with 90% confidence.

Table F.15 Time Delay Uncertainty Data

$\tau_{d,comp}$ (msec)	$\tau_d$ (msec)	$\tau_{d,true}$ (msec)	RP	TASK	PIOR	CHR	RMSTE (deg)	RMSDE (deg)
67	100	88.8	1	2B	2	4	2.2448	1.3308
67	100	86.2	2	1A	3	5	2.4123	1.4206
67	100	86.6	3	1A	3	5	2.2359	1.3466
67	100	89.4	4	2B	3	5	1.8027	0.9954
67	100	89.2	5	2A	3	7	3.6033	2.7323
67	100	88.8	6	2A	4	5.5	2.4926	1.4844
100	100	89	1	2A	2	3	1.8848	1.1951
100	100	88.7	2	2A	3	5	1.7854	1.1597
100	100	87	3	2A	3	4	2.2556	1.3038
100	100	88.4	4	2B	3	5	1.9109	1.2760
100	100	87.8	5	2A	3	5	3.0968	2.1737
100	100	89.9	6	1A	3	4.5	2.5290	1.8706
133	100	88.4	1	2A	3	4	2.0018	1.3889
133	100	86.7	2	2B	3	4	1.7916	1.1356
133	100	88.8	3	2B	3	4	2.0321	0.9731
133	100	84.6	4	2A	3	5	2.0885	1.1317
133	100	85.7	5	1A	3	7	3.8260	2.8009
133	100	84.8	6	2A	2	4	2.1075	1.3212

Table F.16 Time Delay Uncertainty PIO Rating Descriptive Statistics

GROUP	$\tau_{d,comp}$ (msec)	N	MEAN	MIN	MAX	STD	LOWER CI	UPPER CI
RP	67	6	3.0000	2	4	0.6325	2.2461	3.5203
	100	6	2.8333	2	3	0.4082	2.3467	3.1692
	133	6	2.8333	2	3	0.4082	2.3467	3.1692
FTE	67	3	3.3333	3	4	0.5774	2.3600	4.3067
	100	3	3.0000	3	3	0.0000	3.0000	3.0000
	133	3	2.6667	2	3	0.5774	1.6933	3.6400
Pilot	67	3	2.6667	2	3	0.5774	1.6933	3.6400
	100	3	2.6667	2	3	0.5774	1.6933	3.6400
	133	3	3.0000	3	3	0.0000	3.0000	3.0000

Table F.17 Time Delay Uncertainty Cooper-Harper Rating Descriptive Statistics

GROUP	$\tau_{d,comp}$ (msec)	N	MEAN	MIN	MAX	STD	LOWER CI	UPPER CI
RP	67	6	5.2500	4	7	0.9874	4.0729	6.0623
	100	6	4.4167	3	5	0.8010	3.4618	5.0756
	133	6	4.6667	4	7	1.2111	3.2230	5.6629
FTE	67	3	5.8333	5	7	1.0408	4.0786	7.5880
	100	3	4.8333	4.5	5	0.2887	4.3467	5.3200
	133	3	5.3333	4	7	1.5275	2.7581	7.9085
Pilot	67	3	4.6667	4	5	0.5774	3.6933	5.6400
	100	3	4.0000	3	5	1.0000	2.3141	5.6859
	133	3	4.0000	4	4	0.0000	4.0000	4.0000

Table F.18 Time Delay Uncertainty Root Mean Square Tracking Error Descriptive Statistics

GROUP	$\tau_{d,comp}$ (msec)	N	MEAN	MIN	MAX	STD	LOWER CI	UPPER CI
RP	67	6	2.4653	1.8027	3.6033	0.6065	1.7423	2.9642
	100	6	2.2437	1.7854	3.0968	0.5018	1.6456	2.6565
	133	6	2.3079	1.7916	3.8260	0.7522	1.4112	2.9267
FTE	67	3	2.6329	1.8027	3.6033	0.9085	1.1013	4.1644
	100	3	2.5122	1.9109	3.0968	0.5931	1.5123	3.5122
	133	3	2.6740	2.0885	3.8260	0.9977	0.9920	4.3560
Pilot	67	3	2.2977	2.2359	2.4123	0.0994	2.1301	2.4652
	100	3	1.9752	1.7854	2.2556	0.2478	1.5574	2.3930
	133	3	1.9419	1.7916	2.0321	0.1310	1.7211	2.1627

Table F.19 Time Delay Uncertainty Root Mean Square Display Error Descriptive Statistics

GROUP	$\tau_{d,comp}$ (msec)	N	MEAN	MIN	MAX	STD	LOWER CI	UPPER CI
RP	67	6	1.5517	0.9954	2.7323	0.6026	0.8333	2.0474
	100	6	1.4965	1.1597	2.1737	0.4216	0.9939	1.8433
	133	6	1.4586	0.9731	2.8009	0.6742	0.6549	2.0131
FTE	67	3	1.7373	0.9954	2.7323	0.8957	0.2274	3.2473
	100	3	1.7734	1.2760	2.1737	0.4567	1.0035	2.5433
	133	3	1.7513	1.1317	2.8009	0.9139	0.2105	3.2920
Pilot	67	3	1.3660	1.3308	1.4206	0.0480	1.2851	1.4469
	100	3	1.2195	1.1597	1.3038	0.0751	1.0929	1.3462
	133	3	1.1659	0.9731	1.3889	0.2095	0.8126	1.5191

Table F.20 Aerodynamic Sensitivity Analysis Data

$\tau_d$ (msec)	$\tau_{d,true}$ (msec)	RP	TASK	$C_{m_\alpha}$	$C_{m_q}$	$C_{m_{\delta_e}}$	PIO	CHR	RMSTE	RMSDE
100	88.6	1	2A	-20%	-20%	+20%	2	3	1.9934	1.1493
100	86.9	1	2A	+20%	-20%	-20%	3	5	2.0937	1.3732
100	88.4	1	1A	-20%	+20%	-20%	2	4	2.1991	1.3244
100	87.0	1	2B	+20%	+20%	+20%	3	4	2.4193	1.2560
100	87.4	2	1A	-20%	+20%	-20%	3	4	2.6302	1.5346
100	88.1	2	2A	+20%	-20%	-20%	3	5	2.5071	1.6010
100	87.9	2	1A	+20%	+20%	+20%	3	5	2.4751	1.7581
100	88.2	2	2B	-20%	-20%	+20%	3	3	1.5828	1.1283
100	89.7	3	2A	+20%	-20%	-20%	3	4	1.5132	1.1355
100	89.0	3	1A	-20%	+20%	-20%	3	5	2.5713	1.4796
100	89.5	3	2B	+20%	+20%	+20%	3	4	1.8225	1.0244
100	84.7	3	2A	-20%	-20%	+20%	3	5	2.6987	1.1635
100	89.1	4	2A	-20%	-20%	-20%	2	3	1.8390	1.1693
100	87.6	4	2B	-20%	+20%	+20%	3	4	1.8917	1.1683
100	86.6	4	1A	+20%	+20%	-20%	4	6	2.3484	1.4313
100	89.0	4	2A	+20%	-20%	+20%	3	5	1.8311	1.1050
100	89.5	5	2A	+20%	-20%	+20%	3	5	2.1573	1.3780
100	88.8	5	2A	-20%	+20%	+20%	3	6	2.7377	1.7150
100	89.8	5	1A	-20%	-20%	-20%	3	5	2.5948	1.8772
100	88.9	5	2B	+20%	+20%	-20%	3	6	3.8106	2.5350
100	87.5	6	2B	-20%	-20%	-20%	3	5	1.9043	1.1929
100	89.4	6	2B	+20%	-20%	+20%	4	5	2.3204	1.4584
100	89.1	6	2A	20%	20%	-20%	4	5	2.7059	1.8000
100	87.7	6	2B	-20%	20%	20%	3	5	2.6099	1.5412

The student's *t*-tests determined that there was no significant difference between various time delay uncertainties for PIO ratings, Cooper-Harper ratings, RMSTE, and RMSDE with 90% confidence for the RPs treated as a group and for the FTEs.

*F.4.1.2 Response Surface Methodology (RSM) Approach.* The RSM approach was used for Objective 3, MOP 1 to perform an aerodynamic sensitivity analysis in order to investigate the effects of  $C_{m_\alpha}$ ,  $C_{m_q}$ , and  $C_{m_{\delta_e}}$ . Table F.20 lists the data collected for the aerodynamic sensitivity analysis. Due to time constraints,

a full factorial test matrix was not used for data collection. Instead, a sub-optimal test matrix was utilized for data collection. The sub-optimal test matrix blocked on the type of RP. Due to the small number of test points conducted and confounding issues, no interaction effects greater than second order were investigated. This is acceptable due to what is known as the “sparsity of effects” principle which states that most processes are driven by main effects and low order interactions. A RSM approach was used to fit a model to each of the following responses: PIO ratings, Cooper-Harper ratings, RMSTE, and RMSDE. Each response was fitted as a function of five main effects (RP, TASK,  $C_{m_\alpha}$ ,  $C_{m_q}$ ,  $C_{m_{\delta_e}}$ ) and three second order interaction effects ( $C_{m_\alpha} \cdot C_{m_q}$ ,  $C_{m_\alpha} \cdot C_{m_{\delta_e}}$ ,  $C_{m_q} \cdot C_{m_{\delta_e}}$ ). The best fit RSM model for  $PIOR = f(RP, TASK, C_{m_\alpha}, C_{m_q}, C_{m_{\delta_e}}, C_{m_\alpha} \cdot C_{m_q}, C_{m_\alpha} \cdot C_{m_{\delta_e}}, C_{m_q} \cdot C_{m_{\delta_e}})$  was the following:

$$PIOR = 1.7167 + 2500.0 \cdot C_{m_\alpha} \quad (F.3)$$

The RSM approach showed that PIO ratings are significantly affected by  $C_{m_\alpha}$ . Though the effect of  $C_{m_\alpha}$  is statistically significant, it appears that the effect may not be operationally significant. RSM fitted aerodynamic sensitivity PIO ratings remained between 2.5 and 3.5 for changes in  $C_{m_\alpha}$  of  $\pm 20\%$ . The best fit RSM model for  $CHR = f(RP, TASK, C_{m_\alpha}, C_{m_q}, C_{m_{\delta_e}}, C_{m_\alpha} \cdot C_{m_q}, C_{m_\alpha} \cdot C_{m_{\delta_e}}, C_{m_q} \cdot C_{m_{\delta_e}})$  was the following:

$$CHR = 3.1250 + 2916.7 \cdot C_{m_\alpha} \quad (F.4)$$

The RSM approach showed that Cooper-Harper ratings are significantly affected by  $C_{m_\alpha}$ . Though the effect of  $C_{m_\alpha}$  is statistically significant, it is most likely

not operationally significant. RSM fitted aerodynamic sensitivity Cooper-Harper ratings remained between 4 and 5 for changes in  $C_{m_\alpha}$  of  $\pm 20\%$  which is within the traditional Cooper-Harper variation of  $\pm 1$ .

The best fit RSM model for  $RMSTE = f(RP, TASK, C_{m_\alpha}, C_{m_q}, C_{m_{\delta_e}}, C_{m_\alpha} \cdot C_{m_q}, C_{m_\alpha} \cdot C_{m_{\delta_e}}, C_{m_q} \cdot C_{m_{\delta_e}})$  was the following:

$$RMSTE = 1.2103 - 0.0450 \cdot C_{m_q} \quad (F.5)$$

The RSM approach showed that RMSTE is significantly affected by  $C_{m_q}$ . RSM fitted aerodynamic sensitivity RMSTE remained between 2.0 degrees and 3.0 degrees for changes in  $C_{m_q}$  of  $\pm 20\%$ .

The best fit RSM model for  $RMSDE = f(RP, TASK, C_{m_\alpha}, C_{m_q}, C_{m_{\delta_e}}, C_{m_\alpha} \cdot C_{m_q}, C_{m_\alpha} \cdot C_{m_{\delta_e}}, C_{m_q} \cdot C_{m_{\delta_e}})$  was the following:

$$RMSDE = 0.8517 - 0.0246 \cdot C_{m_q} \quad (F.6)$$

The RSM showed that RMSDE is significantly affected by  $C_{m_q}$ . RSM fitted aerodynamic sensitivity RMSDE remained between 1.0 degrees and 2.0 degrees for changes in  $C_{m_q}$  of  $\pm 20\%$ .

RSM was used for Objective 3, MOP 2 to perform an aerodynamic sensitivity analysis in order to investigate the effects of time delay uncertainty. A RSM model was developed for the following responses: PIO ratings, Cooper-Harper ratings, RMSTE, and RMSDE. Each response was fitted with three main effects ( $RP, TASK, \tau_{d,comp}$ ), three second order interaction effects ( $RP \cdot TASK, RP \cdot \tau_{d,comp}, TASK \cdot \tau_{d,comp}$ ), and one third order interaction effect ( $RP \cdot TASK \cdot \tau_{d,comp}$ ).

The best fit RSM model for  $PIOR = f(RP, TASK, \tau_{d,comp}, RP \cdot TASK, RP \cdot \tau_{d,comp}, TASK \cdot \tau_{d,comp}, RP \cdot TASK \cdot \tau_{d,comp})$  was the following:

$$PIOR = 2.8889 \quad (F.7)$$

The RSM showed that PIO ratings are not affected by the type of RP, the task, or the time delay uncertainty.

The best fit RSM model for  $CHR = f(RP, TASK, \tau_{d,comp}, RP \cdot TASK, RP \cdot \tau_{d,comp}, TASK \cdot \tau_{d,comp}, RP \cdot TASK \cdot \tau_{d,comp})$  was the following:

$$CHR = 4.7778 + 0.5556 \cdot RP \quad (F.8)$$

RSM showed that the type of RP significantly affects Cooper-Harper ratings. This result is the opposite of that derived from the student's  $t$ -tests. The student's  $t$ -tests concluded that for each time delay uncertainty, there was no difference between pilot and FTE Cooper-Harper ratings.

The best fit RSM model for  $RMSTE = f(RP, TASK, \tau_{d,comp}, RP \cdot TASK, RP \cdot \tau_{d,comp}, TASK \cdot \tau_{d,comp}, RP \cdot TASK \cdot \tau_{d,comp})$  was the following:

$$RMSTE = 2.3596 + 0.2468 \cdot RP - .3704 \cdot TASK \quad (F.9)$$

This shows that the type of RP and the task significantly affects RMSTE. This result is the opposite of that derived from the student's  $t$ -tests with regards to the type of RP. The student's  $t$ -tests concluded that for each time delay uncertainty,



there was no difference between pilot and FTE RMSTE. RMSTE was smallest for Task 2B and highest for Task 1A.

The best fit RSM model for  $RMSDE \cong f(RP, TASK, \tau_{d,comp}, RP \cdot TASK, RP \cdot \tau_{d,comp}, TASK \cdot \tau_{d,comp}, RP \cdot TASK \cdot \tau_{d,comp})$  was the following:

$$RMSTE = 1.5209 + 0.2332 \cdot RP - .3351 \cdot TASK \quad (F.10)$$

This shows that the type of RP and the task significantly affects RMSDE. This result is the opposite of that derived from the student's  $t$ -tests with regards to the type of RP. The student's  $t$ -tests concluded that for each time delay uncertainty, there was no difference between pilot and FTE RMSDE.

A detailed discussion of the statistical methodologies used in this thesis may be found in the Have Reckon Final Test Report(56). For more information on classical statistics to include the student's  $t$ -test and the  $\chi^2$  test, please see Mendenhall(36). For more information on RSM, please see Reference Myers(40).

## Appendix G. UAV Aerodynamic Model and Time Delay Budget

### G.1 UAV Aerodynamic Model

Since the predictive display algorithm was based on the aerodynamic model of the UAV and total system time delay, it was crucial to have validated parameters prior to the beginning of flight test. Eight flights were conducted with the UAV instrumented with a digital data acquisition system (PID Pod) capable of recording and digitally storing inflight data for later analysis. Programmed test input pitch doublets were used to collect short period mode data. An onboard Global Positioning System (GPS) was used to calibrate the airspeed indicated on the pilot display. Parameter Estimation (Pest) software was used to obtain stability derivatives for use in the predictive display. The results of the parameter estimation were as follows:

$$I_{yy} = 5.25 \text{ slug} \cdot \text{ft}^2 \quad (\text{G.1})$$

$$\text{mass} = 1.426 \text{ slug} \quad (\text{G.2})$$

$$\text{chord} = 1.67 \text{ ft} \quad (\text{G.3})$$

$$\text{span} = 10.0 \text{ ft} \quad (\text{G.4})$$

$$\text{area} = 16.67 \text{ ft}^2 \quad (\text{G.5})$$

$$C_{L_{\delta_e}} = +0.0031 \pm 0.0004 \text{ (per deg)} \quad (\text{G.6})$$

$$C_{L_{\alpha}} = +0.088 \pm 0.005 \text{ (per deg)} \quad (\text{G.7})$$

$$C_{m_{\delta_e}} = -0.018 \pm 0.001 \text{ (per deg)} \quad (\text{G.8})$$

$$C_{m_{\alpha}} = +0.0005 \pm 0.002 \text{ (per deg)} \quad (\text{G.9})$$

$$C_{m_q} = -24 \pm 2 \text{ (per rad)} \quad (\text{G.10})$$

Note that, due to the extremely high damping of the system, the primary stability parameter ( $C_{m_{\alpha}}$ ) was not well identified. Parameter identification flight test time histories with pEst model response overlays can be found in Figure G.1.

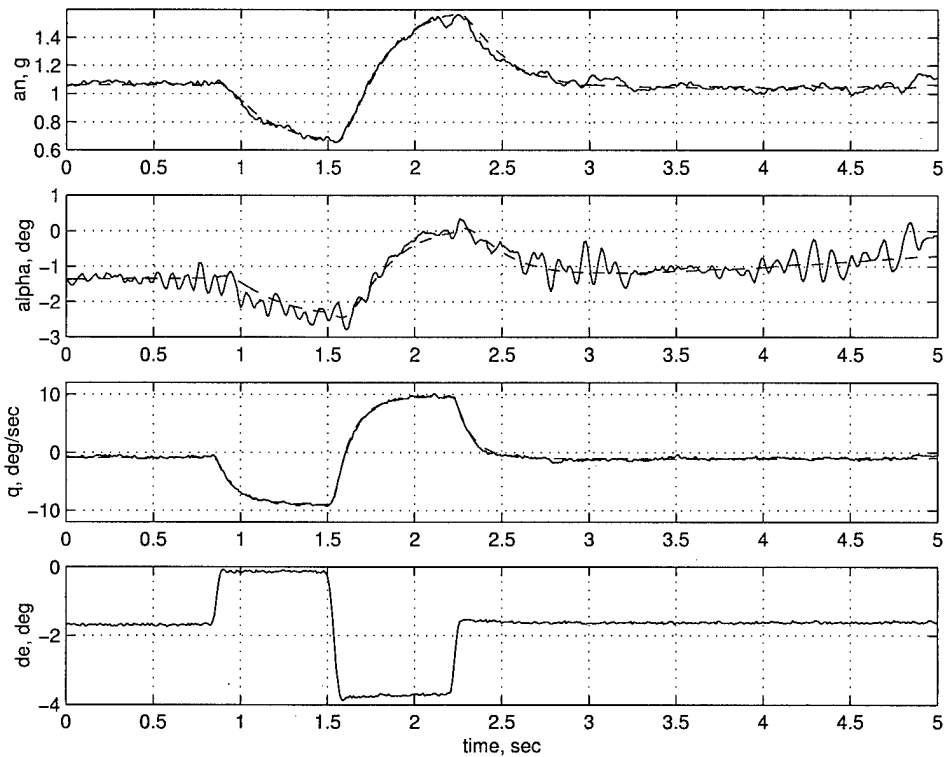


Figure G.1 Parameter Identification Flight Test Data and pEst Model Response

After performing a laboratory calibration of both the PID pod and HUD airdata systems, the test team determined that the HUD display was in units of miles/hour and had a significant bias error. A leastsquares curve fit to the calibration data yielded:

$$KIAS = 5.9 + 1.18 * HUD \quad (G.11)$$

where KIAS is knots indicated airspeed, and HUD is HUD display in mph.

Early flight tests showed that a comfortable airspeed for both the research and safety pilots was a HUD indication of 40 MPH. This resulted in an actual airspeed of 41.3 KCAS. Standard day density at the nominal test altitude (500 feet) above field elevation was used to calculate a test condition dynamic pressure of 5.775 pounds

per square foot. Test conditions were  $\pm 100$  feet from the nominal 500 feet AGL, 40 MPH  $\pm 5$ .

### *G.2 Time Delay Budget*

The baseline system time delay of the UAV system was defined as the time from stick input to elevator movement as seen in the telemetry stream. The time delay measured on the ground was approximately 150 msec based on an average of six measurements. An additional 33 msec delay for integration and display delay gave an overall system time delay of 183 msec.

## Bibliography

1. *RSmith32*. Software Package Version 1.06.02. Ralph H. Smith, 1996,97,98.
2. Bacon, B. J.; and Schmidt D. K. *An Optimal Control Approach to Pilot/Vehicle Analysis and the Neal-Smith Criteria*. AIAA Paper 82-1357, AIAA, 1982.
3. Baron, S.; Kleinman, D. L.; and W. H. Levison. "An Optimal Control Model of Human Response, Part II: Prediction of Human Performance in a Complex Task," *Automatica*, 6:371-382 (1970).
4. Berry, D. T. and others. "In-Flight Evaluation of Control System Pure Time Delays," *Journal of Aircraft*, 19(4):318-323 (April 1982).
5. Berry, Donald T. *Flying Qualities Criteria and Flight Control Design*. AIAA Paper 81-1823, AIAA, 1981.
6. Berry, Donald T. "In-Flight Evaluation of Incremental Time Delays in Pitch and Roll," *Journal of Guidance and Control*, 9(5):573-577 (September 1986).
7. Berry, D. T.; Powers B. G.; Szalai, K. J.; and R. J. Wilson. *A Summary of an In-Flight Evaluation of Control System Pure Time Delays During Landing Using the F-8 DFBW Airplane*. AIAA Paper 80-1626, AIAA, 1980.
8. Captain Jeff Starr, Predator UAV Pilot. "Predator Operator Lessons Learned." Address at UCAV Operator Working Group, May 7 1998.
9. Cardullo, Frank M. and Gary George. *Transport delay Compensation: An Inexpensive Alternative to Increasing Image Generator Update Rate*. AIAA Paper 93-3563, AIAA, 1993.
10. Cooper, George E. and Robert P. Harper Jr. *The Use Of Pilot Rating In The Evaluation Of Aircraft Handling Qualities*. NASA TN D-5153, Washington, D.C.: National Aeronautics And Space Administration, April 1969.
11. Crane, D. F. *Compensation for Time Delay in Flight Simulator Visual Display System*. AIAA Paper 83-1080, AIAA, 1983.
12. Crane, D. Francis. "Flight Simulator Visual Display Delay Compensation." *1981 Winter Simulation Conference Proceedings, Vol. 1*. 59-67. New York: IEEE Press, 1981.
13. Davidson, J. B.; and D. K. Schmidt. *Modified Optimal Control Pilot Model for Computer-Aided Design and Analysis*. NASA-TM- 4384, NASA, 1992.
14. Department of Defense. *Flying Qualities Of Piloted Aircraft*. MIL-STD- 1797A. Washington, D.C.: Government Printing Office, 301 January 1990.

15. Di Franco, Dante A. *In-Flight Investigation of the effects of Higher-Order Control System Dynamics on Longitudinal Handling Qualities*. AFFDL-TR 68-90, Air Force Flight Dynamics Laboratory, 1970.
16. Doman, D. B. *Interactive Flying Qualities Toolbox for Matlab User's Guide*. WL-TR- 95-3070, Flight Dynamics Directorate, 1995.
17. Efremov, A. V. et al. *Analysis of Reasons for Pilot Induced Oscillation Tendency and Development of Criteria for its Prediction*. Technical Report, Moscow Aviation Institute: Pilot/Vehicle Laboratory, 1995.
18. Ema, Tetsuo. "An Experimental Study of Pilot's Control Behavior in System with a Pure Time Delay," *Memoirs of the National Defense Academy, Japan*, 27(2):53-64 (June 1987).
19. Franklin, Gene F. and others. *Feedback Control of Dynamic Systems, Third Edition*. Reading, Massachusetts: Addison-Wesley Publishing Company, 1994.
20. Fulghum, David A. "Unmanned Strike Next for Military," *Aviation Week and Space Technology*, 146(23):47-48 (June, 2 1997).
21. "Gulf War Experience Sparks Review of RPV Priorities," *Aviation Week and Space Technology*, 134(16):86-87 (April, 22 1991).
22. Gum, D. R.; and W. B. Albery. "Time-Delay Problems Encountered in Integrating the Advanced Simulator for Undergraduate Pilot Training," *Journal of Aircraft*, 14(5) (April 1977).
23. Hess, R. A. *A Pilot Modeling Technique for Handling Qualities Research*. AIAA Paper 80-1624, AIAA, 1980.
24. Hess, R. A. *Analysis of Aircraft Longitudinal Handling Qualities*. AIAA Paper 81-1771, AIAA, 1981.
25. Hess, R.A. "Prediction of Pilot Opinion Ratings Using an Optimal Pilot Model," *Human Factors*, 19(5):459-475 (October 1977).
26. Hess, R.A. "Analysis of Aircraft Attitude Control Systems Prone to Pilot-Induced Oscillations," *Journal of Guidance and Control*, 7(1):106-112 (January 1984).
27. Hess, R.A.; and R. M. Kalteis. "Technique for Predicting Longitudinal Pilot-Induced Oscillations," *Journal of Guidance and Control*, 14(1):198-204 (February 1991).
28. Hess, Ronald A. "Effects of Time Delays on Systems Subject to Manual Control," *Journal of Guidance and Control*, 7(4):416-421 (July 1984).
29. Hodgkinson, J. and K. A. Johnston. *Initial Results of an Inflight Simulation of Augmented Dynamics in Fighter Approach and Landing*. AIAA Paper 79-1783, AIAA, 1979.

30. Hodgkinson, J.; Wood, J. R.; and R. H. Hoh. *An Alternate Method of Specifying Bandwidth For Flying Qualities*. AIAA Paper 82-1609, AIAA, 1982.
31. Kleinman, D. L.; Baron, S.; and W. H. Levison. "An Optimal Control Model of Human Response, Part I: Theory and Validation," *Automatica*, 6:357-369 (1970).
32. Leahy, Lt Col Mike and Dr. Larry Birckelbaw. "Industry Day Briefing: Program Description." Briefing at DARPA/USAF UCAV Advanced Technology Demonstrator Industry Day, 23 February 1998.
33. Marshall, John Edward. *Control of Time Delay Systems*. London: The Institution of Electrical Engineers, 1979.
34. McFarland, R. E. *Transport Delay Compensation for Computer Generated Imagery Systems*. NASA JM 100084, Washington, D.C.: National Aeronautics And Space Administration, 1988.
35. McRuer, D. T. et al. *Minimum Flying Qualities, Vol 2: Pilot Modelling for Flying Qualities Applications*. WRDC-TR- 89-3125, Vol. 2, US Air Force Flight Dynamics Laboratory, 1989.
36. Mendenhall, W. and others. *Mathematical Statistics with Applications* (Fourth Edition). PWS-Kent Publishing Company, 1990.
37. Miller, Kimball G. Jr.; and Riley Donald R. "The Effect of Visual-Motion Time Delays on Pilot Performance In a Pursuit Tracking Task." *AIAA Visual and Motion Simulation Conference, Proceedings*. 55-62. Dayton, Ohio April 26-28, 1976: AIAA, 1976.
38. Mitchell, D. G.; Aponso, B. L.; and R. H. Hoh. *Minimum Flying Qualities, Vol. 1*. WRDC-TR- 89-3125, Vol. 1, Air Force Flight Dynamics Laboratory, 1989.
39. Monagan, S. J.; Smith, R. E.; and R. E. Bailey. *Lateral Flying Qualities of Highly Augmented Fighter Aircraft*. AFWAL-TR 81-3171 Vol. 1, Air Force Flight Dynamics Laboratory, 1982.
40. Myers, R.H. and D.C. Montgomery. *Response Surface Methodology*. New York: John Wiley and Sons, 1995.
41. Neal, T. P.; and R.E. Smith. *An Inflight Investigation to Develop Control System Design Criteria for Fighter Airplanes*. AFFDL-TR 70-74, Air Force Flight Dynamics Laboratory, December 1970.
42. Nelson, Robert C. *Flight Stability and Automatic Control, Second Edition*. New York: McGraw-Hill, 1998.
43. Probert, Andrew A. "Uninhabited Combat Aerial Vehicles: Remove The Pilot?," *Airpower Journal*, 11(4):85-89 (Winter 1997).

44. Prosser, Charles F. and Curtiss D. Wiler. *RPV Flying Qualities Design Criteria*. AFFDL-TR 76-125, Air Force Flight Dynamics Laboratory, 1976.
45. R. Wade Allen, Richard J. DiMarco. "Effects of Transport Delays on Manual Control System Performance." *Twentieth Annual Conference on Manual Control*. 185-201. Ames Research Center, Moffett Field, California: NASA, 1984.
46. Ricard, Gilbert L. "Acquisition of Control Skill With Delayed and Compensated Displays," *Human Factors*, 37(3):652-658 (September 1995).
47. Schmidt, D K. "On the Use of the OCM's Quadratic Objective Function as a Pilot Rating Metric." *Proceedings of the 17th Annual Conference on Manual Control*. 305-313. 1981.
48. Scott, William B. "X-36 Testing Gives Boeing Jump on UCAV Work," *Aviation Week and Space Technology*, 148:58-60 (March, 2 1998).
49. Smith, Ralph H. and Norman D. Geddes. *Handling Quality Requirements for Advanced Aircraft Design: Longitudinal Mode*. AFFDL-TR 78-154, Air Force Flight Dynamics Laboratory, August 1979.
50. Smith, Rogers E. *Equivalent System Verification and Evaluation of Augmentation Effects on Fighter Approach and Landing Flying Qualities*. AFWAL-TR-3116, Air Force Flight Dynamics Laboratory, 1981.
51. Smith, Rogers E. and Sarrafian Shahan K. "Effect of Time Delay on Flying Qualities: An Update," *Journal of Guidance and Control*, 9(5):578-584 (September 1986).
52. Sobiski, Donald J. and Frank M. Cardullo. *Predictive Compensation of Visual System Time Delays*. AIAA Paper 87-2434, AIAA, 1987.
53. Stengel, R.F.; and G. E. Miller. "Flight Tests of a Microprocessor Control System," *Journal of Guidance and Control*, 3(6):494-500 (November 1980).
54. Szalai, K. J.; Felleman P. G.; Gera J.; and Glover R. D. *Design and Test Experience With a Troply Redundant Digital Fly-By-Wire Control System*. AIAA Paper 76-1911, AIAA, 1976.
55. Thurling, Andrew J. *Have Reckon Test Plan*. USAF TPS-TP- 99A-03, Edwards AFB, CA: USAF Test Pilot School, August 1999.
56. Thurling, Andrew J., et al. *Limited Evaluation of Unmanned Aerial Vehicle Handling Qualities and System Performance Using a Model-Based Algorithm to Compensate for Time Delay*. AFFTC-TIM- 99-08, Edwards AFB, CA: Air Force Flight Test Center, December 1999.
57. U.S. Army Signal Corps. *Advertisement and Specification for a Heavier-Than-Air Flying Machine*. Signal Corps Specification 486. Washington: Government Printing Office, 23 December 1907.



58. USAF Scientific Advisory Board. *New World Vistas: Air and Space Power for the 21st Century*. Report Series Aircraft and Propulsion Volume. Washington, D.C.: Government Printing Office, 1995.
59. Wilson, J. R. "UAVs: A Bird's-eye View," *Aerospace America*, 38-43 (November 1996).